Temporal and spatial dynamics of trace metal acquisition by prokaryotic communities in the Southern Ocean

Rui Zhang

Sorbonne Université

École Doctorale des Sciences de l'Environnement d'Ile-de-France (ED129)
Laboratoire d'océanographie microbienne (UMR 7621)
Observatoire Océanologique de Banyuls-sur-Mer

Temporal and spatial dynamics of trace metal acquisition by prokaryotic communities in the Southern Ocean

Par Rui Zhang

Thèse de doctorat en Microbiologie
Dirigée par Ingrid Obernosterer et Pavla Debeljak
Présentée et soutenue publiquement le 28 Juin 2024

Devant un jury composé de :

Dr. Mar Benavides ; CRHC-IRD, HDR, Mediterranean Institut of Oceanography, Université Aix Marseille - Rapporteur
Dr. Ludwig Jardillier ; Professeur, Université Paris-Saclay - Rapporteur
Dr. Hélène Planquette ; DR-CNRS, LEMAR, Université Bretagne Occidentale - Examinatrice
Dr. François-Yves Bouget ; DR-CNRS, LOMIC, Sorbonne Université - Président
Dr. Pavla Debeljak ; EC, Sup'Biotech & MNHN - Co-Directrice de thèse
Dr. Ingrid Obernosterer ; DR-CNRS, LOMIC - Directrice de thèse

Dédicace

ACKNOWLEDGEMENTS

During these four years in France, I have had a wonderful time, and I would not have been able to enjoy them without the help of many people. First of all, I would like to thank my supervisor Ingrid Obernosterer for providing me with the opportunity to study abroad and helping me find an apartment in Banyuls-sur-mer. Thank you for taking care of me during the SWINGS cruise, without your help, I could not have adapted quickly to seasick and the life on the cruise. I appreciate your guidance in my research over the past four years. Without your support, this PhD would not have been possible.

Many thanks to my co-supervisor Pavla Debeljak, for guiding me into the basics of bioinformatics at the beginning of my PhD study, without which I would have been lost in the ocean of bioinformatic analysis, and for providing me with bioinformatics guidance throughout my PhD study.

Many thanks to Stéphane, for helping me with sampling while I was on the SWINGS cruise, as well as for help me in data analysis and providing knowledge of marine chemistry during my PhD study.

Many thanks to Eva, for guiding me through the DNA extraction experiment and inviting me for Christmas dinner. Many thanks to Nyree, for providing training in Bio2Mar platform and teaching me how to perform DNA quantification.

Many thanks to Yanhui, for being there for the past two years, we've travelled to so many cities and enjoyed so much delicious food together, I probably wouldn't have had the motivation to travel if it was just me.

Many thanks to Nawal, Jana and Angel for helping me to adapt when I first arrived in Banyuls-sur-mer, for helping me to survive far away from home, for inviting me to parties, hiking, shopping and many thanks to Nawal for teaching me how to swim.

Many thanks to Rhea and Sharvari, for their companionship, help with my thesis, and dinner invitations. Many thanks to all lovely PhD students and Post-Doc of Batiment A: Chloé, Emile, Maxime, Louis, Coco and Anabel.

Many thanks to Jingguang and Ying for helping me when I first arrived in Banyuls-sur-mer, helping me to adapt to life in France and providing me with life’s necessities.

Many thanks to all the researchers in the SWINGS cruise as well as the crew, I had a very enjoyable two months on board. Many thanks to Frédéric Vivier for identifying water masses, Corentin Baudet and Hélène Planquette for providing trace metal data, and Philippe Catala, Olivier Crispi, Audrey Guéneuguès and Barbara Marie for providing cell abundance, major nutrients and DOC data.

Thanks to the teachers and students in EBAME workshop, the courses of fundamentals in statistics and the polar ocean. Thanks for your patience and support. I really learned a lot and enjoyed the classes.

Thanks to China Scholarship Council and Peterson Elites Scholarship, for funding me this 4-year study.

Many thanks to my family and friends in China for your love, encouragement and understanding, and for easing my homesickness. This support has been crucial in the successful completion of my thesis.

Summary

Trace metals such as iron (Fe), manganese (Mn), nickel (Ni), and copper (Cu) play critical roles for the growth and metabolism of phototrophic and non-phototrophic prokaryotic and eukaryotic microorganisms in the ocean, and thereby influence the biogeochemical cycling of major elements. While the impact of Fe limitation on phototrophic microorganisms (phytoplankton) has been extensively investigated, the links between micronutrients and marine microbes remains thus far poorly studied. This thesis investigates the metabolic potential of taxonomically diverse marine microbes to acquire trace metals using a metagenomics approach and thereby provides insights into the contribution of prokaryotic taxa to the cycling of minor and major elements on temporal and spatial scales in the Southern Ocean.

The objective of Chapter 1 is to study the strategy of microbes to acquire different chemical forms of Fe under seasonally changing organic carbon requirements. Based on samples obtained by a remote autonomous sampler, high-resolution seasonal metagenomics observations from the naturally Fe-fertilized region off Kerguelen Island are presented. The results show pronounced, but distinct seasonal patterns in the abundance of genes implicated in the transport of different forms of Fe and organic substrates, of siderophore biosynthesis and carbohydrate active enzymes. The seasonal dynamics suggest a temporal decoupling in the prokaryotic requirements of Fe and organic carbon during the spring phytoplankton bloom and a concerted access to these resources after the summer bloom. Taxonomic assignments revealed differences in the prokaryotic groups harboring genes of a given Fe-related category and pronounced seasonal successions were observed. The ecological strategies provide insights on how Fe could shape microbial community composition, with potential implications for organic matter transformations in the Southern Ocean.

The question of how the availability of trace metals selects for prokaryotic taxa and the potential feedbacks of microbial processes on the trace metal distribution in the ocean is addressed in Chapter 2. The potential reciprocal links between diverse prokaryotic taxa and Fe, Mn, Cu, Ni as well as apparent oxygen utilization (AOU) across 12 well-defined water masses in the Southern Indian Ocean (SWINGS- South West Indian Ocean GEOTRACES GS02 Section cruise) was investigated. Partial Least Square Regression (PLSR) analysis reveals that the water masses are associated with particular latent vectors that are a combination of the spatial distribution of prokaryotic taxa, trace elements and AOU. This

approach provides novel insights on the potential interactions between prokaryotic taxa and trace metals in relation to organic matter remineralization in distinct water masses of the ocean.

In Chapter 3, genes related to trace-metal transport by the prokaryotic communities inhabiting the distinct water masses sampled during the SWINGS cruise were investigated. These results cover 42 samples collected from surface to depth at 13 stations in the Subtropical, Subantarctic, Polar Frontal and Antarctic zones. The abundance of genes associated with the transport of Fe, Mn, Ni and Cu in the free-living (<0.8 μm) and particle-attached fractions (>0.8 μm) were determined both at the community level as well as in metagenome assembled genomes (MAGs). The results reveal differences in the normalized abundance of these genes (GPM) depending on geographic location in surface waters, and among water masses at depth. These latter were particularly pronounced for transporters of siderophores, Mn, Ni and Cu. Each water mass contained a distinct set of abundant MAGs and these were found to differ in their repertoires of trace metal transporters. These observations suggest that the trace metals considered here could play distinct roles in microbial metabolism in different water masses, with potential feedbacks on their cycling in the ocean.

Résumé

Les oligoéléments tels que le fer (Fe), le manganèse (Mn), le nickel (Ni) et le cuivre (Cu) jouent un rôle essentiel dans la croissance et le métabolisme des microorganismes procaryotes et eucaryotes phototrophes et non phototrophes dans l'océan, et influencent ainsi le cycle biogéochimique des principaux éléments. Alors que l'impact de la limitation en Fe sur les microorganismes phototrophes (phytoplancton) a été largement étudié, les liens entre les micronutriments et les procaryotes hétérotrophes restent jusqu'à présent peu explorés. Cette thèse étudie le potentiel métabolique des microbes marins taxonomiquement diversifiés pour acquérir des métaux traces en utilisant une approche métagénomique et donne ainsi un aperçu de la contribution des taxons procaryotes au cycle des éléments nutriments et majeurs à des échelles temporelles et spatiales dans l'Océan Austral.

L'objectif du chapitre 1 est d'étudier la stratégie des procaryotes pour acquérir différentes formes chimiques de Fe au cours de la saison. Sur la base d'échantillons obtenus par un échantillonneur autonome à distance, des observations métagénomiques saisonnières à haute résolution dans la région naturellement fertilisée en Fe au large des îles Kerguelen sont présentées. Les résultats montrent des schémas saisonniers prononcés mais distincts dans l'abondance des gènes impliqués dans le transport de différentes formes de Fe et de substrats organiques, dans la biosynthèse des sidérophores et dans les enzymes impliqués dans la dégradation des sucres. La dynamique saisonnière suggère un découplage temporel des besoins des procaryotes en Fe et en carbone organique pendant l'efflorescence printanière du phytoplancton et un accès concerté à ces ressources en fin d'été. Les assignations taxonomiques ont révélé des différences dans les groupes de procaryotes hébergeant des gènes d'une catégorie donnée liée au Fe et des successions saisonnières prononcées ont été observées. Les stratégies écologiques donnent un aperçu de la manière dont le Fe pourrait façonner la composition de la communauté microbienne, avec des implications potentielles sur la transformation de la matière organique dans l'océan Austral.

La question de savoir comment la disponibilité des métaux traces sélectionne les taxons procaryotes et les rétroactions potentielles des processus microbiens sur la distribution des métaux traces dans l'océan est abordée dans le chapitre 2. Les liens réciproques potentiels entre divers taxons procaryotes et Fe, Mn, Cu, Ni ainsi que l'utilisation apparente de l'oxygène (AOU) dans 12 masses d'eau bien définies du sud de l'océan Indien (SWINGS - South West Indian Ocean GEOTRACES GS02 Section cruise) ont été étudiés. L'analyse

‘Partial Least Square Regression’ (PLSR) révèle que les masses d'eau sont associées à des vecteurs latents particuliers qui sont une combinaison de la distribution spatiale des taxons procaryotes, des éléments traces et de l'AOU. Cette approche fournit de nouvelles informations sur les interactions potentielles entre les taxons procaryotes et les métaux traces en relation avec la reminéralisation de la matière organique dans des masses d'eau distinctes de l'océan.

Dans le chapitre 3, les gènes liés au transport des métaux-traces par les communautés procaryotes habitant les différentes masses d'eau échantillonnées au cours de la campagne SWINGS ont été étudiés. Ces résultats s'appuient 42 échantillons prélevés de la surface jusqu au fond à 13 stations dans la zone subtropicale, subantarctique, frontale polaire et antarctique. L'abondance des gènes associés au transport du Fe, du Mn, du Ni et du Cu dans les fractions libres (<0,8 µm) et attachées aux particules (>0,8 µm) a été déterminée à la fois au niveau de la communauté et dans les ‘metagenome assembled genomes’ (MAG). Les résultats révèlent des différences dans l'abondance normalisée (GPM) en fonction de la localisation géographique dans les eaux de surface et entre les masses d'eau en profondeur. Ces dernières étaient particulièrement prononcées pour les transporteurs de sidérophores, Mn, Ni et Cu. Chaque masse d'eau contenait un ensemble distinct de MAG abondants et ceux-ci se sont révélés différents dans leurs répertoires de transporteurs de métaux traces. Ces observations suggèrent que les métaux traces étudiés ici pourraient jouer des rôles distincts dans le métabolisme microbien dans différentes masses d'eau, avec des rétroactions potentielles sur leur cycle dans l'océan.

Table of Contents

Introduction

1. Physical and biogeochemical characteristics of the Southern Ocean

The Southern Ocean is an oceanographically unique and important region, located in the Southern Hemisphere, comprising 20% of the world's ocean (Fig. 1A). The Southern Ocean, lies south of subtropical fronts (~40°S) to the Antarctic continent (Carter *et al.*, 2008; Chapman *et al.*, 2020), encompassing the interconnected southern portions of the Pacific, Atlantic, and Indian Oceans, and represents the most efficient oceanic carbon sink on the planet (DeVries, 2014; DeVries *et al.*, 2017), while exerting a profound influence on the planet's climate system (Henley *et al.*, 2020; Morley *et al.*, 2020). Compared with other oceans, the Southern Ocean is most notably characterized by the presence of the strongest ocean current on Earth: the Antarctic Circumpolar Current (ACC) (Chapman *et al.*, 2020). The ACC separates the Antarctic from subtropical waters of the other three oceans in terms of ecological and hydrological environments, and divides the Southern Ocean into three zones, with the Subantarctic Zone (SAZ) between the Subantarctic Front (SAF) and the Subtropical Front (STF), the Polar Front Zone (PFZ) between the Polar Front (PF) and the Subantarctic Front (SAF), and the Antarctic Zone (AAZ) to the south of the Polar Front (PF) (Fig. 1B) (Orsi *et al.*, 1995; Carter *et al.*, 2008; Sokolov and Rintoul, 2009). In summary, the Southern Ocean emerges as an important nexus within marine systems, characterized by its unique geographic positioning, profound influence on global climate patterns, and the remarkable characteristics of the Antarctic Circumpolar Current, delineating distinct ecological realms within its expansive domain.

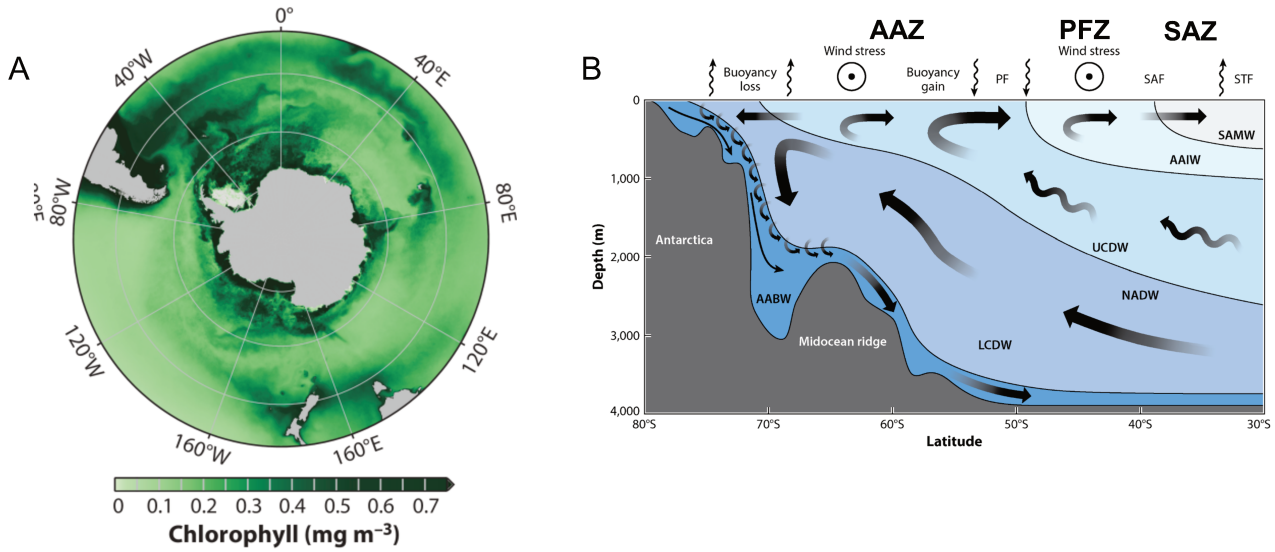

Fig.1 A. Mean 2003–2022 surface chlorophyll concentration in the Southern Ocean computed from the Moderate Resolution Imaging Spectroradiometer (Gray, 2024). B. Schematic view of the Southern Ocean meridional overturning circulation, the locations of ocean fronts and water masses, and atmospheric forcing and fluxes. Abbreviations: AABW, Antarctic Bottom Water; AAIW, Antarctic Intermediate Water; AAZ, Antarctic Zone; LCDW, Lower Circumpolar Deep Water; NADW, North Atlantic Deep Water; PF, polar front; PFZ, Polar Front Zone; SAF, subantarctic front; SAZ, Subantarctic Zone; SAMW, Subantarctic Mode Water; STF, subtropical front; UCDW, Upper Circumpolar Deep Water. Modified from Gent (Gent, 2016).

The oceans consist of a large number of water masses that have no clear boundaries, and water masses are defined as bodies of water with similar physical and chemical properties (such as temperature, salinity and density) and a common history of formation (Castro *et al.*, 1998; Poole and Tomczak, 1999). These physicochemical characteristics are largely influenced by factors such as ocean currents, atmospheric circulation and geographic location. Water masses play a crucial role in ocean circulation and exert significant influence on global climate dynamics, modulating the distribution of heat and the transport of nutrients (Morrison *et al.*, 2015).

The water masses of the Southern Ocean have been relatively well studied and include Subantarctic Mode Waters (SAMW), Antarctic Intermediate Water (AAIW), Upper Circumpolar Deep Water (UCDW), North Atlantic Deep Water (NADW), lower Circumpolar Deep Water (LCDW) and Antarctic Bottom Water (AABW) (Fig. 1B). SAMW is a vertically mixed layer that forms on the equatorial side of the Antarctic Circumpolar Current (ACC), mainly as a result of wintertime surface ocean heat loss and northward cross-frontal fluxes of cool, low-salinity surface water (Rintoul and England, 2002). The AAIW is located below the

SAMW and is one of the major water masses formed around the SAF of the ACC in the Southern Ocean (Talley, 1996, 2003). Circumpolar Deep Water (CDW), located within the ACC, represents the most widely distributed and largest water mass in the Southern Ocean, and is characterized by higher temperature, salinity and nutrients concentrations. CDW exhibits lower concentrations of dissolved oxygen compared to surface waters (Alonso-Sáez *et al.*, 2011), and can be further divided into UCDW and LCDW based on temperature and salinity maximum value, with LCDW typically characterized by higher salinities (34.70-34.75 psu) (Whitworth and Nowlin, 1987). In the Southern Ocean, NADW is transformed to LCDW through upwelling and mixing with other water masses (Park *et al.*, 1993). AABW is defined by seawater with temperature below 2°C, and the upper part of it is LCDW (Sprintall *et al.*, 2013). AABW originates from the Antarctic continental shelf and is a mixture of very cold, salty seawater resulting from the sinking of the ACC (Zhou *et al.*, 2023), and is the largest water mass in the world (Johnson, 2008). The sinking AABW also carries nutrients that are not utilized by marine organisms due to light and Fe limitation, and thus affects the efficiency of the global primary production and the biological carbon pump, which plays a major role in the climate system (Marinov *et al.*, 2006; Marzocchi and Jansen, 2019).

In the present thesis, the following water masses are also considered: Winter Water (WW), Arabian Sea Low Oxygen Water (ASLOW), Subtropical Mode Water (STMW) and South Indian Central Water (SICW). WW is a characteristic of the upper layer in the Southern Ocean during the summer, with very low temperatures (< 2 °C) and increasing salinity with depth (Sabu *et al.*, 2020). The Arabian Sea is one of the oxygen minimum zones (OMZ) in the world's oceans, with an O_2 concentration of <0.5 ml L^{-1} (Singh *et al.*, 2023). STMW is formed mainly by subduction, it is a prominent feature of the upper layer in the western part of the subtropical circulation of the world's oceans (Tsubouchi *et al.*, 2010), and in the Indian Ocean it is characterized by a thermostat covering below the summer thermocline (Tsubouchi *et al.*, 2010). The SICW is formed by subduction of the South Indian Ocean and the temperatures of this water mass range between 9-25°C and have a high salinity (35.2-36 psu) (Purba *et al.*, 2023).

The high-nutrient low-chlorophyll (HNLC) region refers to an ocean area where the concentration of major nutrients such as nitrate and phosphate is high but phytoplankton biomass remains relatively low and constant (Martin and Fitzwater, 1988; Basterretxea *et al.*, 2023). The biomes in the HNLC region cover about 20-30 % of the ocean zone, and the HNLC regions are composed of three main ocean zones: the subarctic North Pacific, the

equatorial Eastern Pacific, and the Southern Ocean (Fig. 2) (Coale *et al.*, 1996; Parekh *et al.*, 2005; Venables and Moore, 2010). Notably, the Southern Ocean emerges as the largest HNLC region in the world, owing to constraints imposed by limited iron (Fe) availability and light penetration, both crucial for primary productivity in marine ecosystems (Boyd, 2002). Mean concentrations of Chlorophyll a are less than 0.3-0.4 μg L^{-1} in most of the Southern Ocean, but can exceeded 1.0 μg L^{-1} during phytoplankton blooms and in coastal and shelf waters (Moore and Abbott, 2000). Phytoplankton blooms in the Southern Ocean are usually dominated by diatoms and are recurrent phenomena observed in various sectors of the Southern Ocean (Quéguiner, 2013; Malviya *et al.*, 2016; Liu *et al.*, 2019).

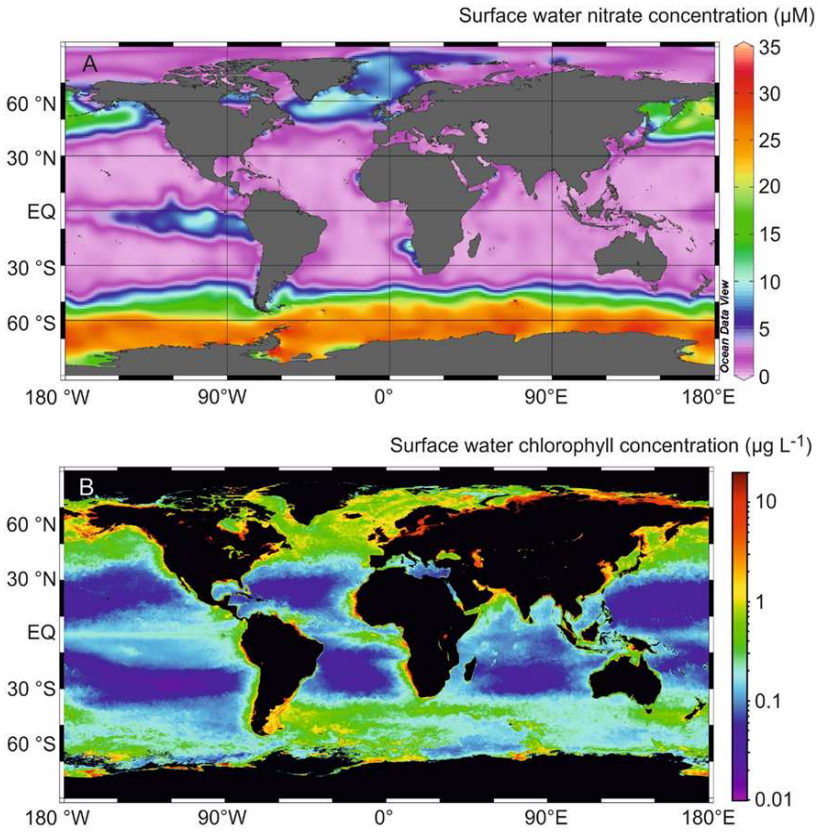

Fig. 2 A. Average nitrate (μM) in 2009. B. Composite chlorophyll a (mg L^{-1}) distributions observed in surface waters in the global ocean in 2009. (Gledhill, 2012)

Fe is an important element required by all organisms. For phytoplankton, Fe is essential for many processes, including biomass production, reduction of nitrate to a usable form, and fixation of atmospheric nitrogen (Schoffman *et al.*, 2016). Although Fe is abundant in the earth's crust, the concentration of available Fe in seawater remains relatively low. Limited dust inputs and the poor solubility of Fe contribute to the low concentrations of Fe (60–200 pmol L^{-1}) in the Southern Ocean compared to other open ocean areas (Jickells *et al.*, 2005; Ellwood *et al.*, 2020). Fe is primarily supplied through upwelling and upward mixing

of deeper, Fe-enriched waters (Boyd and Ellwood, 2010; Tagliabue *et al*., 2014). In the early 90s, John Martin developed the 'iron hypothesis', in which he hypothesized that Fe fertilization in an HNLC region, whether occurring naturally or induced artificially, would stimulate phytoplankton blooms that could sequester atmospheric carbon dioxide, effectively mitigating its concentration, and facilitate its storage through sinking into the deep ocean and sediments (Martin, 1990). The contribution of Fe to primary productivity has been demonstrated through several mesoscale artificial Fe fertilization studies in the Southern Ocean, as well as through research in naturally Fe fertilized areas (Gervais *et al.*, 2002; Blain *et al.*, 2007; Boyd *et al.*, 2007; Yoon *et al.*, 2018).

The Kerguelen Plateau, located in the Indian sector of the Southern Ocean, extends southeast of the Kerguelen islands and has an overall depth of < 700m (Park et al., 2008) (Fig. 3). The interaction of circulation and shallow topography facilitates the transport of Fe from mix layer to the surface waters of the Kerguelen Plateau. This natural Fe-fertilization contributes to the consecutive spring and summer phytoplankton blooms (Blain *et al.*, 2007). Notably, Station A3 is a shallow station (540 m) located on the central Kerguelen Plateau, south of the polar front of the Permanent Open Ocean Zone (POOZ). The unique environmental dynamics surrounding Kerguelen Island offer valuable insights into the impact of natural Fe fertilization on biogeochemical processes in the Southern Ocean and have been intensively studied throughout the past decade (see Special Issues in Deep Sea Research II (2011) dedicated to KEOPS1, Biogeosciences (2015) dedicated to KEOPS2 et Journal of Marine Systems (2021) dedicated to MOBYDICK cruises).

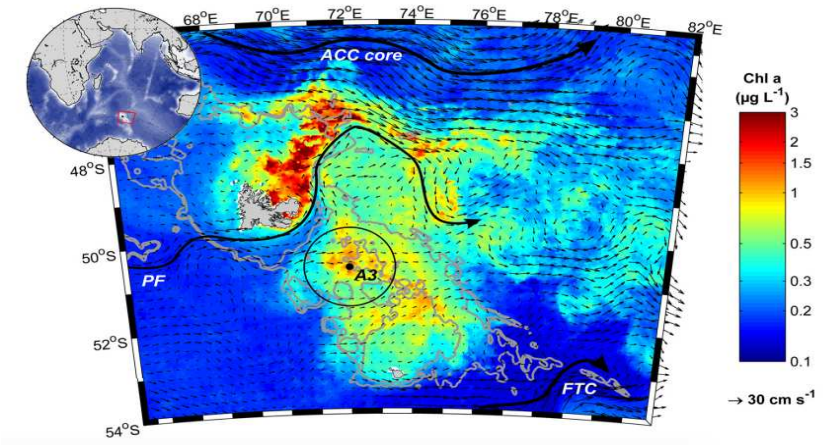

Fig. 3 Localization of the Kerguelen Plateau in the Indian sector of the Southern Ocean and detailed map of the satellite-derived surface Chlorophyll a concentration averaged. Positions of the Antarctic Circumpolar Current core (AAC core), the polar front (PF) and the Fawn Trough Current (FTC) are shown by thick black arrows. (Rembauville *et al.*, 2015)

2. Marine organic matter

Carbon, as a basic element of life, serves as the primary carrier of material and energy cycles within the biosphere (Tanhua *et al.*, 2013). The ocean, the largest carbon pools on Earth's surface, playing an important role in regulating atmospheric CO_2 levels through the process of air-sea exchange (DeVries, 2022). Marine dissolved organic matter (DOM) constitutes one of the most important carbon pools in the ocean (Hansell *et al.*, 2009).

Marine dissolved organic carbon (DOC) exhibits higher concentrations in nearshore and shelf areas as compared to the open ocean (Hansell and Orellana, 2021). This spatial distribution can be attributed to a combination of factors, including the influx of terrestrial organic matter in nearshore areas and a large amount of nutrient input from river systems (Sanchez-Vidal *et al.*, 2013). These nutrient-rich conditions promote phytoplankton growth, consequently elevating the DOC concentrations. The concentration of DOC in surface seawater is higher than that of DOC in deep seawater (Hansell and Orellana, 2021). This is due to the production of DOC occurring predominantly through autotrophic processes in sunlit surface waters. The intricate interplay between various biogeochemical processes within the ocean underscores the pivotal role of DOM in the carbon cycle, influencing global carbon dynamics.

DOM originates from a variety of internal and external sources. Internal sources are primarily associated with biological activities, such as phytoplankton blooms, virus-induced cell lysis, and the transformation of particulate matter, while external sources include inputs from rivers, the atmosphere, and marine sediments (Hedges, 1992). DOM in the ocean can be divided into two distinct fractions. The first category, primarily found in the upper layers of the ocean, comprises freshly produced DOM by phytoplankton. This fraction mainly consists of polysaccharides, proteins, lipids, and other organic compounds. Within this fraction, there are two subcategories: semi-labile dissolved organic carbon (SLDOC) and labile dissolved organic carbon (LDOC) (Hansell and Orellana, 2021). The second category is known as refractory dissolved organic carbon (RDOC), characterized by significantly older radiocarbon ages, an unknown molecular composition, with considerable resistance to biodegradation (Jiao *et al.*, 2014; Hansell and Orellana, 2021).

Marine prokaryotes play an important role in the ocean, contributing significantly to the carbon cycle through the biological pump. The biological pump involves the conversion of inorganic carbon to organic carbon by primary producers in surface seawater through

photosynthesis, and subsequently, the transport of this organic carbon to the deep ocean in the form of particulate organic matter (POM) or DOM via pathways such as sinking (Eppley and Peterson, 1979; Ducklow *et al.*, 2001; Jiao *et al.*, 2010). Heterotrophic prokaryotes utilize this organic matter as a source of carbon and energy for growth. These processes either store carbon in the ocean or recycles it back to the surface through cycling, thereby regulating the carbon balance of marine ecosystems (Fig. 4) (Eppley and Peterson, 1979; Wassmann, 1997; Ducklow *et al.*, 2001; Gehlen *et al.*, 2006; Herndl and Reinthaler, 2013).

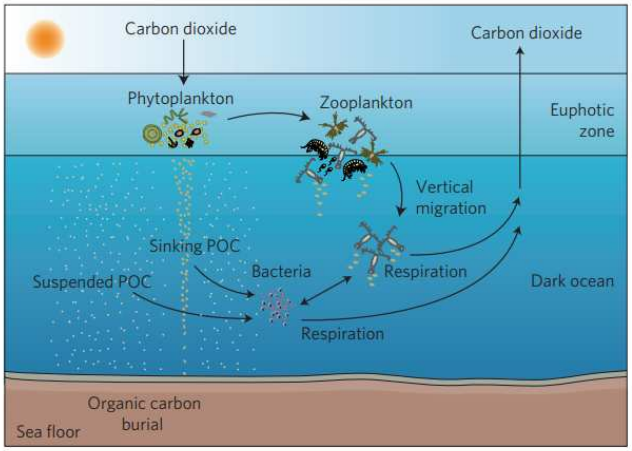

Fig. 4 The biological pump. Phytoplankton in the euphotic zone fix carbon dioxide using solar energy. The particulate organic carbon (POC) produced is grazed on by herbivorous zooplankton, or consumed directly or indirectly by heterotrophic microbes feeding on solubilized remains of phytoplankton. Between 1 and 40% of the primary production is exported out of the euphotic zone, and it exponentially attenuates towards the base of the mesopelagic zone at around 1,000 m depth. Remineralization of organic matter in the oceanic water column converts the organic carbon back to carbon dioxide. Only about 1% of the surface production reaches the sea floor. (Herndl and Reinthaler, 2013)

In addition, Jiao et al. proposed the concept of the Microbial Carbon Pump (MCP) (Jiao *et al.*, 2010), which stated that heterotrophic prokaryotes not only utilize DOC but also contribute to its production, with a portion of it being RDOC (Ogawa *et al.*, 2001). The MCP refers to microbial processes that transform actively labile DOC into inert RDOC (Jiao *et al.*, 2010). It was suggested that the MCP serves as a carbon storage mechanism independent of sinking. Furthermore, it not only stores carbon but also releases nitrogen and phosphorus, thus playing a crucial role in maintaining the sustainability of ocean productivity (Jiao *et al.*, 2010).

3. Trace metals in the ocean

Iron (Fe), manganese (Mn), copper (Cu) and nickel (Ni) are essential micronutrient for marine organisms. They enters the oceans from various sources, including the atmosphere, rivers, hydrothermal vents, and different types of sediments (such as shelf, margin, and bottom sediments) (Little *et al.*, 2014; Richon and Tagliabue, 2019; Tebo and Luther, 2019).

3.1 Iron in the ocean

Iron is now well known that low Fe availability affects phytoplankton primary productivity, community structure, and ecological function, and that it plays a very important role in global ecology and biogeochemistry (Schoffman *et al.*, 2016; Tagliabue *et al.*, 2017; Marchetti, 2019).

Iron in seawater is present as dissolved Fe (dFe; < 0.2 μm or 0.45 μm) and particulate Fe. A fraction of dFe is present in colloidal form (> 0.02 μm), and the remaining fraction is considered truly soluble Fe. The dFe includes inorganic Fe and organic Fe complexed with small organic ligands. (Fig. 5). Inorganic Fe is mainly in the form of ferrous Fe (Fe^{2+}) and ferric Fe (Fe^{3+}), and ferrous Fe is very unstable in the oxygenated environment, and easily oxidized to ferric Fe (Norman *et al.*, 2014). In the ocean usually more than 99.9% of dissolved Fe (dFe) is complexed with ligands, which is the main form of dFe in seawater, and these small organic ligands include siderophores, porphyrins, and domoic acid (Gledhill, 2012). Among them, porphyrins include chlorophylls and chlorophyll breakdown products such as phaeophytin, heme, and vitamin B12, whereas siderophores are organic ligands produced by prokaryotes that bind most dFe in the ocean. There are various types of siderophores in the ocean such as amphiphilic siderophores, photoreactive ferric siderophores, amonabactin, vibrioferrin, and its distribution may be related to prokaryotic abundance as well as prokaryotic productivity (Boyd and Ellwood, 2010; Gledhill, 2012; Chen *et al.*, 2019). The size of colloidal Fe ranges from 1 nm to 0.45 μm, and colloidal Fe is formed by a variety of mechanisms, including the formation of inorganic Fe in combination with large organic ligands or humic substances, and the formation of complexes of organic Fe in conjunction with colloids (Norman *et al.*, 2014). Particulate Fe, for which the size is larger than 0.45 μm, cannot be directly utilized by organisms, but under certain conditions, algae and prokaryotes can release solubilizing substances such as bio enzymes and thereby convert the particulate Fe into available dFe (Naito *et al.*, 2005; Norman *et al.*, 2014).

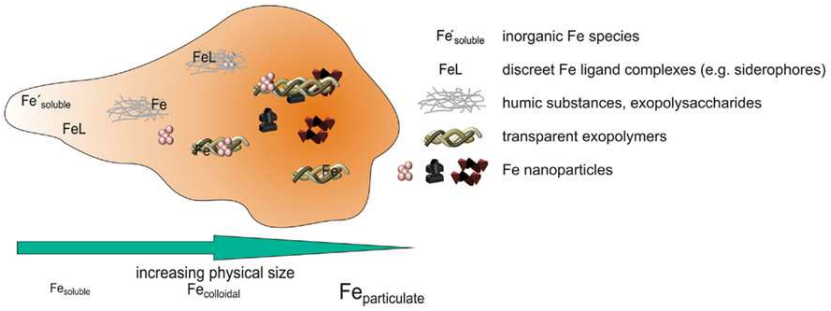

Fig. 5 The forms of iron in seawater. (Gledhill, 2012)

Fe plays a crucial role in heterotrophic prokaryotes, as it is as a cofactor in respiration and its availability also affects the utilization of organic carbon by prokaryotes (Fourquez *et al.*, 2014; Bradley *et al.*, 2020; Sun *et al.*, 2021). Moreover, it's an essential element for various biological processes such as amino acid synthesis, oxidation, and nitrogen fixation (Tandara and Salamunic, 2012; Ilbert and Bonnefoy, 2013); however, the concentration of Fe remains relatively low in the ocean, and therefore, prokaryotes have evolved diverse strategies to take up this element. For example, prokaryotes can acquire ferrous Fe through the Feo protein, ferric Fe through the Fbp protein, and the uptake ferric Fe can be mediated by siderophores, heme, transferrin and lactoferrin (Sandy and Butler, 2009). These mechanisms highlight the adaptive nature of prokaryotes in acquiring Fe, ensuring their survival and proliferation in the ocean.

3.2 Manganese in the ocean

Mn is the third most abundant transition metal in the Earth's crust, following Fe and titanium. Moreover, it ranks as the second most important redox-active metal present in the environment. Notably, the concentration of Mn is 60% greater in the ocean than in the continental crust (Hansel, 2019). Mn exists in various oxidation states in the ocean, primarily encompassing Mn (II), Mn (III), and Mn (IV). Mn that passes through the 0.2 μm filter is considered to be soluble Mn (Graham *et al.*, 1976). Among these soluble forms, Mn (II) is the dominant species in surface seawater. Mn (III) can be both particulate and dissolved when bound to organic complexes, and Mn (IV) exists in a particulate state (Hansel, 2017). Mn can be converted among the three forms by reduction, oxidation and disproportionation reactions (Hansel, 2019), thereby playing a dynamic role in ocean biogeochemistry.

The concentration of dissolved Mn is high in surface seawater, but decreases with depth, mainly due to a combination of photoreduction and sources in the upper ocean (Van Hulten *et al.*, 2017). Notably, dissolved Mn (dMn) concentrations remain relatively constant

throughout much of the deep ocean, typically ranging between approximately 0.10 nM and 0.15 nM (Van Hulten *et al.*, 2017).

Mn holds significant importance for phytoplankton, as all photosynthetic organisms require Mn for water-splitting reactions in oxygenic photosynthesis. Several studies have highlighted not only Fe limitation, but also Mn limitation in the Southern Ocean (Pausch *et al.*, 2019; Browning *et al.*, 2021; Hawco *et al.*, 2022; Anugerahanti and Tagliabue, 2023; Latour *et al.*, 2023). Mn is also extremely important for prokaryotes. Mn is a cofactor for enzymes participating in antioxidant processes (Hansel, 2017). Additionally, Mn(II) serves as a cofactor for enzymes involved in nucleotide metabolism, central carbon metabolism, translation, and signal transduction processes (Hansel, 2017). Moreover, when bound to nucleic acids, proteins, and metabolites within the cell, it also plays roles beyond catalytic functions (Bosma *et al.*, 2021). In many bacilli, Mn (II) is crucial for processes like spore formation and peptide antibiotic production (Bosma *et al.*, 2021). A variety of Mn-oxidizing prokaryotes have been isolated and identified in the ocean. They can impact biological processes such as photosynthesis, carbon fixation, and scavenging of reactive oxygen species, they play an important role in the biogeochemical cycling of various nutrients and trace metals (Hansel, 2017).

Bosma *et al*. proposed that prokaryotes can be divided into three distinct groups based on their preference and utilization of Fe^{2+} or Mn^{2+}: prokaryotes exhibiting an Fe-centered metabolism, those with a Mn-centered metabolism, and those with metabolism centered on neither Fe nor Mn (Bosma *et al.*, 2021). Prokaryotes contain a variety of transporters to uptake Mn, among which MntH is a type of transporter belonging to the NRAMP family, which is an important Mn (II) transporter in prokaryotes, and the ABC (ATP-binding cassette) transporter type MntABC, and a potential third type of importer MntA. There are also a variety of Mn exporters, such as Mn efflux pump (MntP) (Fig. 6) (Bosma *et al.*, 2021).

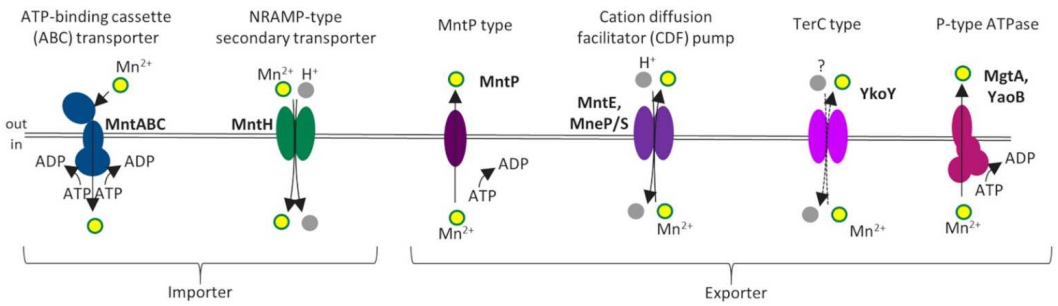

Fig. 6 Manganese transporters in prokaryotes divided into importers and exporters. (Bosma *et al.*, 2021)

3.3 Copper in the ocean

Cu is widely distributed in the environment and holds significant importance in marine biogeochemical research. Within the ocean, Cu exists in diverse forms, primarily represented by Cu(I) and Cu(II) ions, and can be found in dissolved, complexed, and particulate states (Ruacho *et al.*, 2022). In seawater, the predominant form of inorganic Cu is Cu(II) oxidation state, with over 99% of dissolved Cu complexed with organic ligands such as humic-like substances, extracellular polysaccharides, thiols, and other low molecular weight microbial-produced compounds (Ruacho *et al.*, 2022).

The distribution of dissolved Cu in the ocean follows a vertical profile similar to that of nutrients. It tends to be consumed or removed in surface seawater, resulting in higher concentrations at deeper depths, likely due to the remineralization of particulate Cu (Roshan and Wu, 2015; Cui and Gnanadesikan, 2022). The concentrations of dissolved Cu in surface seawater generally range from 0.5 to 5 nmol L^{-1}, with open ocean surface seawater typically exhibiting concentrations below 1 nmol L^{-1} (Bruland and Lohan, 2003; Roshan and Wu, 2015). Previous studies have revealed that the vertical concentration range of dissolved Cu in the Indian Ocean ranges from 1 to 5.49 nmol L^{-1}, while in the Southern Ocean, it ranges from 1.01 to 3.05 nmol L^{-1} (Schlitzer *et al.*, 2018).

Cu, as a trace metal element, plays a crucial role as a cofactor for diverse biological enzymes. These enzymes, including plastocyanin, cytochrome c oxidase, nitrite reductase, azurin, and amine oxidase, rely on Cu for their proper functioning. It is involved in various vital biological processes, including electron transfer, oxidative respiration, denitrification, nitrite reduction, and more. Moreover, in specific cases, Cu can act as a structural component, further highlighting its versatility and significance within biological systems (Argüello *et al.*, 2013). Cu deficiency has been observed to impact the growth and metabolism of some prokaryotes. For instance, Posacka *et al*. noted that Cu deficiency can influence the growth and carbon metabolism of *Flavobacteriia* member *Dokdonia* sp. strain Dokd-P16 (Posacka *et al.*, 2019). However, when Cu accumulates in the cell, it generates harmful reactive oxygen species and interferes with protein functionality by displacing other metal cofactors from crucial sites, rendering it cytotoxic (Gaetke, 2003; Macomber and Imlay, 2009). Furthermore, Cu also affects phytoplankton growth, as well as its capacity to bind with organic ligands. These roles position Cu as a significant contributor to the dynamics of the global carbon and nitrogen cycles.

Due to the dual nature of Cu's bioavailability and toxicity, the cell regulates Cu homeostasis through multiple mechanisms crucial for its effective utilization within the cell and to limit potential toxicity. In eukaryotes, Cu uptake primarily relies on members of the Ctr (Cu transporter) family of transporter proteins (Öhrvik and Thiele, 2015). However, such transporter proteins are not present in prokaryotes. Prokaryotes utilize a variety of mechanisms for Cu uptake, including porins, TonB-dependent importer (e.g., NosA/OprC), and uptake facilitated by chalkophores such as Methanobactin (Mbn) (Andrei *et al.*, 2020). These chalkophores serve as Cu-specific metal carriers. Additionally, prokaryotes employ CopZ, a chaperone protein involved in intracellular Cu transport (Argüello *et al.*, 2013). Prokaryotes employ various mechanisms such as the Cu P-type ATPase CopA, the Cus system, and several other proteins to export Cu, thereby ensuring the maintenance of cellular homeostasis (Fig. 7) (Andrei *et al.*, 2020).

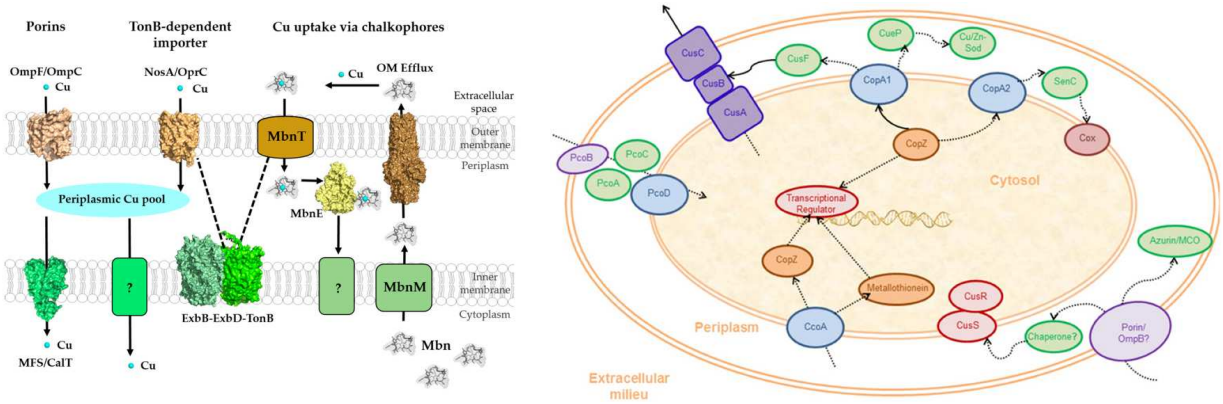

Fig. 7 General view of Cu transporter in prokaryotes. (Argüello *et al.*, 2013; Andrei *et al.*, 2020)

3.4 Nickel in the ocean

Ni is indispensable for a variety of enzymes that play key roles in biological processes. These encompass crucial functions such as nitrogen fixation, nitrogen uptake, carbon fixation, hydrogen metabolism, methane biogenesis, and acid production (Gikas, 2008; John *et al.*, 2022). The sources of Ni in the ocean are diverse, including contributions from rivers and continental shelves. In the ocean, Ni concentrations exhibit a nutrient-like vertical pattern with decrease from the surface to depth, likely attributable to the utilization of dissolved Ni for phytoplankton growth in the surface, followed by Ni sinking and remineralization

processes, ultimately leading to enrichment with depth (Middag *et al.*, 2020; John *et al.*, 2022).

For marine microbes, the most commonly used Ni-dependent proteins are urease and Ni-containing superoxide dismutase (NiSOD). Previous studies have shown Ni plays an important role in phytoplankton metabolic processes, consequently influencing marine primary productivity. Urea is an important source of nitrogen, supporting 5%-50% of marine primary production (Wafar *et al.*, 1995). Studies by Dupont *et al*. have demonstrated that cyanobacteria possess the capability to hydrolyze and utilize urea via the Ni-containing enzyme urease (Dupont *et al.*, 2010). Furthermore, Ni functions as a cofactor for superoxide dismutase (SOD), which is essential for catalyzing the decomposition of toxic superoxide radicals generated during photosynthesis. Some prokaryotes (like *Cyanobacterium Oscillatoria* sp.) exhibit an absolute metabolic dependence on Ni, further underscoring its indispensability within marine ecosystems (Gikas, 2008).

Currently, prokaryotes have multiple mechanisms for Ni uptake. The most well studied ABC-type Ni transporter is the NikABCDE system (Zeer-Wanklyn and Zamble, 2017). Another ATP-dependent input system, Nik/CbiMNQO, has also been identified, which plays a role in the uptake of both Ni and cobalt (Rodionov *et al.*, 2006). The regulation of Ni-dependent processes is primarily controlled by the Ni-dependent regulatory protein NikR, which governs the expression of genes encoding the NikABCDE and NikMNQO systems, as well as other enzymes dependent on Ni (Dosanjh and Michel, 2006). Additionally, secondary Ni/Co transporters such as NiCoT, UreH, and HupE/UreJ have been discovered to contribute to the Ni transport process in prokaryotes (Fig. 8) (Eitinger *et al.*, 2005; Macomber and Hausinger, 2011; Higgins *et al.*, 2012).

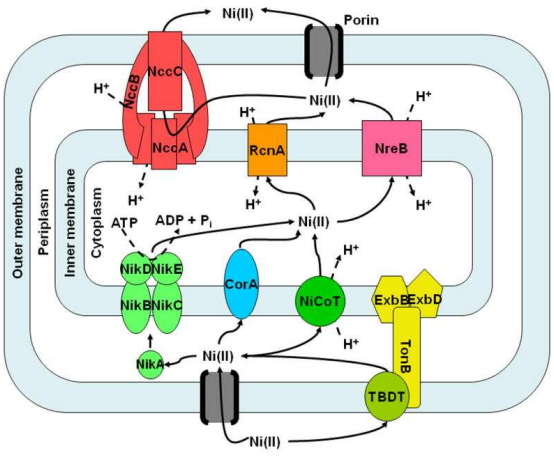

Fig. 8 A representation of selected nickel trafficking pathways in prokaryotes. (Macomber and Hausinger, 2011)

In environments where there is a high concentration of Ni, such as Ni-contaminated soils or water, prokaryotes face the risk of Ni toxicity. To cope with this challenge, prokaryotes have evolved various mechanisms to regulate the levels of Ni within their cells, ensuring intracellular Ni homeostasis and protecting themselves from metal overload (Macomber and Hausinger, 2011). One such mechanism involves the expression of specific genes and proteins that facilitate the efflux of Ni ions from the cell. Two well-known systems involved in Ni resistance are *cnrCBA* (cobalt and nickel resistant) and *nccCBA* (nickel-cobalt-cadmium resistant). These systems typically encode membrane proteins that act as efflux pumps, actively pumping Ni ions out of the cell cytoplasm and into the extracellular space or periplasmic region between the inner and outer membranes. Additionally, prokaryotes possess plasmid-encoded proteins that aid in Ni efflux, like NreB. Another important protein involved in Ni resistance is RcnA, which is capable of pumping both Ni and cobalt ions out of the cytoplasm, thereby reducing their intracellular concentrations and mitigating their toxic effects (Fig. 8). These various mechanisms collectively contribute to the ability of prokaryotes to survive and thrive in Ni-contaminated environments by maintaining Ni homeostasis and preventing metal overload.

4. Functional roles of microbial taxa: Insights via 'omics' approaches

Prokaryotes are key players in the ocean, playing indispensable roles in fundamental biogeochemical processes such as the carbon, nitrogen, sulfur and trace metals cycles (Falkowski *et al.*, 2008; Tagliabue *et al.*, 2017; Zhang *et al.*, 2019; Xu *et al.*, 2021). For a long time, prokaryotes have been studied primarily through culture-based methods. However, it has evolved as a main limiting factor for the exploitation and application of microbial resources that more than 99% of prokaryotes in natural environments cannot be cultivated so far by current isolation and culture methods (Torsvik and Øvreås, 2002). How to fully explore new resources of environmental microorganisms is one of the important subjects of environmental microbiology research at present.

The microbiome refers to the genes and genomes of bacteria, archaea, and eukaryotes, viruses and other microorganisms, and the surrounding environment (Marchesi and Ravel, 2015). In recent years, the development of next generation sequencing (NGS) technology has made it possible to study the microbiome based on non-culture methods, and has promoted the development of microbiome research (White *et al.*, 2016). The 16S rRNA gene is widely used to explore microbial diversity due to its presence in all prokaryotes and its structure, which includes both conserved regions that indicate species affinities and variable regions

that provide species-specific sequences. Furthermore, its utility is enhanced by well-established databases containing reference sequences for prokaryotes. 16S rRNA amplicon sequencing, which involves the amplification and sequencing of targeted regions within the 16S rRNA gene (Claesson *et al.*, 2010), is a representative method for microbial community studies, enabling comprehensive analysis of bacterial and archaeal communities within samples. The analysis workflow primarily involves the identification of operational taxonomic units (OTUs) or Amplicon Sequence Variants (ASVs) through tools like Usearch (Edgar, 2010) or DADA2 (Callahan *et al.*, 2016), followed by taxonomic classification. Subsequently, these data can be further explored through methods such as alpha-diversity (the diversity in a given habitat or ecosystem), beta-diversity (the diversity between samples or communities), or functional prediction. Metagenomes are the sum of the genetic material of all organisms from a given environment, usually unicellular, within a sample (Handelsman *et al.*, 1998). Metagenomics explores microbial genomes in environmental samples via functional gene screening and sequencing, bypassing the need for isolation. It can be used to explore microbial diversity, composition, evolutionary relationship, and functional activity, and environmental interactions. (Simon and Daniel, 2011).

A typical shotgun metagenomics study roughly comprises five steps (Fig. 9) (Quince *et al.*, 2017). Generally, a quantitative analysis of metagenomic species and functional composition can be performed based on reference databases, such as MetaPhlAn2 (Truong *et al.*, 2015) or Kraken2 (Wood and Salzberg, 2014) to achieve sequence species classification, HUMAnN2 (Franzosa *et al.*, 2018) to achieve quantitative functional annotation. However, due to the limited length of the sequence reads, it is hard to provide complete genomic information. Therefore, conducting metagenome de novo assembly and gene prediction helps to obtain more complete genomic information. Metagenomic assembly software includes MEGAHIT (Li *et al.*, 2015) and metaSPAdes (Nurk *et al.*, 2017), gene prediction software such as Prodigal (Hyatt *et al.*, 2010), Prokka (Seemann, 2014) and GeneMarkS-2 (Lomsadze *et al.*, 2018). For the combined analysis of multi-sample or multi-batch metagenome datasets, CD-HIT (Li and Godzik, 2006) is usually used to construct a non-redundancy gene catalogue, so that all samples can be quantified and compared based on a unified reference sequence. The obtained gene catalogue is compared against the function annotation databases, including NCBI NR database, KEGG, COG, TCDB, and Carbohydrate-Active enZYmes Database (Lombard *et al.*, 2014). After assembling the metagenomes, metagenome-assembled genomes (MAGs) can be assembled by binning, which refers to the process of grouping contigs

obtained after assembly separately based on species affiliation (Breitwieser *et al.*, 2019). In recent years, the rapid development of binning software has made it possible to obtain the genomes of non-cultivable microorganisms. Currently commonly used binning tools include MetaBAT 2 (Kang *et al.*, 2019), MaxBin 2 (Wu *et al.*, 2016) and CONCOCT (Alneberg *et al.*, 2014) or use the anvi'o platform (Eren *et al.*, 2015).

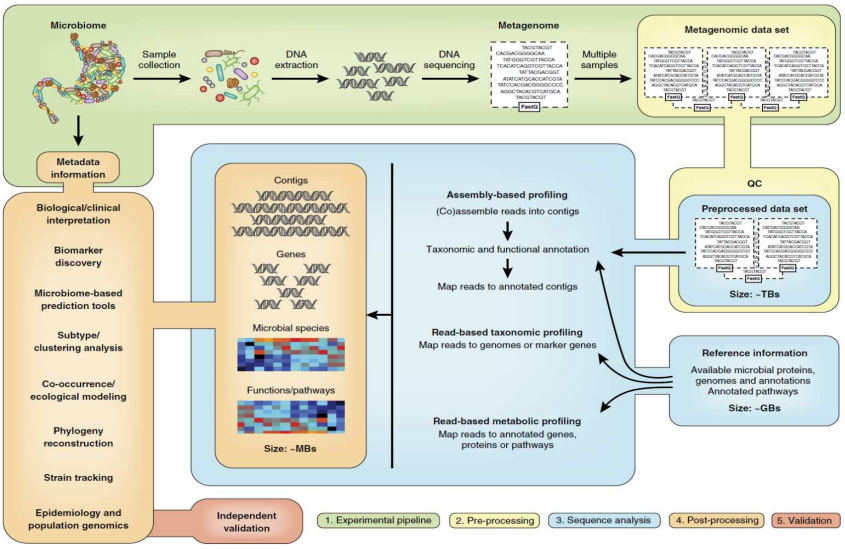

Fig. 9 Summary of a metagenomics pipeline. Step (1): study design and experimental protocol. Step (2): computational pre-processing, such as removal of sequencing adaptors, quality trimming, removal of sequencing duplicates. Step (3): sequence analysis, 'read-based' and 'assembly-based' approaches. Step (4): post-processing, various multivariate statistical techniques can be used to interpret the data. Step (5): validation. (Quince *et al.*, 2017)

Omics approaches have become indispensable tools in global ocean sequencing. The Global Ocean Sampling Expedition (GOS) led by J. Craig Venter has yielded millions of new genes and the genomes of nearly 1,000 uncultured microbial lineages, showcasing the vast genetic diversity hidden in oceans (Yooseph *et al.*, 2007; JCVI, 2022). The tara ocean project (https://www.ebi.ac.uk/services/tara-oceans-data), an initiative by European researchers, which have sampled at 210 sites around the world at depths of up to 1,000 m in the ocean, has led to the creation of a list of marine microbial genes, and the structure and function of the global ocean microbiome was described, contributing to the understanding of global marine microbial ecology (Pesant *et al.*, 2015; Sunagawa *et al.*, 2015, 2020). The unique and dynamic evolutionary patterns of different metals (copper, molybdenum, cobalt, nickel, and selenium) and metalloproteins utilization, as well as the biogeographic distribution of genes encoding trace metals-dependent proteins in diverse marine and non-marine organisms have been explored through metagenomic analyses (Zhang *et al.*, 2019; Xu *et al.*, 2021). A few number of studies have investigated the link between prokaryotic taxa and the forms of Fe

utilized (Hopkinson and Barbeau, 2012; Toulza *et al.*, 2012; Hogle *et al.*, 2016; Debeljak *et al.*, 2019; Sun *et al.*, 2021), and only two studies have extended this investigation to other trace metals (Hogle *et al.*, 2016, Kong *et al*, submitted).

There are still large gaps in our understanding of how trace metals affect microbial metabolism, in particular that of carbon, and the link between prokaryotic communities and trace metals on the temporal and spatial scales, particularly in the Southern Ocean. This thesis aims to address these questions by investigating the spatial and temporal dynamics of trace metal transporters by diverse microbial communities in the Southern Ocean. Notably, this study provides the first high-resolution seasonal metagenomic observations in the Southern Ocean and covers a broad range of water masses. By doing so, it helps us to gain deeper insights into the role of marine prokaryotes in biogeochemical cycles and their interactions with trace metals. Prokaryotes in the ocean include both free-living and particle-attached prokaryotes, each occupying distinct ecological niches within aquatic systems, and exhibit differences in community structure and metabolic functions, contributing uniquely to biogeochemical cycling. In this thesis, I investigated both free-living and particle-attached prokaryotes together.

Chapter 1 aims to better understand the linkages between organic carbon supply, microbial Fe uptake strategies and microbial diversity during an entire season in the naturally fertilized Southern Ocean.

Chapter 2 aims to investigate how the availability of trace metals in water masses affects prokaryotic taxa and the potential feedback of microbial processes on the distribution of trace metals in the ocean.

Chapter 3 aims to explore trace-metal related genes in prokaryotic communities inhabiting distinct water masses, as well as the strategies of trace metal transport by prokaryotes in different water masses.

Reference

Alneberg, J., Bjarnason, B.S., de Bruijn, I., Schirmer, M., Quick, J., Ijaz, U.Z., et al. (2014) Binning metagenomic contigs by coverage and composition. *Nat Methods* **11**: 1144–1146.

Alonso-Sáez, L., Andersson, A., Heinrich, F., and Bertilsson, S. (2011) High archaeal diversity in Antarctic circumpolar deep waters: Biogeography of Archaea in Antarctic waters. *Environmental Microbiology Reports* **3**: 689–697.

Andrei, A., Öztürk, Y., Khalfaoui-Hassani, B., Rauch, J., Marckmann, D., Trasnea, P.-I., et al. (2020) Cu Homeostasis in Bacteria: The Ins and Outs. *Membranes* **10**: 242.

Anugerahanti, P. and Tagliabue, A. (2023) Process controlling iron–manganese regulation of the Southern Ocean biological carbon pump. *Phil Trans R Soc A* **381**: 20220065.

Argüello, J.M., Raimunda, D., and Padilla-Benavides, T. (2013) Mechanisms of copper homeostasis in bacteria. *Front Cell Infect Microbiol* **3**: 73.

Basterretxea, G., Font-Muñoz, J.S., Hernández-Carrasco, I., and Sañudo-Wilhelmy, S.A. (2023) Global variability of high-nutrient low-chlorophyll regions using neural networks and wavelet coherence analysis. *Ocean Sci* **19**: 973–990.

Blain, S., Quéguiner, B., Armand, L., Belviso, S., Bombled, B., Bopp, L., et al. (2007) Effect of natural iron fertilization on carbon sequestration in the Southern Ocean. *Nature* **446**: 1070–1074.

Bosma, E.F., Rau, M.H., van Gijtenbeek, L.A., and Siedler, S. (2021) Regulation and distinct physiological roles of manganese in bacteria. *FEMS Microbiology Reviews* **45**: fuab028.

Bowie, A.R., Van Der Merwe, P., Quéroué, F., Trull, T., Fourquez, M., Planchon, F., et al. (2015) Iron budgets for three distinct biogeochemical sites around the Kerguelen Archipelago (Southern Ocean) during the natural fertilisation study, KEOPS-2. *Biogeosciences* **12**: 4421–4445.

Boyd, P.W. (2002) Environmental factors controlling phytoplankton processes in the Southern Ocean. *J Phycol* **38**: 844–861.

Boyd, P.W. and Ellwood, M.J. (2010) The biogeochemical cycle of iron in the ocean. *Nature Geosci* **3**: 675–682.

Boyd, P.W., Jickells, T., Law, C.S., Blain, S., Boyle, E.A., Buesseler, K.O., et al. (2007) Mesoscale Iron Enrichment Experiments 1993-2005: Synthesis and Future Directions. *Science* **315**: 612–617.

Bradley, J.M., Svistunenko, D.A., Wilson, M.T., Hemmings, A.M., Moore, G.R., and Le Brun, N.E. (2020) Bacterial iron detoxification at the molecular level. *Journal of Biological Chemistry* **295**: 17602–17623.

Breitwieser, F.P., Lu, J., and Salzberg, S.L. (2019) A review of methods and databases for metagenomic classification and assembly. *Briefings in Bioinformatics* **20**: 1125–1136.

Browning, T.J., Achterberg, E.P., Engel, A., and Mawji, E. (2021) Manganese co-limitation of phytoplankton growth and major nutrient drawdown in the Southern Ocean. *Nat Commun* **12**: 884.

Bruland, K.W. and Lohan, M.C. (2003) Controls of Trace Metals in Seawater. In *Treatise on Geochemistry*. Elsevier, pp. 23–47.

Callahan, B.J., McMurdie, P.J., Rosen, M.J., Han, A.W., Johnson, A.J.A., and Holmes, S.P. (2016) DADA2: High-resolution sample inference from Illumina amplicon data. *Nat Methods* **13**: 581–583.

Carter, L., McCave, I.N., and Williams, M.J.M. (2008) Chapter 4 Circulation and Water Masses of the Southern Ocean: A Review. In *Developments in Earth and Environmental Sciences*. Elsevier, pp. 85–114.

Castro, C.G., Pérez, F.F., Holley, S.E., and Ríos, A.F. (1998) Chemical characterisation and modelling of water masses in the Northeast Atlantic. *Progress in Oceanography* **41**: 249–279.

Chapman, C.C., Lea, M.-A., Meyer, A., Sallée, J.-B., and Hindell, M. (2020) Defining Southern Ocean fronts and their influence on biological and physical processes in a changing climate. *Nat Clim Chang* **10**: 209–219.

Chen, J., Guo, Y., Lu, Y., Wang, B., Sun, J., Zhang, H., and Wang, H. (2019) Chemistry and Biology of Siderophores from Marine Microbes. *Marine Drugs* **17**: 562.

Claesson, M.J., Wang, Q., O'Sullivan, O., Greene-Diniz, R., Cole, J.R., Ross, R.P., and O'Toole, P.W. (2010) Comparison of two next-generation sequencing technologies for resolving highly complex microbiota composition using tandem variable 16S rRNA gene regions. *Nucleic Acids Research* **38**: e200–e200.

Coale, K.H., Johnson, K.S., Fitzwater, S.E., Gordon, R.M., Tanner, S., Chavez, F.P., et al. (1996) A massive phytoplankton bloom induced by an ecosystem-scale iron fertilization experiment in the equatorial Pacific Ocean. *Nature* **383**: 495–501.

Cui, M. and Gnanadesikan, A. (2022) Characterizing the Roles of Biogeochemical Cycling and Ocean Circulation in Regulating Marine Copper Distributions. *JGR Oceans* **127**: e2021JC017742.

Debeljak, P., Toulza, E., Beier, S., Blain, S., and Obernosterer, I. (2019) Microbial iron metabolism as revealed by gene expression profiles in contrasted Southern Ocean regimes. *Environ Microbiol* **21**: 2360–2374.

DeVries, T. (2022) The Ocean Carbon Cycle. *Annu Rev Environ Resour* **47**: 317–341.

DeVries, T. (2014) The oceanic anthropogenic CO_2 sink: Storage, air-sea fluxes, and transports over the industrial era. *Global Biogeochemical Cycles* **28**: 631–647.

DeVries, T., Holzer, M., and Primeau, F. (2017) Recent increase in oceanic carbon uptake driven by weaker upper-ocean overturning. *Nature* **542**: 215–218.

Dosanjh, N.S. and Michel, S.L. (2006) Microbial nickel metalloregulation: NikRs for nickel ions. *Current Opinion in Chemical Biology* **10**: 123–130.

Ducklow, H., Steinberg, D., and Buesseler, K. (2001) Upper Ocean Carbon Export and the Biological Pump. *oceanog* **14**: 50–58.

Dupont, C.L., Buck, K.N., Palenik, B., and Barbeau, K. (2010) Nickel utilization in phytoplankton assemblages from contrasting oceanic regimes. *Deep Sea Research Part I: Oceanographic Research Papers* **57**: 553–566.

Edgar, R.C. (2010) Search and clustering orders of magnitude faster than BLAST. *Bioinformatics* **26**: 2460–2461.

Eitinger, T., Suhr, J., Moore, L., and Smith, J.A.C. (2005) Secondary Transporters for Nickel and Cobalt Ions: Theme and Variations. *Biometals* **18**: 399–405.

Ellwood, M.J., Strzepek, R.F., Strutton, P.G., Trull, T.W., Fourquez, M., and Boyd, P.W. (2020) Distinct iron cycling in a Southern Ocean eddy. *Nat Commun* **11**: 825.

Eppley, R.W. and Peterson, B.J. (1979) Particulate organic matter flux and planktonic new production in the deep ocean. *Nature* **282**: 677–680.

Eren, A.M., Esen, Ö.C., Quince, C., Vineis, J.H., Morrison, H.G., Sogin, M.L., and Delmont, T.O. (2015) Anvi'o: an advanced analysis and visualization platform for 'omics data. *PeerJ* **3**: e1319.

Falkowski, P.G., Fenchel, T., and Delong, E.F. (2008) The microbial engines that drive Earth's biogeochemical cycles. *Science* **320**: 1034–1039.

Fourquez, M., Devez, A., Schaumann, A., Guéneuguès, A., Jouenne, T., Obernosterer, I., and Blain, S. (2014) Effects of iron limitation on growth and carbon metabolism in oceanic and coastal heterotrophic bacteria. *Limnol Oceanogr* **59**: 349–360.

Franzosa, E.A., McIver, L.J., Rahnavard, G., Thompson, L.R., Schirmer, M., Weingart, G., et al. (2018) Species-level functional profiling of metagenomes and metatranscriptomes. *Nat Methods* **15**: 962–968.
Gaetke, L. (2003) Copper toxicity, oxidative stress, and antioxidant nutrients. *Toxicology* **189**: 147–163.
Gehlen, M., Bopp, L., Emprin, N., Aumont, O., Heinze, C., and Ragueneau, O. (2006) Reconciling surface ocean productivity, export fluxes and sediment composition in a global biogeochemical ocean model. *Biogeosciences* **3**: 521–537.
Gent, P.R. (2016) Effects of Southern Hemisphere Wind Changes on the Meridional Overturning Circulation in Ocean Models. *Annu Rev Mar Sci* **8**: 79–94.
Gervais, F., Riebesell, U., and Gorbunov, M.Y. (2002) Changes in primary productivity and chlorophyll a in response to iron fertilization in the Southern Polar Frontal Zone. *Limnology & Oceanography* **47**: 1324–1335.
Gikas, P. (2008) Single and combined effects of nickel (Ni(II)) and cobalt (Co(II)) ions on activated sludge and on other aerobic microorganisms: A review. *Journal of Hazardous Materials* **159**: 187–203.
Gledhill, M. (2012) The organic complexation of iron in the marine environment: a review. *Front Microbio* **3**: 69.
Graham, W.F., Bender, M.L., and Klinkhammer, G.P. (1976) Manganese in Narragansett Bay1. *Limnology & Oceanography* **21**: 665–673.
Gray, A.R. (2024) The Four-Dimensional Carbon Cycle of the Southern Ocean. *Annu Rev Mar Sci* **16**: 163–190.
Handelsman, J., Rondon, M.R., Brady, S.F., Clardy, J., and Goodman, R.M. (1998) Molecular biological access to the chemistry of unknown soil microbes: a new frontier for natural products. *Chemistry & Biology* **5**: R245–R249.
Hansel, C.M. (2017) Manganese in Marine Microbiology. In *Advances in Microbial Physiology*. Elsevier, pp. 37–83.
Hansel, C.M. (2019) Manganese Reduction. In *Encyclopedia of Astrobiology*. Gargaud, M., Irvine, W.M., Amils, R., Cleaves, H.J., Pinti, D., Cernicharo Quintanilla, J., and Viso, M. (eds). Berlin, Heidelberg: Springer Berlin Heidelberg, pp. 1–3.
Hansell, D., Carlson, C., Repeta, D., and Schlitzer, R. (2009) Dissolved Organic Matter in the Ocean: A Controversy Stimulates New Insights. *Oceanog* **22**: 202–211.
Hansell, D.A. and Orellana, M.V. (2021) Dissolved Organic Matter in the Global Ocean: A Primer. *Gels* **7**: 128.
Hawco, N.J., Tagliabue, A., and Twining, B.S. (2022) Manganese Limitation of Phytoplankton Physiology and Productivity in the Southern Ocean. *Global Biogeochemical Cycles* **36**: e2022GB007382.
Hedges, J.I. (1992) Global biogeochemical cycles: progress and problems. *Marine Chemistry* **39**: 67–93.
Henley, S.F., Cavan, E.L., Fawcett, S.E., Kerr, R., Monteiro, T., Sherrell, R.M., et al. (2020) Changing Biogeochemistry of the Southern Ocean and Its Ecosystem Implications. *Front Mar Sci* **7**: 581.
Herndl, G.J. and Reinthaler, T. (2013) Microbial control of the dark end of the biological pump. *Nature Geosci* **6**: 718–724.
Higgins, K.A., Carr, C.E., and Maroney, M.J. (2012) Specific Metal Recognition in Nickel Trafficking. *Biochemistry* **51**: 7816–7832.
Hogle, S.L., Thrash, J.C., Dupont, C.L., and Barbeau, K.A. (2016) Trace Metal Acquisition by Marine Heterotrophic Bacterioplankton with Contrasting Trophic Strategies. *Appl Environ Microbiol* **82**: 1613–1624.

Hopkinson, B.M. and Barbeau, K.A. (2012) Iron transporters in marine prokaryotic genomes and metagenomes: Iron transporters in marine prokaryotes. *Environmental Microbiology* **14**: 114–128.
Hyatt, D., Chen, G.-L., LoCascio, P.F., Land, M.L., Larimer, F.W., and Hauser, L.J. (2010) Prodigal: prokaryotic gene recognition and translation initiation site identification. *BMC Bioinformatics* **11**: 119.
Ilbert, M. and Bonnefoy, V. (2013) Insight into the evolution of the iron oxidation pathways. *Biochimica et Biophysica Acta (BBA) - Bioenergetics* **1827**: 161–175.
JCVI (2022) Global Ocean Sampling Expedition.
Jiao, N., Herndl, G.J., Hansell, D.A., Benner, R., Kattner, G., Wilhelm, S.W., et al. (2010) Microbial production of recalcitrant dissolved organic matter: long-term carbon storage in the global ocean. *Nat Rev Microbiol* **8**: 593–599.
Jiao, N., Robinson, C., Azam, F., Thomas, H., Baltar, F., Dang, H., et al. (2014) Mechanisms of microbial carbon sequestration in the ocean – future research directions. *Biogeosciences* **11**: 5285–5306.
Jickells, T.D., An, Z.S., Andersen, K.K., Baker, A.R., Bergametti, G., Brooks, N., et al. (2005) Global Iron Connections Between Desert Dust, Ocean Biogeochemistry, and Climate. *Science* **308**: 67–71.
John, S.G., Kelly, R.L., Bian, X., Fu, F., Smith, M.I., Lanning, N.T., et al. (2022) The biogeochemical balance of oceanic nickel cycling. *Nat Geosci* **15**: 906–912.
Johnson, G.C. (2008) Quantifying Antarctic Bottom Water and North Atlantic Deep Water volumes. *J Geophys Res* **113**: 2007JC004477.
Kang, D.D., Li, F., Kirton, E., Thomas, A., Egan, R., An, H., and Wang, Z. (2019) MetaBAT 2: an adaptive binning algorithm for robust and efficient genome reconstruction from metagenome assemblies. *PeerJ* **7**: e7359.
Latour, P., Strzepek, R.F., Wuttig, K., Van Der Merwe, P., Bach, L.T., Eggins, S., et al. (2023) Seasonality of phytoplankton growth limitation by iron and manganese in subantarctic waters. *Elem Sci Anth* **11**: 00022.
Li, D., Liu, C.-M., Luo, R., Sadakane, K., and Lam, T.-W. (2015) MEGAHIT: an ultra-fast single-node solution for large and complex metagenomics assembly via succinct de Bruijn graph. *Bioinformatics* **31**: 1674–1676.
Li, W. and Godzik, A. (2006) Cd-hit: a fast program for clustering and comparing large sets of protein or nucleotide sequences. *Bioinformatics* **22**: 1658–1659.
Little, S.H., Vance, D., Walker-Brown, C., and Landing, W.M. (2014) The oceanic mass balance of copper and zinc isotopes, investigated by analysis of their inputs, and outputs to ferromanganese oxide sediments. *Geochimica et Cosmochimica Acta* **125**: 673–693.
Liu, Y., Debeljak, P., Rembauville, M., Blain, S., and Obernosterer, I. (2019) Diatoms shape the biogeography of heterotrophic prokaryotes in early spring in the Southern Ocean. *Environmental Microbiology* **21**: 1452–1465.
Lombard, V., Golaconda Ramulu, H., Drula, E., Coutinho, P.M., and Henrissat, B. (2014) The carbohydrate-active enzymes database (CAZy) in 2013. *Nucl Acids Res* **42**: D490–D495.
Lomsadze, A., Gemayel, K., Tang, S., and Borodovsky, M. (2018) Modeling leaderless transcription and atypical genes results in more accurate gene prediction in prokaryotes. *Genome Res* **28**: 1079–1089.
Macomber, L. and Hausinger, R.P. (2011) Mechanisms of nickel toxicity in microorganisms. *Metallomics* **3**: 1153.
Macomber, L. and Imlay, J.A. (2009) The iron-sulfur clusters of dehydratases are primary intracellular targets of copper toxicity. *Proc Natl Acad Sci USA* **106**: 8344–8349.

Malviya, S., Scalco, E., Audic, S., Vincent, F., Veluchamy, A., Poulain, J., et al. (2016) Insights into global diatom distribution and diversity in the world's ocean. *Proc Natl Acad Sci USA* **113**: E1516-25.
Marchesi, J.R. and Ravel, J. (2015) The vocabulary of microbiome research: a proposal. *Microbiome* **3**: 31, s40168-015-0094–5.
Marchetti, A. (2019) A Global Perspective on Iron and Plankton Through the *Tara* Oceans Lens. *Global Biogeochemical Cycles* **33**: 239–242.
Marinov, I., Gnanadesikan, A., Toggweiler, J.R., and Sarmiento, J.L. (2006) The Southern Ocean biogeochemical divide. *Nature* **441**: 964–967.
Martin, J.H. (1990) Glacial-interglacial CO_2 change: The Iron Hypothesis. *Paleoceanography* **5**: 1–13.
Martin, J.H. and Fitzwater, S.E. (1988) Iron deficiency limits phytoplankton growth in the north-east Pacific subarctic. *Nature* **331**: 341–343.
Marzocchi, A. and Jansen, M.F. (2019) Global cooling linked to increased glacial carbon storage via changes in Antarctic sea ice. *Nat Geosci* **12**: 1001–1005.
Middag, R., De Baar, H.J.W., Bruland, K.W., and Van Heuven, S.M.A.C. (2020) The Distribution of Nickel in the West-Atlantic Ocean, Its Relationship With Phosphate and a Comparison to Cadmium and Zinc. *Front Mar Sci* **7**: 105.
Moore, J.K. and Abbott, M.R. (2000) Phytoplankton chlorophyll distributions and primary production in the Southern Ocean. *J Geophys Res* **105**: 28709–28722.
Morley, S.A., Abele, D., Barnes, D.K.A., Cárdenas, C.A., Cotté, C., Gutt, J., et al. (2020) Global Drivers on Southern Ocean Ecosystems: Changing Physical Environments and Anthropogenic Pressures in an Earth System. *Front Mar Sci* **7**: 547188.
Morrison, A.K., Frölicher, T.L., and Sarmiento, J.L. (2015) Upwelling in the Southern Ocean. *Physics Today* **68**: 27–32.
Naito, K., Matsui, M., and Imai, I. (2005) Ability of marine eukaryotic red tide microalgae to utilize insoluble iron. *Harmful Algae* **4**: 1021–1032.
Norman, L., Cabanesa, D.J.E., Blanco-Ameijeiras, S., Moisset, S.A.M., and Hassler, C.S. (2014) Iron Biogeochemistry in Aquatic Systems: From Source to Bioavailability. *Chimia* **68**: 764.
Nurk, S., Meleshko, D., Korobeynikov, A., and Pevzner, P.A. (2017) metaSPAdes: a new versatile metagenomic assembler. *Genome Res* **27**: 824–834.
Ogawa, H., Amagai, Y., Koike, I., Kaiser, K., and Benner, R. (2001) Production of Refractory Dissolved Organic Matter by Bacteria. *Science* **292**: 917–920.
Öhrvik, H. and Thiele, D.J. (2015) The role of Ctr1 and Ctr2 in mammalian copper homeostasis and platinum-based chemotherapy. *Journal of Trace Elements in Medicine and Biology* **31**: 178–182.
Orsi, A.H., Whitworth, T., and Nowlin, W.D. (1995) On the meridional extent and fronts of the Antarctic Circumpolar Current. *Deep Sea Research Part I: Oceanographic Research Papers* **42**: 641–673.
Parekh, P., Follows, M.J., and Boyle, E.A. (2005) Decoupling of iron and phosphate in the global ocean. *Global Biogeochemical Cycles* **19**: 2004GB002280.
Park, Y., Gamberoni, L., and Charriaud, E. (1993) Frontal structure, water masses, and circulation in the Crozet Basin. *J Geophys Res* **98**: 12361–12385.
Park, Y.-H., Fuda, J.-L., Durand, I., and Naveira Garabato, A.C. (2008) Internal tides and vertical mixing over the Kerguelen Plateau. *Deep Sea Research Part II: Topical Studies in Oceanography* **55**: 582–593.
Pausch, F., Bischof, K., and Trimborn, S. (2019) Iron and manganese co-limit growth of the Southern Ocean diatom Chaetoceros debilis. *PLoS ONE* **14**: e0221959.

Pesant, S., Not, F., Picheral, M., Kandels-Lewis, S., Le Bescot, N., Gorsky, G., et al. (2015) Open science resources for the discovery and analysis of Tara Oceans data. *Sci Data* **2**: 150023.

Poole, R. and Tomczak, M. (1999) Optimum multiparameter analysis of the water mass structure in the Atlantic Ocean thermocline. *Deep Sea Research Part I: Oceanographic Research Papers* **46**: 1895–1921.

Posacka, A.M., Semeniuk, D.M., and Maldonado, M.T. (2019) Effects of Copper Availability on the Physiology of Marine Heterotrophic Bacteria. *Front Mar Sci* **5**: 523.

Purba, N.P., Akhir, M.F., Pranowo, W.S., Subiyanto, and Zainol, Z. (2023) Seasonal Water Mass Transformation in the Eastern Indian Ocean from In Situ Observations. *Atmosphere* **15**: 1.

Quéguiner, B. (2013) Iron fertilization and the structure of planktonic communities in high nutrient regions of the Southern Ocean. *Deep Sea Research Part II: Topical Studies in Oceanography* **90**: 43–54.

Quince, C., Walker, A.W., Simpson, J.T., Loman, N.J., and Segata, N. (2017) Shotgun metagenomics, from sampling to analysis. *Nat Biotechnol* **35**: 833–844.

Rembauville, M., Salter, I., Leblond, N., Gueneugues, A., and Blain, S. (2015) Export fluxes in a naturally iron-fertilized area of the Southern Ocean – Part 1: Seasonal dynamics of particulate organic carbon export from a moored sediment trap. *Biogeosciences* **12**: 3153–3170.

Richon, C. and Tagliabue, A. (2019) Insights Into the Major Processes Driving the Global Distribution of Copper in the Ocean From a Global Model. *Global Biogeochemical Cycles* **33**: 1594–1610.

Rintoul, S.R. and England, M.H. (2002) Ekman Transport Dominates Local Air–Sea Fluxes in Driving Variability of Subantarctic Mode Water. *J Phys Oceanogr* **32**: 1308–1321.

Rodionov, D.A., Hebbeln, P., Gelfand, M.S., and Eitinger, T. (2006) Comparative and Functional Genomic Analysis of Prokaryotic Nickel and Cobalt Uptake Transporters: Evidence for a Novel Group of ATP-Binding Cassette Transporters. *J Bacteriol* **188**: 317–327.

Roshan, S. and Wu, J. (2015) The distribution of dissolved copper in the tropical-subtropical north Atlantic across the GEOTRACES GA03 transect. *Marine Chemistry* **176**: 189–198.

Ruacho, A., Richon, C., Whitby, H., and Bundy, R.M. (2022) Sources, sinks, and cycling of dissolved organic copper binding ligands in the ocean. *Commun Earth Environ* **3**: 263.

Sabu, P., Libera, S.A., Chacko, R., Anilkumar, N., Subeesh, M.P., and Thomas, A.P. (2020) Winter water variability in the Indian Ocean sector of Southern Ocean during austral summer. *Deep Sea Research Part II: Topical Studies in Oceanography* **178**: 104852.

Sanchez-Vidal, A., Higueras, M., Martí, E., Liquete, C., Calafat, A., Kerhervé, P., and Canals, M. (2013) Riverine transport of terrestrial organic matter to the North Catalan margin, NW Mediterranean Sea. *Progress in Oceanography* **118**: 71–80.

Sandy, M. and Butler, A. (2009) Microbial Iron Acquisition: Marine and Terrestrial Siderophores. *Chem Rev* **109**: 4580–4595.

Schlitzer, R., Anderson, R.F., Dodas, E.M., Lohan, M., Geibert, W., Tagliabue, A., et al. (2018) The GEOTRACES Intermediate Data Product 2017. *Chemical Geology* **493**: 210–223.

Schoffman, H., Lis, H., Shaked, Y., and Keren, N. (2016) Iron–Nutrient Interactions within Phytoplankton. *Front Plant Sci* **7**: 1223.

Seemann, T. (2014) Prokka: rapid prokaryotic genome annotation. *Bioinformatics* **30**: 2068–2069.

Simon, C. and Daniel, R. (2011) Metagenomic Analyses: Past and Future Trends. *Appl Environ Microbiol* **77**: 1153–1161.
Singh, A.D., Singh, H., Tripathi, S., and Singh, P. (2023) Evolution and dynamics of the Arabian Sea oxygen minimum zone: Understanding the paradoxes. *Evolving Earth* **1**: 100028.
Sokolov, S. and Rintoul, S.R. (2009) Circumpolar structure and distribution of the Antarctic Circumpolar Current fronts: 1. Mean circumpolar paths. *J Geophys Res* **114**: 2008JC005108.
Sprintall, J., Siedler, G., and Mercier, H. (2013) Interocean and Interbasin Exchanges. In *International Geophysics*. Elsevier, pp. 493–518.
Sun, Y., Debeljak, P., and Obernosterer, I. (2021) Microbial iron and carbon metabolism as revealed by taxonomy-specific functional diversity in the Southern Ocean. *ISME J* **15**: 2933–2946.
Sunagawa, S., Acinas, S.G., Bork, P., Bowler, C., Tara Oceans Coordinators, Acinas, S.G., et al. (2020) Tara Oceans: towards global ocean ecosystems biology. *Nat Rev Microbiol* **18**: 428–445.
Sunagawa, S., Coelho, L.P., Chaffron, S., Kultima, J.R., Labadie, K., Salazar, G., et al. (2015) Structure and function of the global ocean microbiome. *Science* **348**: 1261359.
Tagliabue, A., Bowie, A.R., Boyd, P.W., Buck, K.N., Johnson, K.S., and Saito, M.A. (2017) The integral role of iron in ocean biogeochemistry. *Nature* **543**: 51–59.
Talley, L.D. (1996) Antarctic Intermediate Water in the South Atlantic. In *The South Atlantic*. Berlin, Heidelberg: Springer Berlin Heidelberg, pp. 219–238.
Talley, L.D. (2003) Shallow, Intermediate, and Deep Overturning Components of the Global Heat Budget. *J Phys Oceanogr* **33**: 530–560.
Tandara, L. and Salamunic, I. (2012) Iron metabolism: current facts and future decisions. *Biochem Med* 311–328.
Tanhua, T., Bates, N.R., and Körtzinger, A. (2013) The Marine Carbon Cycle and Ocean Carbon Inventories. In *International Geophysics*. Elsevier, pp. 787–815.
Tebo, B.M. and Luther, G.W. (2019) Manganese Cycling in the Oceans. In *Encyclopedia of Water*. Maurice, P. (ed). Wiley, pp. 1–14.
Torsvik, V. and Øvreås, L. (2002) Microbial diversity and function in soil: from genes to ecosystems. *Current Opinion in Microbiology* **5**: 240–245.
Toulza, E., Tagliabue, A., Blain, S., and Piganeau, G. (2012) Analysis of the Global Ocean Sampling (GOS) Project for Trends in Iron Uptake by Surface Ocean Microbes. *PLoS ONE* **7**: e30931.
Truong, D.T., Franzosa, E.A., Tickle, T.L., Scholz, M., Weingart, G., Pasolli, E., et al. (2015) MetaPhlAn2 for enhanced metagenomic taxonomic profiling. *Nat Methods* **12**: 902–903.
Tsubouchi, T., Suga, T., and Hanawa, K. (2010) Indian Ocean Subtropical Mode Water: its water characteristics and spatial distribution. *Ocean Sci* **6**: 41–50.
Van Hulten, M., Middag, R., Dutay, J.-C., De Baar, H., Roy-Barman, M., Gehlen, M., et al. (2017) Manganese in the west Atlantic Ocean in the context of the first global ocean circulation model of manganese. *Biogeosciences* **14**: 1123–1152.
Venables, H. and Moore, C.M. (2010) Phytoplankton and light limitation in the Southern Ocean: Learning from high-nutrient, high-chlorophyll areas. *J Geophys Res* **115**: 2009JC005361.
Wafar, M.V.M., Le Corre, P., and L'Helguen, S. (1995) f-Ratios calculated with and without urea uptake in nitrogen uptake by phytoplankton. *Deep Sea Research Part I: Oceanographic Research Papers* **42**: 1669–1674.

Wassmann, P. (1997) Retention versus export food chains: processes controlling sinking loss from marine pelagic systems. *Hydrobiologia* **363**: 29–57.
White, R.A., Callister, S.J., Moore, R.J., Baker, E.S., and Jansson, J.K. (2016) The past, present and future of microbiome analyses. *Nat Protoc* **11**: 2049–2053.
Whitworth, T. and Nowlin, W.D. (1987) Water masses and currents of the Southern Ocean at the Greenwich Meridian. *J Geophys Res* **92**: 6462–6476.
Wood, D.E. and Salzberg, S.L. (2014) Kraken: ultrafast metagenomic sequence classification using exact alignments. *Genome Biol* **15**: R46.
Wu, Y.-W., Simmons, B.A., and Singer, S.W. (2016) MaxBin 2.0: an automated binning algorithm to recover genomes from multiple metagenomic datasets. *Bioinformatics* **32**: 605–607.
Xu, Y., Cao, J., Jiang, L., and Zhang, Y. (2021) Biogeographic and Evolutionary Patterns of Trace Element Utilization in Marine Microbial World. *Genomics, Proteomics & Bioinformatics* **19**: 958–972.
Yoon, J.-E., Yoo, K.-C., Macdonald, A.M., Yoon, H.-I., Park, K.-T., Yang, E.J., et al. (2018) Reviews and syntheses: Ocean iron fertilization experiments – past, present, and future looking to a future Korean Iron Fertilization Experiment in the Southern Ocean (KIFES) project. *Biogeosciences* **15**: 5847–5889.
Yooseph, S., Sutton, G., Rusch, D.B., Halpern, A.L., Williamson, S.J., Remington, K., et al. (2007) The Sorcerer II Global Ocean Sampling Expedition: Expanding the Universe of Protein Families. *PLoS Biol* **5**: e16.
Zeer-Wanklyn, C.J. and Zamble, D.B. (2017) Microbial nickel: cellular uptake and delivery to enzyme centers. *Current Opinion in Chemical Biology* **37**: 80–88.
Zhang, Y., Ying, H., and Xu, Y. (2019) Comparative genomics and metagenomics of the metallomes. *Metallomics* **11**: 1026–1043.
Zhou, S., Meijers, A.J.S., Meredith, M.P., Abrahamsen, E.P., Holland, P.R., Silvano, A., et al. (2023) Slowdown of Antarctic Bottom Water export driven by climatic wind and sea-ice changes. *Nat Clim Chang* **13**: 701–709.

Chapter 1

Seasonal shifts in Fe-acquisition strategies in Southern Ocean microbial communities revealed by metagenomics and autonomous sampling

Preface

This thesis chapter is part of the Southern Ocean and Climate Project (SOCLIM). I performed all bioinformatic analysis: metagenome assembly and analysis, MAGs analysis. For this chapter, the seawater samples were collected by a remote access sampler that was deployed and recovered by Stéphane Blain and Olivier Crispi. Yan Liu carried out the DNA extractions.

Received: 20 January 2023 | Accepted: 25 April 2023

DOI: 10.1111/1462-2920.16397

RESEARCH ARTICLE

ENVIRONMENTAL MICROBIOLOGY Applied Microbiology International

Seasonal shifts in Fe-acquisition strategies in Southern Ocean microbial communities revealed by metagenomics and autonomous sampling

Rui Zhang[1] | **Pavla Debeljak**[2,3] | **Stephane Blain**[1] | **Ingrid Obernosterer**[1]

[1]Sorbonne Université, CNRS, Laboratoire d'Océanographie Microbienne, LOMIC, Banyuls-sur-Mer, France

[2]Sorbonne Université, Muséum National d'Histoire, Naturelle, CNRS, EPHE, Université des Antilles, Institut de Systématique, Evolution, Biodiversité (ISYEB), Paris, France

[3]SupBiotech, Villejuif, France

Correspondence
Ingrid Obernosterer, CNRS, Sorbonne Université, Laboratoire d'Océanographie Microbienne, LOMIC, F-66650 Banyuls-sur-Mer, France.
Email: ingrid.obernosterer@obs-banyuls.fr

Funding information
China Scholarship Council, Grant/Award Number: 202006220057; Fondation BNP Paribas; Institut Polaire Emile Victor (IPEV); INSU-LEFE-CYBER

Abstract

Iron (Fe) governs the cycling of organic carbon in large parts of the Southern Ocean. The strategies of diverse microbes to acquire the different chemical forms of Fe under seasonally changing organic carbon regimes remain, however, poorly understood. Here, we report high-resolution seasonal metagenomic observations from the region off Kerguelen Island (Indian Sector of the Southern Ocean) where natural Fe-fertilization induces consecutive spring and summer phytoplankton blooms. Our data illustrate pronounced, but distinct seasonal patterns in the abundance of genes implicated in the transport of different forms of Fe and organic substrates, of siderophore biosynthesis and carbohydrate-active enzymes. The seasonal dynamics suggest a temporal decoupling in the prokaryotic requirements of Fe and organic carbon during the spring phytoplankton bloom and a concerted access to these resources after the summer bloom. Taxonomic assignments revealed differences in the prokaryotic groups harbouring genes of a given Fe-related category and pronounced seasonal successions were observed. Using MAGs we could decipher the respective Fe- and organic substrate-related genes of individual taxa assigned to abundant groups. The ecological strategies related to Fe-acquisition provide insights on how this element could shape microbial community composition with potential implications on organic matter transformations in the Southern Ocean.

INTRODUCTION

Organic carbon and iron (Fe) are essential elements for heterotrophic prokaryotes and from a metabolic point of view the two elements are intimately linked. Organic substrates provide building units for the cell and carbon metabolism is a source of energy, but a large number of enzymes involved in carbon-related pathways require Fe as a cofactor. The acquisition of both elements is therefore essential for a cell to thrive in a given environment. The concentration of marine organic matter varies on spatial and temporal scales and a large diversity of substrates with highly variable degrees of bioavailability make up this pool (Moran et al., 2016). The concentration of inorganic nutrients can regulate the utilization of labile forms of organic matter, and Fe could be a rate-limiting micro-nutrient in high-nutrient low-chlorophyll (HNLC) regions (Obernosterer et al., 2015).

The marine Fe pool is made up by various dissolved and particulate forms originating from biological, lithogenic or authigenic sources (Tagliabue et al., 2017), but the availability of these different forms of Fe to prokaryotes remains poorly investigated (Debeljak et al., 2021; Hogle et al., 2022; Manck et al., 2022). The presence of multiple chemical forms of Fe is both a challenge and an opportunity for prokaryotes which have evolved a large panel of uptake strategies. Fe requirements and resource acquisition mechanisms vary among taxa (Hopkinson & Barbeau, 2012).

Roseobacter genomes contain genes for multiple Fe uptake mechanisms, while SAR11 has a reduced set of transporters (Hogle et al., 2016; Roe et al., 2013). Siderophore biosynthesis appears to be restricted to a few prokaryotic groups, and many of these belong to *Gammaproteobacteria* (Hopkinson & Barbeau, 2012; Manck et al., 2022; Payne et al., 2016). By contrast, transporters of siderophore-bound Fe are more widespread (Debeljak et al., 2021; Hogle et al., 2022; Hopkinson & Barbeau, 2012), a differentiation that can lead to potential cross feeding (Cordero et al., 2012). The prevalence of specific Fe uptake strategies was shown to be linked to Fe concentrations across large spatial scales (Toulza et al., 2012). Together, this results in a complex interplay between the genomic and physiological properties of individual microbes and their interaction among each other and with their micro-environment.

Responses of microbial communities from HNLC waters to additions of Fe and organic carbon in short-term bottle incubation experiments largely depend on location and season (Obernosterer et al., 2015). Although these experiments provide evidence that Fe and organic carbon can constrain prokaryotic growth, they do not inform on potential acclimation of microbes to changes in the supply of these elements. The aim of the present study was to better understand the link between microbial Fe uptake strategies, organic matter supply and microbial diversity in the Southern Ocean. Our specific objectives were first to determine the seasonal dynamics in the functional repertoire of Fe and organic substrate acquisition genes and second to identify the microbial community members harbouring these genes under varying organic matter supply. We carried out our study in the region off Kerguelen Island, a suitable environment because the intense spring and summer phytoplankton blooms induced by natural Fe fertilization (Blain et al., 2007) result in pronounced seasonal patterns related to Fe and organic carbon availability. To address these objectives in an ocean region that is difficult to access due to logistic constraints, we used an autonomous in situ sampler providing high-resolution observations over an entire seasonal cycle.

EXPERIMENTAL PROCEDURES

Sample collection

We used 12 seawater samples collected with a Remote Access Sampler (RAS-500®, Mac Lane) from 25 October 2016 to 24 February 2017 in surface waters (40 m) of the Kerguelen plateau in the Indian sector of the Southern Ocean (Station A3, 527 m overall depth; Figure 1). The technical aspects of the RAS and its mooring and the collection of seawater are described in detail in Blain et al. (Blain et al., 2021). Briefly, three samples (500 mL each) were collected at each time point; for inorganic nutrient analyses, one sample was filtered in situ through an 0.8-µm polycarbonate (PC) filter (47 mm diameter, Nuclepore, Whatman, Sigma-Aldrich, St Louis, MO, USA), and for phytoplankton and prokaryotic diversity (Blain et al., 2021; Liu et al., 2020), two samples remained unfiltered.

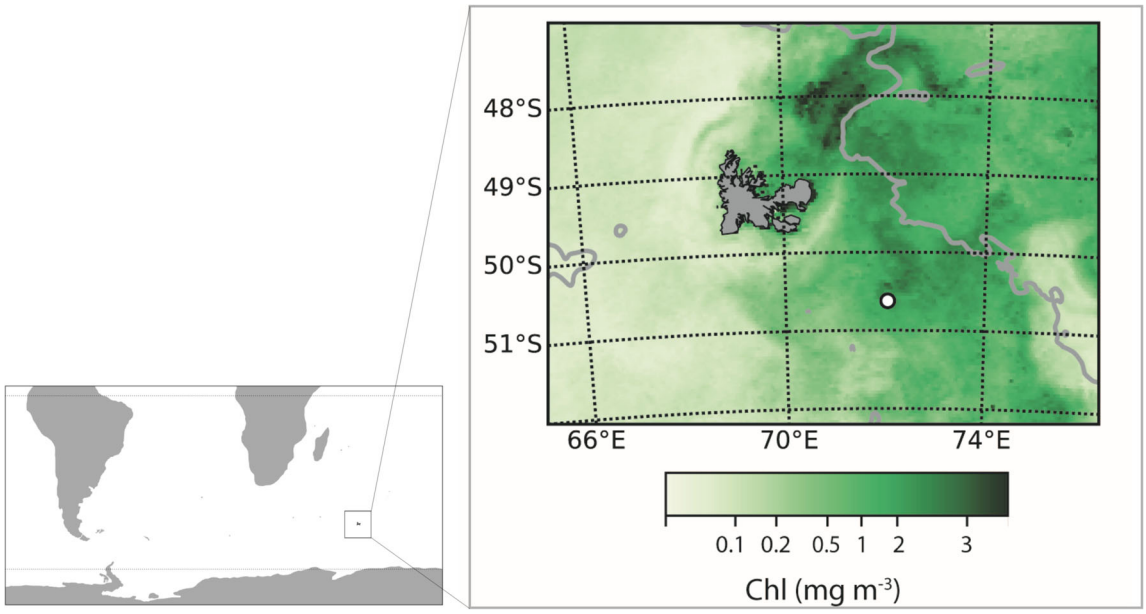

FIGURE 1 Map of the region around Kerguelen Island and location of the deployment of the remote autonomous sampler (white dot). Insert shows global position of Kerguelen Island as indicated by a square. Monthly composite of chlorophyll for November 2016. Modified from Blain et al. (Blain et al., 2022).

Fixatives (mercuric chloride or glutaraldehyde) were added to the sample bags prior to sampling. Upon recovery of the RAS, seawater for metagenomic analyses (fixed with mercuric chloride) was filtered sequentially through 0.8- and 0.2-μm PC filters (47 mm diameter, Nuclepore, Whatman, Sigma-Aldrich) and both filters were kept at −80°C until DNA extraction. Only the DNA extracted from the 0.2-μm filters were used for metagenomic analyses. Temperature and salinity were obtained from sensors mounted on the RAS.

DNA extraction and metagenome sequencing

Total DNA was extracted from 0.2-μm PC filters using the DNeasy PowerWater Kit (Qiagen) according to the manufacturer's instructions with a few modifications. Each filter was cut into small pieces with the scissors, and added solution PW1 and incubated at 65°C for 10 min to promote cell lysis, the complete details of DNA extraction are given in the study by Liu et al. (2020). DNA concentration was measured using quantus fluorometer (Promega) with QuantiFluor® Double stranded DNA (dsDNA) system. Metagenome samples ($n = 12$) were sequenced with an Illumina NovaSeq 6000 system using 2 × 150 bp chemistry at Fasteris SA, Inc. (Switzerland), and yielded 59–83 Mio pairs of metagenomic reads per sample, corresponding to a total of 263.8 GB (Table S1). The data sets are available in the European Nucleotide Archive (ENA) repository at https://www.ebi.ac.uk/ena under the project ID PRJEB56376.

Metagenome assembly

The raw reads were checked with FastQC v0.11.9 and processed with Trimmomatic (v 0.32) (Bolger et al., 2014). The short reads that passed the quality control were individually assembled by MEGAHIT v1.2.9 (D. Li et al., 2015; parameters used --presets meta-large). We also used metaSPAdes v3.14.1 (Nurk et al., 2017; parameters used *-k* 21, 33, 55, 77, 99, 127) to assemble short reads for comparison. MetaQuast with default parameters was used to evaluate metagenomic assembly (Mikheenko et al., 2016). For assembly using MEGAHIT, the total number of contigs varies between 0.1 and 1.6 Mio with an average length of 600 bp (Table S2). For the assembly using metaSPAdes, the total number of contigs varies between 0.3 and 1.8 Mio with an average length of 500 bp (Table S2). Due to the length of N50, we decided to continue the analysis from the MEGAHIT assembly results.

Metagenomic analysis

Open reading frames (ORFs) were predicted using Prodigal v2.6.3 (Hyatt et al., 2010, parameters used -p meta; Table S3). CD-HIT v4.8.1 (W. Li & Godzik, 2006, parameters used -c 1 -aS 1 -g 1) was used to construct a non-redundant protein database pooling the 12 samples (10,984,076 proteins). Based on the non-redundant protein sequence number, we constructed the non-redundant gene sequence set. Salmon v1.4.0 (Patro et al., 2017) was used for read recruitment of the short reads to the non-redundant gene sequences collection, and for the quantification of each gene in each sample (parameters used -incompatPrior 0.0 --seqBias --gcBias --biasSpeedSamp 5 -validateMappings). The quantified protein occurrences for each sample were normalized as genes per kilobase million (GPM) using the following formula:

$$\mathrm{GPM} = 10^6 \times \frac{\text{total reads mapped to genes}/\text{gene length in bp}}{\text{sum}(\text{total reads mapped to genes}/\text{gene length in bp})}.$$

This value can be applied to the metagenomes to remove the effect of library size and gene length, and GPM are thus comparable among samples.

To detect genes that are involved in Fe-related pathways, we used FeGenie (Garber et al., 2020) based on individual contig files for alignment and annotation (parameters used --meta -t 8 --norm). FeGenie is a bioinformatics tool to annotate iron-related genes by combining a Hidden Markov Model (HMM) and BLAST. HMM is a probabilistic model used for gene finding of sequencing data. The authors of FeGenie have constructed their own database of HMMs for Fe related genes by obtaining HMMs from Pfam/TIGRFAMS or by manually constructing HMMs. The HMMs were calibrated through queries against the NCBI's database. Bit score cutoffs that optimally delineate between true and false positives among hits from the non-redundant protein database were identified by manually inspecting each hmm search result. In the present study, we used this comprehensive library to identify proteins that are related to Fe transport and storage, and siderophore biosynthesis and transport (Table S4). The genes identified from the present dataset passed the recommended bit score cutoffs. Different pathways can share homologous genes, as is the case for example in siderophore biosynthesis. HMMs developed in FeGenie are sensitive to the entirety of each gene family. In the metagenomes used here, not all domains of a given siderophore pathway were detected at each time point (see Figure S3). This is most likely due to the overall lower GPMs of siderophore biosynthesis genes as compared to other Fe-related genes, and thus a limit of

detection at our sequencing depth. In order to obtain GPM for the identified FeGenie proteins, each protein sequence related to the Fe pathway in each sample was retrieved in fasta format and mapped against the non-redundant protein database using DIAMOND blastp. Proteins at 100% similarity were retrieved with the according GPM.

For the taxonomic affiliation of Fe-related genes, sequences were obtained using Centrifuge v1.0.4 (Kim et al., 2016) by searching against the GTDB database (Parks et al., 2022) and the alignments with highest score were kept. We then calculated the relative contribution of a prokaryotic group assigned to a gene of interest. The limitation of this approach is that taxonomy is assigned based on relatively short sequencing length of the individual genes; for this reason, we considered mainly the family level and used metagenome-assembled genomes (MAGs) for a more resolutive description. Therefore, the GPM for each Fe-related gene in each sample were summed separately (corresponding to *a*), the GPM per taxa associated with each Fe-related gene in each sample were summed (corresponding to *b*), and the relative contribution of the prokaryotic group was calculated as *b*/*a*.

Organic substrate transporter annotation was carried out based on the non-redundant protein sequences set against the Transporter Classification Database (TCDB; Saier, 2006) using DIAMOND blastp (parameters used --more-sensitive -e 1e-5), and amino acid similarity of ≥70% was chosen as threshold for further analysis. Carbohydrate-active enzymes (CAZymes) were annotated based on the non-redundant protein sequences set using hmmsearch against the dbCAN database (*e*-value <1 × 10–10, coverage >0.3) (Zhang et al., 2018). The domain with the highest coverage was selected for sequences overlapping multiple CAZymes domains. The phylogenetic affiliation of organic substrate transporters and CAZymes sequences and the relative contribution of prokaryotic groups was determined using the same method as described above.

Visualization of data was performed using the packages ggplot2 in the R v4.0.3 and SigmaPlot v14.5 software. The heatmap was generated using the pheatmap package in the R v 4.0.3, with Euclidean distance as the distance function.

Analysis of MAGs

One MAG assigned to each SAR11 and *Nitrincolaceae*, and two MAGs assigned each to *Polaribacter* and *Rhodobacteraceae* were downloaded from data previously published by Sun et al. (2021). The seawater samples from which the MAGs were constructed were collected from three sites in the Kerguelen region including the study site of the RAS deployment. After sequencing, metagenomes were assembled and binned using the methods described by Sun et al. (2021). MAGs were reassessed using CheckM (v1.1.2; Parks et al., 2015) for completeness, and the completeness of the six MAGs used in the present study ranged from 55% to 94% (Table S5). The Average Nucleotide Identity (ANI) values between MAGs, calculated using the OrthoANIu algorithm (Yoon et al., 2017), were below 95%. ORFs of MAGs were predicted using Prodigal v2.6.3 (Hyatt et al., 2010; parameters used -p meta) and functional annotation of MAGs was carried out using the same method as above. To estimate the abundance of MAGs and their Fe- and organic substrate transporter and CAZymes-related genes across the 12 metagenomes, we first used Bowtie2 v2.4.4 (Langmead & Salzberg, 2012) with default parameters to recruit short reads from the 12 metagenomes and samtools (H. Li et al., 2009) was used to convert the resulting SAM files into sorted and indexed BAM files. We used anvi'o v7.1 (Eren et al., 2015) to profile short metagenomic reads aligned to MAGs to estimate coverage statistics per metagenome. Briefly, we first used the program 'anvi-gen-contigs-database' turning MAGs into a contigs-db, then used the program 'anvi-profile' to process the BAM file and generate individual anvi'o profile database, and used the program 'anvi-merge' to merge these individual profiles into a final merged profile database which stored the coverage statistics of each MAGs in the 12 metagenomes. Finally, the program 'anvi-summarize' generated mean coverage values of each MAG and each gene within them across the 12 metagenomes and was visualized by the program 'anvi-interactive' in 'gene mode'.

RESULTS

Environmental context

The site of the RAS deployment is located southeast of Kerguelen Island in the Indian Sector of the Southern Ocean (Figure 1). This naturally Fe-fertilized region has been extensively studied during previous oceanographic cruises focusing on distinct time periods, that are early spring, mid and late summer (projects KEOPS1&2 and MOBYDICK). The deployment of the RAS from 25 October 2016 to 24 February 2017 has for the first time provided a full seasonal picture of the physical context (Pellichero et al., 2020), inorganic nutrient concentrations and characteristics of the consecutive phytoplankton blooms and their carbon and trace element export (Blain et al., 2021, 2022). Briefly, the spring phytoplankton bloom started in late October and peaked by mid-November and the summer bloom occurred in early January (Figure S1A). Diatoms dominated both blooms but varied considerably in their composition between seasons (Blain et al., 2021). Surface

water temperature steadily increased from 1.70°C to 4.17°C over the course of the sampling period. Concentrations of nitrate (range 21.95 to 27.69 μM) and silicic acid (range 2.45–8.24 μM) decreased during the observation period, while ammonium concentrations (range 0.3 to 2 μM) reached a maximum in late December (Figure S1B; Blain et al., 2021).

Seasonal trends in Fe and C transporters

In total, 28,662 Fe-related genes were annotated in the FeGenie database, 66,005 genes related to substrate transport in the TCDB database and 136,460 genes related to enzymatic activity in the CAZymes database. Fe-related genes exhibited lowest normalized gene abundances (genes per kilobase million, GPM; 10–600 GPM), followed by organic carbon membrane transporters (600–1400 GPM) and CAZymes (7000–12,000 GPM).

Normalized gene abundances (GPM) of each of these categories revealed pronounced seasonal patterns (Figure 2). Transporters of Fe ions (Fe^{3+}, Fe^{2+}) (Figure 2A), siderophores and heme (Figure 2B) had the highest GPM after the blooms. Increases in GPM occurred rapidly after the spring bloom and with a time lag of about 1 month after the summer bloom. Siderophore biosynthesis genes had one peak during the spring bloom, and a second peak after the summer bloom in parallel with various Fe transporters (Figure 2B). Organic substrate transporters revealed the highest GPM during the spring bloom and a smaller peak was observed 1 month after the summer bloom (Figure 2C). Organic substrate transporters increased also during the final spring bloom decline, following the seasonal peak in CAZymes.

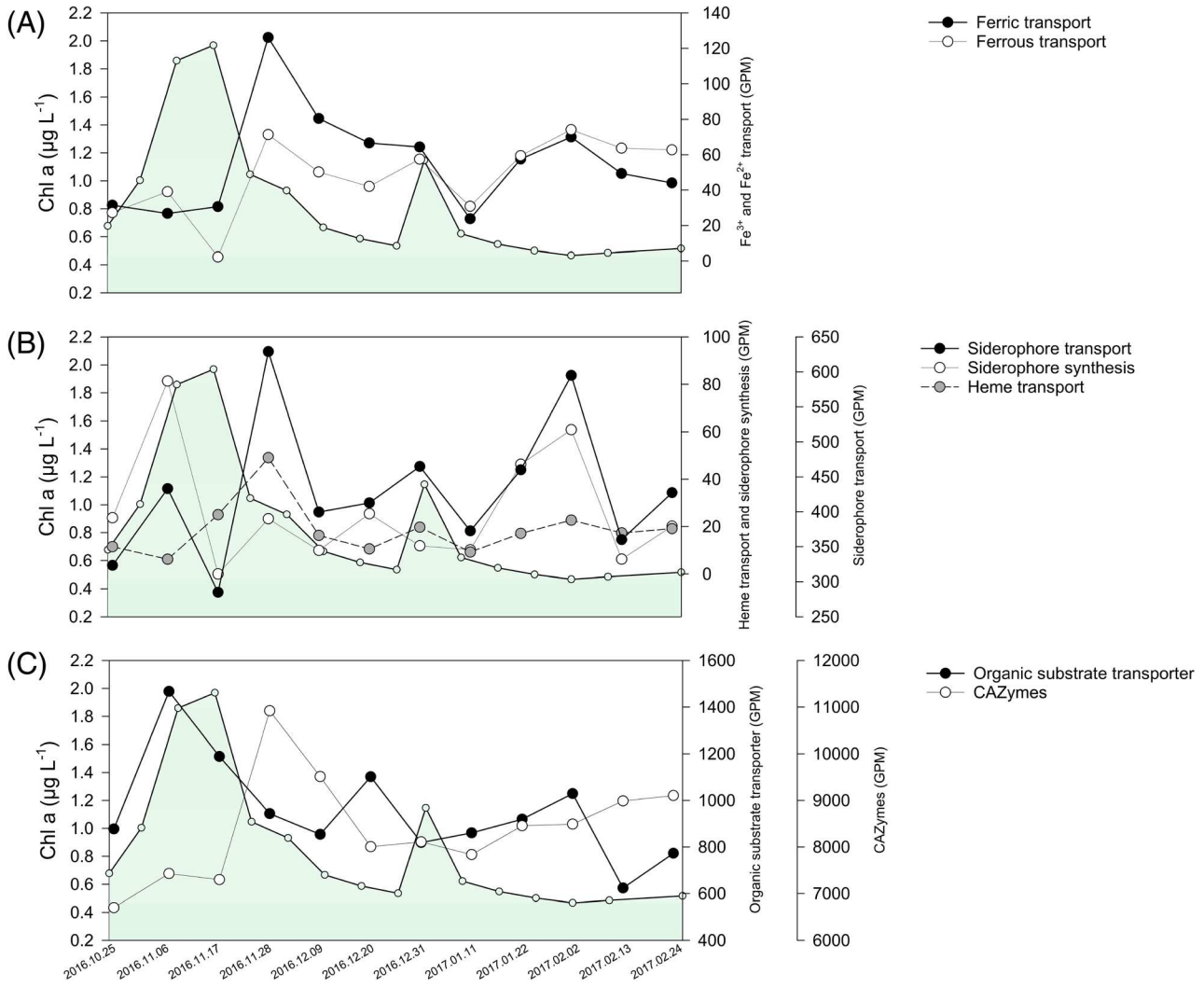

FIGURE 2 Temporal changes of Chlorophyll *a* (green shaded area) and abundance of genes for Fe^{3+} and Fe^{2+} transporters (A), siderophore-bound Fe and heme transporters and siderophore biosynthesis (B) and carbon substrate transporters and carbohydrate-active enzymes (CAZymes) (C). Normalized gene abundances are given in genes per kilobase million (GPM) (see 'Experimental Procedures' for details).

The most abundant transporters of Fe^{3+} ions were *fbpABC*, *fut*A1/A2 and *fbpB-futB*, and the dominant Fe^{2+} ion transporter genes were *feoAB* and *efeUOB* (Figure 3A; Table S4). Siderophore uptake genes were dominated by the *exbB-exbD-tonB* complex and among the genes identified for the transport of specific siderophores were those of pyoverdin (*fpv*), aerobactin (*hat*), ferric enterobactin (*pir*), ferripyochelin (*fpt*), and vibrioferrin (*pvu*) (Figure 3B). We further identified four siderophore biosynthesis clusters related to pyochelin

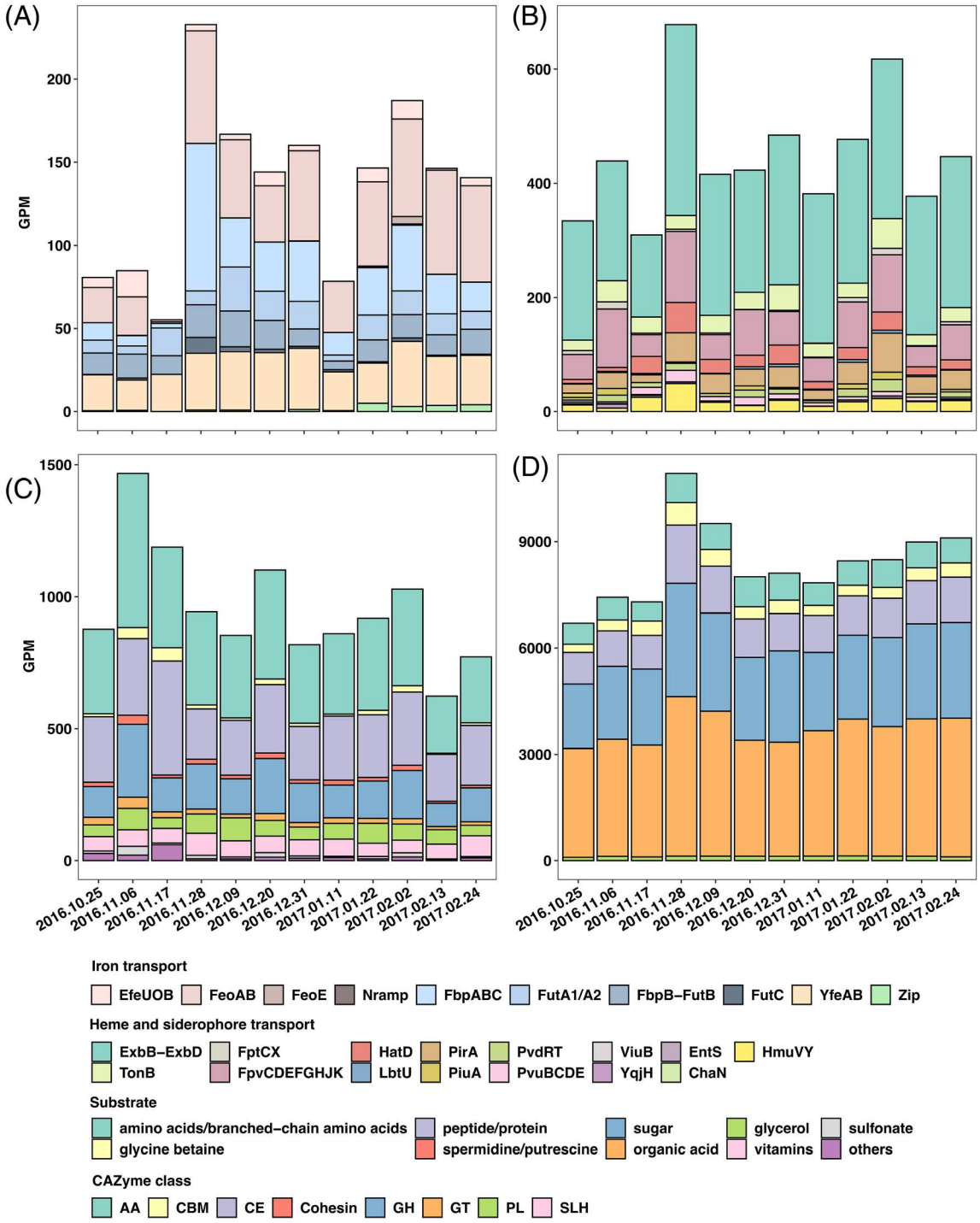

FIGURE 3 Abundance of individual genes contributing to Fe^{3+} and Fe^{2+} transport (A), heme and siderophore transport (B), organic substrate transport (C) and carbohydrate-active enzymes (CAZymes, D) at the 12 time points. Transporters of fatty acids, lipoproteins, ammonia, exopolysaccharides and urea are pooled as 'others'. CAZyme classes include auxiliary activities (AA), carbohydrate-binding modules (CBM), carbohydrate esterases (CE), cohesin, glycoside hydrolases (GH), glycosyltransferases (GT), polysaccharide lyases (PL) and S-layer homology domain (SLH). Normalized gene abundances are given in genes per kilobase million (GPM) (see 'Experimental Procedures' for details).

(*pch*), pyoverdin (*pvd*), rhizobactin (*rhb*) and vanchrobactin (*vab*) (Figures S2 and S3). Among other Fe-related genes identified, a seasonal trend driven by the two phytoplankton blooms was also detectable for Fe regulation (*fur*, *dtxR*, *fecR*), while genes for iron storage (*ftn*) remained stable over time (Figure S2). Transporters of organic substrates were dominated by those for amino acids and proteins, followed by sugars, glycerol and organic acids, and transporters for vitamins were also present throughout the season (Figure 3C). During the sampling period, 379 families of CAZymes were identified, among which 191 glycoside hydrolase (GH) families, 82 glycosyltransferase (GT) families, 41 polysaccharide lyase (PL) families, 34 carbohydrate-binding module (CBM) class families, 16 carbohydrate esterase (CE) families and 13 auxiliary activities (AA) families (Figure 3D).

To obtain a more detailed picture of the seasonal patterns of genes involved in Fe and organic substrate acquisition, we determined the similarity in the temporal trend among individual genes (Figure 4). This analysis highlights four periods. The first period, corresponding to the spring bloom (6 November and 17 November), was characterized by seasonally highest GPM of genes coding for siderophore synthesis (e.g., Pyochelin [*pch*], Pyoverdin [*pvd*], Vanchrobactin [*vab*]) and transport (e.g., catecholate receptor [*piu*], ferripyochelin [*fpt*], Vibriobactin [*viuB*]), concurrently with several organic substance transporters, such as amino acids, sugars, spermidine/putrescine and sulfonates. During the second period that corresponds to the immediately following decline of the spring bloom (28 November), concurrent peaks in transporters of Fe^{3+} ions (*fbp, fut*), heme (*hmu*) and siderophores (e.g., Vibrioferrin [*pvu*], Aerobactin [*haf*], Pyoverdin [*fpv*]) were observed. This period further revealed high GPM of several CAZymes (GT, CE, GH). The third period extends from the final declining phase of the spring bloom to the summer bloom (9 December, 20 December and 31 December) and was characterized by enhanced GPM of transporters of Fe^{3+} ions (*fbpB-futB*, *futA1*/*A2*, *yfe*). The fourth period is represented by two sampling dates

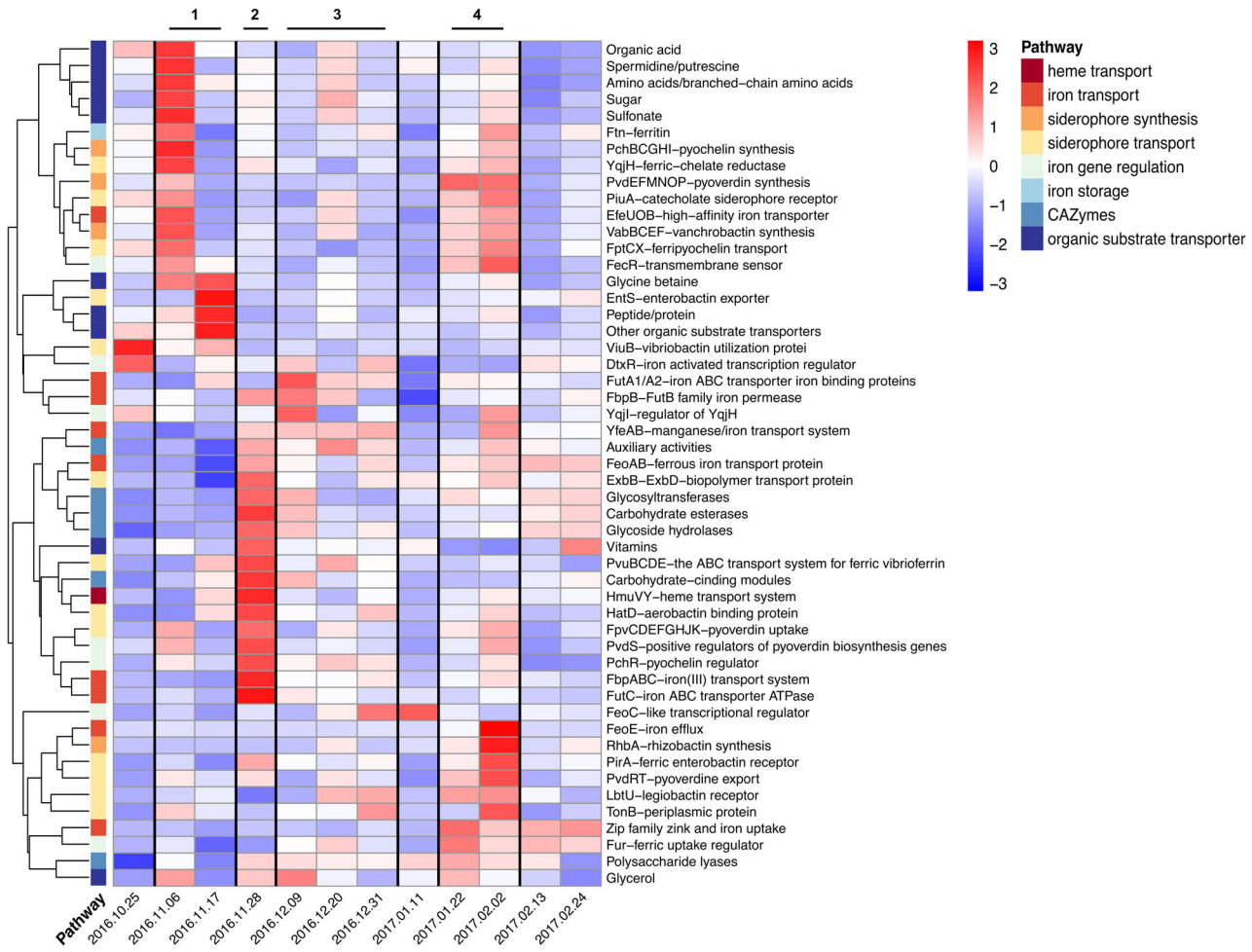

FIGURE 4 Heatmap illustrates the seasonal patterns of genes involved in Fe and organic substrate transporters and related processes. Similarity between genes is based on Euclidian distance cluster analysis. Colour intensity is determined by *Z*-score transformed normalized gene abundances (GPM). The vertical lines separate the four periods.

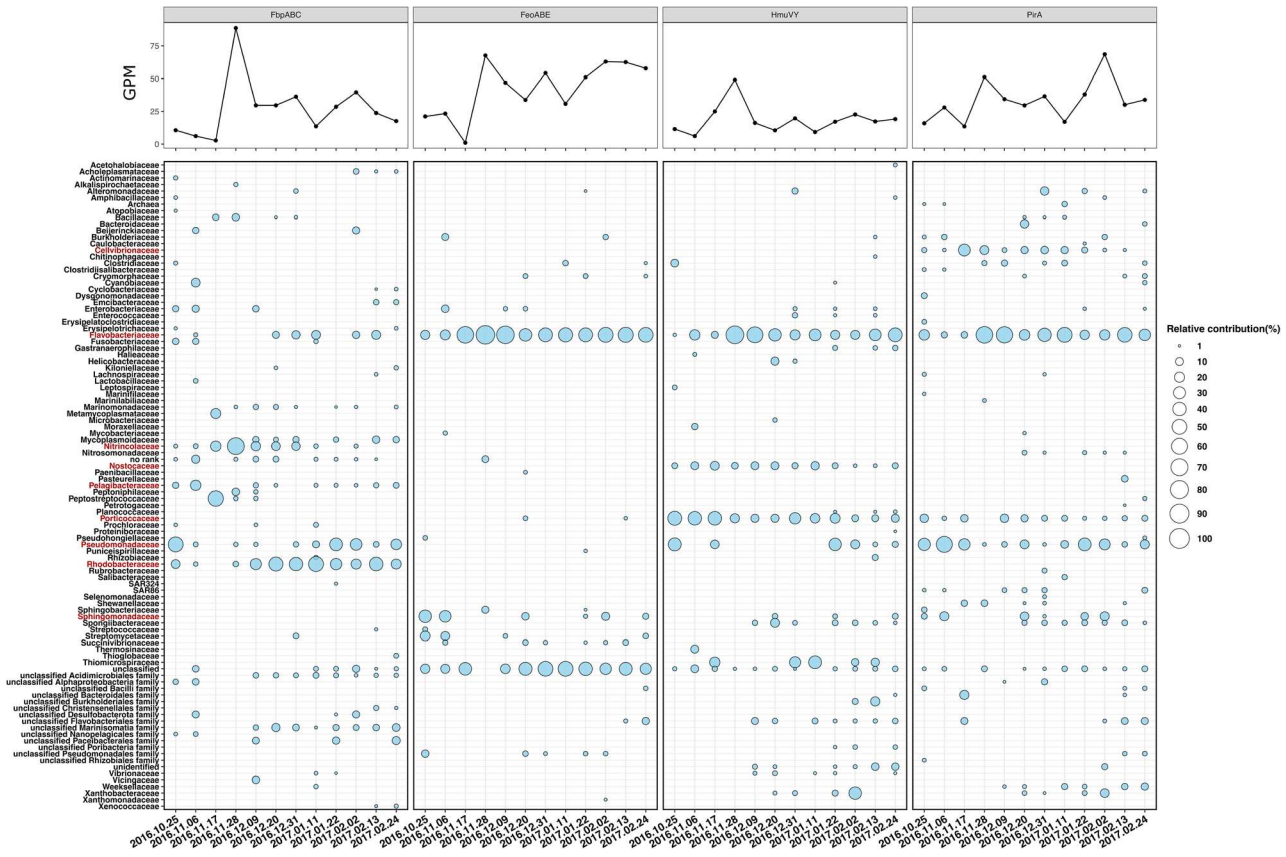

FIGURE 5 Temporal changes of normalized gene abundance (GPM) and relative contribution of prokaryotic groups to specific genes associated with Fe^{3+}, Fe^{2+}, heme and siderophore transport. Prokaryotic groups are based on the family level. Prokaryotic groups discussed in the text are marked in red.

1 month after the summer bloom (22 January and 2 February). Siderophore synthesis genes present already during the first phase re-emerged (e.g. *Pch*, *Pvd*, *Vab*) in combination with a new group of siderophore synthesis (e.g., Rhizobactin [*rhb*]) and transport (Ferric Enterobactin [*pir*], Legiobactin [*lbt*]) genes. During the fourth period, transporters of Fe peaked in parallel with those of organic compounds and siderophore synthesis genes, a pattern that contrasted our observations during the spring bloom.

Linking function to taxonomy at the family level

These temporal changes in the functional repertoire were paralleled by shifts in the prokaryotic community composition (Liu et al., 2020) raising the question of the link between microbial diversity and Fe and organic substrate acquisition. To investigate whether the genes of interest were harboured by specific prokaryotic groups, we assigned the taxonomy of the individual genes belonging to the different gene categories. We illustrate here the taxonomic assignments of four genes, each representing the transport of a distinct form of Fe and each characterized by a marked seasonal trend; these are transport of Fe^{3+} ions (*fbp*) and Fe^{2+} ions (*feo*), of heme (*hmu*) and the siderophore ferric enterobactin receptor (*pir*) (Figure 5). The taxonomic assignments of other Fe-related genes are illustrated in Figure S4. The transporter *fbp* (Fe^{3+} ions) was assigned to several prokaryotic groups and their respective relative contributions changed considerably over time (Figure 5). During the spring bloom (Period 1) when GPM were low, transport of Fe^{3+} ions was assigned to *Pseudomonadaceae*, *Pelagibacteraceae* and *Rhodobacteraceae*, while *Nitrincolaceae* dominated the taxonomic assignments (75% of all *fbp* genes) when GPM peaked during the bloom decline (Period 2). *Rhodobacteraceae* (in particular the genus *Amylibacter*, Figure S5) were the most abundant contributors to *fbp* (19%–51%) during the remaining season and *Pseudomonadaceae* had an increasing share towards the end of the season (4%–35%). A contrasting picture was obtained for *feo* (transport of Fe^{2+} ions) that was assigned to mainly two groups, *Sphingomonadaceae* in early spring (Period 1; 28%–39%) and *Flavobacteriaceae* throughout the remaining season (16%–89%). *Flavobacteriaceae* were dominated by the genus *Polaribacter* (Figure S5) during the spring bloom decline (Period 2). Heme uptake (*hmu*) revealed a seasonal

abundance pattern similar to that of *fbp*, but had distinct taxonomic assignments. *Porticoccaceae* (7%–43%), *Flavobacteriaceae* (2%–76%) and *Nostocaceae* (2%–14%) were the main contributors to heme uptake throughout the season. During the bloom decline (Phase 2) when *hmu* peaked *Polaribacter irgensii* (*Flavobacteriaceae*) had a dominant contribution, and *Cellulophaga*, *hydrogenovibrio* and *Kordia* (*Flavobacteriaceae*; Figure S5) prevailed over the remaining season. The ferric enterobactin receptor *pir* had a seasonal abundance pattern different to that of heme, with peaks during Periods 1 and 4, but overall similar taxonomic assignments at the family level. *Flavobacteriaceae* (6%–66%), with substantial contributions of *Polaribacter*, *Pseudomonadaceae* and *Porticoccaceae* (1%–13%) were the dominant contributors to *pir*, and *Sphingomonadaceae* (0%–15%) and *Cellvibrionacaea* (0%–30%) had seasonally variable contributions. The taxonomic assignments of genes encoding for organic substrate transporters and CAZymes revealed overall small differences in the prokaryotic groups contributing to each category, but marked temporal changes in their relative contributions were observed, in particular during Period 2 (Figures S6 and S7).

Genome-resolved functional potential

To obtain insights on the functional potential for the acquisition of both Fe and organic substrates, we used previously published MAGs obtained from samples collected in the Kerguelen region, including our study site (Sun et al., 2021). We choose MAGs belonging to SAR11, *Nitrincolaceae*, *Rhodobacteracea* and the genus *Polaribacter* (*Flavobacteriaceae*) (Figure 6 and

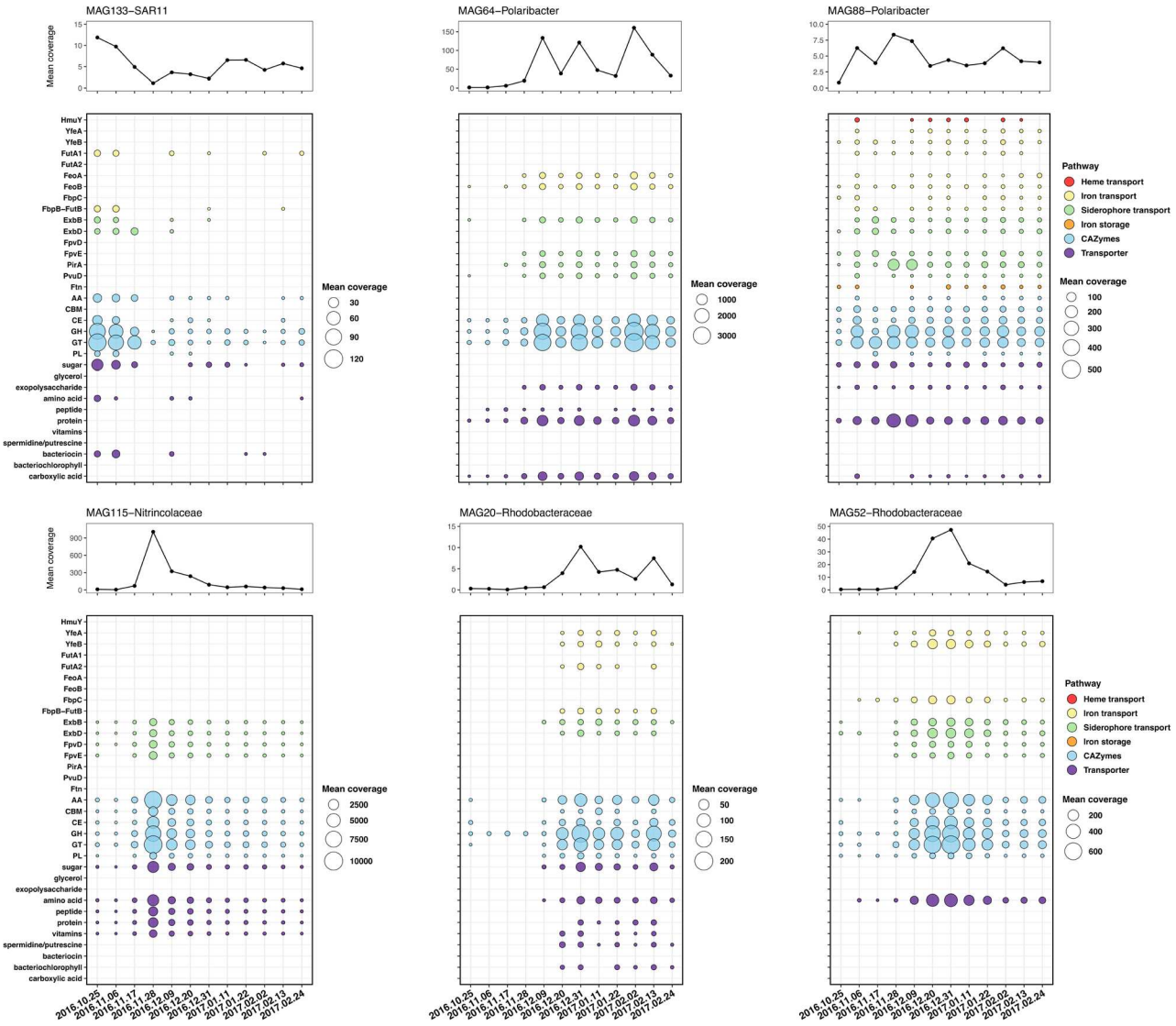

FIGURE 6 Mean coverage of MAGs in the 12 samples and inventories of genes related to Fe and organic substrate transport and CAZymes. Mean coverage on the upper panel represents the average depth of coverage across contig (the coverage of each nucleotide in a contig divided by the length of the contig). Mean coverage on the lower panel represents the Σ coverage of each bp in a gene/gene length.

Table S5). These MAGs belong to prokaryotic groups with substantial contributions to the different gene categories (Figures 5 and S5–S7). Furthermore, ASVs belonging to each of these groups were shown to be abundant and have pronounced seasonal relative abundance patterns, based on 16S rRNA gene sequencing from the same RAS deployment (Liu et al., 2020). Mapping our metagenomic short reads to these MAGs revealed that they largely varied in their respective coverages and had each a distinct seasonal trend. SAR11 MAG133 had slightly higher coverage in early spring as compared to the remaining season. By contrast, *Nitrincolaceae* MAG115 revealed one sharp peak during Period 2. The two *Rhodobacteraceae* MAGs had both higher coverage during the transition between the spring and summer blooms (Period 3). By contrast, the two *Polaribacter* MAGs differed in their overall coverage and their seasonal dynamics. The inventories of the Fe-acquisition and organic substrate-acquisition genes provided some insights on the metabolic versatility of these MAGs. SAR11 MAG133 harboured a reduced set of Fe (*fut*, *fbp*B-*fut*B, Fe^{3+} ions) and organic substrate (sugars and amino acids) transporters. In *Nitrincolaceae* MAG115, we identified transporters for siderophore-bound Fe (*exbB-exbD* complex and *fpv* for pyoverdin) and for several organic substrates (sugars, amino acids, peptides) and vitamins. Both *Rhodobacteraceae* MAGs harboured transporters for Fe^{3+} ions (*yfe*, *fbp*), but appear to differ in their potential of organic substrate acquisition. We identified transporters of several substrates in *Rhodobacteraceae* MAG20 while only amino acid transporters were detected in *Rhodobacteraceae* MAG52. Among the MAGs considered here, *Polaribacter* MAG88 had the most diverse Fe-gene inventory, including heme and bacterioferritin, absent from MAG64. The two *Polaribacter* MAGs harboured both transporters of Fe^{2+} ions (*feo*), proteins and carboxylic acids.

DISCUSSION

We observed pronounced seasonal patterns in the prevalence of genes for the transport of Fe and organic substrates by prokaryotic communities in the Southern Ocean. The acquisition of Fe was temporally decoupled from that of organic carbon over the course of the spring phytoplankton bloom, while a concerted access to both elements occurred after the summer bloom. These dynamics on the community level likely result from seasonal changes in the requirements of Fe and organic carbon and the functional capabilities to acquire the different chemical forms in which these elements are present by diverse microbial taxa. Using metagenome assembled genomes, we illustrate differences in the Fe and organic substrate acquisition repertoires among abundant prokaryotic taxa. These observations combined with marked seasonal changes in microbial community composition (Liu et al., 2020) provide new insights on the potential ecological niches of prokaryotes in the Fe- and organic carbon-constrained Southern Ocean.

Seasonal microbial response to phytoplankton blooms induced by natural iron fertilization

Natural Fe-fertilization in the region off Kerguelen Island leads to annually occurring phytoplankton blooms that impact ecosystem structure and functioning (Blain et al., 2007). Heterotrophic prokaryotes respond markedly to these blooms in terms of growth, biomass production and respiration and thereby contribute to the processing of a substantial fraction of primary production during different seasons (Christaki et al., 2021). The microbial communities present and active in these naturally Fe-fertilized waters vary over the course of the bloom (Liu et al., 2020) and are distinct to communities in surrounding HNLC waters during different seasons (Hernandez-Magana et al., 2021; Landa et al., 2016; West et al., 2008). Differences among prokaryotic taxa in Fe requirements and acquisition strategies as well as in the metabolic potential for the uptake of diverse phytoplankton-derived organic substrates could be one underlying mechanism (Debeljak et al., 2019; Teeling et al., 2012). Niche differentiation in relation to Fe and organic carbon was recently described on a spatial scale (Sun et al., 2021), but a temporal perspective is thus far lacking.

Microbial strategies and Fe sources during the spring bloom

The prevalence of organic substrate transporters during the spring bloom (Period 1) points to a community that rapidly responds to the supply of labile phytoplankton-derived substrates. Organic carbon has been identified as a growth-limiting resource for the winter community in the Kerguelen region (Landa et al., 2016; Obernosterer et al., 2015). Our data suggest that amino acids, organic acids, sugars and sulfonates are the most prominent substances utilized, confirmed by metatranscriptomics and metaproteomics data at the same study site (Debeljak et al., unpublished) and as reported previously from phytoplankton blooms in other marine environments (Teeling et al., 2012; T. B. Francis, Bartosik, et al., 2021). The seasonal pattern of organic substrate transporters was, however, decoupled from that of Fe-transporters during the spring bloom, raising the question of how prokaryotes meet their Fe-requirements.

Dissolved Fe concentrations are high in surface waters in early spring (0.16 nM) (Quéroué et al., 2015), but heterotrophic prokaryotes compete with fast growing small phytoplankton for this Fe source (Fourquez et al., 2015). As reported for diverse members of this clade (Dinasquet et al., 2022; Liu et al., 2020), SAR11 MAG133 was abundant in early spring. The small streamlined genomes of SAR11 (Giovannoni, 2017) have reduced Fe-uptake repertoires (Hogle et al., 2016), as observed also for SAR11 MAG133 (Fe^{3+} ion transporters *fut*, *fbp*B-*fut*B). Using MICRO-CARD-FISH, SAR11 accounted for about 25% of community Fe uptake, while the contribution to leucine uptake was 50% in early spring in fertilized and HNLC waters (Fourquez et al., 2016), indicating an efficient organic substrate utilization even under conditions when access to Fe is constrained. Low Fe requirements and an efficient transport of Fe and organic substrates could be a strategy of SAR11 to take advantage of the pool of labile substrates supplied by phytoplankton.

Lithogenic particles present a potentially important source of Fe in early spring above the Kerguelen plateau (Blain et al., 2022). This Fe source is geochemically complex and needs to be rendered biologically available via dissolution as for example through the binding to high affinity ligands (Kalinowski et al., 2000). Among the strongest binding ligands are catecholate-type siderophores and particle-associated prokaryotes were shown to express the genes implicated in the respective biosynthesis pathways (Debeljak et al., 2021). The prevalence of a catecholate-type siderophore receptor gene (*piu*) during spring indicates that this Fe source could in part account for the prokaryotic demand. Taxonomic assignments revealed that *Pseudomonadaceae* were the most prominent group harbouring this receptor, an observation that supports previous findings on the role of this group in siderophore biosynthesis and uptake (Schalk et al., 2020). An alternative strategy could be the utilization of an internal reservoir, such as Fe stored in specific proteins (bacterioferritin, Ftn) (Andrews et al., 2003). This capacity was shown for strains belonging to *Pseudoalteromonas* (Mazzotta et al., 2020) and several prokaryotic groups, in particular *Flavobacteriaceae*, *Halieaceae* and *Altermonadaceae* contributed to the expression of the respective genes above the Kerguelen plateau in early spring (Debeljak et al., 2019). We identified the gene coding for ferritin in *Polaribacter* MAG88, which had increased coverage during spring, in contrast to *Polaribacter* MAG64 that lacked this gene and revealed enhanced coverage later in the season. These observations illustrate potential niche differentiation among closely related taxa. The utilization of internal Fe stored as ferritin by some taxa could be a possible mechanism for the apparent temporal decoupling in requirements of organic substrates and Fe.

Fe acquisition strategies during the spring bloom decline

Microbial gene inventories related to Fe and organic carbon transport drastically changed during the decline of the spring bloom (Period 2). The prevalence of all CAZyme families indicates the presence of a chemically different pool of organic matter and the need to cleave polysaccharides to access organic carbon (Teeling et al., 2012). The synchronized enhancement in the GPM of different types of Fe-transporters, including those for Fe^{3+} and Fe^{2+} ions, Fe bound to siderophores (Vibrioferrin [*pvu*], Aerobactin [*hat*], Pyoverdin [*fpv*]) and heme suggest an increased prokaryotic Fe demand in response to the shift in the organic carbon regime during the phytoplankton bloom decline. In contrast to early spring, remineralization is a key process providing different sources of Fe to the system. Our observations allow us to provide insights into possible Fe and organic carbon-related strategies of three bacterial groups with distinct abundance patterns.

Nitrincolaceae, represented by MAG115, rapidly responded to the bloom decline. The marked seasonal pattern of MAG115, reaching highest coverages of all MAGs considered here, matched the relative abundances of the respective ASVs as determined from 16S rRNA gene sequences (Liu et al., 2020). *Nitrincolaceae* dominated the taxonomic assignments of transporters of Fe^{3+} ions (*fbp*) during the bloom decline and MAG115 harboured several siderophore uptake genes, such as pyoverdine (*fpv*), a siderophore containing catecholate and hydroxamate groups. MAG115 also contained a large repertoire of organic substrate transporters indicating its capacity in the uptake of various labile compounds (B. Francis, Urich, et al., 2021). The rapid response to a pulsed supply of organic carbon by taking advantage of its potential to utilize different forms of Fe suggests a copiotrophic metabolic strategy, and idea that is further supported by the concurrent expression both at the transcriptomic and proteomic level of genes related to Fe and organic carbon transport by *Nitrincolaceae* MAG115 (Debeljak et al., unpublished).

Polaribacter MAG88 (*Flavobacteriaceae*) also responded to the bloom decline, but its coverage remained comparatively low. This MAG harboured a large repertoire of transporters for organic substrates and Fe, and among the latter we identified the heme transporter *hmu*. Heme is a porphyrin-bound source of Fe that can account for a large fraction of cellular Fe concentrations in phytoplankton and can become a source to heterotrophs when cells are destroyed such as by viral lysis or grazing (Honey et al., 2013). Utilization of heme was demonstrated experimentally for strains belonging to the *Roseobacter* clade (Hogle et al., 2017; Roe et al., 2013), but many other abundant microbial groups appear to lack heme transporters (Hogle et al., 2017). In the present study,

Flavobacteriaceae had a substantial share of the taxonomic assignments of heme transporters (*hmu*), in particular during the bloom decline. Our data suggest that members belonging to *Flavobacteriaceae* could use this source of Fe, to account for its requirements during the degradation of phytoplankton derived organic substances. This potential niche specialization could play an important role in large particles where access to this source of Fe is facilitated.

Both *Roseobacter* MAGs had increased coverage during the transition between the spring decline and summer bloom, matching observations of members of this clade at the ASVs level (Liu et al., 2020). Although functional Fe-profiles were overall similar for both MAGs, MAG20 appears to have a larger organic substrate repertoire than MAG52. An analysis of *Roseobacter* genomes revealed the presence of multiple and diverse pathways for the acquisition of inorganic and organically bound Fe and several copies of ABC transporters (Hogle et al., 2016). This indicates that this group can make use of a variety of chemical forms of Fe, an idea that is supported by observations on the transcriptomic (Debeljak et al., 2019, 2021) level. This versatility with respect to Fe transport let us hypothesize that specialization of organic substrate utilization could be the underlying mechanism for the similar seasonal patterns of the two *Roseobacter* MAGs.

Parallel Fe and C acquisition following the productive season

Despite the smaller magnitude of the summer phytoplankton bloom as compared to spring, the community functional repertoire markedly changed with a time lag of about 1 month, contrasting the rapid response to the spring bloom. The late summer period is characterized by slightly higher concentrations of dissolved organic carbon and seasonally highest prokaryotic abundance (Christaki et al., 2021; Hernandez-Magana et al., 2021) and remineralization presents the main source of Fe (Blain et al., 2008; Sarthou et al., 2008). These environmental conditions could be favourable for the energetically costly biosynthesis of siderophores, supported by our observation of the diverse assemblage of genes for the acquisition of siderophore-bound Fe at the end of the season. Among these the gene of the siderophore receptor *pir* (ferric enterobactin receptor) was assigned to *Flavobacteriaceae*, and the two *Polaribacter* MAGs harboured both this gene. Many members of *Flavobacteriaceae*, including *Polaribacter*, are specialized in the degradation of complex compounds, such as polysaccharides (Kappelmann et al., 2019; Xing et al., 2015). Our results indicate that the concurrent access to organic substrates and siderophore-bound Fe could be a strategy that renders these taxa efficient degraders of organic matter in the Southern Ocean.

By considering transporters for different forms of Fe and organic carbon, two elements that were shown to constrain prokaryotic growth in the Southern Ocean, we provide insights on temporal dynamics in nutrient acquisition at the community level. The distinct seasonal patterns in Fe transporters with respect to those of organic substrates suggest that there could be a switch in nutrient requirements along the season. Our results extend the use of biomarker genes that have allowed to identify nutrient stress of specific microbial groups on spatial scales (Garcia et al., 2020; Saito et al., 2014; Ustick et al., 2021). The taxon-specific genomic capacities to access the different chemical forms of Fe could be the basis for ecological niches and drive the observed changes in prokaryotic community composition (Liu et al., 2020) as an acclimation to the supply of phytoplankton-derived organic matter in this naturally fertilized region of the Southern Ocean.

AUTHOR CONTRIBUTIONS

Rui Zhang: Data curation (equal); formal analysis (equal); methodology (equal); visualization (equal); writing – review and editing (supporting). **Pavla Debeljak:** Conceptualization (supporting); data curation (equal); formal analysis (equal); investigation (supporting); methodology (equal); supervision (equal); writing – review and editing (supporting). **Stephane Blain:** Conceptualization (equal); funding acquisition (equal); investigation (equal); project administration (equal); resources (equal); supervision (supporting); validation (supporting); writing – review and editing (supporting). **Ingrid Obernosterer:** Conceptualization (equal); funding acquisition (equal); investigation (equal); project administration (equal); resources (equal); supervision (lead); validation (equal); visualization (equal); writing – original draft (lead); writing – review and editing (lead).

ACKNOWLEDGEMENTS

The authors thank the team of the Technical Division of the Institute of the Sciences of the Universe (DT-INSU) for the design and construction of the mooring for the RAS. The authors thank the captains and the crews of the R/V Marion Dufresne for their support during the deployment and the recovery of the RAS. The project Southern Ocean and Climate (SOCLIM) was supported by the Climate Initiative of the BNP Paribas Foundation, the French Polar Institute (Institut Polaire Paul Emile Victor) and the French program LEFE-CYBER of the CNRS-INSU. The authors thank Yan Liu who carried out the DNA extraction. The authors thank the French Institute of Bioinformatics (IFB; https://www.france-bioinformatique.fr) for providing computing resources. The authors thank to the reviewers for their insightful comments on a previous version of this manuscript. This work is part of the PhD thesis of R.Z. supported by the China Scholarship Council (CSC; No. 202006220057).

CONFLICT OF INTEREST STATEMENT

The authors declare no competing interests.

DATA AVAILABILITY STATEMENT

The data sets generated and analysed during the current study are available in the European Nucleotide Archive (ENA) repository at https://www.ebi.ac.uk/ena under the project ID PRJEB56376.

ORCID

Pavla Debeljak https://orcid.org/0000-0002-5542-0358
Ingrid Obernosterer https://orcid.org/0000-0002-2530-8111

REFERENCES

Andrews, S.C., Robinson, A.K. & Rodríguez-Quiñones, F. (2003) Bacterial iron homeostasis. *FEMS Microbiology Reviews*, 27, 215–237.

Blain, S., Planquette, H., Obernosterer, I. & Guéneuguès, A. (2022) Vertical flux of trace elements associated with lithogenic and biogenic carrier phases in the Southern Ocean. *Global Biogeochemical Cycles*, 36, 5.

Blain, S., Quéguiner, B., Armand, L., Belviso, S., Bombled, B., Bopp, L. et al. (2007) Effect of natural iron fertilization on carbon sequestration in the Southern Ocean. *Nature*, 446, 1070–1074.

Blain, S., Rembauville, M., Crispi, O. & Obernosterer, I. (2021) Synchronized autonomous sampling reveals coupled pulses of biomass and export of morphologically different diatoms in the Southern Ocean. *Limnology & Oceanography*, 66, 753–764.

Blain, S., Sarthou, G. & Laan, P. (2008) Distribution of dissolved iron during the natural iron-fertilization experiment KEOPS (Kerguelen Plateau, Southern Ocean). *Deep Sea Research Part II: Topical Studies in Oceanography*, 55, 594–605.

Bolger, A.M., Lohse, M. & Usadel, B. (2014) Trimmomatic: a flexible trimmer for Illumina sequence data. *Bioinformatics*, 30, 2114–2120.

Christaki, U., Gueneugues, A., Liu, Y., Blain, S., Catala, P., Colombet, J. et al. (2021) Seasonal microbial food web dynamics in contrasting Southern Ocean productivity regimes. *Limnology and Oceanography*, 66, 108–122.

Cordero, O.X., Ventouras, L.-A., DeLong, E.F. & Polz, M.F. (2012) Public good dynamics drive evolution of iron acquisition strategies in natural bacterioplankton populations. *Proceedings of the National Academy of Sciences United States of America*, 109, 20059–20064.

Debeljak, P., Blain, S., Bowie, A., Merwe, P., Bayer, B. & Obernosterer, I. (2021) Homeostasis drives intense microbial trace metal processing on marine particles. *Limnology & Oceanography*, 66, 3842–3855.

Debeljak, P., Toulza, E., Beier, S., Blain, S. & Obernosterer, I. (2019) Microbial iron metabolism as revealed by gene expression profiles in contrasted Southern Ocean regimes. *Environmental Microbiology*, 21, 2360–2374.

Dinasquet, J., Landa, M. & Obernosterer, I. (2022) SAR11 clade microdiversity and activity during the early spring blooms off Kerguelen Island, Southern Ocean. *Environmental Microbiolgy Reports*, 1758-2229, 13117–13916.

Eren, A.M., Esen, Ö.C., Quince, C., Vineis, J.H., Morrison, H.G., Sogin, M.L. et al. (2015) Anvi'o: an advanced analysis and visualization platform for 'omics data. *PeerJ*, 3, e1319.

Fourquez, M., Beier, S., Jongmans, E., Hunter, R. & Obernosterer, I. (2016) Uptake of leucine, chitin, and iron by prokaryotic groups during spring phytoplankton blooms induced by natural iron fertilization off Kerguelen Island (Southern Ocean). *Frontiers in Marine Science*, 3, 256.

Fourquez, M., Obernosterer, I., Davies, D.M., Trull, T.W. & Blain, S. (2015) Microbial iron uptake in the naturally fertilized waters in the vicinity of the Kerguelen Islands: phytoplankton–bacteria interactions. *Biogeosciences*, 12, 1893–1906.

Francis, B., Urich, T., Mikolasch, A., Teeling, H. & Amann, R. (2021) North Sea spring bloom-associated Gammaproteobacteria fill diverse heterotrophic niches. *Environmental Microbiome*, 16, 15.

Francis, T.B., Bartosik, D., Sura, T., Sichert, A., Hehemann, J.-H., Markert, S. et al. (2021) Changing expression patterns of TonB-dependent transporters suggest shifts in polysaccharide consumption over the course of a spring phytoplankton bloom. *The ISME Journal*, 15, 2336–2350.

Garber, A.I., Nealson, K.H., Okamoto, A., McAllister, S.M., Chan, C. S., Barco, R.A. et al. (2020) FeGenie: a comprehensive tool for the identification of iron genes and iron gene neighborhoods in genome and metagenome assemblies. *Frontiers in Microbiology*, 11, 37.

Garcia, C.A., Hagstrom, G.I., Larkin, A.A., Ustick, L.J., Levin, S.A., Lomas, M.W. et al. (2020) Linking regional shifts in microbial genome adaptation with surface ocean biogeochemistry. *Philosophical Transactions of the Royal Society B: Biological Sciences*, 375, 20190254.

Giovannoni, S.J. (2017) SAR11 bacteria: the most abundant plankton in the oceans. *Annual Review of Marine Science*, 9, 231–255.

Hernandez-Magana, A.E., Liu, Y., Debeljak, P., Crispi, O., Marie, B., Koedooder, C. et al. (2021) Prokaryotic diversity and activity in contrasting productivity regimes in late summer in the Kerguelen region (Southern Ocean). *Journal of Marine Systems*, 221, 103561.

Hogle, S.L., Brahamsha, B. & Barbeau, K.A. (2017) Direct heme uptake by phytoplankton-associated *Roseobacter* bacteria. *mSystems*, 2, e00124-16.

Hogle, S.L., Hackl, T., Bundy, R.M., Park, J., Satinsky, B., Hiltunen, T. et al. (2022) Siderophores as an iron source for picocyanobacteria in deep chlorophyll maximum layers of the oligotrophic ocean. *The ISME Journal*, 16, 1636–1646.

Hogle, S.L., Thrash, J.C., Dupont, C.L. & Barbeau, K.A. (2016) Trace metal acquisition by marine heterotrophic bacterioplankton with contrasting trophic strategies. *Applied and Environmental Microbiology*, 82, 1613–1624.

Honey, D., Gledhill, M., Bibby, T., Legiret, F., Pratt, N., Hickman, A. et al. (2013) Heme b in marine phytoplankton and particulate material from the North Atlantic Ocean. *Marine Ecology Progress Series*, 483, 1–17.

Hopkinson, B.M. & Barbeau, K.A. (2012) Iron transporters in marine prokaryotic genomes and metagenomes: iron transporters in marine prokaryotes. *Environmental Microbiology*, 14, 114–128.

Hyatt, D., Chen, G.-L., LoCascio, P.F., Land, M.L., Larimer, F.W. & Hauser, L.J. (2010) Prodigal: prokaryotic gene recognition and translation initiation site identification. *BMC Bioinformatics*, 11, 119.

Kalinowski, B.E., Liermann, L.J., Givens, S. & Brantley, S.L. (2000) Rates of bacteria-promoted solubilization of Fe from minerals: a review of problems and approaches. *Chemical Geology*, 169, 357–370.

Kappelmann, L., Krüger, K., Hehemann, J.-H., Harder, J., Markert, S., Unfried, F. et al. (2019) Polysaccharide utilization loci of North Sea Flavobacteriia as basis for using SusC/D-protein expression for predicting major phytoplankton glycans. *The ISME Journal*, 13, 76–91.

Kim, D., Song, L., Breitwieser, F.P. & Salzberg, S.L. (2016) Centrifuge: rapid and sensitive classification of metagenomic sequences. *Genome Research*, 26, 1721–1729.

Landa, M., Blain, S., Christaki, U., Monchy, S. & Obernosterer, I. (2016) Shifts in bacterial community composition associated with increased carbon cycling in a mosaic of phytoplankton blooms. *The ISME Journal*, 10, 39–50.

Langmead, B. & Salzberg, S.L. (2012) Fast gapped-read alignment with Bowtie 2. *Nature Methods*, 9, 357–359.
Li, D., Liu, C.-M., Luo, R., Sadakane, K. & Lam, T.-W. (2015) MEGAHIT: an ultra-fast single-node solution for large and complex metagenomics assembly via succinct de Bruijn graph. *Bioinformatics*, 31, 1674–1676.
Li, H., Handsaker, B., Wysoker, A., Fennell, T., Ruan, J., Homer, N. et al. (2009) The Sequence Alignment/Map format and SAMtools. *Bioinformatics*, 25, 2078–2079.
Li, W. & Godzik, A. (2006) Cd-hit: a fast program for clustering and comparing large sets of protein or nucleotide sequences. *Bioinformatics*, 22, 1658–1659.
Liu, Y., Blain, S., Crispi, O., Rembauville, M. & Obernosterer, I. (2020) Seasonal dynamics of prokaryotes and their associations with diatoms in the Southern Ocean as revealed by an autonomous sampler. *Environmental Microbiology*, 22, 3968–3984.
Manck, L.E., Park, J., Tully, B.J., Poire, A.M., Bundy, R.M., Dupont, C.L. et al. (2022) Petrobactin, a siderophore produced by Alteromonas, mediates community iron acquisition in the global ocean. *The ISME Journal*, 16, 358–369.
Mazzotta, M.G., McIlvin, M.R. & Saito, M.A. (2020) Characterization of the Fe metalloproteome of a ubiquitous marine heterotroph, *Pseudoalteromonas* (BB2-AT2): multiple bacterioferritin copies enable significant Fe storage. *Metallomics*, 12, 654–667.
Mikheenko, A., Saveliev, V. & Gurevich, A. (2016) MetaQUAST: evaluation of metagenome assemblies. *Bioinformatics*, 32, 1088–1090.
Moran, M.A., Kujawinski, E.B., Stubbins, A., Fatland, R., Aluwihare, L.I., Buchan, A. et al. (2016) Deciphering Ocean carbon in a changing world. *Philosophical Transactions of the Royal Society B: Biological Sciences*, 113, 3143–3151.
Nurk, S., Meleshko, D., Korobeynikov, A. & Pevzner, P.A. (2017) metaSPAdes: a new versatile metagenomic assembler. *Genome Research*, 27, 824–834.
Obernosterer, I., Fourquez, M. & Blain, S. (2015) Fe and C co-limitation of heterotrophic bacteria in the naturally fertilized region off the Kerguelen Islands. *Biogeosciences*, 12, 1983–1992.
Parks, D.H., Chuvochina, M., Rinke, C., Mussig, A.J., Chaumeil, P.-A. & Hugenholtz, P. (2022) GTDB: an ongoing census of bacterial and archaeal diversity through a phylogenetically consistent, rank normalized and complete genome-based taxonomy. *Nucleic Acids Research*, 50, D785–D794.
Parks, D.H., Imelfort, M., Skennerton, C.T., Hugenholtz, P. & Tyson, G.W. (2015) CheckM: assessing the quality of microbial genomes recovered from isolates, single cells, and metagenomes. *Genome Research*, 25, 1043–1055.
Patro, R., Duggal, G., Love, M.I., Irizarry, R.A. & Kingsford, C. (2017) Salmon provides fast and bias-aware quantification of transcript expression. *Nature Methods*, 14, 417–419.
Payne, S.M., Mey, A.R. & Wyckoff, E.E. (2016) Vibrio iron transport: evolutionary adaptation to life in multiple environments. *Microbiology and Molecular Biology Reviews*, 80, 69–90.
Pellichero, V., Boutin, J., Claustre, H., Merlivat, L., Sallée, J. & Blain, S. (2020) Relaxation of wind stress drives the abrupt onset of biological carbon uptake in the Kerguelen bloom: a multisensor approach. *Geophysical Research Letters*, 47, 9.
Quéroué, F., Sarthou, G., Planquette, H.F., Bucciarelli, E., Chever, F., van der Merwe, P. et al. (2015) High variability in dissolved iron concentrations in the vicinity of the Kerguelen Islands (Southern Ocean). *Biogeosciences*, 12, 3869–3883.
Roe, K.L., Hogle, S.L. & Barbeau, K.A. (2013) Utilization of heme as an iron source by marine Alphaproteobacteria in the Roseobacter clade. *Applied and Environmental Microbiology*, 79, 5753–5762.
Saier, M.H. (2006) TCDB: the Transporter Classification Database for membrane transport protein analyses and information. *Nucleic Acids Research*, 34, D181–D186.
Saito, M.A., McIlvin, M.R., Moran, D.M., Goepfert, T.J., DiTullio, G.R., Post, A.F. et al. (2014) Multiple nutrient stresses at intersecting Pacific Ocean biomes detected by protein biomarkers. *Science*, 345, 1173–1177.
Sarthou, G., Vincent, D., Christaki, U., Obernosterer, I., Timmermans, K.R. & Brussaard, C.P.D. (2008) The fate of biogenic iron during a phytoplankton bloom induced by natural fertilisation: impact of copepod grazing. *Deep Sea Research Part II: Topical Studies in Oceanography*, 55, 734–751.
Schalk, I.J., Rigouin, C. & Godet, J. (2020) An overview of siderophore biosynthesis among fluorescent Pseudomonads and new insights into their complex cellular organization. *Environmental Microbiology*, 22, 1447–1466.
Sun, Y., Debeljak, P. & Obernosterer, I. (2021) Microbial iron and carbon metabolism as revealed by taxonomy-specific functional diversity in the Southern Ocean. *The ISME Journal*, 15, 2933–2946.
Tagliabue, A., Bowie, A.R., Boyd, P.W., Buck, K.N., Johnson, K.S. & Saito, M.A. (2017) The integral role of iron in ocean biogeochemistry. *Nature*, 543, 51–59.
Teeling, H., Fuchs, B.M., Becher, D., Klockow, C., Gardebrecht, A., Bennke, C.M. et al. (2012) Substrate-controlled succession of marine bacterioplankton populations induced by a phytoplankton bloom. *Science*, 336, 608–611.
Toulza, E., Tagliabue, A., Blain, S. & Piganeau, G. (2012) Analysis of the Global Ocean Sampling (GOS) project for trends in iron uptake by surface ocean microbes. *PLoS One*, 7, e30931.
Ustick, L.J., Larkin, A.A., Garcia, C.A., Garcia, N.S., Brock, M.L., Lee, J.A. et al. (2021) Metagenomic analysis reveals global-scale patterns of ocean nutrient limitation. *Science*, 372, 287–291.
West, N.J., Obernosterer, I., Zemb, O. & Lebaron, P. (2008) Major differences of bacterial diversity and activity inside and outside of a natural iron-fertilized phytoplankton bloom in the Southern Ocean. *Environmental Microbiology*, 10, 738–756.
Xing, P., Hahnke, R.L., Unfried, F., Markert, S., Huang, S., Barbeyron, T. et al. (2015) Niches of two polysaccharide-degrading Polaribacter isolates from the North Sea during a spring diatom bloom. *The ISME Journal*, 9, 1410–1422.
Yoon, S.-H., Ha, S., Lim, J., Kwon, S. & Chun, J. (2017) A large-scale evaluation of algorithms to calculate average nucleotide identity. *Antonie Van Leeuwenhoek*, 110, 1281–1286.
Zhang, H., Yohe, T., Huang, L., Entwistle, S., Wu, P., Yang, Z. et al. (2018) dbCAN2: a meta server for automated carbohydrate-active enzyme annotation. *Nucleic Acids Research*, 46, W95–W101.

SUPPORTING INFORMATION

Additional supporting information can be found online in the Supporting Information section at the end of this article.

How to cite this article: Zhang, R., Debeljak, P., Blain, S. & Obernosterer, I. (2023) Seasonal shifts in Fe-acquisition strategies in Southern Ocean microbial communities revealed by metagenomics and autonomous sampling. *Environmental Microbiology*, 25(10), 1816–1829. Available from: https://doi.org/10.1111/1462-2920.16397

Supplementary material

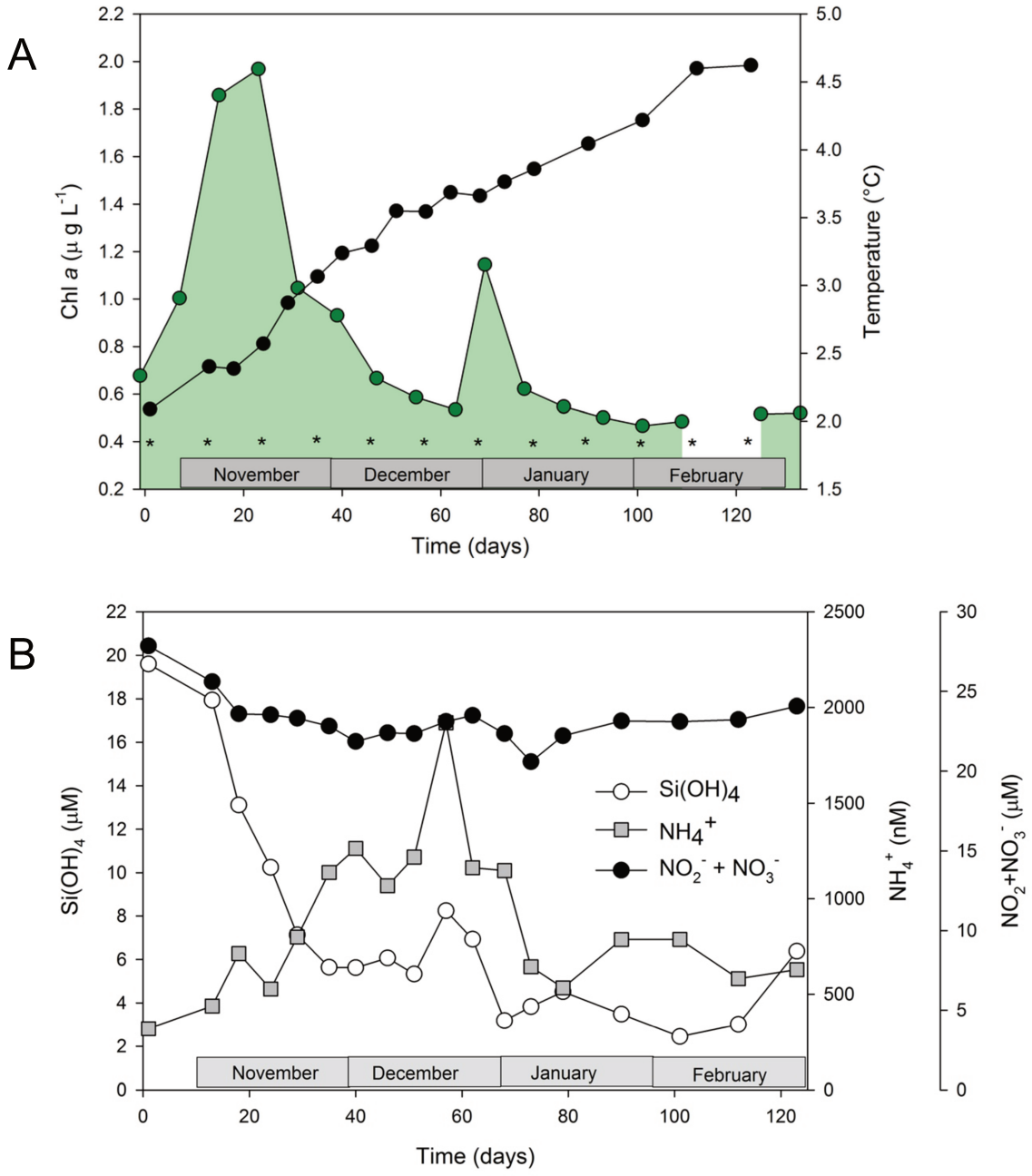

Figure S1. A. Temporal changes of Chlorophyll a (green shaded area) and temperature (black circles) during the period of RAS deployment. B. Temporal changes of silicic acid ($Si(OH)_4$), ammonium (NH^{4+}) and nitrite+nitrate ($NO^{2-} + NO^{3-}$) during the period of sampling (25 October 2016 to 24 February 2017). Data are from Liu *et al*. (Liu *et al.*, 2020).

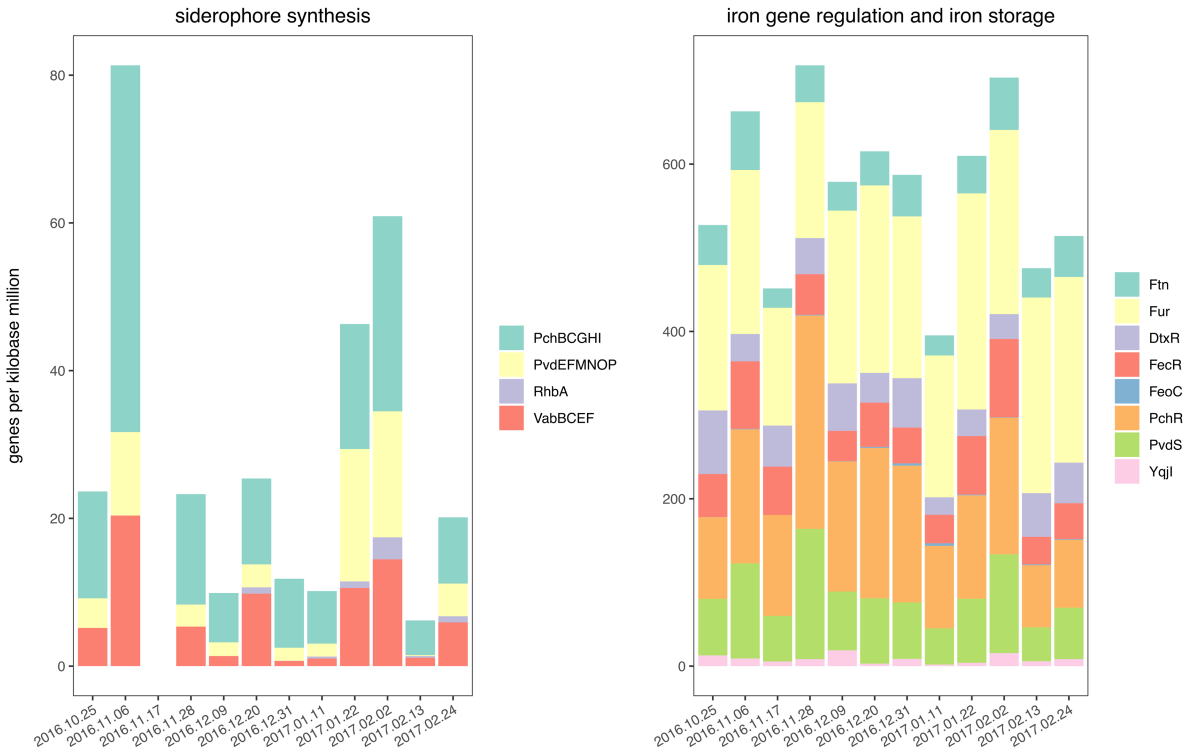

Figure S2. Abundance of genes related to siderophore synthesis, iron gene regulation and storage at the 12 time points. Gene abundance is represented by genes per kilobase million (GPM).

Figure S3. Abundance of individual genes related to heme oxygenase, heme transport, iron transport, siderophore synthesis, siderophore transport, iron gene regulation and storage at the 12 time points. Gene abundance is represented by genes per kilobase million (GPM).

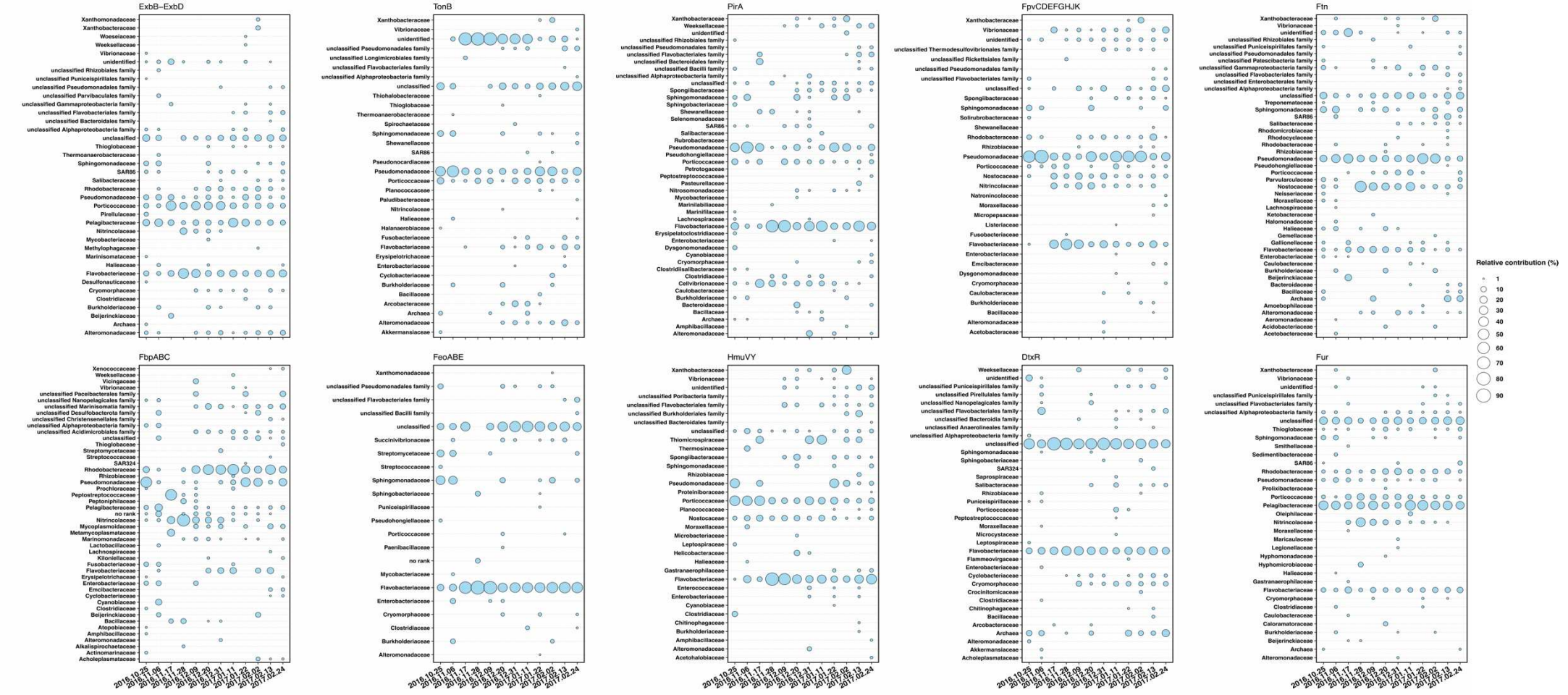

Figure S4. Relative contribution of prokaryotic groups to specific genes associated with $Fe^{3+}$and Fe^{2+} ions, heme and siderophore transport. Prokaryotic groups are based on family level.

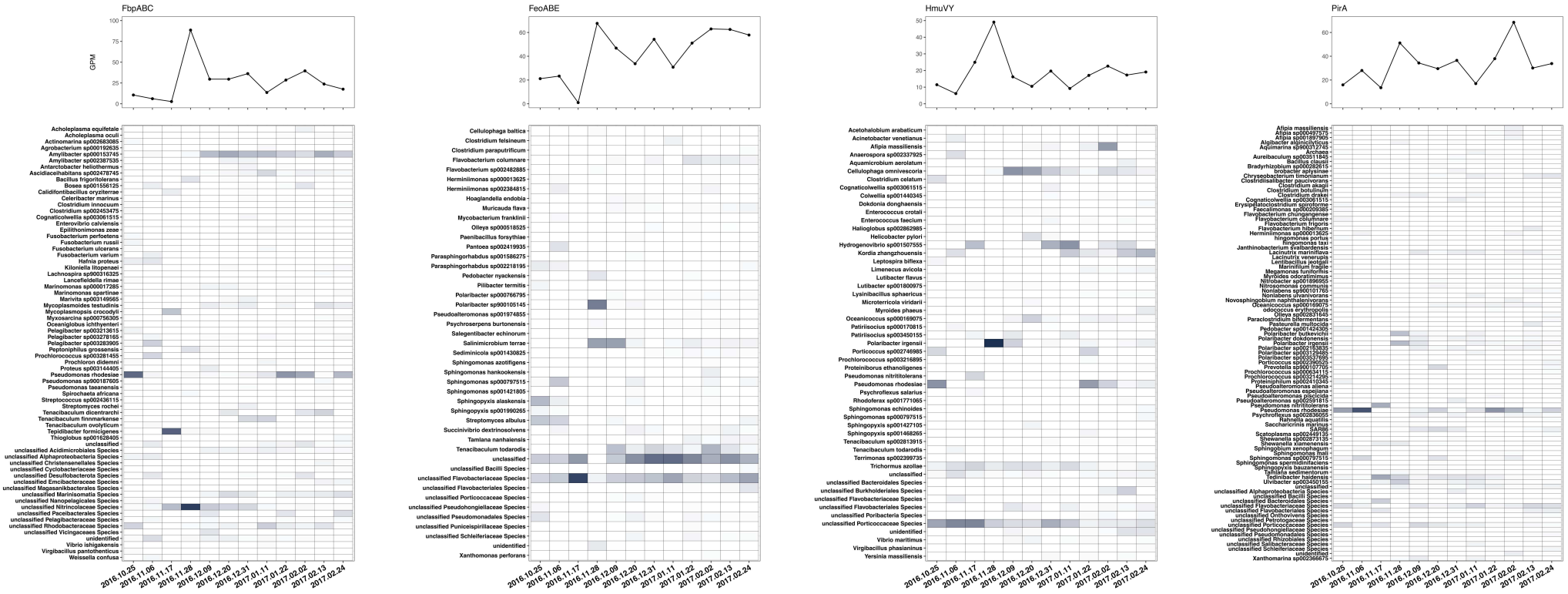

Figure S5. Temporal changes of normalized gene abundance (GPM) and relative contribution of prokaryotic groups to specific genes associated with $Fe^{3+}$and Fe^{2+} ions, heme and siderophore transport. Taxonomic assignments are based on the species level.

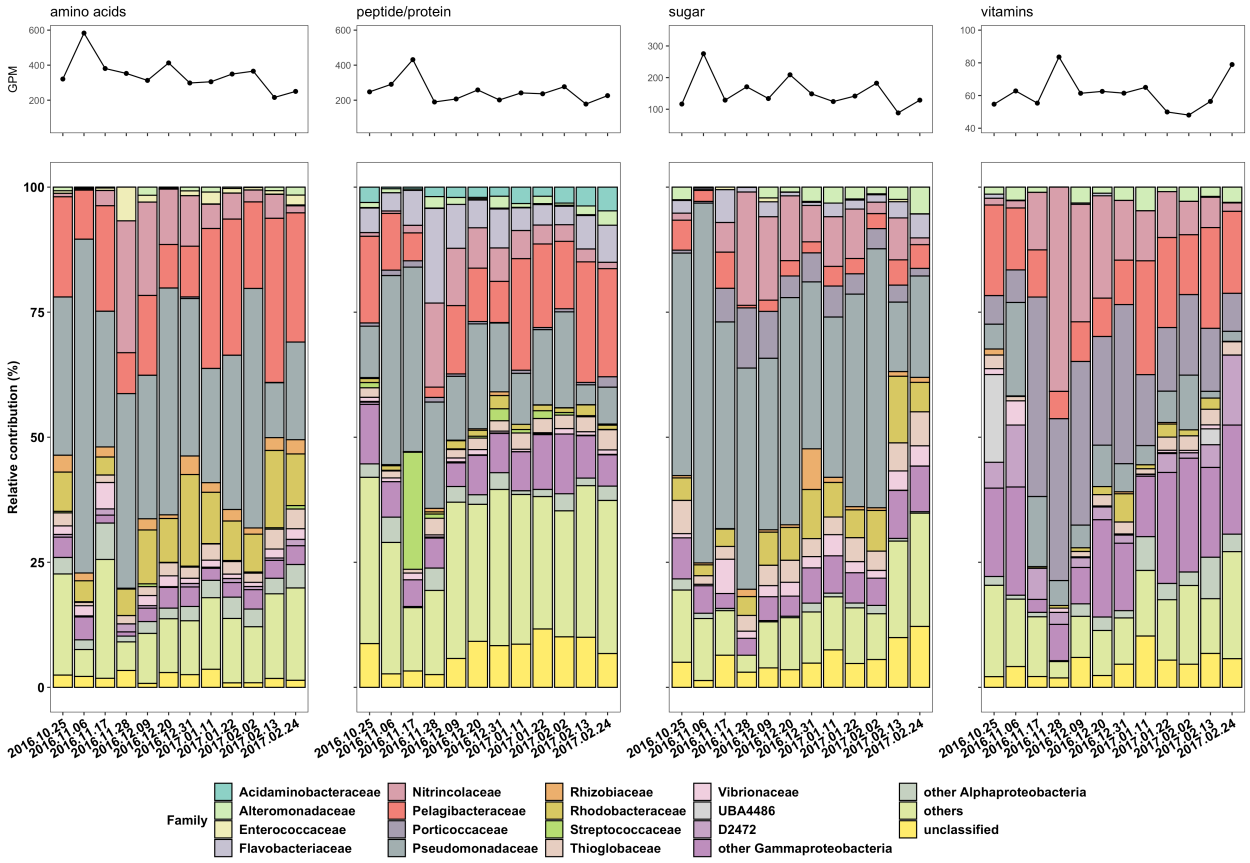

Figure S6. Temporal changes of normalized gene abundance (GPM) and relative contribution of prokaryotic groups to specific genes associated with organic substrate transporters. Prokaryotic groups are based on the family level.

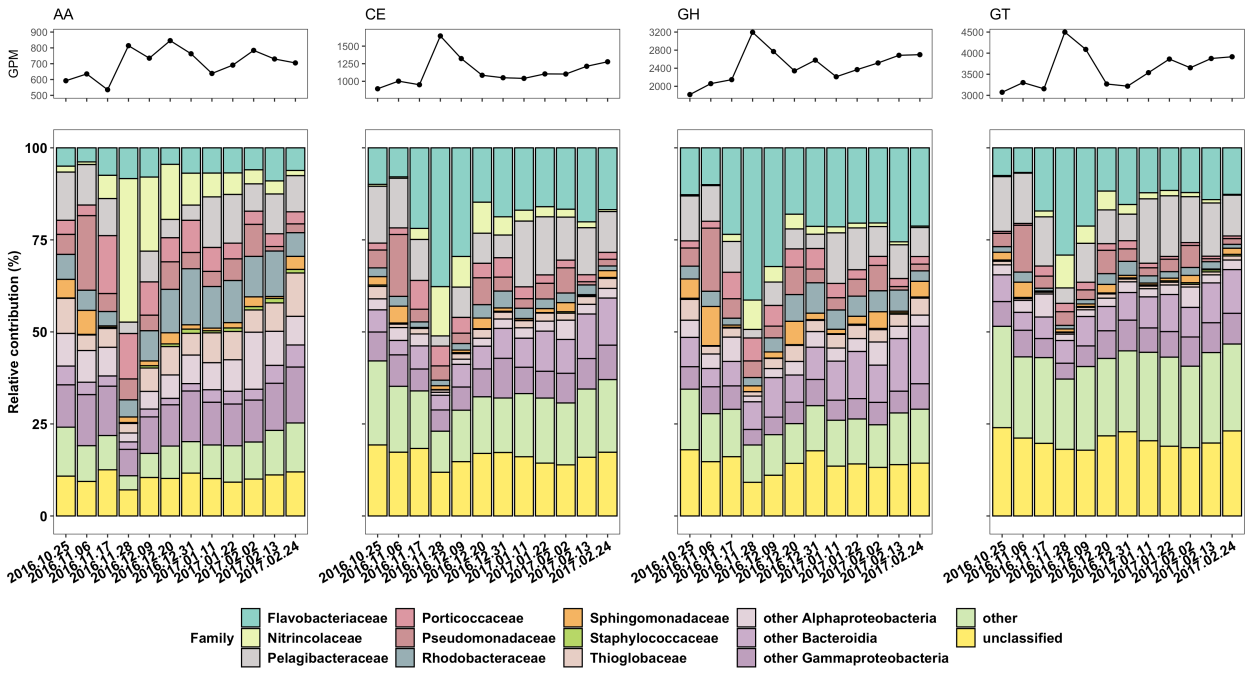

Figure S7. Temporal changes of normalized gene abundance (GPM) and relative contribution of prokaryotic groups to specific genes associated with CAZymes. Prokaryotic groups are based on the family level.

Table S1. Sequencing information

Samples	Sampling date	Number of paired reads	Size in Mb
AFQF-48	2016.10.25	63778294	19133
AFQF-49	2016.11.06	71480812	21443
AFQF-50	2016.11.17	59318585	17794
AFQF-51	2016.11.28	67938556	20381
AFQF-52	2016.12.09	82243763	24672
AFQF-53	2016.12.20	83432464	25029
AFQF-54	2016.12.31	82312116	24693
AFQF-55	2017.01.11	69349995	20804
AFQF-56	2017.01.22	78128006	23437
AFQF-57	2017.02.02	71959548	21587
AFQF-58	2017.02.13	77098475	23128
AFQF-59	2017.02.24	72339662	21701

Table S2. The result of metagenome assembly using MEGAHIT and metaSPAdes

Samples	Contigs[1]	Average len. (bp)[1]	N50 len. (bp)[1]*	Contigs[2]	Average len. (bp)[2]	N50 len. (bp)[2]*
AFQF-48	874699	630	1110	1285537	465	936
AFQF-49	777516	674	1190	1139395	496	971
AFQF-50	211989	684	1183	356050	457	931
AFQF-51	163698	767	1882	300133	505	1379
AFQF-52	790640	693	1274	1102283	525	1109
AFQF-53	815239	709	1461	1168811	529	1190
AFQF-54	1047771	737	1567	1299701	596	1392
AFQF-55	502376	685	1299	860516	460	958
AFQF-56	1527120	684	1296	1774089	566	1195
AFQF-57	958096	680	1333	1200534	544	1201
AFQF-58	1520326	676	1295	1664748	577	1245
AFQF-59	954652	676	1428	1399578	519	1101

* are based on contigs of size >= 500 bp

1 are based on the result of metagenome assembly using MEGAHIT

2 are based on the result of metagenome assembly using metaSPAdes

Table S3. The result of ORF calling on individual assemblies

Samples	Total number of predicted proteins
AFQF-48	1222967
AFQF-49	1118516
AFQF-50	306892
AFQF-51	246170
AFQF-52	1157204
AFQF-53	1194864
AFQF-54	1566689
AFQF-55	725137
AFQF-56	2218886
AFQF-57	1383251
AFQF-58	2190695
AFQF-59	1376380

Table S4. List of iron related genes

Table S5. Statistics and taxonomy assignment of the metagenome-assembled genomes (MAGs)

Table S4 and Table S5 can be found at this link (https://enviromicro-journals.onlinelibrary.wiley.com/doi/abs/10.1111/1462-2920.16397)

Reference

Liu, Y., Blain, S., Crispi, O., Rembauville, M., and Obernosterer, I. (2020) Seasonal dynamics of prokaryotes and their associations with diatoms in the Southern Ocean as revealed by an autonomous sampler. *Environ Microbiol* **22**: 3968–3984.

Chapter 2

Tagging of water masses with covariance of trace metals and prokaryotic taxa in the Southern Ocean

Rui Zhang[1], Stéphane Blain[1], Corentin Baudet[2], Hélène Planquette[2], Frédéric Vivier[3], Philippe Catala[1], Olivier Crispi[1], Audrey Guéneuguès[1], Barbara Marie[1], Pavla Debeljak[4], Ingrid Obernosterer[1*]

Manuscript was accepted by Limnology and Oceanography Letters

[1] CNRS, Sorbonne Université, Laboratoire d'Océanographie Microbienne, LOMIC, F-66650 Banyuls/mer, France.
[2] Université Bretagne Occidentale, CNRS, IRD, Ifremer, UMR 6539, LEMAR, F-29280 Plouzané, France.
[3] LOCEAN-IPSL, CNRS, Sorbonne Université, Paris, France.
[4] Sorbonne Université, Muséum National d'Histoire Naturelle, CNRS, EPHE, Université des Antilles, Institut de Systématique, Evolution, Biodiversité (ISYEB), F-75005, Paris, France.

[*] Corresponding author

Preface

This thesis chapter is part of the South Indian Ocean GEOTRACES Section (SWINGS) project. I collected the seawater samples, and performed the DNA extractions and conducted all bioinformatic analysis. For this chapter, water masses were identified by Frédéric Vivier, the trace metal data were provided by Corentin Baudet and Hélène Planquette, the data of cell abundance, major nutrients and DOC were provided by Philippe Catala, Olivier Crispi, Audrey Guéneuguès and Barbara Marie.

Abstract

Marine microbes are strongly interrelated to trace metals in the ocean. How the availability of trace metals selects for prokaryotic taxa and the potential feedbacks of microbial processes on the trace metal distribution in the ocean remains poorly understood. We investigate here the potential reciprocal links between diverse prokaryotic taxa and iron (Fe), manganese (Mn), copper (Cu), Nickel (Ni) as well as apparent oxygen utilization (AOU) across 12 well-defined water masses in the Southern Indian Ocean (SWINGS- South West Indian Ocean GEOTRACES GS02 Section cruise). Applying Partial Least Square Regression (PLSR) analysis we show that the water masses are associated with particular latent vectors that are a combination of the spatial distribution of prokaryotic taxa, trace elements and AOU. This approach provides novel insights on the potential interactions between prokaryotic taxa and trace metals in relation to organic matter remineralization in distinct water masses of the ocean.

Introduction

The ocean is a dynamical system where hydrological features shape the seascape at multiple scales (Kavanaugh et al. 2014). Hydrographically defined water masses can constrain biogeochemical processes resulting in vertical or horizontal gradients of major nutrients and trace metals (Jenkins et al. 2015). In parallel, the composition of microbial communities that are key mediators in nutrient cycling, varies among ocean basins and along geographical ranges and depth layers (Galand et al. 2010; Agogué et al. 2011; Salazar et al. 2016; Raes et al. 2018; Liu et al. 2019; Sow et al. 2022). Frontal systems, upwelling and mesoscale eddies can structure community composition on a regional scale (Baltar et al. 2010; Lekunberri et al. 2013; Hernando-Morales et al. 2017). Specific hydrographic and biogeochemical properties, among which the concentration of major nutrients, were identified as factors with potential reciprocal influence on these biogeographic patterns in the ocean (Hanson et al. 2012).

Trace metals, such as iron (Fe), manganese (Mn), nickel (Ni) and copper (Cu), play crucial roles in microbial growth and metabolism (Morel and Price 2003) and are therefore important micronutrients (Lohan and Tagliabue 2018). In heterotrophic prokaryotes, Fe is essential in the respiratory chain (Andrews et al. 2003), thus Fe availability affects the processing of organic carbon (Fourquez et al. 2014). Mn (II) serves as a cofactor for various enzymes involved in the central carbon metabolism and in antioxidant activity (Hansel 2017). Ni has been identified as an indispensable element for nitrogen fixation (Glass and Dupont 2017) and for chemolithotrophic prokaryotes (Gikas 2008). Cu acts as a cofactor for numerous proteins involved in redox reactions, oxidative respiration, denitrification, and other processes (Argüello et al. 2013). Cu deficiency can affect microbial growth of some prokaryotic taxa, but certain concentrations of dissolved Cu can also be toxic to heterotrophic prokaryotes or phytoplankton in the ocean (Moffett et al. 1997; Debelius et al. 2011, Posacka et al. 2019).

The biological roles of Fe, Ni and Cu result in nutrient like vertical profiles in the offshore ocean with low concentrations in surface waters due to biological uptake by auto- and heterotrophic microbes, and increases with depth due to remineralization of sinking material. The magnitude of these uptake and remineralization processes is tightly linked to the composition of the microbial community and its metabolic capabilities. The expected nutrient like profile is not observed for Mn due to the photoproduction of the soluble form of Mn (II) in surface waters and the biologically mediated production of insoluble MnOx at depth (Sunda et al. 1983). Adding to this complexity, transport and mixing largely influence the

large-scale distribution of these trace metals (Thi Dieu Vu and Sohrin 2013; Latour et al. 2021; Chen et al. 2023). The GEOTRACES program has made major advances in the determination of the trace metal content of water masses across the global ocean, but the interplay with the microbial community remains to date poorly understood. In this context, the main objective of the present study was to investigate the potential interactive effect between trace elements and microbes, and how these could influence chemical and biological water-mass specific properties across 12 well-defined water masses in the Southern Indian Ocean (SWINGS- South West Indian Ocean Geotraces Section cruise, GEOTRACES GS02 section).

Materials and methods

Environmental context

Samples were collected during the SWINGS cruise between January 10 and March 8 2021. The 23 stations sampled for the present study (Fig. 1A) were located in the Subtropical Zone (STZ) (Station 2, 3, 5, 8, 11), Subantarctic Zone (SAZ) (Station 14, 15, 16, 38), the Polar Frontal Zone (PFZ) (Station 21, 25, 31, 33, 36), and the Antarctic Zone (AAZ) (29, 30, 42, 44, 45, 46, 58, 63, 68). Surface water (20m) sampled at each of these stations are assigned to these geographical zones, and the samples below the mixed layer were categorized into 12 water masses according to their physicochemical properties (Fig. 1B). Water masses were identified at each station from the vertical profile of physical properties (Fig. S1) and geographical considerations, in particular the location of main Southern Ocean fronts as determined by Park et al (Park et al. 2019). The most abundant water masses of the Southern Ocean were identified from their neutral density, γ^n (Orsi et al. 1999; Bindoff and McDougall 2000; Talley et al. 2011), with highest values in water masses close to the bottom decreasing upwards; Antarctic Bottom Water (AABW, $\gamma^n > 28.27$ kg m^{-3}), Lower Circumpolar Deep Water (LCDW, $\gamma^n > 27.8$), Upper Circumpolar Deep Water (UCDW, $\gamma^n > 27.5$) and Antarctic Intermediate Water (AAIW, $\gamma^n > 27.2$). Within the LCDW density range, the presence of North Atlantic Deep Water (NADW) was determined from the salinity criterion S> 34.8 (Park et al. 1993, 2001). In the Aghulas Current sector, Arabian Sea Low Oxygen Water (ASLOW) was identified as a low-oxygen (< 165 μmol/kg) subsurface layer near $\gamma^n = 25.5$, whereas Red Sea Overflow Water (RSOW) was identified as interleaving saline layers within the AAIW salinity minimum, following Beal et al (Beal et al. 2006). The presence of mode waters (STMW) was assessed from the detection of a homogeneous low-potential vorticity layer in their corresponding density range.

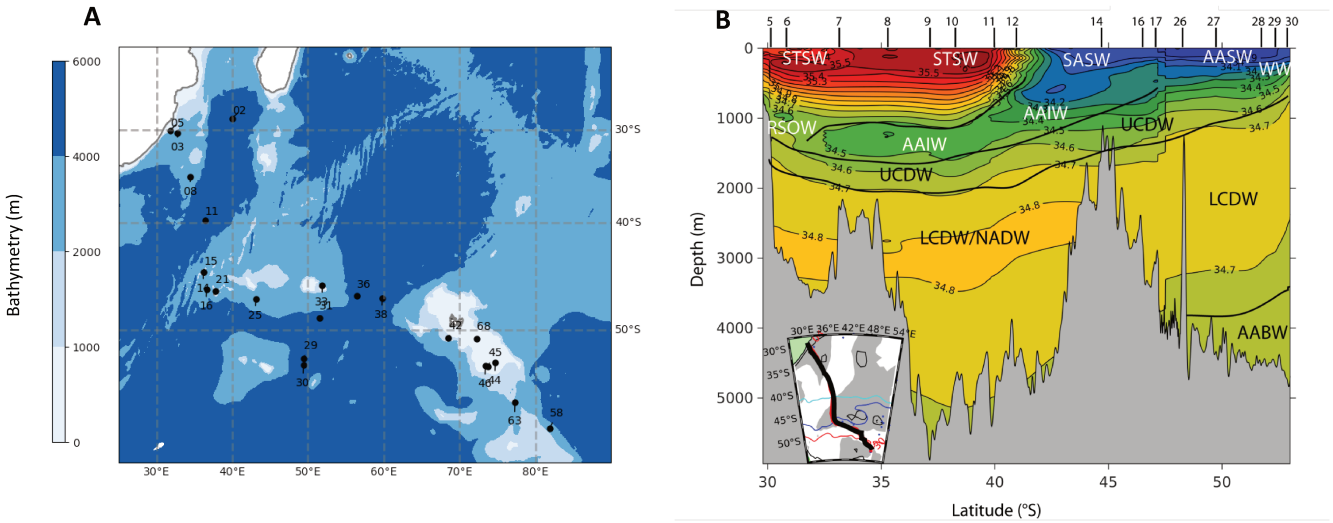

Fig.1. A. Map of stations sampled for the present study during the SWINGS cruise in the Indian Sector of the Southern Ocean. Color shading represents bathymetry and the black line contours South Africa (25°- 35° E) and Madagascar (45°-50°E). B. A cross-section (inserted map) showing the vertical distribution of some water masses sampled at the stations indicated on the upper x-axis. Lines indicate salinity. STSW, Subtropical Surface Water; SASW, Sub Antarctic Surface Water; ASW, Antarctic Surface Water; WW, Winter water; AAIW, Antarctic Intermediate Water; RSOW, Red Sea Overflow Water; UCDW, Upper Circumpolar Deep Water; LCDW, Lower Circumpolar Deep Water; LCDW/NADW, Lower Circumpolar Deep Water/ North Atlantic Deep Water; AABW, Antarctic Bottom Water. The full list of water masses is provided in Fig. 2.

All seawater samples dedicated to microbial community composition were collected using 12 L Niskin bottles mounted on a rosette equipped with conductivity, temperature and depth (CTD) sensors (SeaBird SBE911plus). Seawater (6L) was sequentially passed through 0.8 µm polycarbonate (PC) filters (47 mm diameter, Nuclepore, Whatman, Sigma Aldrich, St Louis, MO) and 0.22 µm Sterivex filter units (Sterivex, Millipore, EMD, Billerica, MA). The cells concentrated on the 0.8 µm filters were considered particle-attached (PA) and those on the 0.22 µm filters as free-living (FL). The filters were stored at -80°C until returned to the home laboratory for DNA extraction. Sample collection, preservation and analyses of major nutrients, trace elements and dissolved oxygen were determined using standard protocols and are described in the Supplemental Methods and data are available under doi https://doi.org/10.17882/99983.

DNA extraction and sequencing

Total DNA was extracted from the 0.8 µm filters and the 0.22 µm Sterivex filter units using the DNeasy PowerWater Kit (Qiagen) according to the manufacturer's instructions with a few modifications described in the Supplementary Methods. The V4–V5 region of the 16S rRNA gene was amplified using primer sets 515F-Y (5'-GTGYCAGCMGCCGCGGTAA) and 926-

R (5'-CCGYCAATTYMTTTRAGTTT) as described elsewhere (Parada et al. 2016), and PCR amplification was performed as described previously (Liu et al. 2020). 16S rRNA gene amplicons were sequenced with Illumina MiSeq V3 2 × 300 bp chemistry at the platform Biosearch Technologies (Berlin, Germany). Data are available in the European Nucleotide Archive (ENA) repository at https://www.ebi.ac.uk/ena under the project ID PRJEB63680.

Data analysis

16S rRNA gene sequences were demultiplexed using the Illumina bcl2fastq v2.20 at the platform Biosearch Technologies (Berlin, Germany). The PCR primers and adapters of 16S rRNA gene sequences were trimmed with cutadapt v1.15. Amplicon sequencing variants (ASV) were produced in R using DADA2 package (v1.24) (Callahan et al. 2016) with the following parameters: truncLen=c(240,210), maxN=0, maxEE=c(3,5), truncQ=2. This pipeline includes the following steps: filter and trim, dereplication, sample inference, merge paired reads and chimera removal. A total of 12,847 unique amplicon sequence variants (ASVs) were obtained from the 172 samples collected (FL and PA prokaryotes combined). Taxonomic assignment of ASVs were performed using the DADA2-formatted SILVA SSU Ref NR99 138 database (Quast et al. 2012). The number of reads per sample varied between 2,633 and 241,954. Singletons and sequences belonging to Eukaryotes, chloroplasts and mitochondria were removed. To obtain the same number of reads for all samples, the dataset was randomly subsampled to 4,493 reads per sample with the function rarefy_even_depth by the Phyloseq package (v1.40) (McMurdie and Holmes 2013) in R. After subsampling 10,138 ASVs were obtained in total, of which 5,847 ASVs from the FL fraction (n=76) and 6,461 ASVs from the PA fraction (n=80).

All statistical analyses were performed using the R 4.2.1 version. Non-metric dimensional scaling (NMDS) ordinations were generated based on Bray–Curtis dissimilarity (Legendre and Gallagher 2001) using the ordinate function in the Phyloseq package. Analysis of similarity (ANOSIM) was performed via the vegan package (v2.6) (Dixon 2003) to test for significant differences in microbial communities between water masses. The dendrograms are based on Bray Curtis dissimilarity using the UPGMA algorithm on Hellinger transformed data (Legendre and Gallagher 2001). To test the association of the FL prokaryotic community composition and environmental factors, Partial-Least-Squares Regression (PLSR) (Guebel and Torres 2013) analysis with cross-validation was performed using pls v2.8 package (Mevik and Wehrens 2007) in R with the relative abundance of abundant ASVs as the Y variables and the environmental factors as the X variables (data are available under doi

https://doi.org/10.17882/99983). Scale-transformation of the data matrix was performed to standardize before data input to the model. The regression coefficients were extracted with the function coef by the pls package in R and the heatmap was generated by pheatmap package (v1.0.12) in R. For the identification of indicator ASVs for surface waters and deep water masses, the IndVal index from the labdsv package (v2.0) (Roberts 2019) in R was used. This index takes into account the specificity, fidelity and relative abundance of the ASVs in the different water masses and surface waters.

Results and discussion

Structuring of microbial communities by water masses

In surface waters microbial communities clustered according to geographical zone and frontal system, and in the subsurface the clustering was driven by water mass (Fig. 2). This spatial structuring was significant for both FL (ANOSIM, R=0.8651, P=0.0001) and PA communities (ANOSIM, R=0.714, P=0.0001). Hierarchical clustering dendrograms and low entanglement values between dendrograms of both size fractions (Fig. S2) further illustrate that the structuring effect of water masses is similar for FL and PA microbial communities. For a given water mass the composition of the microbial communities was, however, significantly different between size fractions (Fig. S3-5 and Suppl. Results), suggesting that factors that are dependent and independent of size fraction together both influence the observed biogeographical patterns. Particles are known to host distinct communities and the nature of the particles can shape the associated prokaryotic assemblages (Baumas and Bizic 2023). Sinking particles were suggested to act as vectors for microbes across the water column (Mestre et al. 2018), an idea that is supported by the about 2-fold lower number of indicator species for a given water mass for the PA (121) as compared to the FL (213) communities (Fig. S6, Table S1-2, and Suppl. Results). Taken together, these observations point to a complex interplay between processes specific to the particle-sphere and habitat-type independent factors, such as temperature or hydrostatic pressure, to shape the prokaryotic community composition.

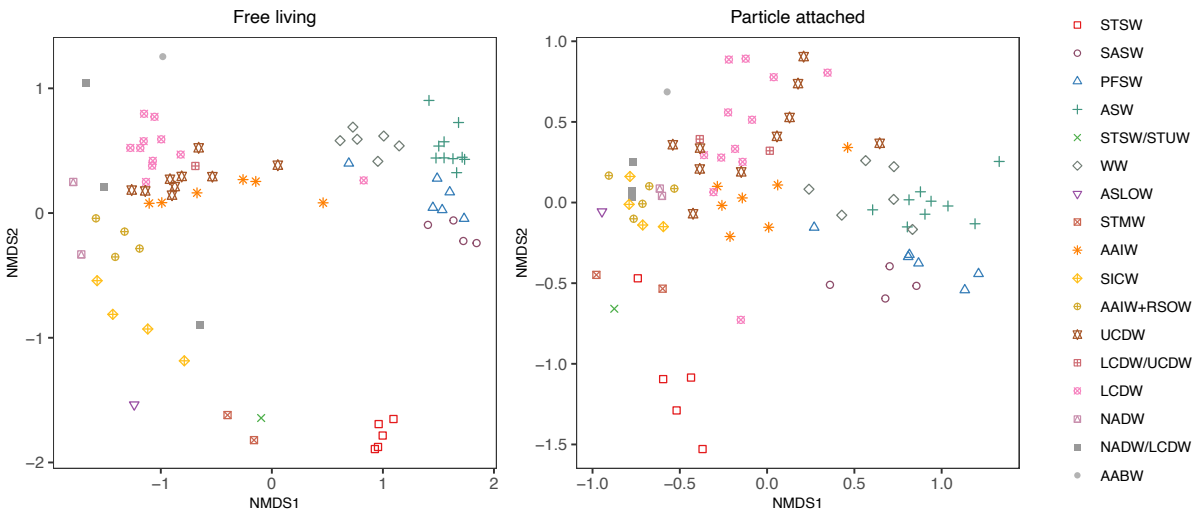

Fig.2. Non-Metric Multidimensional Scaling (NMDS) plots of free-living (FL) and particle-attached (PA) prokaryotic communities based on Bray-Curtis dissimilarity. ANOSIM statistics: FL, R: 0.8651, Significance: 1e-04; PA, R: 0.714, Significance: 1e-04. STSW, Subtropical Surface Water; SASW, Sub Antarctic Surface Water; PFSW, Polar Frontal Surface water; ASW, Antarctic Surface Water; STSW/STUW, Subtropical Surface Water/ Subtropical Underwater; WW, Winter water; ASLOW, Arabian Sea Low Oxygen Water; STMW, Subtropical Mode Water; AAIW, Antarctic Intermediate Water; SICW, South Indian Central Water; AAIW+RSOW, Antarctic Intermediate Water mixed with Red Sea Overflow Water; UCDW, Upper Circumpolar Deep Water; LCDW/UCDW, Lower Circumpolar Deep Water/Upper Circumpolar Deep Water; LCDW, Lower Circumpolar Deep Water; NADW, North Atlantic Deep Water; NADW/LCDW, North Atlantic Deep Water/Lower Circumpolar Deep Water; AABW, Antarctic Bottom Water.

Microbial 'biogeo'gradients

Identifying the factors that select for microbial taxa and understanding the potential feedbacks of microbes on the biogeochemical properties of the water mass they thrive in remains challenging. In this context, the role of trace elements in the ocean interior has, to the best of our knowledge, never been considered. To explore the potential reciprocal links between environmental and microbial parameters, we used Partial Least Square Regression (PLSR, or also Projection of Latent Structure Regression). PLSR is a multivariate regression model based on a simultaneous PCA on two matrices which achieves the best relationships between them (Dunn 2020). An advantage of PLSR is that it prevents the bias of co-linearity a facet not taken into consideration by PCA. PLSR has been successfully applied to determine the ecological vectors associated with carbon flux or trace metal export (Rembauville et al. 2015; Blain et al. 2022), to predict the partitioning of carbon among microbial community members based on bio-optical properties (Rembauville et al. 2017) or to link biodiversity and carbon fluxes (Guidi et al. 2016). We carried out PLSR using only

those available environmental parameters for which a reciprocal influence can be expected, that are the concentrations of the major nutrients nitrate (NO_3^-) and phosphate (PO_4^{3-}), the trace elements manganese (Mn), iron (Fe), nickel (Ni) and copper (Cu), and Apparent Oxygen Utilization (AOU). We considered only ASVs with a relative abundance of ≥ 5% in at least one sample, (22 ASVs, Table S3) as abundant taxa are expected to dominate the interplay with nutrients in different water masses. To confirm this idea, we also performed a PLSR analysis with ASVs with a relative abundance of ≥ 1%. We carried out the PLSR analysis with ASVs in the FL fraction, because the concentrations of major and trace nutrients were only available in the dissolved phase.

The PLSR analysis revealed that the three first latent vectors explained 61%, 16% and 9% of the covariance (Fig. 3A and B; Fig. S7). Therefore, any sample associated with a water mass, which was initially described by 29 variables (7 environmental factors and 22 ASVs) can now be described in a 3-dimensional space. This reduction in complexity facilitates the examination of whether water masses are associated with particular latent vectors which we propose to call microbial 'biogeo'-gradients (BG). These BGs are a combination of the spatial distribution of environmental factors and ASVs. Our results show that BG1 discriminates deep, cold water masses (UCDW, LCDW, AAIW) (negative signs) from warmer and more saline subtropical waters (STSW/STUW, STMW, ASLOW) (positive signs) (Fig. 3C and D). BG2 mainly discriminates WW (negative sign) (Fig. 3C and E). BG3 provides a partitioning between NADW/LCDW and WW (positive sign) and AAIW and UCDW (negative sign) (Fig. 3C and F). The PLSR analysis performed with ASVs ≥ 1% relative abundance (246 ASVs) confirmed this result, as the ASVs with < 5% relative abundance are close to the origin of the latent vector space and thus do not have a strong discriminative power (Fig. S8).

Physical properties of water masses are set by the conditions at the formation and the subsequent transport and mixing in the ocean interior. These abiotic processes, together with additional biotic transformations contribute to structure on the one hand the distribution of environmental parameters (Fig. S9-11; data are available under doi https://doi.org/10.17882/99983) and on the other hand the distribution of prokaryotic taxa as discussed above (Fig. S4-5 and S12). Our observations that BGs are good descriptors of water masses suggest that they provide clues on the possible interactions between environmental factors and prokaryotic taxa that together contribute to the structuring of latent vectors in the 3-dimensional space.

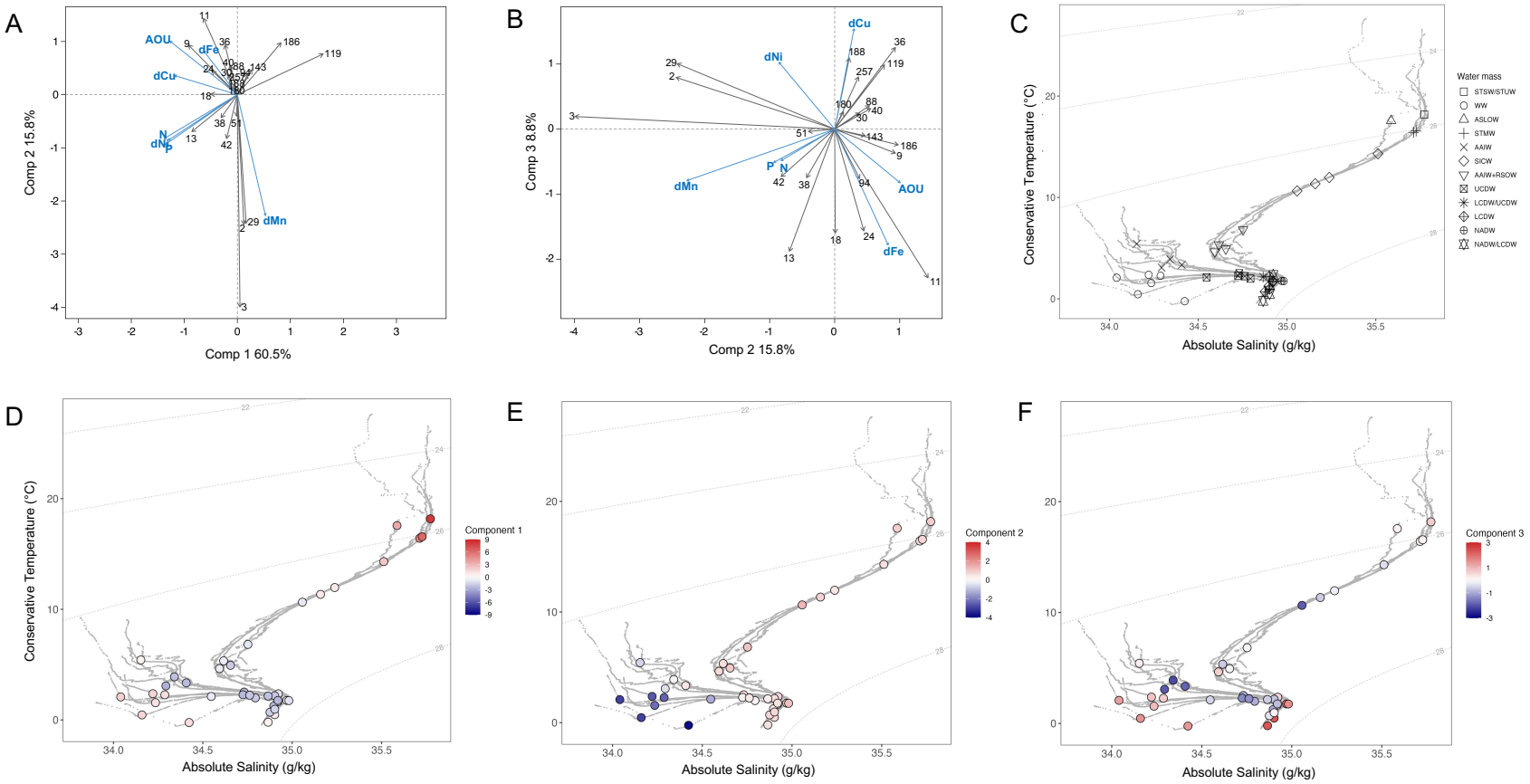

Fig.3. A. Partial least squares regression (PLSR) analysis linking abundant ASVs (relative abundance ⩾ 5% in at least one sample) with environmental variables. Blue labels describe the environmental variables (AOU, apparent oxygen utilization; P, phosphate; N, nitrate; dMn, dissolved manganese; dFe, dissolved iron; dNi, dissolved nickel; dCu, dissolved copper) whereas grey labels describe the ASVs (detailed in Fig. 4). Shown are components 1 and 2. B. Components 2 and 3 of the PLSR analysis C. Temperature-salinity diagram and localization of samples collected in different water masses and used for PLSR. D. Temperature-salinity diagram and localization of samples. The color coding corresponds to the first component of scores of samples extracted from PLSR. E. As for panel C, but the color coding corresponds to the second component of scores of samples extracted from PLSR F. As for panel C, but the color coding corresponds to the third component of scores of samples extracted from PLSR.

We discuss in the following these possible reciprocal feedbacks that are the basis of the nature of the BGs. BG1 is dominated by processes linked to remineralization as indicated by the contribution of AOU (Fig. 3A). Therefore, the gradients of the other contributors to BG1 (Fe, Cu, N, P, Ni, and ASVs) across different water masses could be related to this process. Our analysis highlights several ASVs (9, 11, 13, 18, 24) as potential key drivers of remineralization processes (Fig. 3A). BG2 has a more complex structure because it is defined as a gradient with opposite trends between Fe, AOU and the related ASVs (9, 11, 24) and Mn, N, P, Ni and the related ASVs (2, 3, 29). BG3 captures contrasted conditions with opposite gradients between Fe, AOU and the associated ASVs (9, 11, 13, 18, 24, 94), and Ni and Cu associated with another group of ASVs (36, 119, 188, 257) (Fig. 3B and S7).

All three BGs are related to remineralization, an observation that is not surprising as this process occurs in all water masses. The regression coefficients, which summarize the information contained in the different BGs, reveal 12 ASVs with a positive relationship with AOU (Fig. 4). The concurrently positive regression coefficients of these ASVs with Fe could indicate that either this element stimulates their metabolic activity and contribution to remineralization or the enhanced supply of Fe by these microbial taxa through remineralization. However, these ASVs could further be partitioned in different groups revealing that Cu is potentially an important discriminating factor. One group of ASVs (11, 13, 18, 24, 38, 94) thrives in low Cu conditions, while another group of ASVs (ASV 9, 30, 40, 88) accommodates with high Cu concentrations. This observation could suggest that the group with negative regressions is either sensitive to the toxicity of Cu or that these ASVs extensively use Cu. Consequently, ASVs belonging to this latter group are potential contributors to the remineralization of Cu.

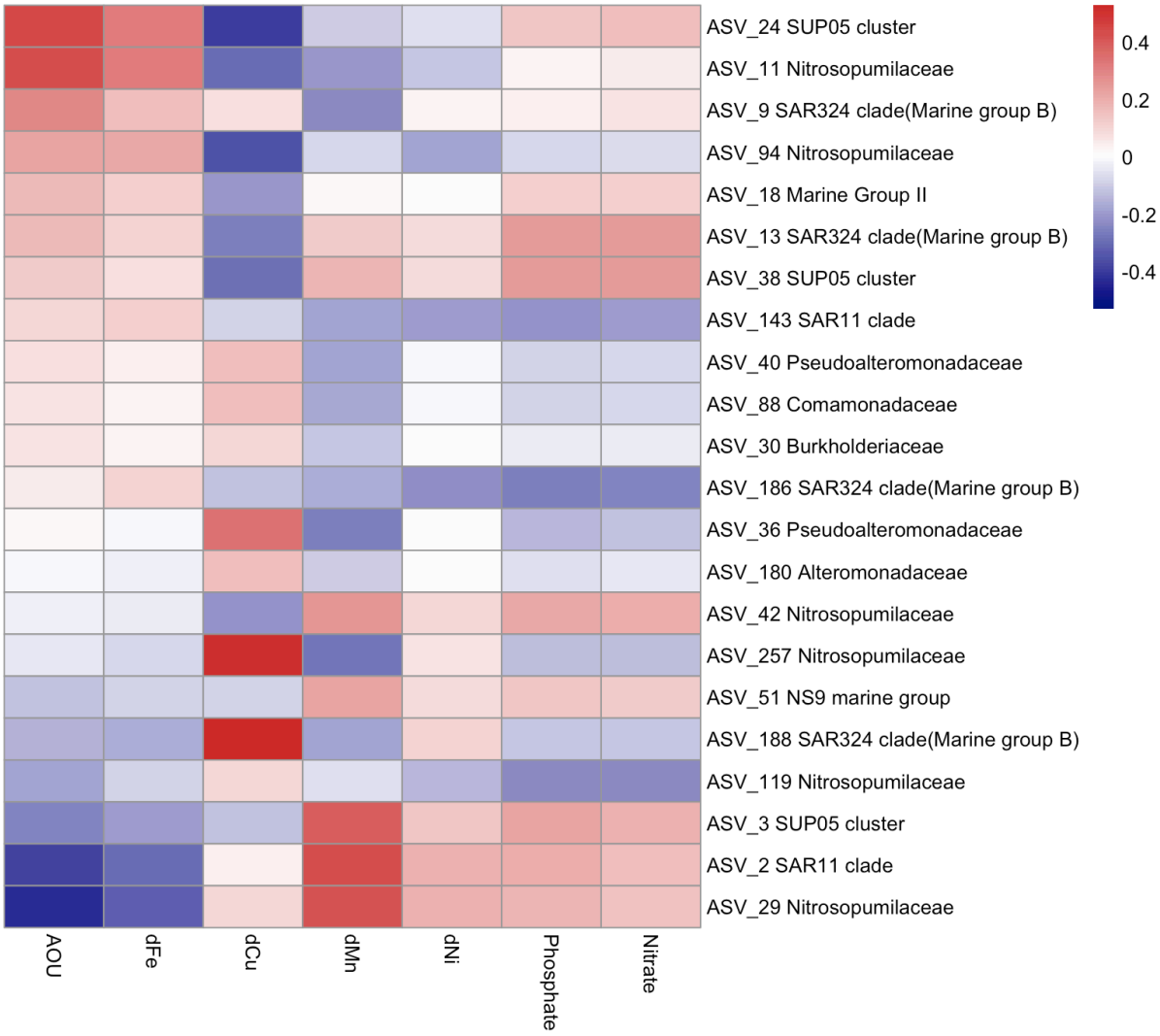

Fig.4 Heatmap based on the regression coefficients of abundant free-living prokaryotes (relative abundance of ASVs ≥ 5% in at least one sample) and environmental variables. The regression coefficients are extracted from the PLSR model.

Negative regression coefficients with AOU were observed with several ASVs suggesting that their activity is decoupled from the remineralization of organic matter. Among these, 3 ASVs (2, 3, 29) had positive regression coefficients with Mn and to a lesser extent with N, P and Ni. These ASVs were highlighted by BG2 that tags WW (Fig. 3E), young water masses with low AOU, typical of HNLC-type waters with high concentrations of N, P and low concentrations of Fe. In the case of Mn, the prokaryotic mediated oxidation of Mn (II) to insoluble Mn (IV) can lead to low Mn concentrations, while photoinduced, organically mediated reduction of Mn (IV, III) can result in high concentrations of this trace element in surface waters (Sunda and Huntsman 1994). This could pinpoint the ASVs with negative regression coefficients (257, 188 and 119) as potential mediators of this reduction (Jones et al. 2020). Another group

of ASVs (36, 119, 188, 257) revealed positive regression coefficients with Cu and were significant contributors to BG3, a good marker of NADW/LCDW. The absence of positive regression coefficients with AOU suggests that these ASVs are not Cu remineralizers, but that they are able to thrive in high Cu concentration (~ 1.7 nM in NADW and LCDW). This group also contains ASVs that have high negative regression coefficients with Mn.

Our data provide novel insights on the potential interactions between abundant ASVs and trace metals in relation to organic matter remineralization. Among these ASVs, only 7 ASVs were detected by the indicator species analysis (Fig. S6) illustrating the potential of PLSR analysis to identify key microbes if combined with appropriate biogeochemical parameters. Together, these results provide a new view on the parallel distribution of biogeochemical variables and prokaryotic taxa in distinct water masses. Because our results are based on the ASV-level, the limited functional knowledge does not allow to infer the specific pathways involved in trace element cycling by these prokaryotes. However, our results provide the opportunity to identify testable hypotheses on the underlying mechanisms, as illustrated for a few specific taxa below.

We observed that distinct ASVs belonging to the same family revealed opposite regression coefficients with trace elements. This was the case for example of ASVs belonging to *Nitrosopumilaceae.* While ASV 11 and 94 had positive regression coefficients with Fe and negative ones with Cu, ASV 29 and 119 revealed the opposite patterns. *Nitrosopumilaceae* are well-known chemolithoautotrophic ammonia-oxidizers (Qin et al. 2016), but this family also contains members with heterotrophic metabolism (Pester et al. 2011; Aylward and Santoro 2020). Fe- and Cu- availability appears to shape the ecological niches of different strains belonging to this group (Shafiee et al. 2019, 2021). A similar differentiation was observed for ASVs of the SUP05 cluster (ASV 24 and 38 vs ASV 3). Strong positive regressions with Cu were further detected for ASV188 (SAR324 clade, Marine group B), ASV 36 (*Pseudoalteromonadaceae*) and ASV 188 (*Alteromonadacea*). Culture work revealed a range of physiological responses and consequences on cellular carbon metabolism among diverse bacterial strains to Cu gradients (Posacka et al. 2019), illustrating that the requirements of this trace metal or the sensitivities towards its toxicity is highly variable. Insights on the contrasting interplays between trace metals and prokaryotic taxa, including closely related ones, could be gained through the investigation of the gene inventories of the metabolic pathways of interest. Quantifying the genes of the respective transporters as well as of metabolisms involving trace elements in the water masses where these taxa are abundant,

and describing the gene repertoire of representative MAGs could be a possible way to further investigate the ecological niches of ASVs in relation to trace metals in future studies.

Data availability statement

The data sets generated and analysed during the current study are available in the European Nucleotide Archive (ENA) repository at https://www.ebi.ac.uk/ena under the project ID PRJEB63680. Environmental and biogeochemical data are available under doi https://doi.org/10.17882/99983.

References

Agogué, H., D. Lamy, P. R. Neal, M. L. Sogin, and G. J. Herndl. 2011. Water mass-specificity of bacterial communities in the North Atlantic revealed by massively parallel sequencing: BACTERIAL ASSEMBLAGES IN NORTH ATLANTIC OCEAN. Molecular Ecology **20**: 258–274. doi:10.1111/j.1365-294X.2010.04932.x

Andrews, S. C., A. K. Robinson, and F. Rodríguez-Quiñones. 2003. Bacterial iron homeostasis. FEMS Microbiol Rev **27**: 215–237. doi:10.1016/S0168-6445(03)00055-X

Argüello, J. M., D. Raimunda, and T. Padilla-Benavides. 2013. Mechanisms of copper homeostasis in bacteria. Front. Cell. Infect. Microbiol. **3**. doi:10.3389/fcimb.2013.00073

Aylward, F. O., and A. E. Santoro. 2020. Heterotrophic Thaumarchaea with Small Genomes Are Widespread in the Dark Ocean N. Bouskill [ed.]. mSystems **5**: e00415-20. doi:10.1128/mSystems.00415-20

Baltar, F., J. Arístegui, J. M. Gasol, I. Lekunberri, and G. J. Herndl. 2010. Mesoscale eddies: hotspots of prokaryotic activity and differential community structure in the ocean. ISME J **4**: 975–988. doi:10.1038/ismej.2010.33

Baumas, C., and M. Bizic. 2023. Did you say marine snow? Zooming into different types of organic matter particles and their importance in the open ocean carbon cycle. preprint Life Sciences.

Beal, L. M., T. K. Chereskin, Y. D. Lenn, and S. Elipot. 2006. The Sources and Mixing Characteristics of the Agulhas Current. Journal of Physical Oceanography **36**: 2060–2074. doi:10.1175/JPO2964.1

Bindoff, N. L., and T. J. McDougall. 2000. Decadal Changes along an Indian Ocean Section at 32°S and Their Interpretation. J. Phys. Oceanogr. **30**: 1207–1222. doi:10.1175/1520-0485(2000)030<1207:DCAAIO>2.0.CO;2

Blain, S., H. Planquette, I. Obernosterer, and A. Guéneuguès. 2022. Vertical Flux of Trace Elements Associated With Lithogenic and Biogenic Carrier Phases in the Southern Ocean. Global Biogeochemical Cycles **36**. doi:10.1029/2022GB007371

Bosma, E. F., M. H. Rau, L. A. van Gijtenbeek, and S. Siedler. 2021. Regulation and distinct physiological roles of manganese in bacteria. FEMS Microbiology Reviews **45**: fuab028. doi:10.1093/femsre/fuab028

Callahan, B. J., P. J. McMurdie, M. J. Rosen, A. W. Han, A. J. A. Johnson, and S. P. Holmes. 2016. DADA2: High-resolution sample inference from Illumina amplicon data. Nat Methods **13**: 581–583. doi:10.1038/nmeth.3869

Chen, X.-G., D. Rusiecka, M. Gledhill, and others. 2023. Ocean circulation and biological processes drive seasonal variations of dissolved Al, Cd, Ni, Cu, and Zn on the Northeast Atlantic continental margin. Marine Chemistry **252**: 104246. doi:10.1016/j.marchem.2023.104246

Debelius, B., J. M. Forja, and L. M. Lubián. 2011. Toxicity of copper, nickel and zinc to Synechococcus populations from the Strait of Gibraltar. Journal of Marine Systems **88**: 113–119. doi:10.1016/j.jmarsys.2011.02.009

Dixon, P. 2003. VEGAN, a package of R functions for community ecology. Journal of Vegetation Science **14**: 927–930. doi:10.1111/j.1654-1103.2003.tb02228.x

Dunn, K. 2020. Process Improvement Using Data. https://learnche.org/pid/PID.pdf?10d109.

Fourquez, M., A. Devez, A. Schaumann, A. Guéneuguès, T. Jouenne, I. Obernosterer, and S. Blain. 2014. Effects of iron limitation on growth and carbon metabolism in oceanic and coastal heterotrophic bacteria. Limnol. Oceanogr. **59**: 349–360. doi:10.4319/lo.2014.59.2.0349

Galand, P. E., M. Potvin, E. O. Casamayor, and C. Lovejoy. 2010. Hydrography shapes bacterial biogeography of the deep Arctic Ocean. ISME J **4**: 564–576. doi:10.1038/ismej.2009.134

Gikas, P. 2008. Single and combined effects of nickel (Ni(II)) and cobalt (Co(II)) ions on activated sludge and on other aerobic microorganisms: A review. Journal of Hazardous Materials **159**: 187–203. doi:10.1016/j.jhazmat.2008.02.048

Glass, J. B., and C. L. Dupont. 2017. Oceanic Nickel Biogeochemistry and the Evolution of Nickel Use, p. 12–26. *In* D. Zamble, M. Rowińska-Żyrek, and H. Kozlowski [eds.], The Biological Chemistry of Nickel. The Royal Society of Chemistry.

Guebel, D. V., and N. V. Torres. 2013. Partial Least-Squares Regression (PLSR), p. 1646–1648. *In* W. Dubitzky, O. Wolkenhauer, K.-H. Cho, and H. Yokota [eds.], Encyclopedia of Systems Biology. Springer New York.

Guidi, L., S. Chaffron, L. Bittner, and others. 2016. Plankton networks driving carbon export in the oligotrophic ocean. Nature **532**: 465–470. doi:10.1038/nature16942

Hansel, C. M. 2017. Manganese in Marine Microbiology, p. 37–83. *In* Advances in Microbial Physiology. Elsevier.

Hanson, C. A., J. A. Fuhrman, M. C. Horner-Devine, and J. B. H. Martiny. 2012. Beyond biogeographic patterns: processes shaping the microbial landscape. Nat Rev Microbiol **10**: 497–506. doi:10.1038/nrmicro2795

Hernando-Morales, V., J. Ameneiro, and E. Teira. 2017. Water mass mixing shapes bacterial biogeography in a highly hydrodynamic region of the Southern Ocean: Water mixing shapes bacterial biogeography. Environ Microbiol **19**: 1017–1029. doi:10.1111/1462-2920.13538

Jenkins, W. J., W. M. Smethie, E. A. Boyle, and G. A. Cutter. 2015. Water mass analysis for the U.S. GEOTRACES (GA03) North Atlantic sections. Deep Sea Research Part II: Topical Studies in Oceanography **116**: 6–20. doi:10.1016/j.dsr2.2014.11.018

Jones, M. R., G. W. Luther, and B. M. Tebo. 2020. Distribution and concentration of soluble manganese(II), soluble reactive Mn(III)-L, and particulate MnO2 in the Northwest Atlantic Ocean. Marine Chemistry **226**: 103858. doi:10.1016/j.marchem.2020.103858

Kavanaugh, M. T., B. Hales, M. Saraceno, Y. H. Spitz, A. E. White, and R. M. Letelier. 2014. Hierarchical and dynamic seascapes: A quantitative framework for scaling pelagic biogeochemistry and ecology. Progress in Oceanography **120**: 291–304. doi:10.1016/j.pocean.2013.10.013

Latour, P., K. Wuttig, P. Van Der Merwe, and others. 2021. Manganese biogeochemistry in the Southern Ocean, from Tasmania to Antarctica. Limnology & Oceanography **66**: 2547–2562. doi:10.1002/lno.11772

Legendre, P., and E. D. Gallagher. 2001. Ecologically meaningful transformations for ordination of species data. Oecologia **129**: 271–280. doi:10.1007/s004420100716

Lekunberri, I., E. Sintes, D. De Corte, T. Yokokawa, and G. J. Herndl. 2013. Spatial patterns of bacterial and archaeal communities along the Romanche Fracture Zone (tropical Atlantic). FEMS Microbiol Ecol **85**: 537–552. doi:10.1111/1574-6941.12142

Liu, Y., S. Blain, O. Crispi, M. Rembauville, and I. Obernosterer. 2020. Seasonal dynamics of prokaryotes and their associations with diatoms in the Southern Ocean as revealed by an autonomous sampler. Environ Microbiol **22**: 3968–3984. doi:10.1111/1462-2920.15184

Liu, Y., P. Debeljak, M. Rembauville, S. Blain, and I. Obernosterer. 2019. Diatoms shape the biogeography of heterotrophic prokaryotes in early spring in the Southern Ocean. Environmental Microbiology **21**: 1452–1465. doi:10.1111/1462-2920.14579

Lohan, M. C., and A. Tagliabue. 2018. Oceanic Micronutrients: Trace Metals that are Essential for Marine Life. Elements **14**: 385–390. doi:10.2138/gselements.14.6.385

Martin, M. 2011. Cutadapt removes adapter sequences from high-throughput sequencing reads. EMBnet j. **17**: 10. doi:10.14806/ej.17.1.200

McMurdie, P. J., and S. Holmes. 2013. phyloseq: An R Package for Reproducible Interactive Analysis and Graphics of Microbiome Census Data M. Watson [ed.]. PLoS ONE **8**: e61217. doi:10.1371/journal.pone.0061217

Mestre, M., C. Ruiz-González, R. Logares, C. M. Duarte, J. M. Gasol, and M. M. Sala. 2018. Sinking particles promote vertical connectivity in the ocean microbiome. Proc. Natl. Acad. Sci. U.S.A. **115**. doi:10.1073/pnas.1802470115

Mevik, B.-H., and R. Wehrens. 2007. The **pls** Package: Principal Component and Partial Least Squares Regression in *R*. J. Stat. Soft. **18**. doi:10.18637/jss.v018.i02

Moffett, J. W., L. E. Brand, P. L. Croot, and K. A. Barbeau. 1997. Cu speciation and cyanobacterial distribution in harbors subject to anthropogenic Cu inputs. Limnol. Oceanogr. **42**: 789–799. doi:10.4319/lo.1997.42.5.0789

Morel, F. M. M., and N. M. Price. 2003. The Biogeochemical Cycles of Trace Metals in the Oceans. Science **300**: 944–947. doi:10.1126/science.1083545

Orsi, A. H., G. C. Johnson, and J. L. Bullister. 1999. Circulation, mixing, and production of Antarctic Bottom Water. Progress in Oceanography **43**: 55–109. doi:10.1016/S0079-6611(99)00004-X

Parada, A. E., D. M. Needham, and J. A. Fuhrman. 2016. Every base matters: assessing small subunit rRNA primers for marine microbiomes with mock communities, time series and global field samples: Primers for marine microbiome studies. Environ Microbiol **18**: 1403–1414. doi:10.1111/1462-2920.13023

Park, Y., E. Charriaud, P. Craneguy, and A. Kartavtseff. 2001. Fronts, transport, and Weddell Gyre at 30°E between Africa and Antarctica. J. Geophys. Res. **106**: 2857–2879. doi:10.1029/2000JC900087

Park, Y., L. Gamberoni, and E. Charriaud. 1993. Frontal structure, water masses, and circulation in the Crozet Basin. J. Geophys. Res. **98**: 12361–12385. doi:10.1029/93JC00938

Park, Y. -H., T. Park, T. -W. Kim, and others. 2019. Observations of the Antarctic Circumpolar Current Over the Udintsev Fracture Zone, the Narrowest Choke Point in the Southern Ocean. JGR Oceans **124**: 4511–4528. doi:10.1029/2019JC015024

Pester, M., C. Schleper, and M. Wagner. 2011. The Thaumarchaeota: an emerging view of their phylogeny and ecophysiology. Current Opinion in Microbiology **14**: 300–306. doi:10.1016/j.mib.2011.04.007

Posacka, A. M., D. M. Semeniuk, and M. T. Maldonado. 2019. Effects of Copper Availability on the Physiology of Marine Heterotrophic Bacteria. Front. Mar. Sci. **5**: 523. doi:10.3389/fmars.2018.00523

Qin, W., W. Martens-Habbena, J. N. Kobelt, and D. A. Stahl. 2016. *Candidatus* Nitrosopumilaceae, p. 1–2. *In* W.B. Whitman [ed.], Bergey's Manual of Systematics of Archaea and Bacteria. Wiley.

Quast, C., E. Pruesse, P. Yilmaz, J. Gerken, T. Schweer, P. Yarza, J. Peplies, and F. O. Glöckner. 2012. The SILVA ribosomal RNA gene database project: improved data processing and web-based tools. Nucleic Acids Research **41**: D590–D596. doi:10.1093/nar/gks1219

Raes, E. J., L. Bodrossy, J. Van De Kamp, and others. 2018. Oceanographic boundaries constrain microbial diversity gradients in the South Pacific Ocean. Proc. Natl. Acad. Sci. U.S.A. **115**. doi:10.1073/pnas.1719335115

Rembauville, M., N. Briggs, M. Ardyna, and others. 2017. Plankton Assemblage Estimated with BGC-Argo Floats in the Southern Ocean: Implications for Seasonal Successions and Particle Export. JGR Oceans **122**: 8278–8292. doi:10.1002/2017JC013067

Rembauville, M., I. Salter, N. Leblond, A. Gueneugues, and S. Blain. 2015. Export fluxes in a naturally iron-fertilized area of the Southern Ocean – Part 1: Seasonal dynamics of particulate organic carbon export from a moored sediment trap. Biogeosciences **12**: 3153–3170. doi:10.5194/bg-12-3153-2015

Roberts, D. W. 2019. labdsv: Ordination and multivariate analysis for ecology.

Salazar, G., F. M. Cornejo-Castillo, V. Benítez-Barrios, E. Fraile-Nuez, X. A. Álvarez-Salgado, C. M. Duarte, J. M. Gasol, and S. G. Acinas. 2016. Global diversity and biogeography of deep-sea pelagic prokaryotes. ISME J **10**: 596–608. doi:10.1038/ismej.2015.137

Schreiber, D. R., A. S. Gordon, and F. Millero J. 1985. The toxicity of copper to the marine bacterium *Vibrio alginolyticus*. Can. J. Microbiol. **31**: 83–87. doi:10.1139/m85-016

Shafiee, R. T., P. J. Diver, J. T. Snow, Q. Zhang, and R. E. M. Rickaby. 2021. Marine ammonia-oxidising archaea and bacteria occupy distinct iron and copper niches. ISME COMMUN. **1**: 1. doi:10.1038/s43705-021-00001-7

Shafiee, R. T., J. T. Snow, Q. Zhang, and R. E. M. Rickaby. 2019. Iron requirements and uptake strategies of the globally abundant marine ammonia-oxidising archaeon, Nitrosopumilus maritimus SCM1. ISME J **13**: 2295–2305. doi:10.1038/s41396-019-0434-8

Sow, S. L. S., M. V. Brown, L. J. Clarke, and others. 2022. Biogeography of Southern Ocean prokaryotes: a comparison of the Indian and Pacific sectors. Environmental Microbiology **24**: 2449–2466. doi:10.1111/1462-2920.15906

Sunda, W. G., and S. A. Huntsman. 1994. Photoreduction of manganese oxides in seawater. Marine Chemistry **46**: 133–152. doi:10.1016/0304-4203(94)90051-5

Sunda, W. G., S. A. Huntsman, and G. R. Harvey. 1983. Photoreduction of manganese oxides in seawater and its geochemical and biological implications. Nature **301**: 234–236. doi:10.1038/301234a0

Talley, L. D., G. L. Pickard, W. J. Emery, and J. H. Swift, eds. 2011. Descriptive physical oceanography: an introduction, 6. ed. Elsevier, AP.

Thi Dieu Vu, H., and Y. Sohrin. 2013. Diverse stoichiometry of dissolved trace metals in the Indian Ocean. Sci Rep **3**: 1745. doi:10.1038/srep01745

Supplementary material

Supplementary Methods

Sample collection and analysis of environmental parameters

Enumeration of prokaryotic abundance. To determine the abundance of prokaryotic cells, raw seawater samples (1.45 mL) were fixed with glutaraldehyde (1% final concentration), incubated at 4°C for 30 minutes, shock-frozen in liquid nitrogen and stored at -80°C until analyzed back in the home laboratory. The prokaryotic cell abundance was determined by flow cytometry as described previously (Hernandez-Magana et al. 2021). Counts were performed on a FACSCanto II flow cytometer (Becton Dickinson) equipped with 3 air-cooled lasers: blue (argon 488 nm), red (633 nm) and violet (407 nm). Cells were stained with SYBR Green I (Invitrogen – Molecular Probes) at 0.025% (vol/vol) final concentration for 15 min at room temperature in the dark. Stained prokaryotic cells were discriminated and enumerated according to their right-angle light scatter (SSC) and green fluorescence at 530/30 nm. In a plot of green versus red fluorescence, non-autofluorescent cells were distinguished from autofluorescent cells. Fluorescent beads (1.002 µm; Polysciences Europe) were systematically added to each analyzed sample as internal standard. The cell abundance was determined from the flow rate, which was calculated with TruCount beads (BD biosciences).

Concentration of trace metals. To sample seawater for trace metal determination, the trace metal clean rosette equipped with 24 GO-FLO bottles was deployed using a Kevlar wire. GO-FLO bottles and all sampling material were cleaned before the cruise following the GEOTRACES cookbook (Cutter et al. 2017). Immediately after recovery, the rosette was transferred into a clean container for sampling trace elements. Particle levels were controlled with a particle counter (Lighthouse HH3016) and when levels were adequate for ISO class 6 levels, sampling could begin. Bottles were pressurized with 0.2 µm-filtered nitrogen (Air Liquide®).

Samples dedicated to dissolved trace metal analyses were filtered on-line through a 0.45µm polyethersulfone filter (Supor®) and collected in duplicates in acid-cleaned 60mL LDPE bottles. All samples were acidified within 24h of collection with hydrochloric acid (HCl, ultrapure grade, Merck, final pH 1.8).

Concentrations of dissolved iron (dFe), manganese (dMn), copper (dCu), nickel (dNi) were analyzed using the preconcentration system seaFAST-pico™ coupled to a high-resolution magnetic sector field inductively-coupled plasma mass spectrometer (SF-ICP-MS, Element

XR – Pôle Spectrométrie Ocean, Brest) following Tonnard et al. (Tonnard et al. 2020). Acidified MQ water with hydrochloric acid (HCl, ultrapure grade, Merck, 0.2‰, final pH 1.8) (n=9) was analyzed and used as the analytical blank (dFe=0.14±0.05 nmol L-1, dMn=0.08±0.04 nmol L-1, dCu=0.05±0.01 nmol L-1, dNi=0.06±0.01 nmol L-1). All trace metal data were above the detection limit (LOD), defined as three times the standard deviation (sd) of the blank. The reproducibility of our analyses has been verified with duplicat analyses (n=22). Reference seawater (NASS-7) and GEOTRACES consensus (GSC and GSP) seawaters were used to certify the accuracy of our analyses.

measured reference	dFe (nmol L^{-1})	dMn (nmol L^{-1})	dCu (nmol L^{-1})	dNi (nmol L^{-1})
NASS 7 (n=10)	**5.87±0.62**	**12.52±0.87**	**2.60±0.16**	**3.74±0.16**
	6.23±0.46	*13.65±1.09*	*3.16±0.22*	*4.14±0.30*
GSC (n=15)	**1.76±0.35**	**1.87±0.31**	**1.08±0.19**	**3.81±0.66**
	1.53±0.12	*2.18±0.07*	*1.10±0.15*	*4.39±0.20*
GSP (n=2)	**0.18±0.02**	**0.65±0.04**	**0.55±0.08**	**2.77±0.06**
	0.16±0.04	*0.78±0.03*	*0.57±0.05*	*2.60±0.10*

Concentration of inorganic nutrients. To collect samples for the determination of the concentration of phosphate (PO_4^{3-}), nitrate (NO_3^-) and nitrite (NO_2^-), syringes (50 mL) were directly connected to the spigot of the Niskin bottles. The samples were drawn through a 0.45 µm Uptidisc (Whatman) adapted for the syringe. The samples (25 mL) were poisoned with mercuric chloride ($HgCl_2$, 20 mg L^{-1}, final concentration) and stored in the dark at room temperature for later analysis in the home lab as described in (Blain et al. 2015). Analyses were done on a segmented flow analyzer (Skalar) equipped with colorimetric detection using methods described in (Aminot and Kérouel 2007). The accuracy of the methods was assessed using reference material (Certipur, Merck). The precisions were in the range of 1–4 %, and the limit of detection was 0.02 µM for nitrate and nitrite, and 0.03 µM for phosphate.

Concentration of dissolved organic carbon (DOC). The concentration of DOC was determined in samples filtered through two combusted (450 °C, 4 h) GF/F filters. Subsamples of 10 mL (in duplicate) were transferred to pre-combusted glass ampoules and acidified with H_3PO_4 (final pH = 2). The sealed glass ampoules were stored in the dark at room temperature until analysis. DOC concentrations were measured on a Shimadzu TOC-L analyzer as described previously (Hernandez-Magana et al. 2021). Consensus reference material (batch #04-21 DSR (700 m) consensus value [43-45] µM) provided in sealed glass ampoules

(https://hansell-lab.earth.miami.edu/consensus-reference-material/index.html) was injected every 12 to 17 samples to insure stable operating conditions. The measured DOC concentration of this reference material was on average 44.7±2.0 µM.

Apparent Oxygen Utilization (AOU). Dissolved oxygen concentrations (O_2 meas) were measured using the calibrated oxygen sensor mounted on the CTD frame. The concentration of oxygen at saturation (O_2 sat) was calculated using the solubility equation provided by Garcia et al (Garcia and Gordon 1992), using temperature and salinity measured by the CTD sensor. AOU was derived using the equation AOU = O_2 sat - O_2 meas.

DNA extraction

The Sterivex cartridges were opened according to Perrine's method (Cruaud et al. 2017), and the 0.22 µm membranes were cut into small pieces and transferred to 2 mL microtubes (Eppendorf). The 0.8 µm membranes were also cut into pieces. To promote cell lysis, a solution containing PW1 and lysozyme was added to the microtubes and incubated at 37°C for 45 min. To digest the proteins in the cell lysate a proteinase K solution was added and incubated at 55°C for 1 h. DNA was then extracted following the manufacturer's instructions of the DNeasy PowerWater Kit (Qiagen). DNA concentrations were measured by a quantus fluorometer (Promega) with the QuantiFluor® Double stranded DNA (dsDNA) system.

Supplementary Results

Microbial community composition

Regardless of free-living or particle-attached prokaryotes, prokaryotic communities from STSW differ from those in other zones of surface seawater (Fig. 2), where free-living prokaryotes from STSW were dominated by *Cyanobiaceae*, SAR11, SAR86, SAR116 and *Actinomarinaceae*, while other surface seawaters were dominated by SAR11, *Flavobacteriaceae*, *Rhodobacteraceae* and SAR86. The free-living prokaryotes from ASW also have abundant *Thioglobaceae* (Fig. S4), as well as particle-attached prokaryotes from STSW were primarily dominated by *Cyanobiaceae* and *Flavobacteriaceae* compared to other surface seawaters, with lower abundance of *Haileaceae*, *Rhodobacteraceae*, and *Rubritaleaceae* (Fig. S5). The free-living prokaryotic communities in seawater collected from below the surface contained abundant *Nitrosopumilaceae*, SAR406 and SAR324, whereas particle-attached prokaryotes in seawater collected from below the surface exhibited a greater number of ASVs compared to the free-living prokaryotic communities in surface seawater (Fig. S4 and S5).

Biogeographical barriers of water masses and sampling zones define specific prokaryotic taxa in different samples

To further investigate whether each water mass or surface seawater contains specific prokaryotic taxa, the indicator species analysis was performed for each water mass or surface seawater. A total of 213 indicator species were identified in all samples of free-living prokaryotic communities, while 121 indicator species were identified in all samples of particle-attached prokaryotic communities. The list of indicator species, along with their indicator values and contributions to the prokaryotic community were shown in Table S1 and S2, where the contribution of indicator species to the free-living and particle-attached prokaryotic community is significantly lower in the STMW, AAIW, AICW, AAIW+RSOW, UCDW, LCDW and NADW/LCDW compared to other water masses and surface seawaters (Fig. S6), and indicator species in STSW contributed more than 60% to the free-living prokaryotic community, whereas indicator species in AABW contributed over 50% to the particle-attached prokaryotic community (Fig. S6). With the exception of ASW and STSW, there was rarely overlap between indicator species in free-living prokaryotic communities and those in particle-attached prokaryotic communities. The dominant indicator species of prokaryotic communities present in different water masses or surface seawaters belong to distinct taxa. For instance, for indicator species in free-living prokaryotic communities, *Cyanobiaceae* and SAR11 dominate in STSW, *Flavobacteriaceae* and SAR86 dominate in SASW, *Rhodobacteraceae* dominate in PFSW, and *Flavobacteriaceae*, *Nitrincolaceae*, and *Rhodobacteraceae* dominate in ASW, *Thioglobaceae* are the dominant indicator species in WW, while *Nitrosopumliaceae* dominate in AAIW and AAIW+RSOW. In contrast, for indicator species in particle-attached prokaryotic communities, *Cyanobiaceae* and *Rhodobacteraceae* dominate in STSW, *Cyanobiaceae* and *Flavobacteriaceae* dominate in SASW, *Halieaceae* dominate in PFSW, *Flavobacteriaceae* dominate in ASW, and *Pirellulaceae* dominate in WW (Fig. S6).

Reference

Aminot, A., and R. Kérouel. 2007. Dosage automatique des nutriments dans les eaux marines. Méthodes en flux continu, Ifremer.

Blain, S., J. Capparos, A. Guéneuguès, I. Obernosterer, and L. Oriol. 2015. Distributions and stoichiometry of dissolved nitrogen and phosphorus in the iron-fertilized region near Kerguelen (Southern Ocean). Biogeosciences **12**: 623–635. doi:10.5194/bg-12-623-2015

Cruaud, P., A. Vigneron, M.-S. Fradette, S. J. Charette, M. J. Rodriguez, C. C. Dorea, and A. I. Culley. 2017. Open the Sterivex ™ casing: An easy and effective way to improve DNA extraction yields: *DNA extraction from Sterivex ™ filters* . Limnol. Oceanogr. Methods **15**: 1015–1020. doi:10.1002/lom3.10221

Cutter, G., K. Casciotti, P. Croot, W. Geibert, L.-E. Heimbürger, M. Lohan, H. Planquette, and T. Van De Flierdt. 2017. Sampling and Sample-handling Protocols for GEOTRACES Cruises. Version 3, August 2017. GEOTRACES International Project Office.

Garcia, H. E., and L. I. Gordon. 1992. Oxygen solubility in seawater: Better fitting equations. Limnol. Oceanogr. **37**: 1307–1312. doi:10.4319/lo.1992.37.6.1307

Hernandez-Magana, A. E., Y. Liu, P. Debeljak, O. Crispi, B. Marie, C. Koedooder, and I. Obernosterer. 2021. Prokaryotic diversity and activity in contrasting productivity regimes in late summer in the Kerguelen region (Southern Ocean). Journal of Marine Systems **221**: 103561. doi:10.1016/j.jmarsys.2021.103561

Tonnard, M., H. Planquette, A. R. Bowie, and others. 2020. Dissolved iron in the North Atlantic Ocean and Labrador Sea along the GEOVIDE section (GEOTRACES section GA01). Biogeosciences **17**: 917–943. doi:10.5194/bg-17-917-2020

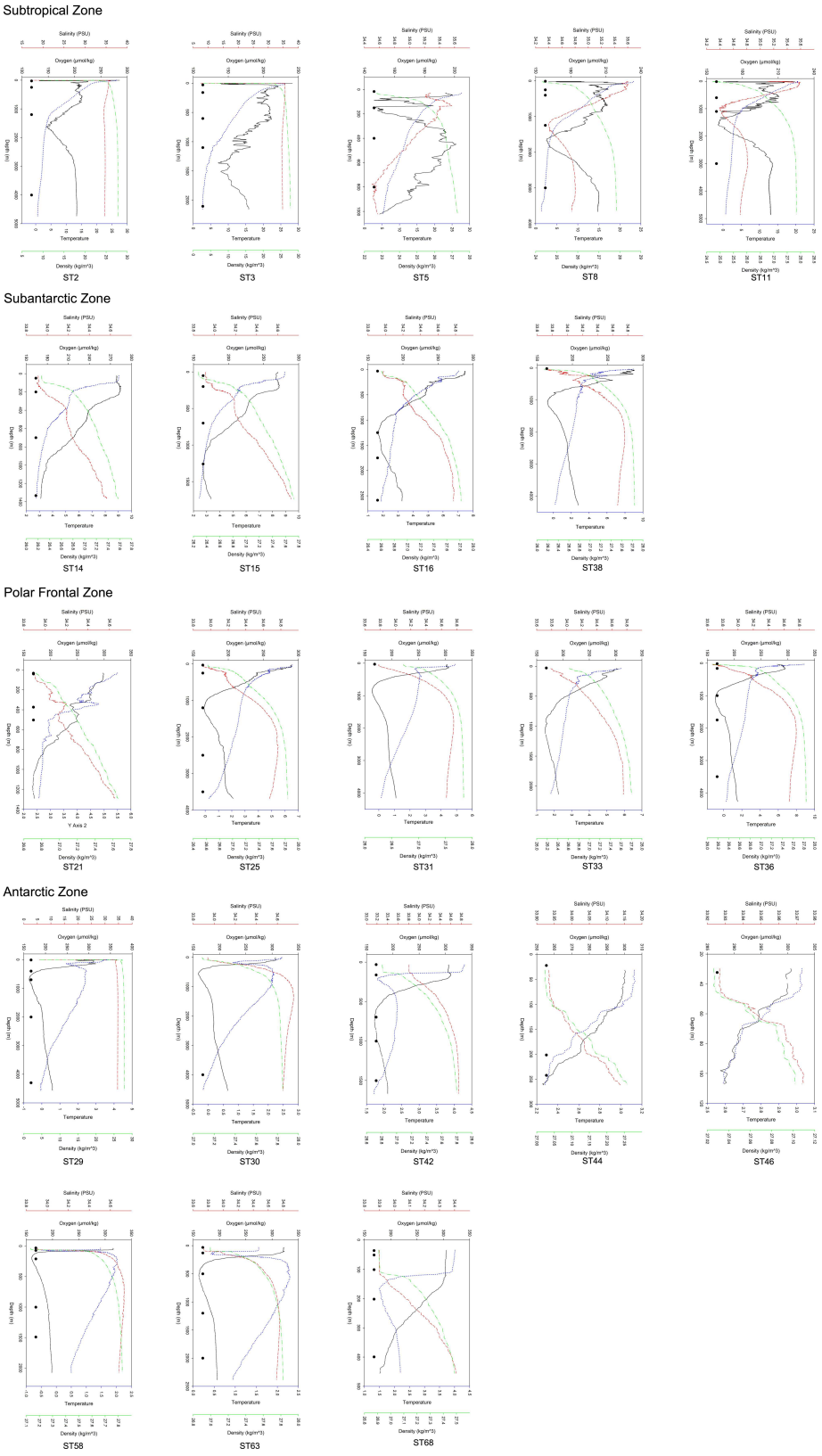

Fig. S1. Vertical profiles of temperature (blue), salinity (red), oxygen (black) and density (green) at the stations sampled in the present study. Dots represent the depths at which samples were collected.

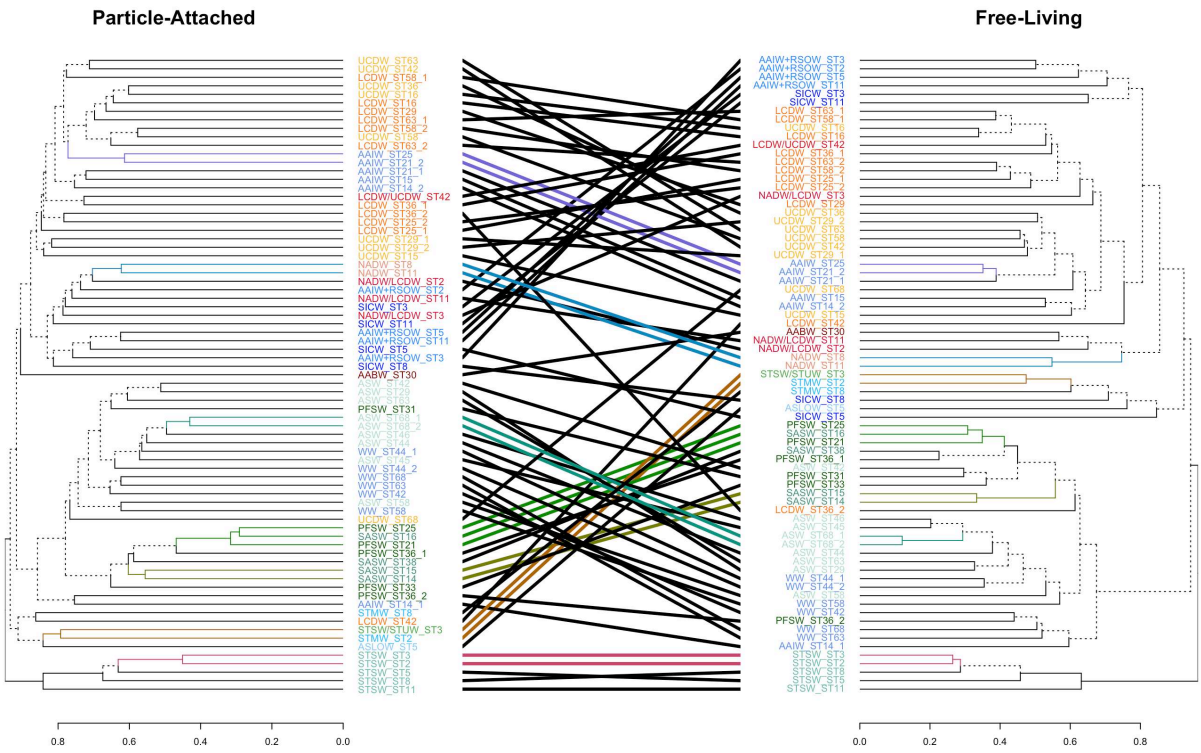

Fig. S2. Tanglegram showing hierarchical clustering of particle-attached and free-living prokaryotic community structure based on Bray-Curtis distances using the UPGMA method (entanglement=0.21). Entanglement is a measure between 1 (full entanglement) and 0 (no entanglement). A lower entanglement coefficient corresponds to a good alignment. Only those samples for which community composition of free living and particle attached prokaryotes are available are used here.

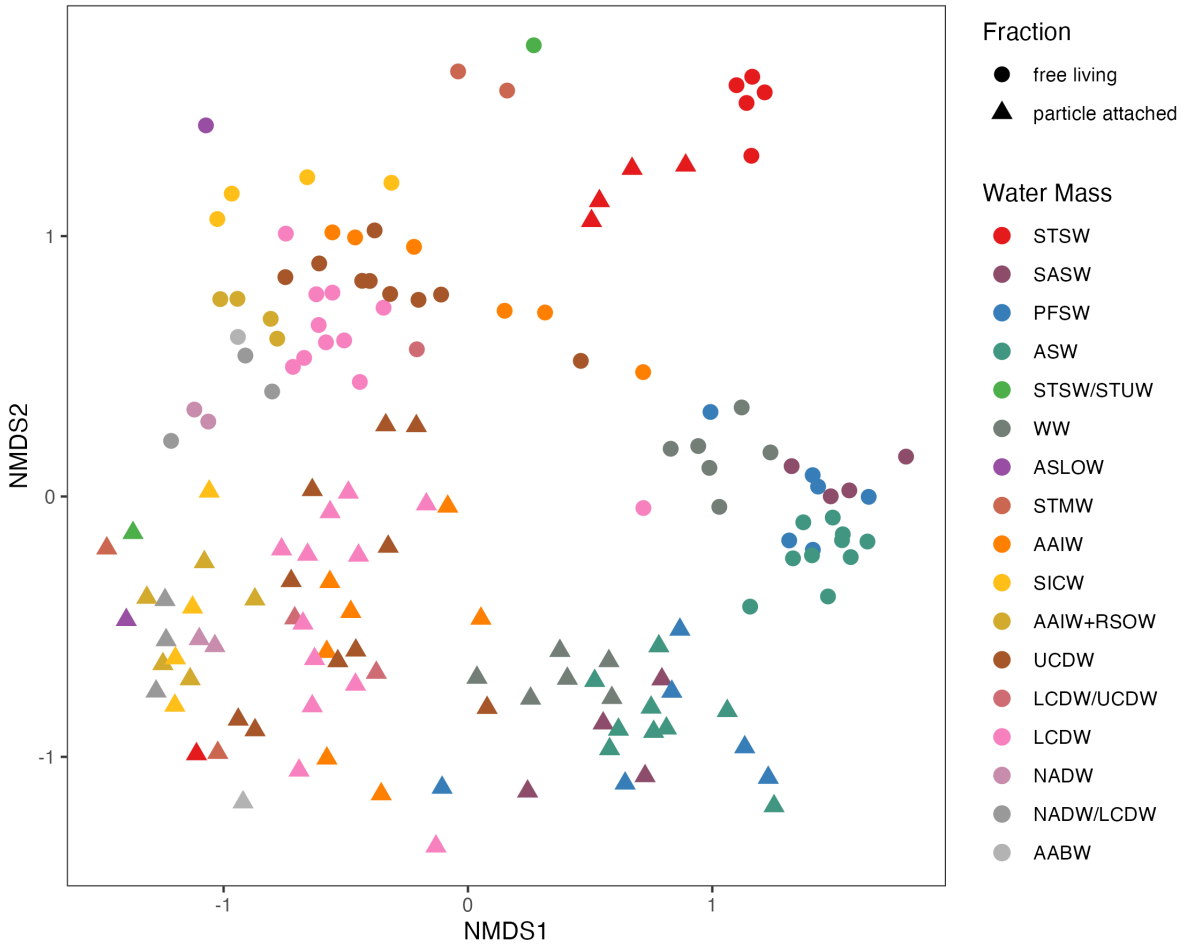

Fig. S3. Non-Metric Multidimensional Scale (NMDS) plots of free-living (circles) and particle-attached (triangles) prokaryotic communities based on Bray-Curtis dissimilarity. ANOSIM statistic: R: 0.7133, Significance: 1e-04.

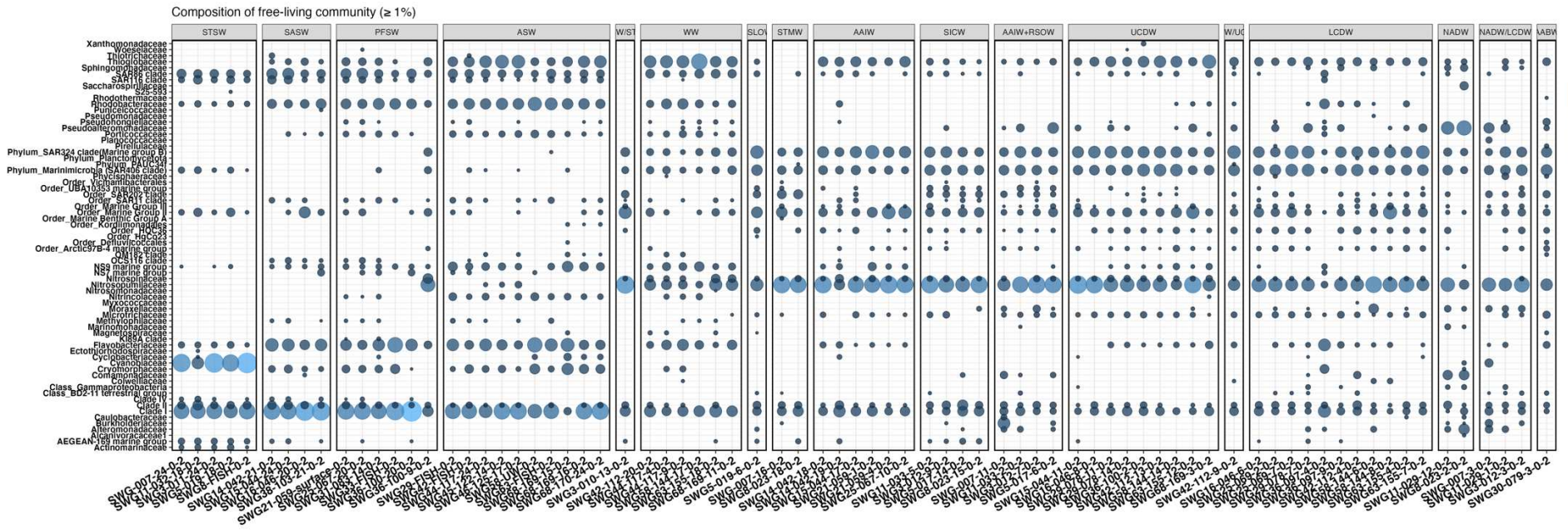

Fig. S4. Composition of the free-living prokaryotic communities in all samples of the present study. Taxonomic assignments are based on the Family level and only ASVs with a relative abundance of more than 1% in at least one sample are shown.

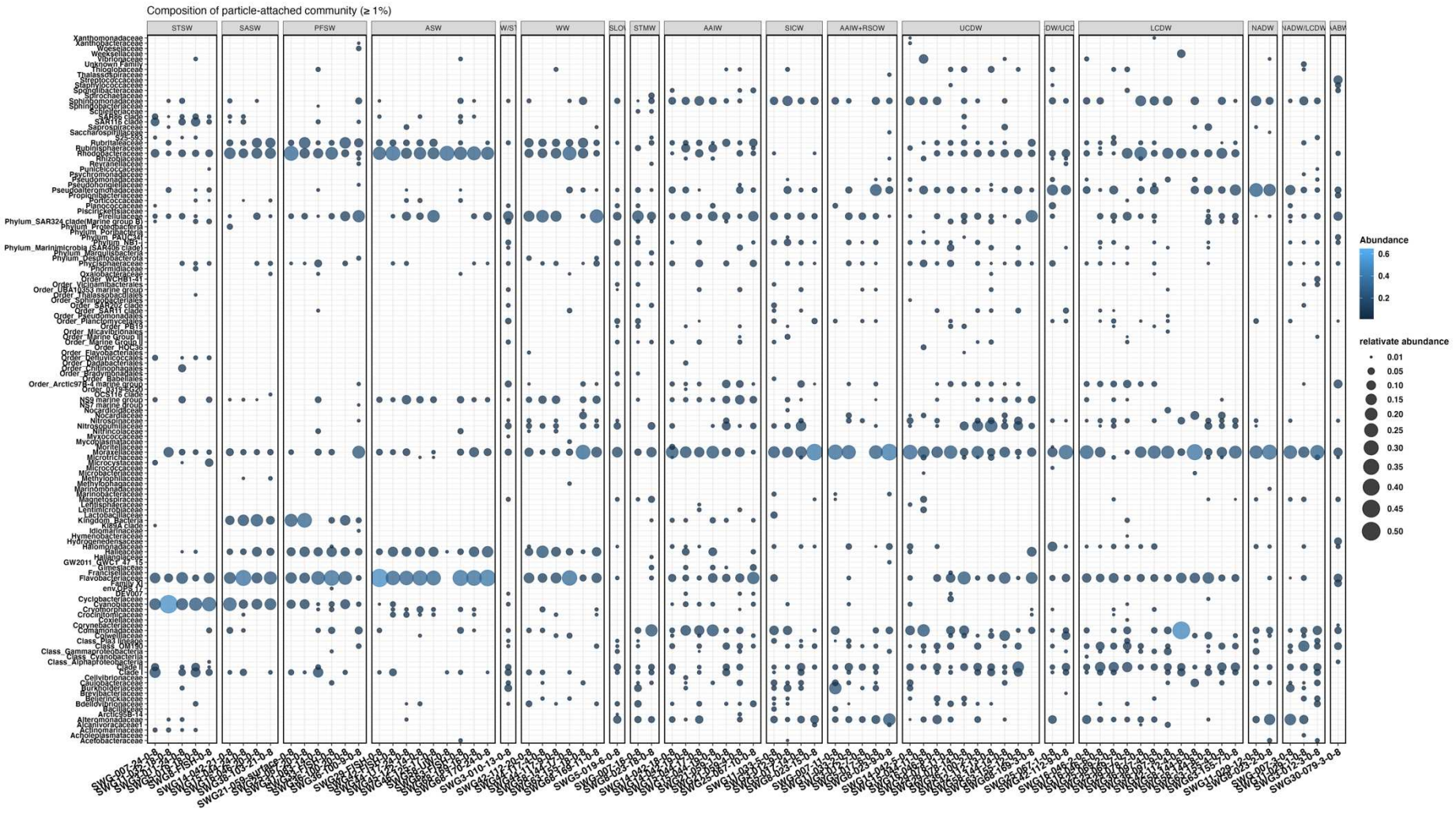

Fig. S5. Composition of the particle-attached prokaryotic communities in all samples of the present study. Taxonomic assignments are based on the Family level and only ASVs with a relative abundance of more than 1% in at least one sample are shown.

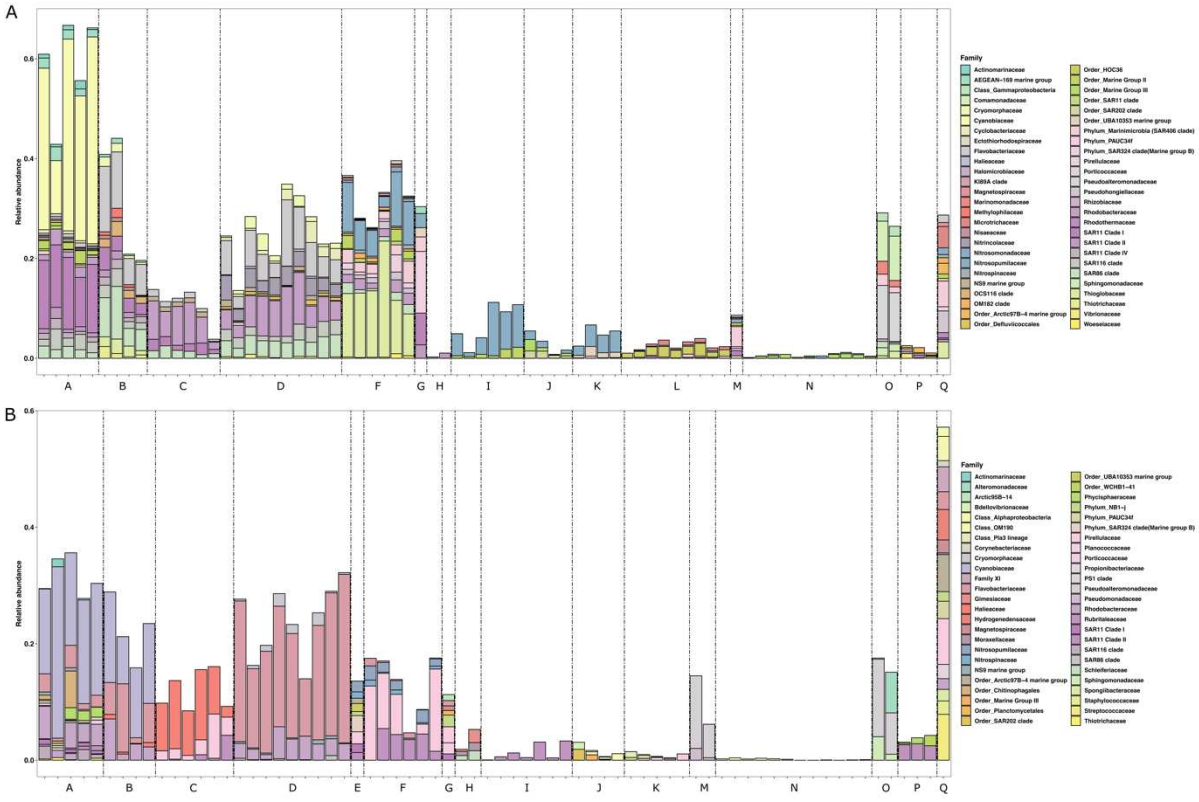

Fig. S6. Contribution of different indicator ASVs and their taxonomy in each sample (A, free-living prokaryotic community; B, particle-attached prokaryotic community). Surface waters and water masses were separated by vertical dashed lines. Taxonomic assignments are based on the Family level. A, STSW; B, SASW; C, PFSW; D, ASW; E, STSW/STUW; F, WW; G, ASLOW; H, STMW; I, AAIW; J, SICW; K, AAIW+RSOW; L, UCDW; M, LCDW/UCDW; N, LCDW; O, NADW; P, NADW/LCDW; Q, AABW.

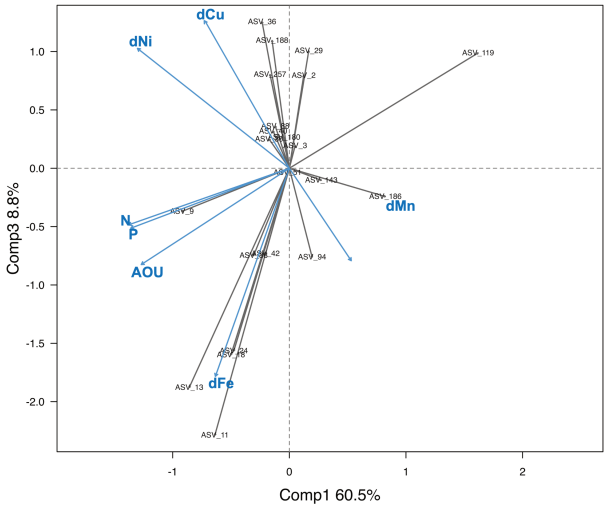

Fig. S7. Partial least squares regression analysis (PLSr) linking abundant ASVs (relative abundance ≥ 5% in at least one sample) with environmental variables. Blue short labels describe the environmental variables (AOU, apparent oxygen utilization; P, phosphate; N, nitrate; dMn, dissolved manganese; dFe, dissolved iron; dNi, dissolved nickel; dCu, dissolved copper) whereas grey short labels describe the ASVs.

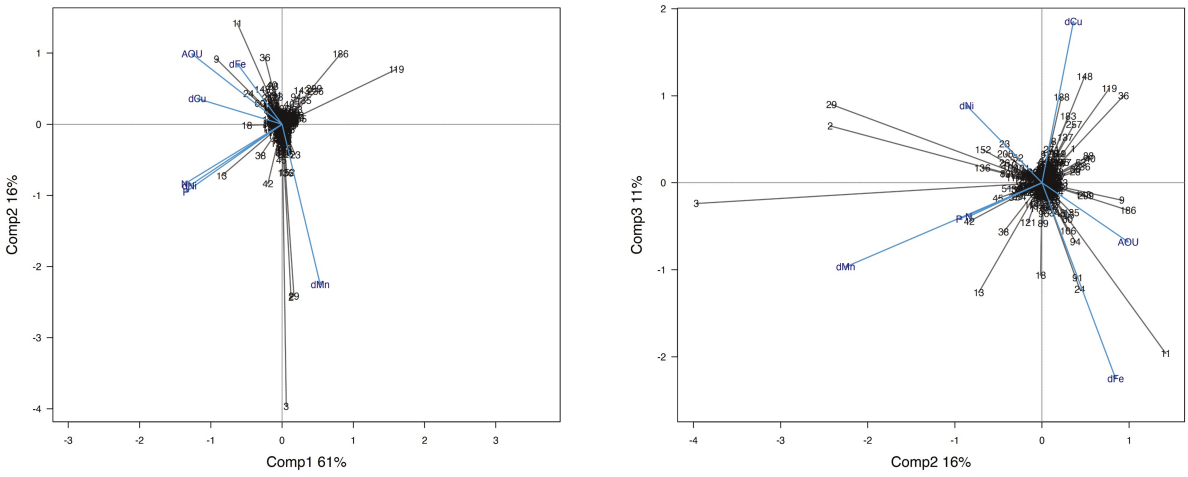

Fig. S8. Partial least squares regression analysis (PLSr) linking abundant ASVs (relative abundance ≥ 1% in at least one sample) with environmental variables. Blue short labels describe the environmental variables (AOU, apparent oxygen utilization; P, phosphate; N, nitrate; dMn, dissolved manganese; dFe, dissolved iron; dNi, dissolved nickel; dCu, dissolved copper) whereas grey short labels describe the ASVs.

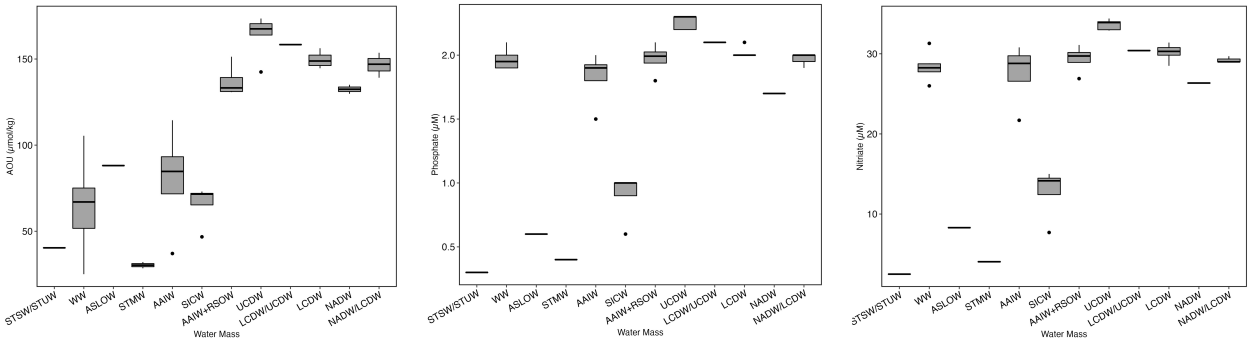

Fig. S9. The concentration of apparent oxygen utilization (AOU, μmol kg^{-1}), phosphate (μM) and nitrate (μM) in different surface waters and water masses (STSW/STUW, n=1; WW, n=6; ASLOW, n=1; STMW, n=2; AAIW, n=4; SICW, n=4; AAIW+RSOW, n=4; UCDW, n=5, LCDW/UCDW, n=1; LCDW, n=6; NADW, n=2; NADW/LCDW, n=3).

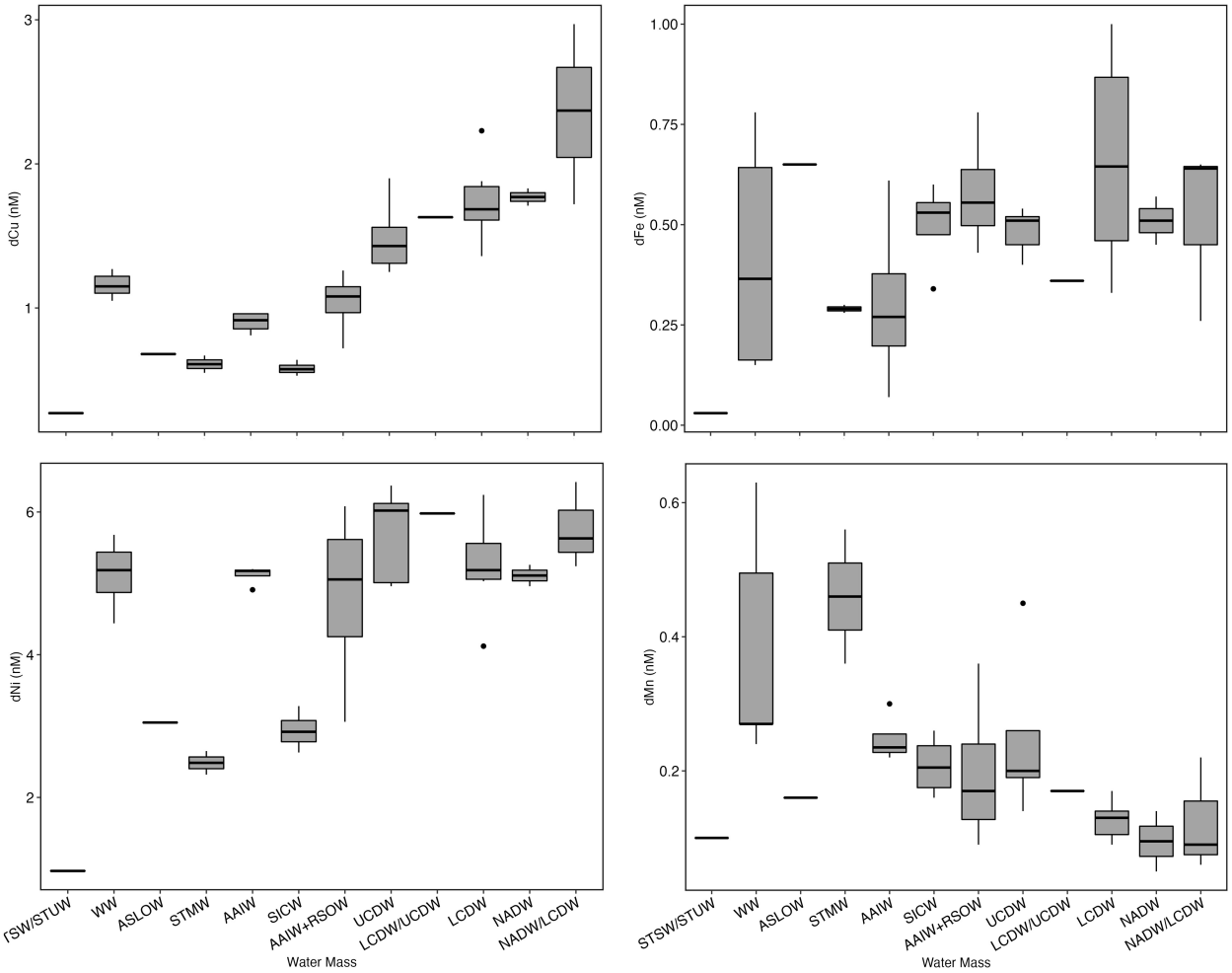

Fig. S10. The concentration of dissolved Cu (nM), dissolved Fe (nM), dissolved Ni (nM) and dissolved Mn (nM) in different surface waters and water masses (STSW/STUW, n=1; WW, n=6; ASLOW, n=1; STMW, n=2; AAIW, n=4; SICW, n=4; AAIW+RSOW, n=4; UCDW, n=5, LCDW/UCDW, n=1; LCDW, n=6; NADW, n=2; NADW/LCDW, n=3).

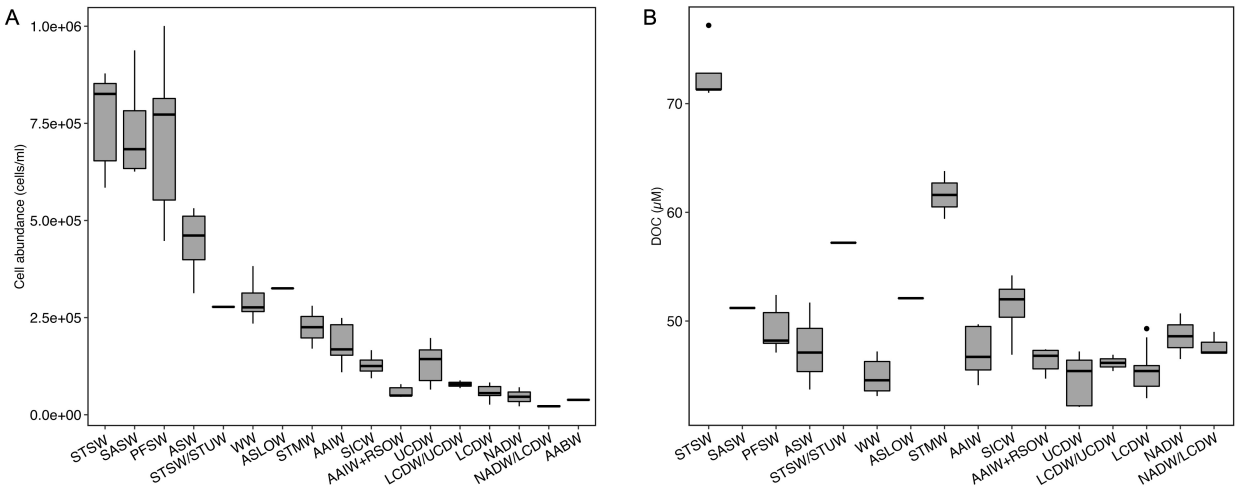

Fig. S11. A. Cell abundance of prokaryotes in different surface waters and water masses (STSW, n=5; SASW, n=4; PFSW, n=6; ASW, n=10; STSW/STUW, n=1; WW, n=6; ASLOW, n=1; STMW, n=2; AAIW, n=7; SICW, n=4; AAIW+RSOW, n=5; UCDW, n=10, LCDW/UCDW, n=2; LCDW, n=15; NADW, n=2; NADW/LCDW, n=3; AABW, n=1). B. DOC concentrations in different surface waters and water masses (STSW, n=5; SASW, n=4; PFSW, n=6; ASW, n=10; STSW/STUW, n=1; WW, n=6; ASLOW, n=1; STMW, n=2; AAIW, n=7; SICW, n=4; AAIW+RSOW, n=5; UCDW, n=10, LCDW/UCDW, n=2; LCDW, n=12; NADW, n=2; NADW/LCDW, n=3).

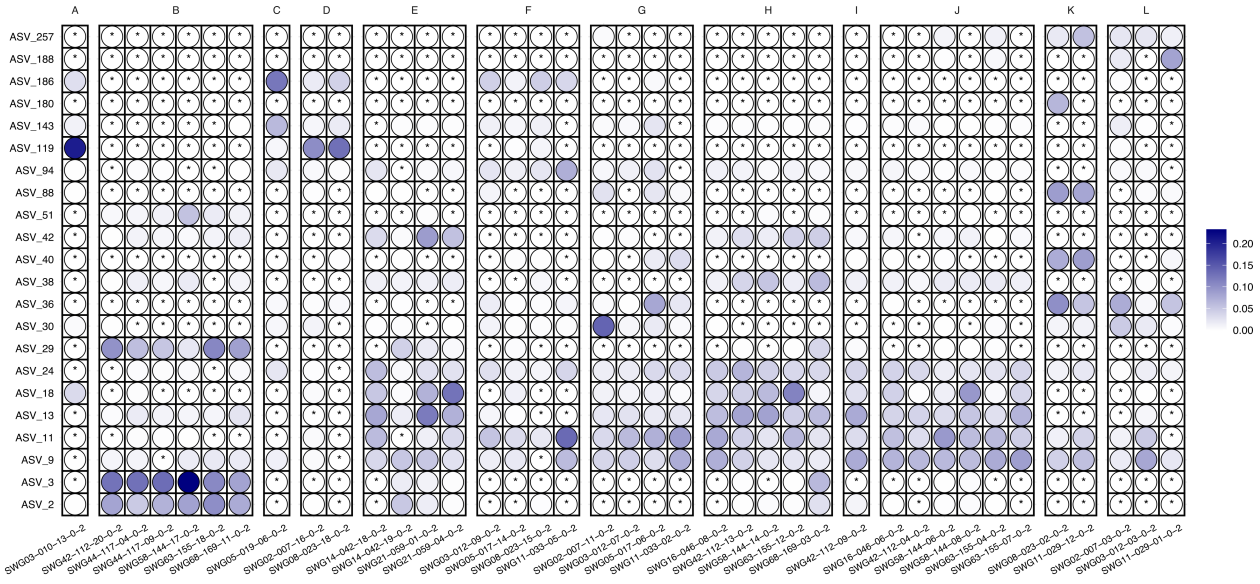

Fig.S12. Relative abundance of 22 abundant ASVs (relative abundance of ASVs >=5% in at least one sample) in different free-living prokaryotic community samples. Asterisks indicates that the relative abundance of ASV is 0. A. STSW/STUW; B. WW; C. ASLOW; D. STMW; E. AAIW; F. SICW; G. AAIW+RSOW; H. UCDW; I. LCDW/UCDW; J. LCDW; K. NADW; L. NADW/LCDW.

Table S1. List of indicator species with their indicator value, p-value and frequency in each surface water and water mass in the free-living prokaryotic community.

Water Mass	Family	Indicator Value	p-value	Frequency
ASW	ASV_78_Cryomorphaceae	0.48	0.029	23
	ASV_132_Cyclobacteriaceae	0.70	0.002	33
	ASV_214_Flavobacteriaceae	0.52	0.001	21
	ASV_32_Flavobacteriaceae	0.41	0.003	32
	ASV_456_Flavobacteriaceae	0.62	0.049	12
	ASV_49_Flavobacteriaceae	0.39	0.044	37
	ASV_70_Flavobacteriaceae	0.68	0.001	17
	ASV_80_Flavobacteriaceae	0.52	0.001	23
	ASV_5_Halieaceae	0.40	0.027	27
	ASV_104_Nitrincolaceae	0.61	0.001	24
	ASV_72_Nitrincolaceae	0.48	0.002	28
	ASV_168_NS9 marine group	0.69	0.001	13
	ASV_262_Order_Defluviicoccales	0.45	0.009	23
	ASV_539_Porticoccaceae	0.50	0.031	16
	ASV_147_Rhodobacteraceae	0.52	0.004	23
	ASV_34_Rhodobacteraceae	0.59	0.001	26
	ASV_57_Rhodobacteraceae	0.54	0.001	31
	ASV_87_Rhodobacteraceae	0.70	0.01	20
	ASV_505_SAR116 clade	0.73	0.002	13
	ASV_71_SAR116 clade	0.43	0.001	31
	ASV_100_SAR86 clade	0.65	0.001	23
	ASV_103_SAR86 clade	0.70	0.001	27
	ASV_707_SAR86 clade	0.65	0.028	9
	ASV_545_Thiotrichaceae	0.48	0.047	13
STSW	ASV_304_Actinomarinaceae	0.89	0.001	6
	ASV_1030_AEGEAN-169 marine group	0.80	0.015	4
	ASV_261_AEGEAN-169 marine group	0.89	0.001	8
	ASV_3144_AEGEAN-169 marine group	0.80	0.047	4
	ASV_187_SAR11 Clade I	1.00	0.001	5
	ASV_209_SAR11 Clade I	0.75	0.001	8
	ASV_256_SAR11 Clade I	0.83	0.001	6
	ASV_484_SAR11 Clade I	0.80	0.027	4
	ASV_567_SAR11 Clade I	0.80	0.009	4
	ASV_58_SAR11 Clade I	0.68	0.002	13

	ASV_702_SAR11 Clade I	1.00	0.001	5
	ASV_769_SAR11 Clade I	0.80	0.003	4
	ASV_780_SAR11 Clade I	0.80	0.017	4
	ASV_807_SAR11 Clade I	0.80	0.009	4
	ASV_910_SAR11 Clade I	0.80	0.036	4
	ASV_462_SAR11 Clade II	0.83	0.021	6
	ASV_520_SAR11 Clade II	1.00	0.001	5
	ASV_561_SAR11 Clade IV	0.74	0.029	6
	ASV_840_SAR11 Clade IV	0.86	0.032	8
	ASV_287_Cyanobiaceae	0.80	0.012	4
	ASV_451_Cyanobiaceae	0.80	0.012	4
	ASV_470_Cyanobiaceae	0.80	0.012	4
	ASV_56_Cyanobiaceae	0.94	0.001	7
	ASV_625_Cyanobiaceae	0.80	0.01	4
STSW	ASV_642_Cyanobiaceae	0.80	0.018	4
	ASV_65_Cyanobiaceae	0.96	0.001	6
	ASV_8_Cyanobiaceae	0.86	0.001	14
	ASV_833_Cyanobiaceae	0.80	0.008	4
	ASV_912_Cyanobiaceae	0.80	0.01	4
	ASV_495_Cyclobacteriaceae	0.80	0.01	4
	ASV_474_Flavobacteriaceae	0.80	0.044	4
	ASV_783_Flavobacteriaceae	1.00	0.001	5
	ASV_660_Halieaceae	1.00	0.001	5
	ASV_926_KI89A clade	1.00	0.001	5
	ASV_611_NS9 marine group	0.80	0.03	4
	ASV_1525_OCS116 clade	0.72	0.042	6
	ASV_1087_Order_Marine Group II	0.73	0.043	5
	ASV_548_Order_Marine Group II	0.80	0.045	4
	ASV_729_Order_Marine Group II	0.95	0.001	6
	ASV_759_Order_Marine Group II	0.80	0.043	4
	ASV_1017_Order_Marine Group III	0.72	0.05	7
	ASV_613_SAR406 clade	0.77	0.025	5
	ASV_392_Rhodobacteraceae	0.80	0.045	4
	ASV_395_Rhodobacteraceae	0.99	0.001	6
	ASV_467_Rhodobacteraceae	0.77	0.044	8
	ASV_541_Rhodobacteraceae	0.68	0.048	5
	ASV_1048_SAR116 clade	0.82	0.001	6

	ASV_191_SAR116 clade	0.95	0.001	7
	ASV_290_SAR116 clade	0.95	0.001	7
	ASV_388_SAR116 clade	0.92	0.001	6
	ASV_483_SAR86 clade	0.80	0.03	4
	ASV_499_SAR86 clade	0.93	0.001	8
	ASV_569_SAR86 clade	0.77	0.023	5
	ASV_584_SAR86 clade	1.00	0.001	5
SASW	ASV_574_AEGEAN-169 marine group	0.76	0.01	10
	ASV_166_Cryomorphaceae	0.50	0.012	28
	ASV_112_Flavobacteriaceae	0.46	0.003	32
	ASV_124_Flavobacteriaceae	0.41	0.014	23
	ASV_129_Flavobacteriaceae	0.55	0.003	25
	ASV_21_Flavobacteriaceae	0.52	0.019	28
	ASV_394_Flavobacteriaceae	0.86	0.001	7
	ASV_204_Methylophilaceae	0.45	0.049	28
	ASV_269_Nisaeaceae	0.39	0.014	26
	ASV_122_OCS116 clade	0.42	0.023	33
	ASV_156_SAR11 Clade I	0.59	0.01	27
	ASV_350_SAR11 Clade II	0.60	0.001	24
	ASV_195_SAR11 Clade IV	0.59	0.001	23
	ASV_169_SAR116 clade	0.69	0.002	20
	ASV_216_SAR86 clade	0.65	0.03	16
	ASV_243_SAR86 clade	0.60	0.03	8
	ASV_509_SAR86 clade	0.80	0.001	8
	ASV_92_SAR86 clade	0.55	0.014	28
	ASV_182_Thioglobaceae	0.49	0.015	17
	ASV_213_Thiotrichaceae	0.53	0.046	23
PFSW	ASV_123_SAR11 Clade I	0.38	0.031	29
	ASV_140_NS9 marine group	0.43	0.002	27
	ASV_177_Flavobacteriaceae	0.55	0.001	18
	ASV_26_Rhodobacteraceae	0.41	0.027	25
	ASV_260_Rhodobacteraceae	0.45	0.01	22
	ASV_33_Rhodobacteraceae	0.36	0.006	30
	ASV_387_SAR11 Clade I	0.56	0.014	12
	ASV_6_Rhodobacteraceae	0.32	0.045	32
	ASV_819_Flavobacteriaceae	0.54	0.031	12
	ASV_82_SAR86 clade	0.32	0.015	29

WW	ASV_29_Candidatus Nitrosopumilus	0.54	0.041	34
	ASV_749_Family_Ectothiorhodospiraceae	0.67	0.004	19
	ASV_201_Family_OM182 clade	0.45	0.002	29
	ASV_109_Family_SAR86 clade	0.36	0.01	29
	ASV_178_Lentibacter	0.43	0.001	29
	ASV_510_LS-NOB	0.66	0.004	12
	ASV_883_Magnetospira	0.72	0.013	11
	ASV_684_Nitrosomonas	0.65	0.027	13
	ASV_267_Order_Marine Group II	0.76	0.001	15
	ASV_320_Order_SAR11 clade	0.33	0.049	27
	ASV_117_Pseudohongiella	0.40	0.001	30
	ASV_139_Roseobacter clade NAC11-7 lineage	0.39	0.003	32
	ASV_210_SAR324 clade(Marine group B)	0.64	0.023	22
	ASV_136_SAR406 clade	0.63	0.002	24
	ASV_375_SAR406 clade	0.57	0.001	21
	ASV_3_SUP05 cluster	0.48	0.001	36
	ASV_817_Sva0996 marine group	0.68	0.002	15
	ASV_537_Woeseia	0.77	0.001	16
ASLOW	ASV_5394_AEGEAN-169 marine group	1.00	0.044	1
	ASV_1443_Nitrosopumilaceae	0.79	0.043	3
	ASV_724_Order UBA10353 marine group	0.89	0.05	2
	ASV_143_SAR11 Clade I	0.52	0.041	40
	ASV_3042_SAR11 Clade II	0.98	0.049	3
	ASV_186_SAR324 clade(Marine group B)	0.57	0.048	10
	ASV_2261_SAR406 clade	0.79	0.045	6
	ASV_442_SAR406 clade	0.48	0.031	15
	ASV_4703_SAR406 clade	0.89	0.04	2
STMW	ASV_2579_SAR11 Clade II	0.81	0.046	3
AAIW	ASV_1371_Nitrosopumilaceae	0.83	0.001	6
	ASV_42_Nitrosopumilaceae	0.48	0.01	38
	ASV_424_Nitrosopumilaceae	0.68	0.032	10
	ASV_688_Order_Marine Group II	0.67	0.013	11
	ASV_809_Order_Marine Group II	0.79	0.027	7
AAIW+RSOW	ASV_1981_Nitrosopumilaceae	0.90	0.006	7
	ASV_91_Nitrosopumilaceae	0.33	0.025	34
	ASV_422_Order_UBA10353 marine group	0.62	0.045	16
	ASV_1825_SAR324 clade(Marine group B)	0.71	0.039	7

SICW	ASV_805_Nitrosopumilaceae	0.71	0.032	11
	ASV_716_Order_Marine Group III	0.81	0.043	6
	ASV_741_Order_SAR202 clade	1.00	0.001	4
UCDW	ASV_286_Microtrichaceae	0.46	0.035	24
	ASV_981_Nitrosopumilaceae	0.54	0.014	14
	ASV_105_Order_HOC36	0.32	0.024	37
	ASV_1948_Rhodobacteraceae	0.72	0.035	9
	ASV_763_SAR406 clade	0.52	0.039	17
LCDW	ASV_650_Nitrosopumilaceae	0.56	0.042	11
	ASV_384_Order_Marine Group III	0.91	0.001	10
NADW	ASV_59_Class_Gammaproteobacteria	0.44	0.014	46
	ASV_88_Comamonadaceae	0.77	0.021	19
	ASV_318_Marinomonadaceae	0.78	0.028	11
	ASV_40_Pseudoalteromonadaceae	0.72	0.007	26
	ASV_46_Pseudoalteromonadaceae	0.39	0.043	38
	ASV_410_Rhizobiaceae	0.80	0.031	12
	ASV_328_SAR406 clade	0.59	0.035	13
	ASV_341_SAR86 clade	0.46	0.033	21
	ASV_133_Sphingomonadaceae	0.73	0.013	19
	ASV_1452_Thioglobaceae	0.98	0.002	3
NADW/LCDW	ASV_246_Order_Arctic97B-4 marine group	0.80	0.001	12
	ASV_869_Order_Marine Group II	0.47	0.04	14
	ASV_2150_SAR11 Clade I	0.97	0.001	6
	ASV_2284_SAR406 clade	0.94	0.001	7
	ASV_329_Vibrionaceae	0.82	0.046	6
LCDW/UCDW	ASV_44_Flavobacteriaceae	0.76	0.007	11
	ASV_1601_Halomicrobiaceae	0.65	0.003	12
	ASV_982_Microtrichaceae	0.73	0.004	10
	ASV_1172_Nitrosopumilaceae	0.82	0.001	8
	ASV_792_Nitrosopumilaceae	0.54	0.025	11
	ASV_837_Order_HOC36	0.81	0.003	8
	ASV_543_Order_SAR202 clade	0.32	0.034	26
	ASV_891_Phylum_PAUC34f	0.61	0.001	17
	ASV_1539_SAR11 Clade I	0.83	0.004	9
	ASV_617_SAR11 Clade I	0.52	0.012	12
	ASV_629_SAR11 Clade I	0.60	0.001	12
	ASV_1817_SAR324 clade(Marine group B)	0.72	0.038	6

LCDW/UCDW	ASV_814_SAR324 clade(Marine group B)	0.60	0.025	9
	ASV_116_SAR406 clade	0.31	0.031	35
	ASV_1332_SAR406 clade	0.78	0.001	10
	ASV_1564_SAR406 clade	0.73	0.008	7
	ASV_327_SAR406 clade	0.51	0.044	21
	ASV_402_SAR406 clade	0.42	0.01	19
	ASV_645_SAR406 clade	0.54	0.003	13
	ASV_244_Sphingomonadaceae	0.78	0.025	5
AABW	ASV_1651_Flavobacteriaceae	0.95	0.006	4
	ASV_39_Flavobacteriaceae	0.89	0.001	11
	ASV_978_Magnetospiraceae	0.88	0.011	6
	ASV_1447_Marinimicrobia (SAR406 clade)	0.95	0.004	3
	ASV_271_Marinimicrobia (SAR406 clade)	0.61	0.043	13
	ASV_409_Marinimicrobia (SAR406 clade)	0.47	0.046	19
	ASV_839_Marinimicrobia (SAR406 clade)	0.77	0.003	14
	ASV_84_Microtrichaceae	0.49	0.006	30
	ASV_832_Nitrosopumilaceae	0.73	0.039	6
	ASV_151_Nitrospinaceae	0.43	0.001	24
	ASV_2148_OM182 clade	0.99	0.008	2
	ASV_1373_Order_Arctic97B-4 marine group	0.71	0.022	10
	ASV_319_Order_Arctic97B-4 marine group	0.97	0.009	2
	ASV_948_Order_Arctic97B-4 marine group	0.74	0.019	6
	ASV_412_Order_Marine Group II	0.47	0.023	21
	ASV_1057_Order_UBA10353 marine group	0.75	0.023	7
	ASV_247_Pirellulaceae	0.54	0.001	22
	ASV_179_Pseudohongiellaceae	0.74	0.007	17
	ASV_2778_Pseudohongiellaceae	0.86	0.02	4
	ASV_1753_Rhodothermaceae	0.89	0.042	5
	ASV_962_SAR11 Clade I	0.61	0.002	13
	ASV_393_SAR11 Clade II	0.70	0.005	8
	ASV_291_Thioglobaceae	0.77	0.037	9

Table S2. List of indicator species with their indicator value, p-value and frequency in each surface water and water mass in the particle-attached prokaryotic community.

Water Mass	Family	Indicator Value	p-value	Frequency
ASW	ASV_78_Cryomorphaceae	0.80	0.001	11
	ASV_10_Flavobacteriaceae	0.35	0.018	45
	ASV_17_Flavobacteriaceae	0.73	0.003	25
	ASV_32_Flavobacteriaceae	0.61	0.001	24
	ASV_49_Flavobacteriaceae	0.50	0.003	21
	ASV_50_Flavobacteriaceae	0.47	0.03	26
	ASV_70_Flavobacteriaceae	0.91	0.001	12
	ASV_283_NS9 marine group	0.58	0.044	14
	ASV_34_Rhodobacteraceae	0.59	0.004	19
	ASV_87_Rhodobacteraceae	0.59	0.045	17
	ASV_100_SAR86 clade	0.61	0.044	10
STSW	ASV_1310_Actinomarinaceae	0.60	0.047	3
	ASV_56_Cyanobiaceae	0.79	0.004	5
	ASV_586_Cyanobiaceae	0.59	0.032	5
	ASV_65_Cyanobiaceae	0.91	0.001	11
	ASV_8_Cyanobiaceae	0.78	0.016	8
	ASV_966_Cyanobiaceae	0.78	0.044	5
	ASV_378_Flavobacteriaceae	0.80	0.042	4
	ASV_516_Flavobacteriaceae	0.80	0.014	4
	ASV_564_Flavobacteriaceae	0.80	0.041	4
	ASV_783_Flavobacteriaceae	1.00	0.001	5
	ASV_611_NS9 marine group	0.80	0.049	4
	ASV_361_Order_Chitinophagales	0.59	0.05	6
	ASV_317_Phycisphaeraceae	1.00	0.001	5
	ASV_686_Porticoccaceae	0.80	0.026	4
	ASV_1427_PS1 clade	0.80	0.027	4
	ASV_392_Rhodobacteraceae	0.80	0.047	4
	ASV_395_Rhodobacteraceae	0.80	0.036	4
	ASV_467_Rhodobacteraceae	0.80	0.02	4
	ASV_469_Rhodobacteraceae	0.80	0.015	4
	ASV_475_Rhodobacteraceae	0.80	0.028	4
	ASV_541_Rhodobacteraceae	0.80	0.026	4
	ASV_758_Rhodobacteraceae	0.80	0.035	4
	ASV_1151_Rubritaleaceae	0.80	0.04	4
	ASV_256_SAR11 Clade I	0.80	0.008	4
	ASV_520_SAR11 Clade II	0.80	0.034	4
	ASV_290_SAR116 clade	0.80	0.028	4
	ASV_388_SAR116 clade	0.80	0.026	4
	ASV_703_SAR324 clade(Marine group B)	0.77	0.014	5

	ASV_1359_Thiotrichaceae	0.80	0.04	4
SASW	ASV_25_Cyanobiaceae	0.57	0.001	33
	ASV_309_Cyanobiaceae	1.00	0.001	4
	ASV_478_Flavobacteriaceae	0.97	0.001	5
	ASV_86_Flavobacteriaceae	0.83	0.007	9
	ASV_673_Halieaceae	0.72	0.017	7
	ASV_75_Rhodobacteraceae	0.60	0.028	20
STSW/STUW	ASV_119_Nitrosopumilaceae	0.80	0.042	2
	ASV_4520_Nitrospinaceae	1.00	0.034	1
	ASV_958_Order_Arctic97B-4 marine group	0.83	0.031	4
	ASV_3143_Order_UBA10353 marine group	1.00	0.026	1
	ASV_486_Phylum_NB1-j	0.60	0.001	17
	ASV_1965_Pirellulaceae	0.95	0.033	2
	ASV_1998_Pirellulaceae	0.93	0.031	2
	ASV_181_SAR11 Clade I	0.88	0.016	7
	ASV_217_SAR11 Clade II	0.68	0.05	9
	ASV_186_SAR324 clade(Marine group B)	0.72	0.048	4
	ASV_354_SAR324 clade(Marine group B)	0.82	0.034	6
PFSW	ASV_5_Halieaceae	0.30	0.024	36
	ASV_97_Pirellulaceae	0.63	0.029	28
	ASV_364_Rubritaleaceae	0.67	0.05	10
WW	ASV_310_Flavobacteriaceae	0.67	0.019	13
	ASV_29_Nitrosopumilaceae	0.88	0.001	11
	ASV_152_Nitrospinaceae	0.75	0.018	8
	ASV_20_Pirellulaceae	0.50	0.042	22
	ASV_67_Rubritaleaceae	0.54	0.013	17
ASLOW	ASV_1815_Arctic95B-14	0.93	0.037	5
	ASV_3428_Flavobacteriaceae	0.97	0.033	2
	ASV_1513_Magnetospiraceae	0.92	0.025	3
	ASV_937_Order_Planctomycetales	0.78	0.027	6
	ASV_2235_Phylum_NB1-j	0.98	0.047	2
	ASV_2768_Phylum_NB1-j	0.85	0.036	3
	ASV_1185_Pirellulaceae	0.84	0.034	2
	ASV_2973_Pirellulaceae	0.95	0.034	3
	ASV_427_Planococcaceae	0.72	0.039	10
	ASV_3381_SAR11 Clade I	1.00	0.047	1
STMW	ASV_622_Gimesiaceae	1.00	0.004	2
	ASV_527_Moraxellaceae	0.77	0.033	5
	ASV_572_Schleiferiaceae	0.76	0.05	3
AAIW	ASV_212_Rubritaleaceae	0.65	0.006	24
AAIW+RSOW	ASV_1201_Class_Pla3 lineage	0.80	0.045	4
	ASV_960_Phylum_NB1-j	0.76	0.035	5

	ASV_911_Pirellulaceae	0.80	0.035	4
SICW	ASV_1474_Bdellovibrionaceae	0.72	0.047	5
	ASV_535_Class_OM190	0.71	0.046	4
	ASV_1396_Order_Marine Group III	0.50	0.049	2
	ASV_1862_Order_SAR202 clade	0.50	0.047	2
LCDW	ASV_797_Class_OM190	0.68	0.005	11
NADW	ASV_180_Alteromonadaceae	0.96	0.035	4
	ASV_40_Pseudoalteromonadaceae	0.62	0.016	33
	ASV_133_Sphingomonadaceae	0.49	0.04	28
NADW/LCDW	ASV_1400_Phycisphaeraceae	0.65	0.049	3
	ASV_2659_Order_WCHB1-41	0.66	0.039	3
	ASV_53_SAR11 Clade II	0.39	0.001	30
LCDW/UCDW	ASV_141_Pseudoalteromonadaceae	0.49	0.021	22
	ASV_19_Pseudoalteromonadaceae	0.43	0.025	46
	ASV_857_Pseudomonadaceae	0.93	0.006	6
AABW	ASV_1008_Spongiibacteraceae	0.88	0.018	6
	ASV_1757_Class_Alphaproteobacteria	0.99	0.032	2
	ASV_1221_Class_OM190	0.97	0.043	2
	ASV_2022_Class_OM190	1.00	0.03	1
	ASV_1171_Corynebacteriaceae	0.80	0.016	9
	ASV_848_Family XI	1.00	0.04	1
	ASV_556_Flavobacteriaceae	0.94	0.001	11
	ASV_1051_Hydrogenedensaceae	1.00	0.04	1
	ASV_1610_Hydrogenedensaceae	1.00	0.041	1
	ASV_589_Magnetospiraceae	0.73	0.034	12
	ASV_978_Magnetospiraceae	0.87	0.032	4
	ASV_222_Nitrosopumilaceae	0.58	0.036	8
	ASV_319_Order_Arctic97B-4 marine group	0.94	0.003	4
	ASV_777_Order_Arctic97B-4 marine group	0.84	0.004	9
	ASV_2349_Phylum_NB1-j	1.00	0.042	1
	ASV_1554_Phylum_PAUC34f	1.00	0.042	1
	ASV_2525_Phylum_PAUC34f	1.00	0.037	1
	ASV_1160_Pirellulaceae	1.00	0.036	1
	ASV_247_Pirellulaceae	0.91	0.005	13
	ASV_864_Propionibacteriaceae	0.96	0.001	11
	ASV_174_Rhodobacteraceae	0.42	0.047	21
	ASV_54_Staphylococcaceae	0.75	0.032	15
	ASV_1468_Streptococcaceae	1.00	0.036	1
	ASV_2018_Streptococcaceae	1.00	0.04	1
	ASV_873_Streptococcaceae	1.00	0.034	1

Table S3. Taxonomic of 22 abundant ASVs (ASVs with a relative abundance of ≥ 5% in at least one sample).

ASV	Kingdom	Phylum	Class	Order	Family	Genus	Species
ASV_11	Archaea	Crenarchaeota	Nitrososphaeria	Nitrosopumilales	Nitrosopumilaceae	Family_Nitrosopumilaceae	Family_Nitrosopumilaceae
ASV_119	Archaea	Crenarchaeota	Nitrososphaeria	Nitrosopumilales	Nitrosopumilaceae	Candidatus Nitrosopelagicus	Genus_Candidatus Nitrosopelagicus
ASV_13	Bacteria	SAR324 clade(Marine group B)	Phylum_SAR324 clade	Phylum_SAR324 clade	Phylum_SAR324 clade	Phylum_SAR324 clade	Phylum_SAR324 clade
ASV_143	Bacteria	Proteobacteria	Alphaproteobacteria	SAR11 clade	Clade I	Clade Ib	Genus_Clade Ib
ASV 18	Archaea	Thermoplasmatota	Thermoplasmata	Marine Group II	Order Marine Group II	Order Marine Group II	Order Marine Group II
ASV 180	Bacteria	Proteobacteria	Gammaproteobacteria	Enterobacterales	Alteromonadaceae	Aestuariibacter	aggregatus
ASV 186	Bacteria	SAR324 clade(Marine group B)	Phylum SAR324 clade	Phylum SAR324 clade	Phylum SAR324 clade	Phylum SAR324 clade	Phylum SAR324 clade
ASV 188	Bacteria	SAR324 clade(Marine group B)	Phylum SAR324 clade	Phylum SAR324 clade	Phylum SAR324 clade	Phylum SAR324 clade	Phylum SAR324 clade
ASV 2	Bacteria	Proteobacteria	Alphaproteobacteria	SAR11 clade	Clade I	Clade Ia	Genus Clade Ia
ASV 24	Bacteria	Proteobacteria	Gammaproteobacteria	Pseudomonadales	Thioglobaceae	SUP05 cluster	Genus SUP05 cluster
ASV 257	Archaea	Crenarchaeota	Nitrososphaeria	Nitrosopumilales	Nitrosopumilaceae	Family Nitrosopumilaceae	Family Nitrosopumilaceae
ASV 29	Archaea	Crenarchaeota	Nitrososphaeria	Nitrosopumilales	Nitrosopumilaceae	Candidatus Nitrosopumilus	Genus Candidatus Nitrosopumilus
ASV 3	Bacteria	Proteobacteria	Gammaproteobacteria	Pseudomonadales	Thioglobaceae	SUP05 cluster	Genus SUP05 cluster
ASV 30	Bacteria	Proteobacteria	Gammaproteobacteria	Burkholderiales	Burkholderiaceae	Cupriavidus	metallidurans
ASV 36	Bacteria	Proteobacteria	Gammaproteobacteria	Enterobacterales	Pseudoalteromonadaceae	Pseudoalteromonas	Genus Pseudoalteromonas
ASV 38	Bacteria	Proteobacteria	Gammaproteobacteria	Pseudomonadales	Thioglobaceae	SUP05 cluster	Genus SUP05 cluster
ASV 40	Bacteria	Proteobacteria	Gammaproteobacteria	Enterobacterales	Pseudoalteromonadaceae	Pseudoalteromonas	Genus Pseudoalteromonas
ASV 42	Archaea	Crenarchaeota	Nitrososphaeria	Nitrosopumilales	Nitrosopumilaceae	Candidatus Nitrosopumilus	Genus Candidatus Nitrosopumilus
ASV 51	Bacteria	Bacteroidota	Bacteroidia	Flavobacteriales	NS9 marine group	Family NS9 marine group	Family NS9 marine group
ASV_88	Bacteria	Proteobacteria	Gammaproteobacteria	Burkholderiales	Comamonadaceae	Aquabacterium	parvum
ASV_9	Bacteria	SAR324 clade(Marine group B)	Phylum_SAR324 clade	Phylum_SAR324 clade	Phylum_SAR324 clade	Phylum_SAR324 clade	Phylum_SAR324 clade
ASV_94	Archaea	Crenarchaeota	Nitrososphaeria	Nitrosopumilales	Nitrosopumilaceae	Family_Nitrosopumilaceae	Family_Nitrosopumilaceae

Chapter 3

Spatial variations in microbial trace metal transporters across surface and deep water masses of the Southern Ocean

Rui Zhang[1], Pavla Debeljak[2], Sharvari Gadegaonkar[1], Corentin Baudet[3], Hélène Planquette[3], Stéphane Blain[1], Ingrid Obernosterer[1*]

[1] CNRS, Sorbonne Université, Laboratoire d'Océanographie Microbienne, LOMIC, F-66650 Banyuls/mer, France.
[2] Sorbonne Université, Muséum National d'Histoire Naturelle, CNRS, EPHE, Université des Antilles, Institut de Systématique, Evolution, Biodiversité (ISYEB), F-75005, Paris, France.
[3] Université Bretagne Occidentale, CNRS, IRD, Ifremer, UMR 6539, LEMAR, F-29280 Plouzané, France.

* Corresponding author

Preface

This thesis chapter is part of the South Indian Ocean GEOTRACES Section (SWINGS) cruise. I collected the samples, and performed the DNA extractions and conducted all bioinformatic analysis. The trace metal data were provided by Corentin Baudet and Hélène Planquette.

Abstract

Trace metals are essential for the growth and metabolism of marine prokaryotes. While the concentrations of trace metals have been quantified on large spatial scales and in different water masses, the links between microbial metabolism and trace metals remains poorly understood. In this study, we aimed to address this question by investigating genes related to trace-metal transport by prokaryotic communities inhabiting distinct water masses in the Indian Sector of the Southern Ocean. Using a metagenomics approach, we analyzed 42 samples collected from 13 different stations in the Subtropical, Subantarctic, Polar Frontal and Antarctic zones during the SWINGS cruise. We searched for genes associated with the transport of Fe, Mn, Ni and Cu in the free-living (<0.8 μm) and particle-attached (>0.8 μm) fractions at the community level as well as in metagenome assembled genomes (MAGs). Our results reveal differences in the normalized abundance of these genes (GPM) depending on geographic location in surface waters and among water masses at depth. These latter were particularly pronounced for transporters of siderophores, Mn, Ni and Cu. Each water mass contained a distinct set of abundant MAGs and these were found to differ in their repertoires of trace metal transporters. Our observations suggest that these trace metals could play distinct roles in microbial metabolism in different water masses, with potential feedbacks on their cycling in the ocean.

Introduction

Prokaryotes are widely distributed across the ocean, constituting approximately 70% and 75% of the total biomass in surface and deep waters respectively (Fuhrman *et al.*, 1989). These prokaryotic communities exhibit significant functional diversity and play a crucial role in influencing the biogeochemical cycles of marine ecosystems (Pedrós-Alió, 2006; Azam and Malfatti, 2007; Falkowski *et al.*, 2008; Buchan *et al.*, 2014; Lechtenfeld *et al.*, 2015). Prokaryotes rely on macroelements such as carbon (C), oxygen (O), hydrogen (H), nitrogen (N), sulphur (S) and phosphorous (P), to derive their nutritional and metabolic requirements. Micronutrients, such as the trace metals in the marine ecosystems are crucial for the sustenance and are major cofactors in varying metabolic processes. Iron (Fe) is highly limiting in marine ecosystems due to its fairly low solubility, though it is the most essential nutrient for microbial heterotrophic metabolism, particularly in processes such as respiration, nitrogen fixation and consumption of N. Limited Fe availability regulates the productivity of phytoplankton, processing of organic carbon by prokaryotes, the structure of communities, and the functioning of ecosystems across extensive areas of the world's oceans (Moore *et al.*, 2001; Gledhill, 2012; Fourquez *et al.*, 2014; Bradley *et al.*, 2020; Sun *et al.*, 2021). Microbes produce and utilize siderophores, which are potent molecules that bind iron, to obtain Fe from its limiting environment. They contribute largely to Fe availability as a part of the iron-binding ligand pool in seawater (Park *et al.*, 2023). Furthermore, heterocyclic cofactor molecules containing iron i.e., heme play a crucial role in enzymatic processes such as photosynthesis, respiration and assimilation of N (Hogle *et al.*, 2014).

Additionally, trace metals such as manganese (Mn), nickel (Ni), and copper (Cu) are considered to be important components of many essential metalloproteins in prokaryotes. Manganese (Mn) serves as a cofactor for various enzymes participating in central carbon metabolism, nucleotide metabolism, photosynthesis, peptide cleavage, antioxidant activity, translation, and signaling (Hansel, 2017; Bosma *et al.*, 2021). Nickel (Ni) acts as an essential micronutrient and is indispensable for chemolithotrophic prokaryotes, it is an essential cofactor for some pathogen virulence factors (Gikas, 2008; Maier and Benoit, 2019), plays a key role in methanogenesis, N utilization and fixation. Ni is further an essential cofactor of super oxide dismutase (SOD) cleaving superoxidase radicals generated via photosynthesis and processes related to organic matter degradation. Copper (Cu) acts as a cofactor for numerous proteins involved in redox reactions, oxidative respiration, denitrification, photosynthesis, N and S cycling. Cu is required for the optimum functioning of

phytoplankton especially in plastocyanin containing species (Argüello *et al.*, 2013; Kong and Price, 2020).

In order to thrive in different water masses, prokaryotes adopt different strategies, in response to varying physicochemical and nutrient conditions. Water masses refer to extensive bodies of water characterized by similar physical and chemical attributes such as temperature, salinity, and density (Emery, 2001). Water masses exhibit gradients in major and trace metal concentrations. It has been shown that the composition of prokaryotic communities varies across water bodies (Lekunberri *et al.*, 2013; Hernando-Morales *et al.*, 2017; Milici *et al.*, 2017; Vipindas *et al.*, 2023). While links between ocean characteristics such as temperature, depth, nutrients, and community composition have been established (Raes *et al.*, 2018), little is known on the role of trace metals influencing prokaryotic community composition (Zhang *et al*., in revision).

The free-living (FL) and particle-attached (PA) fractions represent different niches in the aquatic system, they have shown to differ in their microbial community structure and therefore, contribute in a different way to the biogeochemical cycles due to the underlying metabolic differences. Although FL and PA microbes employ similar approaches to acquire trace metals, the specific mechanisms can differ depending on the microbial lifestyle, the physical and chemical attributes of their surroundings. The PA and FL communities have displayed large taxonomic and phylogenic dissimilarities (Leu *et al.*, 2022; Urvoy *et al.*, 2022). There is an increasing number of studies utilizing omics approaches to investigate the metabolic potential of prokaryotes in these size-fractions (Sunagawa *et al.*, 2015) . This technology aids in the exploration of the complex dynamics in marine microbial community structure and function.

In this study, we collected a total of 42 samples from 13 stations in the Subtropical, Subantarctic or Polar Frontal and Antarctic zones during the SWINGS cruises. Our samples covering 8 water masses and 4 surface waters and encompass both FL and PA prokaryotic communities. We investigate the community composition of the FL and PA prokaryotic communities as well as the gene abundances of the trace metal transporters at the community level and the level of metagenome assembled genomes (MAGs). Our objective is to examine if the communities and abundant MAGs vary in their potential of trace metal acquisition as an adaptation to varying micro-nutrient conditions or due to metabolic pathways requiring a given trace metal.

Materials and methods

Sample collection

Sampling was conducted during the SWINGS cruise from 10th January to 8th March 2021. The 13 sampling stations in this study were located in the Subtropical Zone (STZ), Subantarctic Zone (SAZ), the Polar Frontal Zone (PFZ) and the Antarctic Zone (AAZ) (Fig. 1).

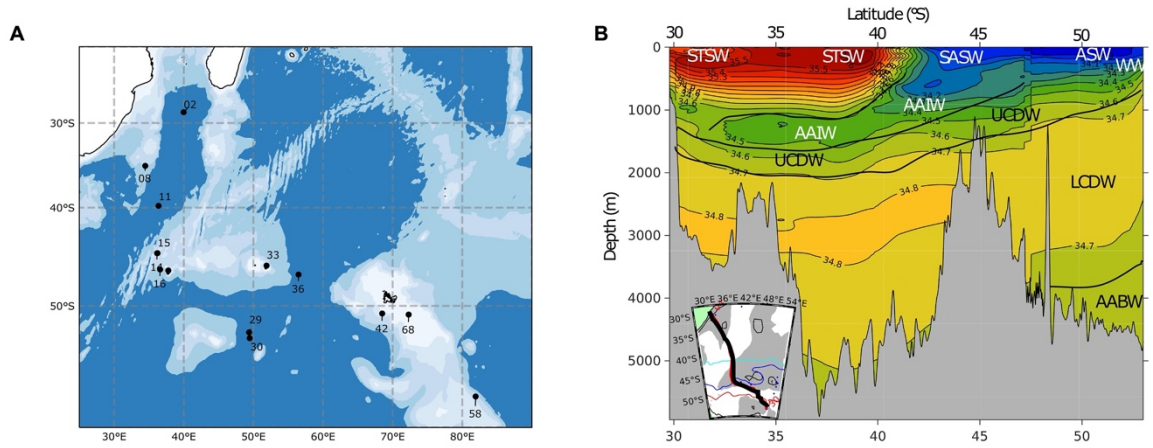

Fig.1. A. Map of stations sampled for the present study during the SWINGS cruise. B. A cross-section (inserted map) showing the vertical distribution of some water masses. STSW, Subtropical Surface Water; SASW, Sub Antarctic Surface Water; ASW, Antarctic Surface Water; WW, Winter water; AAIW, Antarctic Intermediate Water; UCDW, Upper Circumpolar Deep Water; LCDW, Lower Circumpolar Deep Water; AABW, Antarctic Bottom Water. The full list of water masses is provided in Table 1.

The seawater in the sampling zone was classified into 8 water masses and 4 surface water types (Subtropical Surface Water (STSW), Sub Antarctic Surface Water (SASW), Polar Frontal Surface water (PFSW), Antarctic Surface Water (ASW)) based on the physical and chemical properties of seawater such as temperature, salinity, oxygen concentration, depth, and latitude and longitude. Seawater samples (6L) were collected at each sampling site using 12 L Niskin bottles equipped with conductivity, temperature and depth (CTD) sensors (SeaBird SBE911plus). The collected seawater was then sequentially filtered through 0.8 µm polycarbonate filters (47 mm diameter, Nuclepore, Whatman, Sigma Aldrich, St Louis, MO) and 0.22 µm Sterivex filter units (Sterivex, Millipore, EMD, Billerica, MA). The prokaryotes collected on the 0.8 µm filters were classified as particle-attached, while those collected on the 0.22 µm filters were identified as free-living prokaryotes. A total of 42 seawater samples were collected, comprising 23 free-living and 19 particle-attached samples. Notably, the particle-attached samples covering only 7 out of the 8 identified water masses compared to

the free-living samples. Both the 0.8 μm polycarbonate filters and 0.22 μm Sterivex filter units were stored at -80°C until returned to the home laboratory for DNA extraction.

DNA extraction and sequencing

Total DNA extraction was performed from 0.8 μm polycarbonate filters and 0.22 μm Sterivex filter units using the DNeasy PowerWater Kit (Qiagen) following the manufacturer's instructions with a few modifications. Sterivex units were opened according to Perrine's methods (Cruaud *et al.*, 2017). The 0.8 and 0.22 filter membranes were then cut into small pieces using scissors and transferred to the new 2 mL Eppendorf tubes. Subsequently, solution PW1 and a lysozyme solution were added, and the mixture was incubated at 37°C for 45 minutes to promote cell lysis, and then a proteinase K solution was added and incubated at 55°C for 1 h to digest the proteins in the cell lysate, the remaining steps were carried out following the manufacturer's instructions. DNA concentrations were measured using a Promega Quantus fluorometer with the QuantiFluor® Double stranded DNA (dsDNA) system. The V4–V5 region of the 16S rRNA gene was amplified using primer sets 515F-Y (5'-GTGYCAGCMGCCGCGGTAA) and 926-R (5'-CCGYCAATTYMTTTRAGTTT) as described elsewhere (Parada *et al.*, 2016). 16S rRNA gene amplicons were sequenced with Illumina MiSeq V3 2 × 300 bp chemistry at the Biosearch Technologies platform (Berlin, Germany). Metagenomes were sequenced with an Illumina NovaSeq 6000 system using 2 × 150 bp chemistry at Fasteris SA, Inc. (Switzerland), and the details were shown in Table S1.

16S amplicons analysis

16S rRNA gene sequences were demultiplexed using the Illumina bcl2fastq v2.20 at the platform Biosearch Technologies (Berlin, Germany). The PCR primers and adapters of 16S rRNA gene sequences were trimmed with cutadapt v1.15. Amplicon sequence variants (ASV) inference was performed in R using DADA2 package with the parameters: truncLen=c(240,210), maxN=0, maxEE=c(3,5), truncQ=2, this pipeline encompassed filter and trim, dereplication, sample inference, merge paired reads and chimeras removal steps. A total of 3459 unique ASVs were identified from both free-living and particle-attached prokaryotic samples. Taxonomic assignment of ASVs was achieved using the DADA2-formatted SILVA SSU Ref NR99 138 database at the species level.

The number of ASVs per sample exhibited variability, ranging from 3187 to 162,490.

For analyses of community composition in each sample, the dataset was randomly subsampled to the lowest number of reads (3187) per sample with the function rarefy_even_depth by the Phyloseq package in R to obtain the same number of reads for all samples (McMurdie and Holmes, 2014). All statistical analyses in this study were conducted using the R 3.4.2 version. Non-metric dimensional scaling (NMDS) ordinations were generated based on Bray–Curtis dissimilarity, utilizing the ordinate function in the Phyloseq package (McMurdie and Holmes, 2013). Prokaryotic community compositions were visualized using ggplot2 based on annotated sequences. The results were described in the supplementary material (Fig. S1).

Metagenome assembly and functional profiling

The raw reads underwent quality assessment using FastQC v0.11.9 and subsequent preprocessing was carried out using Trimmomatic (v 0.32) as described by Bolger et al. (Bolger *et al.*, 2014). Following quality control, the retained short reads were individually assembled using MEGAHIT v1.2.9 (Li *et al.*, 2015) with specific parameters (--min-contig-len 1000 --presets meta-large). The resulting contigs exhibited N50 lengths ranging from 1.4k to 3.5k. The Open Reading Frames (ORFs) in this study were predicted using Prodigal v2.6.3 (Hyatt *et al.*, 2010) with the following parameters: -p meta. To create a non-redundant protein database pooling the 42 samples, CD-HIT v4.8.1 (Li and Godzik, 2006) was used for clustering with the parameters: -c 1 -aS 1 -g 1. The resulting non-redundant gene sequence set was constructed based on the non-redundant protein sequence numbers (18,497,675 proteins). For read recruitment of short reads to the non-redundant gene sequence collection and quantification of each gene in each sample, Salmon v1.4.0 (Patro *et al.*, 2017) was used. The specific parameters utilized were: --meta -incompatPrior 0.0 --seqBias --gcBias --biasSpeedSamp 5 -validateMappings. To make the protein occurrences comparable across samples, the data was normalized as genes per kilobase million (GPM). The GPM calculation is defined as follows: GPM = 1M × (mapped genes/gene length)/ (sum of mapped reads/gene length).

To identify genes associated with the iron cycle pathway, we used FeGenie (Garber *et al.*, 2020) based on the non-redundant protein sequence set for alignment and annotation (parameters used --meta). FeGenie generated its own database of HMMs based on iron-related genes and was used for the identification of proteins involved in intracellular Fe cycling and transport. To identify genes associated with trace metal transporters, the non-redundant protein sequence set was against the KEGG database using GhostKOALA

(Kanehisa *et al.*, 2016) and KofamKOALA (Aramaki *et al.*, 2020). In this study, two specific Mn-related uptake transporters were detected in all samples: the NRAMP (natural resistance-associated macrophage protein) family type transporter MntH, and the ABC (ATP-binding cassette) type transporter MntABC. Additionally, two Mn-efflux transporters, MntP and MneA, were detected, along with non-specific Mn uptake transporter genes. Most of the genes associated with copper transport identified in the free-living and particle-attached samples were exporter and efflux genes, and only one was an uptake gene (SLC31A1, CTR1). Details of trace metal transporters can be found in Table S2.

To better evaluate the presence and abundance of genes in the PA and FL samples, we performed the corresponding calculations with reference to the Particle Association Niche Index (PAN Index) (Salazar *et al.*, 2015). This index was computed through an abundance-weighted average approach: for a given gene, we documented its abundance in each sample along with the corresponding size fraction of the sample. We assigned a value of 0 to FL samples and a value of 1 to PA samples. Subsequently, we determined the abundance-weighted average of these values. Thus, the PAN index value for a gene that occurs only in the PA sample is 1, and the value for a gene that occurs only in the FL sample is 0. For genes evenly distributed between FL and PA samples, the PAN index value would be 0.5.

Binning

The individual metagenome assemblies (contigs ≥ 2500 bp) underwent a comprehensive binning process to yield higher quality metagenome-assembled genomes (MAGs). This binning process utilized MetaWRAP (v1.3) (Uritskiy *et al.*, 2018) with two binning tools: MaxBin2 (v2.2.5) (Wu *et al.*, 2016) and MetaBAT2 (v2.12.1) (Kang *et al.*, 2019). Subsequent refinement was carried out by the Bin_refinement module in MetaWRAP (v1.3). First, mixed bin sets were created by combining bin sets generated by MaxBin2 and MetaBAT2, and then the selection of the best MAGs was based on the completeness and contamination for each MAG in these three sets as evaluated by the CheckM (Parks *et al.*, 2015). To enhance the quality of the MAGs, the sequence reads from the metagenome were mapped to each MAG. The MAGs were then reassembled using the reassemble_bins module in MetaWRAP, contributing to an improvement in their overall quality. Following this reassembly step, the MAGs were reevaluated by CheckM. A total of 1103 MAGs were retained based on the thresholds of completeness greater than or equal to 50% and contamination less than or equal to 10%. To reduce redundancy (Evans and Denef, 2020), all reassembled MAGs were dereplicated using dRep (Olm *et al.*, 2017) with the following parameters: -comp 50 -con 10 -

nc 0.25 -pa 0.9 -sa 0.95. Subsequently, 556 MAGs were retained based on the 95% average nucleotide identities (ANI). Within this set, the completeness of 157 MAGs greater than or equal to 90%, the completeness of 270 MAGs greater than or equal to 80%, and the completeness of 361 MAGs greater than or equal to 70%.

To calculate the abundance of each MAG across samples, we first employed Bowtie2 v2.4.4 (Langmead and Salzberg, 2012) with default parameters to map short reads from 42 metagenomes. Subsequently, samtools (Li *et al.*, 2009) were utilized to convert resulting SAM files into sorted and indexed BAM files. Anvi'o v7.1 (Eren *et al.*, 2015) was then used to profile short metagenomic reads aligned to MAGs, enabling the estimation of coverage statistics for each metagenome, and the details are as described by Zhang (Zhang *et al.*, 2023). ORFs were predicted for all MAGs using Prodigal. Functional annotation was conducted using GhostKOALA (Kanehisa *et al.*, 2016) and KofamKOALA (Aramaki *et al.*, 2020), and METABOLIC (v4.0) (Zhou *et al.*, 2022). Genes associated with the iron cycle pathway were identified using FeGenie (Garber *et al.*, 2020). The details of methodology are the same method as above. Taxonomic classification of 556 MAGs was refined using GTDB-Tk v2.3.0 (Parks *et al.*, 2022), referencing the GTDB database release 214, and the classify_wf function with default parameters was used for this purpose. Maximum Likelihood (ML) phylogenetic trees were constructed using IQ-Tree (v2.0.3) (Nguyen *et al.*, 2015) with the following parameters: -m TESTMERGE -bb 1000 -bnni. The resulting trees were then visualized using iTOL (Letunic and Bork, 2007).

Results and Discussion

Concentration of trace metals in the sampled water masses

During the SWINGS cruise, a total of 42 seawater samples were collected, comprising 23 free-living samples and 19 particle-attached samples. These samples encompassed 4 surface seawater samples (10-30 m) and 8 different water masses, as detailed in Table 1.

Table 1. List of water masses and the number in free-living and particle-attached samples.

Acronym	Water mass	Free-living samples	Particle-attached samples
STSW	Subtropical Surface Water	3	3
SASW	Sub Antarctic Surface Water	3	2
PFSW	Polar Frontal Surface water	2	1
ASW	Antarctic Surface Water	4	3
WW	Winter water	1	0
STMW	Subtropical Mode Water	1	1
AAIW	Antarctic Intermediate Water	1	1
SICW	South Indian Central Water	2	2
UCDW	Upper Circumpolar Deep Water	3	3
LCDW	Lower Circumpolar Deep Water	1	1
NADW	North Atlantic Deep Water	1	1
AABW	AntArctic Bottom Water	1	1

The concentration of dissolved iron (dFe) varied between 0.3-0.5 nM in surface seawater, except for two samples near the Kerguelen Island where the concentration was < 0.1 nM (Fig. 2). The concentration of dissolved manganese (dMn) in the STSW was notably higher (~ 1.5 nM) as compared to other surface seawater samples (< 0.3 nM). Conversely, the concentration of dissolved nickel (dNi) was lower in STSW (2 nM) compared to other surface seawater samples (5 nM). The concentrations of dFe, dNi and dCu tended to be highest in LCDW, NADW and AABW, while dMn concentrations were highest in STSW (Fig. 2).

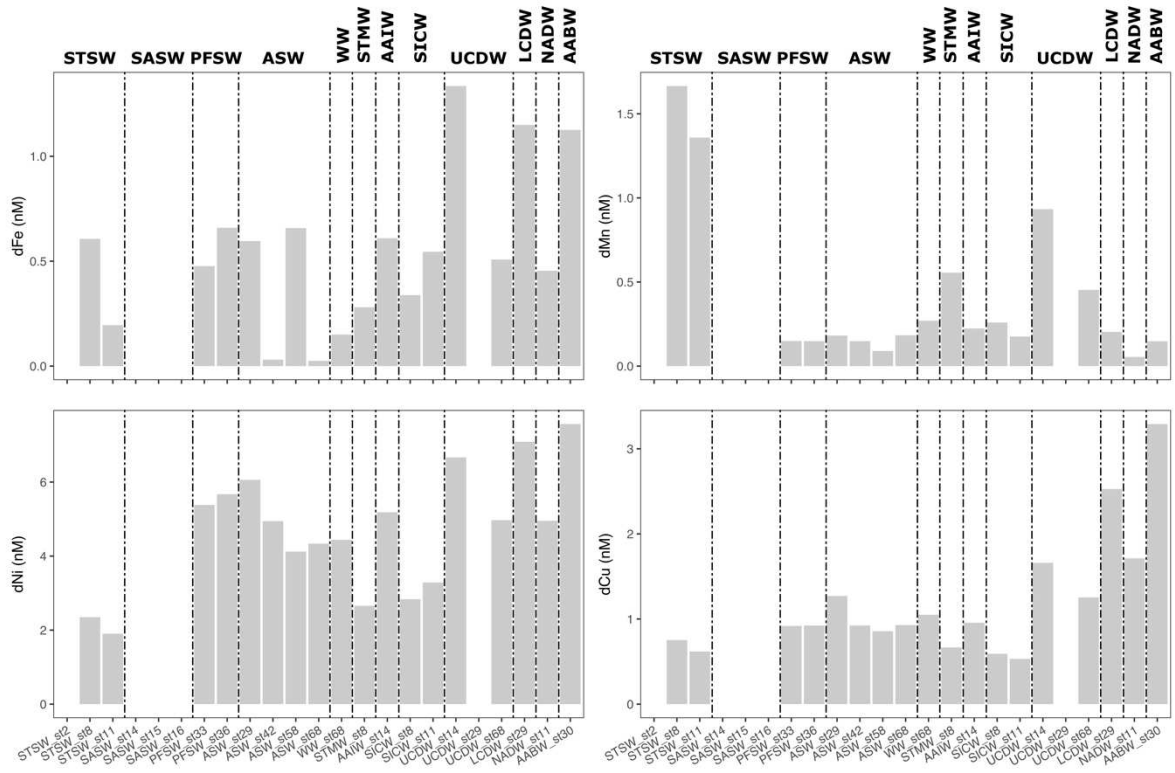

Fig. 2 Concentrations of dissolved trace metals; note the difference in y-axis. UCDW at Station 14 has been identified as a hydrothermal vent site (Baudet *et al*., 2024). Data are from Corentin Baudet and Hélène Planquette (LEMAR). No data available for SASW and for UCDW at station 29.

Abundance of trace metal transporters in different water masses

The transporter genes identified in our data revealed differences in GPM across a latitudinal gradient in surface waters and among water masses at depth. We focus our description here on the FL fraction. The acquisition of Fe was dominated by transporters of ferric Fe (Fe^{3+}; *fbp*, *fbp-futB*, *fut* A1/A2) across stations and depths and transporters of ferrous Fe (Fe^{2+}; *efe*UOB, *feoAB*) had substantially lower GPM (Fig. 3A and Fig. S2). The transporter Yfe (Fe/Mn) revealed a marked decrease in the GMP between surface (STSW, SASW, PFSW, ASW) and deeper water masses, mirroring the pattern observed for Mn transporters (Fig. 3C and Fig. S2). *feoE* representing Fe efflux revealed slightly higher abundances in WW and UCDW (at Station 68). GPM of these Fe-related transporter genes combined revealed an increasing trend from STSW towards ASW, and overall small variations were observed among the deeper water masses.

The most abundant siderophore transport genes detected were *fpv* (pyoverdine), *pirA* (ferric enterobactin), *hatD* (aerobactin) and *viuB* (vibriobactin) and *hmu* was the main heme transport system (Fig. 3B and Fig. S2), and these transporters increased from STSW to ASW.

These observations indicate an increased inventory of diverse iron uptake genes in surface waters that have been characterized as Fe-limited systems (PFSW, ASW) as compared to STSW. Siderophore transporters had overall lower GPM in deeper waters, with the exception of LCDW and NADW. Our results suggest a water-mass specific distribution of these specific siderophore transporter genes, which contrasts the pattern observed for inorganic iron transporters.

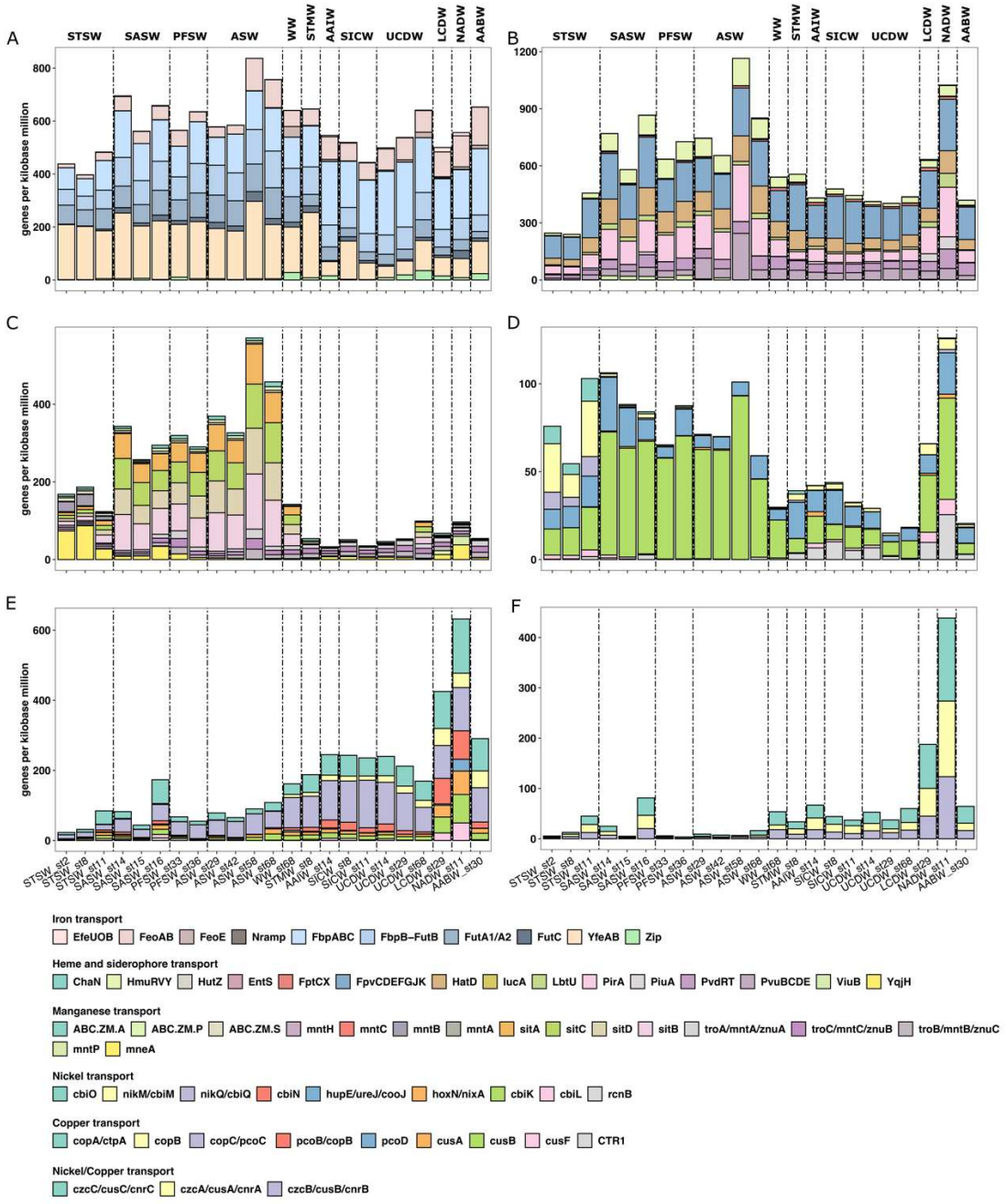

Fig. 3. The abundance of genes in free-living samples for Fe^{3+} and Fe^{2+} transporters (A), heme and siderophore transporters (B), manganese transporters (C), nickel transporters (D), copper transporters (E), and nickel/copper transporters (F). Normalized gene abundances are given in genes per kilobase million (GPM).

Transporters of Mn were substantially higher in surface waters of the Subantarctic, Polar Frontal and Antarctic zones as compared to the corresponding deep waters (Fig. 3C, Fig. S3 C and Fig. S4). Communities in STSW had a distinct set of Mn transporters as compared to the other surface waters. The *sitABCD* transport system (Mn/Fe) dominated in SASW, PFSW and ASW (Fig. 3C and Fig. S4), and the transport system *tro*, *mnt*, *znu* (Mn/ Zn/ Fe) was more prominent in deeper waters (Fig. 3C, Fig. S3 C and Fig. S4). Two putative Mn exporters, *mntP* and *mneA*, were detected in our data with increased GPM in STSW, LCDW and NADW, both in the FL and PA communities (Fig. 3C, Fig. S3 C and Fig. S4). As for transporters of Fe and siderophores, GMP of Mn transporters increased from STSW to ASW.

In the case of Ni, we observed a clear differentiation in the types of transporter genes among water masses. While *cbiO (*Co/Ni*)*, *nikM*/*cbiM (*Co/Ni*)*, *hup*/*ure*/*cooJ* (Ni) and *cbik* (Ni) had a roughly equal contribution in STSW, *cbik* dominated in SASW, PFSW and ASW, and *cbik* and *hup*/*ure*/*cooJ* had a similar share at depth (Fig. 3D and Fig. S4). The increase in GPM from STSW to ASW was only observed for *cbik*, this observation aligns with the trend of increasing concentration of dNi from STSW to ASW. GPM of Ni transporters were again lower in deeper as compared to surface waters, with the exception of LCDW and NADW (Fig. 3D). Most of the genes associated with Cu identified in both FL and PA samples were Cu efflux or resistance genes (*copC/pcoC*, *pcoB/copB*, *cusABF*), with the exception of CTR1 (Fig. 3E and Fig. S3 E). Independent of their putative function, their GPM revealed an inverse pattern as compared to that of Mn and Ni, with low GPM in surface increasing with depth. Highest GPM were observed in LCDW and NADW. A similar pattern was observed for Ni/Cu efflux genes (Fig. 3F and Fig. S3 F).

In the PA fraction, we also observed marked differences in trace metal related transporters across samples, exhibiting patterns similar to the FL fraction for Cu and Cu/Ni, but not for the other trace metals (Fig. 3 and Fig. S3). To compare the gene abundances in the FL to the PA fraction, the PAN index was calculated. Our analysis revealed that genes related Fe transport, including Fe^{3+}, Fe^{2+} and siderophore transport, were not preferentially present in either fraction, while genes related to Mn, Ni and Cu transport were more abundant in PA as compared to FL communities (Fig. S5). Some of these genes showed distinct patterns between surface and deeper layers, such as the siderophore transporter genes and *sitABCD* genes, which were more abundant in FL samples in surface seawater and in PA samples in deeper depth layers (Fig. S5).

When comparing trace metal concentrations in surface seawater across different sampling zones, we observed marked differences in the concentration of dMn and dNi, particularly in the STSW samples. Notably, dMn concentrations in STSW were higher than in other surface seawater samples, whereas dNi concentrations were lower (Fig. 2). This could contribute to the observation that FL prokaryotes in these samples carried different type and abundances of genes related to Ni and Mn transport as compared to other samples. *Cyanobiaceae* were found to dominate the FL prokaryotic community in STSW. These communities exhibited a higher abundance of genes associated with Ni/Co and Mn transport, such as *cbiOMQ*, *mntABC*, and *mneA*. Ni and Co play important roles in the cellular physiology of *Cyanobiaceae* (Dupont *et al.*, 2012; Rodriguez and Ho, 2014). CbiOMQ has been identified as the major Ni/Co transporter in several *Cyanobiaceae* genomes (Rodionov *et al.*, 2006), which may explain its higher abundance in STSW of FL samples. *Cyanobiaceae* utilize Mn for photosynthesis, and high Mn concentrations in the environment can cause Mn accumulation in *Cyanobiaceae* (Allen and Martin, 2007; Eisenhut, 2019). To regulate intracellular Mn homeostasis, *Cyanobiaceae* possess pathways such as *mntABC* (uptake) and *mneA* (export), which facilitate Mn uptake and regulation.

Genes associated with heme, siderophore, Ni, and Cu transport exhibited their highest abundance in LCDW and NADW as compared to other water masses, in both the FL and PA fractions (Fig. 3 and Fig. S3). The high abundance of these genes was, however, not associated with a marked difference in trace metal concentrations in these as compared to other water masses. LCDW is formed by mixing NADW with AABW (Park *et al.*, 1993; Sprintall *et al.*, 2013), and the migration of water masses promotes the dispersal of prokaryotes, resulting in similar prokaryotic communities between LCDW and NADW (Fig. S1). This could lead to similar trace metal transport strategies for prokaryotes in LCDW and NADW.

The distribution of MAGs across samples

In order to better understand the metabolic potential of dominant prokaryotes across different water masses, we constructed metagenome assembled genomes (MAG). After dereplication, 556 MAGs (≥ 50% completeness and ≤ 10% potential contamination) were constructed from 42 metagenomes, of which 72 MAGs belonged to *Archaea* and 484 MAGs belonged to *Bacteria*. These 72 archaeal MAGs belong to 4 phyla, 4 classes, 5 orders and 7 families. The families of archaeal MAGs were *Poseidoniaceae* (31 MAGs), *Thalassarchaeaceae* (29 MAGs), *Nitrosopumiaceae* (5 MAGs), *CG-Epi 1* (3 MAGs), *UBA57* (2 MAGs), *ARS21* (1

MAG) and *UBA12382* (1 MAG). The FL samples had higher abundances of archaeal MAGs among the water masses as compared to the PA samples across all 7 families (Fig. S6). The diverse MAGs belonging to *Poseidoniaceae* were more abundant in surface waters (STSW, SASW, PFSW, ASW) than at depth. By contrast, MAGs belonging to *Thalassarchaeaceae* and *Nitrosopumilaceae* had higher coverages at depth (WW, STMW, SICW, UCDW, LCDW, NADW, AABW) as compared to the surface ocean. Most of the other archaeal MAGs that we constructed were also abundant in deeper water masses with an exception to one MAG belonging to CG-epi1 that was abundant in STSW (Fig. S6).

The 484 bacterial MAGs constructed in this study belong to 19 phyla 32 classes, 89 orders and 150 families. These MAGs mainly belong to the phyla *Pseudomonadota, Bacteroidota* and *Planctomycetota*. Similar to archaeal MAGs, the bacterial MAGs exhibited distinct distribution patterns in surface seawater and water masses in the FL samples, whereas they were more homogeneously distributed in the PA samples (Fig. S7). *Bacteroidota* MAGs were more abundant in surface as compared to deep water masses. However, SAR324, *Nitrospinota*, *Marinisomatota*, *Gemmatimonadota*, *Actinomycetota* and *Chloroflexota* were more abundant in deep ocean water masses as compared to surface seawater.

Abundant MAGs across samples

We then focused our investigation on the most abundant MAGs for surface waters (STSW, SASW, PFSW and ASW) and for water masses (WW, AAIW, SICW, UCDW, LCDW and NADW). These MAGs were defined as those 10 MAGs with the highest mean coverage in a given sample. They accounted for 55-84% of the total mean coverage of all the MAGs (completeness >= 70%) constructed in these samples.

For these abundant MAGs with the highest mean coverage in STSW, SASW, PFSW and ASW in the FL samples we retaining a total of 55 MAGs (Fig. 4). The MAGs with high mean coverage in STSW were distinct to the other surface samples, and they mostly belonged to *Acidimicrobiales*, *Thalassarchaeaceae*, *Cyanobiaceae*, *Halieaceae*, *Parvibaculales* and *Flavobacteriaceae*. MAGs from Site 11 revealed several taxa belonging to *Poseidoniaceae* and *Burkholderiaceae* (Fig. 4 and Table S3). This is consistent with the observation that the community composition of prokaryotes in STSW is different as compared to other surface water samples (Fig. S1). While several of the top 10 MAGs were shared between SASW, PFSW, and ASW, a number of differences were noted. SASW contained MAGs with higher mean coverage belonging to *Rhodobacteraceae, Porticoccaceae, Schleiferiaceae, Pseudohongiellaceae, Woeseiaceae* and *Poseidoniaceae*, and PFSW and ASW contained MAGs with higher mean coverage belonging to *Porticoccaceae*, *Flavobacteriaceae*,

Schleiferiaceae, *Cyclobacteriaceae* and *Emcibacteraceae* (Fig. 4 and Table S3). Functional annotation revealed, that most of these abundant MAGs harbored genes associated with Fe, heme and siderophore transport (Fig. 4). AF79_bin_3_Cyanobiaceae with high mean coverage in STSW was found to carry genes related to Mn (*mntABC* and *mneA*) and Ni (*cbiL*) transport, and several other MAGs with high mean coverage in STSW harbored genes related to Cu efflux (*copA*), consistent with the observed gene types and abundance present in STSW at the community level (Fig. 3). Using annotation results based on the Metabolic_v4.0 database, we further observed that these MAGs with high mean coverage in STSW carried genes encoding amylolytic enzymes compared to MAGs with high mean coverage in other surface seawater (Fig. 4 and Table S4). Furthermore, these MAGs with high mean coverage in surface seawater were found to carry more genes related to oxidative phosphorylation compared to those with high mean coverage in the six water masses mentioned later (Table S4). This points to specific taxonomic and functional adaptations within microbial communities in these distinct surface water masses. When we performed a comparative analysis of the top 10 MAGs between the FL and PA samples, we found that there were 14 MAGs common in both size fractions, and these MAGs carry similar genes related to trace metals transport (Fig. 4).

The abundant MAGs in terms of mean coverage in WW, AAIW, SICW, UCDW, LCDW and NADW for the free-living samples resulted in a total of 36 MAGs (Fig. 5). Six clades have been identified of the SAR324 cluster in recent years, these clades possess a broad metabolic potential including both heterotrophic and autotrophic pathways, and they can make up to 30% of the bacterial community (Malfertheiner *et al.*, 2022). Therefore, due to the ubiquitous nature of SAR324, its (AF88_bin_40_NAC60-12) abundance was high in each water mass of the FL samples (Fig. 5 and S1).

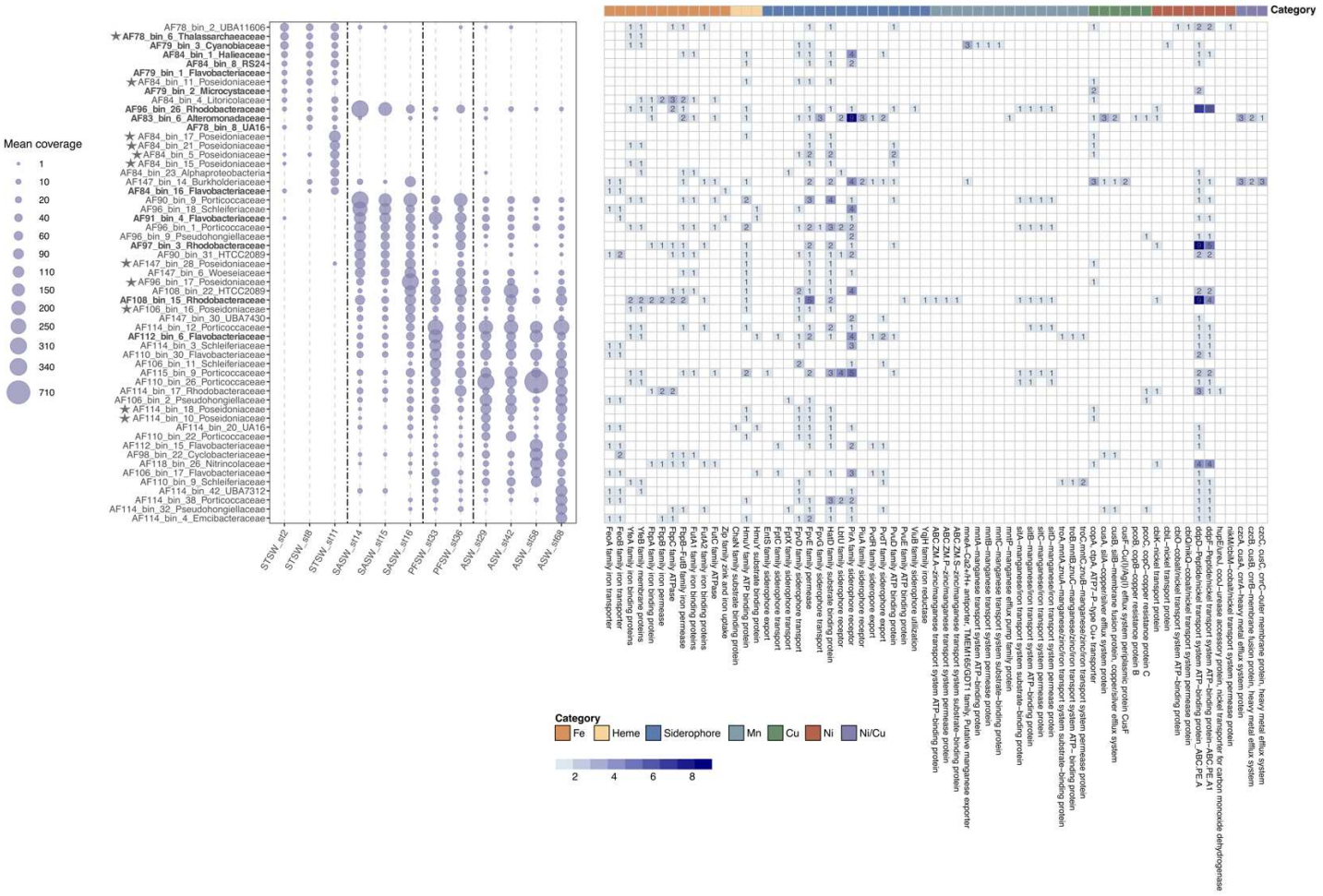

Fig. 4 The mean coverage of each MAG in free-living samples and the distribution of trace metals transport genes in the MAGs. Only the top 10 abundant MAGs in STSW, SASW, PFSW and ASW for the free-living sample are shown here. The surface water was separated by dashed line, and the order of the surface water is STSW, SASW, PFSW and ASW. Archaeal MAGs are marked in asterisk. The common top10 MAGs between the FL and PA fraction are shown in bold.

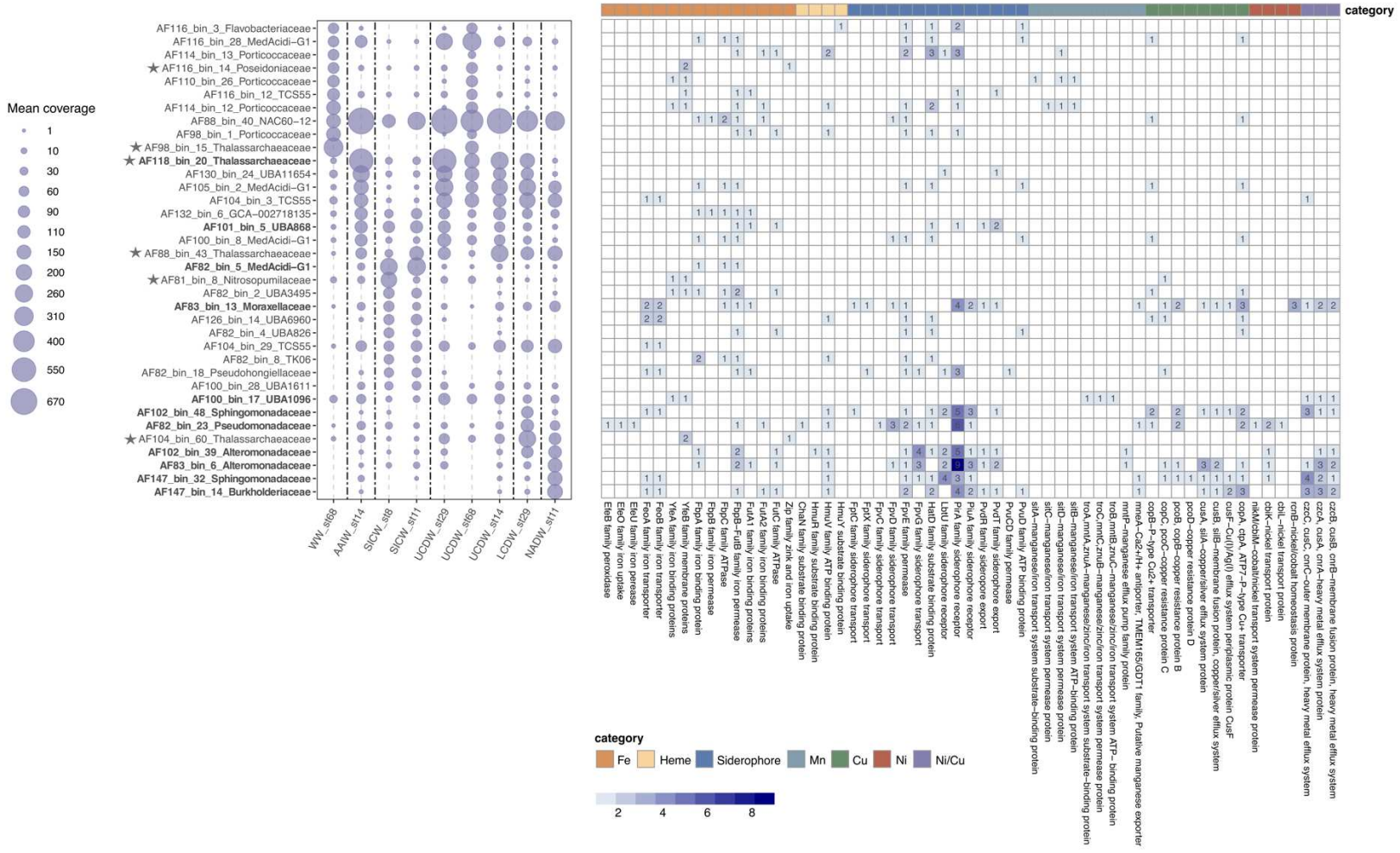

Fig. 5 The mean coverage of each MAG in free-living samples and the distribution of trace metals transport genes in the MAGs. Only the top 10 abundant MAGs in WW, AAIW, SICW, UCDW, LCDW and NADW for the free-living sample are shown here. The water masses were separated by dashed line, the order of the water masses is WW, AAIW, SICW, UCDW, LCDW and NADW. Archaeal MAGs are marked in asterisk. The common top10 MAGs between the FL and PA fraction are shown in bold.

The MAGs with high mean coverage in WW were overall absent from other water masses, except for one sample collected in UCDW at station 68, a site that is located above the shallow Kerguelen plateau. The MAGs with the highest mean coverage in WW belong to *Thalassarchaeaceae* (Archaea), while others belong to *Porticoccaceae*, SAR324, *Marinisomatales*, *Poseidoniaceae*, MedAcidi-G1 and *Flavobacteriaceae* (Fig. 5 and Table S5). Functional annotation revealed that most of these MAGs with high mean coverage in WW harbor genes associated with Fe (*yfeAB*, *fbpB-futB*, *futA1* and *futC*), heme (*hmuY*), siderophore (*fpvE*, *hatD* and *pirA*) and Mn transport (*sitABCD*) (Fig. 5). Additionally, these MAGs contain genes involved in amino acid utilization, fatty acid degradation, cellulose degradation, chitin degradation, fermentation, and oxidative phosphorylation (Table S6). In AAIW and UCDW, there were similar MAGs exhibiting higher mean coverage, attributed to SAR324, *Thalassarchaeaceae*, UBA11654, MedAcidi-G1, among others (Fig. 5 and Table S5). Contrasted with MAGs with high mean coverage in WW, these MAGs lack genes associated with heme and Mn transport, while containing more genes related to Fe (*feoAB* and *fbpABC*) and Cu transport (Fig. 5). Moreover, annotation results based on the Metabolic_v4.0 database revealed similar genes detected in the MAGs with high mean coverage in AAIW and UCDW to those MAGs with high mean coverage in WW, such as genes related to fatty acid degradation, but genes associated with cellulose degradation were not detected (Table S6).

The MAGs with higher mean coverage in SICW mainly belong to SAR324, *Thalassarchaeaceae*, MedAcidi-G1, *Nitrosopumilaceae* and UBA3495 (formerly SAR202 group III). In comparison to MAGs with high mean coverage in WW, these MAGs contained more genes related to ferrous (*feoAB*) and siderophore (*fptCX*, *piu* and *pvd*) transport (Fig. 5). This implies that these MAGs with high mean coverage in the SICW may be able to access Fe by transporting ferripyochelin, catecholate siderophore and pyoverdine compared to other MAGs. Among these, one of the MAGs (*Moraxellaceae*) was detected to carry both genes related to Cu and Ni transport. Furthermore, some of these MAGs were found to contain genes associated with aerobic CO oxidation (Table S6), suggesting that these MAGs may be able to adapt to organic carbon limitation in SICW through this survival strategy.

There are similar MAGs with higher mean coverage in LCDW and NADW, which predominantly belong to SAR324, *Thalassarchaeaceae*, MedAcidi-G1, *Burkholderiales*, *Sphingomonadales*, *Alteromonadaceae* and *Pseudomonadaceae* (Fig. 5 and Table S5). Some MAGs only with high mean coverage in LCDW and NADW, such as *Burkholderiales*, *Sphingomonadales*, *Alteromonadaceae* and *Thalassarchaeaceae*, were observed to harbor more genes associated with Fe^{2+} (*efeUOB* and *feoAB*), heme, siderophore, Cu, and Ni

transport as well as Mn efflux (*mntP* and *mneA*) compared to other MAGs (Fig. 5 and Table S5). Additionally, these MAGs were found to contain genes related to formaldehyde oxidation, fermentation, aromatic degradation, oxidative phosphorylation, nitrogen metabolism, and sulfur metabolism, suggesting that these MAGs are adapting to the conditions of these deep water masses through multiple strategies (Table S6). Furthermore, our research revealed that these MAGs with Ni transporter proteins, which were abundant in LCDW and NADW (AF82_bin_23, AF102_bin_39, AF83_bin_6, AF147_bin_32, AF147_bin_14), commonly harbor genes associated with nitrite reduction to ammonium (*nrfA*, *nifBD*), in contrast to MAGs with high mean coverage in WW (Table 2). This implies a potential dependency on Ni as a cofactor for the utilization of inorganic nitrogen substrates in these MAGs.

Table 2. The count of nitrogen-related genes detected in the abundant MAGs in WW, AAIW, SICW, UCDW, LCDW and NADW for the free-living samples.

Gene	AF104_bin_3*	AF81_bin_8*	AF83_bin_13*	AF82_bin_18*	AF104_bin_29*	AF100_bin_17*	AF82_bin_23*	AF102_bin_39*	AF83_bin_6*	AF147_bin_32*	AF147_bin_14*
amoA-Ammonia oxidation	0	1	0	0	0	0	0	0	0	0	0
amoB-Ammonia oxidation	0	1	0	0	0	0	0	0	0	0	0
amoC-Ammonia oxidation	0	1	0	0	0	0	0	0	0	0	0
narG-Nitrate reduction	0	0	0	0	0	0	0	0	1	0	1
narH-Nitrate reduction	0	0	0	0	0	0	0	0	1	0	1
nrfA-Nitrite reduction to ammonia	1	0	0	0	0	0	1	1	1	0	0
nirB-Nitrite reduction to ammonia	0	0	2	0	0	0	2	0	0	1	2
nirD-Nitrite reduction to ammonia	0	0	1	0	0	1	1	0	0	1	1
norB-Nitric oxide reduction	0	0	0	0	0	0	0	0	0	0	1
norC-Nitric oxide reduction	1	0	0	0	1	0	0	0	0	0	0
ureC-Urease	0	1	0	2	0	1	1	0	0	0	1
ureB-Urease	0	1	0	1	0	1	1	0	0	0	1
ureA-Urease	0	1	0	1	0	1	1	0	0	0	1

*AF104_bin_3 is present in AAIW/UCDW/LCDW/NADW; AF81_bin_8, AF83_bin_13, and AF82_bin_18 are present in SICW; AF104_bin_29 is present in SICW/UCDW/LCDW/NADW; AF100_bin_17 is present in UCDW; AF82_bin_23 present in LCDW; AF102_bin_39, AF83_bin_6, AF147_bin_32, and AF147_bin_14 are present in NADW.

We further identified those abundant MAGs that were shared between the FL and PA samples across the five water masses (SICW, AAIW, UCDW, LCDW, and NADW). Our analysis revealed 11 MAGs, which belong to *Verrucomicrobiae*, *Gammaproteobacteria*, *Alphaproteobacteria*, *Poseidoniia* and *Acidimicrobiia*. Among these MAGs, AF101_bin_5_UBA868 and AF82_bin_5_MedAcidi-G1, exhibited high mean coverage in SICW and AAIW (Fig. 5). These MAGs were found to carry genes associated with Fe^{3+} and siderophore transport, amino acid utilization, fatty acid degradation, fermentation, aerobic CO oxidation, and oxidative phosphorylation (Fig. 5 and Table S6), indicative of heterotrophic lifestyles (Baltar *et al.*, 2023; Roda-Garcia *et al.*, 2023). Notably, AF101_bin_5_UBA868 also harbors sulfur oxidizing genes, aligning with previous observations identifying UBA868 as a key sulfur oxidizer beneath the Ross Ice Shelf in Antarctica (Baltar *et al.*, 2023). In the PA communities, we observed a significantly higher mean coverage of AF83_bin_13_Moraxellaceae (*Acinetobacter junii*) compared to the FL communities (Fig. 5). This MAG carries genes associated with Fe, Ni, and Cu transporters. *Acinetobacter Junii* which are abundantly present in the ocean are aerobic heterotrophic bacteria (Bergey's Manual of systematic bacteriologym Volume 2). Therefore, these communities have capabilities to perform carbon and dissimilatory inorganic nitrogen and sulfur cycling, indicative to the requirement of higher utilization of Fe, Ni and Cu transporters. Furthermore, AF102_bin_48_Sphingomonadaceae (*Qipengyuania citrea*), AF82_bin_23_Pseudomonadaceae (*Halopseudomonas pachastrellae*), AF102_bin_39_Alteromonadaceae (*Pseudoalteromonas lipolytica*), AF83_bin_6_Alteromonadaceae (*Pseudoalteromonas gelatinilytica*), AF147_bin_14_Burkholderiaceae (*Aquabacterium*) and AF147_bin_32_Sphingomonadaceae (*Sphingopyxis*) were abundant in LCDW and NADW in both FL and PA samples (Fig. 5). These MAGs were found to carry genes related not only to Fe, heme, and siderophore transport but also to Ni and Cu transport (Fig. 5). This observation is consistent with our findings of peaks in genes associated with Cu and Ni transport in the LCDW and NADW. We also found that dominant MAGs in deep water masses (LCDW and NADW) contain genes related to C1 metabolism, fermentation, aromatic degradation, oxidative phosphorylation, and sulfur metabolism (Table S6), suggesting that these MAGs can carry out diverse metabolisms (Peres *et al.*, 2023; Torres-Beltrán *et al.*, 2021; Coutinho *et al.*, 2023).

Reference

Allen, J.F. and Martin, W. (2007) Out of thin air. 610–612.

Aramaki, T., Blanc-Mathieu, R., Endo, H., Ohkubo, K., Kanehisa, M., Goto, S., and Ogata, H. (2020) KofamKOALA: KEGG Ortholog assignment based on profile HMM and adaptive score threshold. *Bioinformatics* **36**: 2251–2252.

Argüello, J.M., Raimunda, D., and Padilla-Benavides, T. (2013) Mechanisms of copper homeostasis in bacteria. *Front Cell Infect Microbiol* **3**:.

Azam, F. and Malfatti, F. (2007) Microbial structuring of marine ecosystems. *Nat Rev Microbiol* **5**: 782–791.

Baltar, F., Martínez-Pérez, C., Amano, C., Vial, M., Robaina-Estévez, S., Reinthaler, T., et al. (2023) A ubiquitous gammaproteobacterial clade dominates expression of sulfur oxidation genes across the mesopelagic ocean. *Nat Microbiol* **8**: 1137–1148.

Bolger, A.M., Lohse, M., and Usadel, B. (2014) Trimmomatic: a flexible trimmer for Illumina sequence data. *Bioinformatics* **30**: 2114–2120.

Bosma, E.F., Rau, M.H., van Gijtenbeek, L.A., and Siedler, S. (2021) Regulation and distinct physiological roles of manganese in bacteria. *FEMS Microbiology Reviews* **45**: fuab028.

Bradley, J.M., Svistunenko, D.A., Wilson, M.T., Hemmings, A.M., Moore, G.R., and Le Brun, N.E. (2020) Bacterial iron detoxification at the molecular level. *Journal of Biological Chemistry* **295**: 17602–17623.

Buchan, A., LeCleir, G.R., Gulvik, C.A., and González, J.M. (2014) Master recyclers: features and functions of bacteria associated with phytoplankton blooms. *Nat Rev Microbiol* **12**: 686–698.

Coutinho, F.H., Silveira, C.B., Sebastián, M., Sánchez, P., Duarte, C.M., Vaqué, D., et al. (2023) Water mass age structures the auxiliary metabolic gene content of free-living and particle-attached deep ocean viral communities. *Microbiome* **11**: 118.

Cruaud, P., Vigneron, A., Fradette, M.-S., Charette, S.J., Rodriguez, M.J., Dorea, C.C., and Culley, A.I. (2017) Open the Sterivex ™ casing: An easy and effective way to improve DNA extraction yields: *DNA extraction from Sterivex ™ filters . Limnol Oceanogr Methods* **15**: 1015–1020.

Dupont, C.L., Johnson, D.A., Phillippy, K., Paulsen, I.T., Brahamsha, B., and Palenik, B. (2012) Genetic Identification of a High-Affinity Ni Transporter and the Transcriptional Response to Ni Deprivation in Synechococcus sp. Strain WH8102. *Appl Environ Microbiol* **78**: 7822–7832.

Eisenhut, M. (2019) Manganese Homeostasis in Cyanobacteria. *Plants* **9**: 18.

Emery, W.J. (2001) Water Types And Water Masses. In *Encyclopedia of Ocean Sciences*. Elsevier, pp. 3179–3187.

Eren, A.M., Esen, Ö.C., Quince, C., Vineis, J.H., Morrison, H.G., Sogin, M.L., and Delmont, T.O. (2015) Anvi'o: an advanced analysis and visualization platform for 'omics data. *PeerJ* **3**: e1319.

Evans, J.T. and Denef, V.J. (2020) To Dereplicate or Not To Dereplicate? *mSphere* **5**: e00971-19.

Falkowski, P.G., Fenchel, T., and Delong, E.F. (2008) The Microbial Engines That Drive Earth's Biogeochemical Cycles. *Science* **320**: 1034–1039.

Fourquez, M., Devez, A., Schaumann, A., Guéneuguès, A., Jouenne, T., Obernosterer, I., and Blain, S. (2014) Effects of iron limitation on growth and carbon metabolism in oceanic and coastal heterotrophic bacteria. *Limnol Oceanogr* **59**: 349–360.

Fuhrman, J., Sleeter, T., Carlson, C., and Proctor, L. (1989) Dominance of bacterial biomass in the Sargasso Sea and its ecological implications. *Mar Ecol Prog Ser* **57**: 207–217.

Garber, A.I., Nealson, K.H., Okamoto, A., McAllister, S.M., Chan, C.S., Barco, R.A., and Merino, N. (2020) FeGenie: A Comprehensive Tool for the Identification of Iron Genes and Iron Gene Neighborhoods in Genome and Metagenome Assemblies. *Front Microbiol* **11**: 37.

Gikas, P. (2008) Single and combined effects of nickel (Ni(II)) and cobalt (Co(II)) ions on activated sludge and on other aerobic microorganisms: A review. *Journal of Hazardous Materials* **159**: 187–203.

Gledhill, M. (2012) The organic complexation of iron in the marine environment: a review. *Front Microbio* **3**:.

Hansel, C.M. (2017) Manganese in Marine Microbiology. In *Advances in Microbial Physiology*. Elsevier, pp. 37–83.

Hernando-Morales, V., Ameneiro, J., and Teira, E. (2017) Water mass mixing shapes bacterial biogeography in a highly hydrodynamic region of the Southern Ocean: Water mixing shapes bacterial biogeography. *Environ Microbiol* **19**: 1017–1029.

Hogle, S.L., Barbeau, K.A., and Gledhill, M. (2014) Heme in the marine environment: from cells to the iron cycle. *Metallomics* **6**: 1107–1120.

Hyatt, D., Chen, G.-L., LoCascio, P.F., Land, M.L., Larimer, F.W., and Hauser, L.J. (2010) Prodigal: prokaryotic gene recognition and translation initiation site identification. *BMC Bioinformatics* **11**: 119.

Kanehisa, M., Sato, Y., and Morishima, K. (2016) BlastKOALA and GhostKOALA: KEGG Tools for Functional Characterization of Genome and Metagenome Sequences. *Journal of Molecular Biology* **428**: 726–731.

Kang, D.D., Li, F., Kirton, E., Thomas, A., Egan, R., An, H., and Wang, Z. (2019) MetaBAT 2: an adaptive binning algorithm for robust and efficient genome reconstruction from metagenome assemblies. *PeerJ* **7**: e7359.

Kong, L. and Price, N.M. (2020) Identification of copper-regulated proteins in an oceanic diatom, *Thalassiosira oceanica* 1005. *Metallomics* **12**: 1106–1117.

Langmead, B. and Salzberg, S.L. (2012) Fast gapped-read alignment with Bowtie 2. *Nat Methods* **9**: 357–359.

Lechtenfeld, O.J., Hertkorn, N., Shen, Y., Witt, M., and Benner, R. (2015) Marine sequestration of carbon in bacterial metabolites. *Nat Commun* **6**: 6711.

Lekunberri, I., Sintes, E., De Corte, D., Yokokawa, T., and Herndl, G.J. (2013) Spatial patterns of bacterial and archaeal communities along the Romanche Fracture Zone (tropical Atlantic). *FEMS Microbiol Ecol* **85**: 537–552.

Letunic, I. and Bork, P. (2007) Interactive Tree Of Life (iTOL): an online tool for phylogenetic tree display and annotation. *Bioinformatics* **23**: 127–128.

Leu, A.O., Eppley, J.M., Burger, A., and DeLong, E.F. (2022) Diverse Genomic Traits Differentiate Sinking-Particle-Associated versus Free-Living Microbes throughout the Oligotrophic Open Ocean Water Column. *mBio* **13**: e01569-22.

Li, D., Liu, C.-M., Luo, R., Sadakane, K., and Lam, T.-W. (2015) MEGAHIT: an ultra-fast single-node solution for large and complex metagenomics assembly via succinct de Bruijn graph. *Bioinformatics* **31**: 1674–1676.

Li, H., Handsaker, B., Wysoker, A., Fennell, T., Ruan, J., Homer, N., et al. (2009) The Sequence Alignment/Map format and SAMtools. *Bioinformatics* **25**: 2078–2079.

Li, W. and Godzik, A. (2006) Cd-hit: a fast program for clustering and comparing large sets of protein or nucleotide sequences. *Bioinformatics* **22**: 1658–1659.

Maier, R. and Benoit, S. (2019) Role of Nickel in Microbial Pathogenesis. *Inorganics* **7**: 80.

Malfertheiner, L., Martínez-Pérez, C., Zhao, Z., Herndl, G.J., and Baltar, F. (2022) Phylogeny and Metabolic Potential of the Candidate Phylum SAR324. *Biology* **11**: 599.

McMurdie, P.J. and Holmes, S. (2013) phyloseq: An R Package for Reproducible Interactive Analysis and Graphics of Microbiome Census Data. *PLoS ONE* **8**: e61217.
McMurdie, P.J. and Holmes, S. (2014) Waste Not, Want Not: Why Rarefying Microbiome Data Is Inadmissible. *PLoS Comput Biol* **10**: e1003531.
Milici, M., Vital, M., Tomasch, J., Badewien, T.H., Giebel, H.-A., Plumeier, I., et al. (2017) Diversity and community composition of particle-associated and free-living bacteria in mesopelagic and bathypelagic Southern Ocean water masses: Evidence of dispersal limitation in the Bransfield Strait: Bacteria in the deep Southern Ocean. *Limnol Oceanogr* **62**: 1080–1095.
Moore, J.K., Doney, S.C., Glover, D.M., and Fung, I.Y. (2001) Iron cycling and nutrient-limitation patterns in surface waters of the World Ocean. *Deep Sea Research Part II: Topical Studies in Oceanography* **49**: 463–507.
Nguyen, L.-T., Schmidt, H.A., Von Haeseler, A., and Minh, B.Q. (2015) IQ-TREE: A Fast and Effective Stochastic Algorithm for Estimating Maximum-Likelihood Phylogenies. *Molecular Biology and Evolution* **32**: 268–274.
Olm, M.R., Brown, C.T., Brooks, B., and Banfield, J.F. (2017) dRep: a tool for fast and accurate genomic comparisons that enables improved genome recovery from metagenomes through de-replication. *The ISME Journal* **11**: 2864–2868.
Parada, A.E., Needham, D.M., and Fuhrman, J.A. (2016) Every base matters: assessing small subunit rRNA primers for marine microbiomes with mock communities, time series and global field samples: Primers for marine microbiome studies. *Environ Microbiol* **18**: 1403–1414.
Park, J., Durham, B.P., Key, R.S., Groussman, R.D., Bartolek, Z., Pinedo-Gonzalez, P., et al. (2023) Siderophore production and utilization by marine bacteria in the North Pacific Ocean. *Limnology & Oceanography* **68**: 1636–1653.
Park, Y., Gamberoni, L., and Charriaud, E. (1993) Frontal structure, water masses, and circulation in the Crozet Basin. *J Geophys Res* **98**: 12361–12385.
Parks, D.H., Chuvochina, M., Rinke, C., Mussig, A.J., Chaumeil, P.-A., and Hugenholtz, P. (2022) GTDB: an ongoing census of bacterial and archaeal diversity through a phylogenetically consistent, rank normalized and complete genome-based taxonomy. *Nucleic Acids Research* **50**: D785–D794.
Parks, D.H., Imelfort, M., Skennerton, C.T., Hugenholtz, P., and Tyson, G.W. (2015) CheckM: assessing the quality of microbial genomes recovered from isolates, single cells, and metagenomes. *Genome Res* **25**: 1043–1055.
Patro, R., Duggal, G., Love, M.I., Irizarry, R.A., and Kingsford, C. (2017) Salmon provides fast and bias-aware quantification of transcript expression. *Nat Methods* **14**: 417–419.
Pedrós-Alió, C. (2006) Marine microbial diversity: can it be determined? *Trends in Microbiology* **14**: 257–263.
Peres, F.V., Paula, F.S., Bendia, A.G., Gontijo, J.B., De Mahiques, M.M., and Pellizari, V.H. (2023) Assessment of prokaryotic communities in Southwestern Atlantic deep-sea sediments reveals prevalent methanol-oxidising Methylomirabilales. *Sci Rep* **13**: 12782.
Raes, E.J., Bodrossy, L., Van De Kamp, J., Bissett, A., Ostrowski, M., Brown, M.V., et al. (2018) Oceanographic boundaries constrain microbial diversity gradients in the South Pacific Ocean. *Proc Natl Acad Sci USA* **115**:.
Roda-Garcia, J.J., Haro-Moreno, J.M., and López-Pérez, M. (2023) Evolutionary pathways for deep-sea adaptation in marine planktonic Actinobacteriota. *Front Microbiol* **14**: 1159270.
Rodionov, D.A., Hebbeln, P., Gelfand, M.S., and Eitinger, T. (2006) Comparative and Functional Genomic Analysis of Prokaryotic Nickel and Cobalt Uptake Transporters:

Evidence for a Novel Group of ATP-Binding Cassette Transporters. *J Bacteriol* **188**: 317–327.

Rodriguez, I.B. and Ho, T.-Y. (2014) Diel nitrogen fixation pattern of Trichodesmium: the interactive control of light and Ni. *Sci Rep* **4**: 4445.

Salazar, G., Cornejo-Castillo, F.M., Borrull, E., Díez-Vives, C., Lara, E., Vaqué, D., et al. (2015) Particle-association lifestyle is a phylogenetically conserved trait in bathypelagic prokaryotes. *Molecular Ecology* **24**: 5692–5706.

Sprintall, J., Siedler, G., and Mercier, H. (2013) Interocean and Interbasin Exchanges. In *International Geophysics*. Elsevier, pp. 493–518.

Sun, Y., Debeljak, P., and Obernosterer, I. (2021) Microbial iron and carbon metabolism as revealed by taxonomy-specific functional diversity in the Southern Ocean. *ISME J* **15**: 2933–2946.

Sunagawa, S., Coelho, L.P., Chaffron, S., Kultima, J.R., Labadie, K., Salazar, G., et al. (2015) Structure and function of the global ocean microbiome. *Science* **348**: 1261359.

Torres-Beltrán, M., Vargas-Gastélum, L., Magdaleno-Moncayo, D., Riquelme, M., Herguera-García, J.C., Prieto-Davó, A., and Lago-Lestón, A. (2021) The metabolic core of the prokaryotic community from deep-sea sediments of the southern Gulf of Mexico shows different functional signatures between the continental slope and abyssal plain. *PeerJ* **9**: e12474.

Uritskiy, G.V., DiRuggiero, J., and Taylor, J. (2018) MetaWRAP—a flexible pipeline for genome-resolved metagenomic data analysis. *Microbiome* **6**: 158.

Urvoy, M., Gourmelon, M., Serghine, J., Rabiller, E., L'Helguen, S., and Labry, C. (2022) Free-living and particle-attached bacterial community composition, assembly processes and determinants across spatiotemporal scales in a macrotidal temperate estuary. *Sci Rep* **12**: 13897.

Vipindas, P.V., Venkatachalam, S., Jabir, T., Yang, E.J., Cho, K.-H., Jung, J., et al. (2023) Water Mass Controlled Vertical Stratification of Bacterial and Archaeal Communities in the Western Arctic Ocean During Summer Sea-Ice Melting. *Microb Ecol* **85**: 1150–1163.

Wu, Y.-W., Simmons, B.A., and Singer, S.W. (2016) MaxBin 2.0: an automated binning algorithm to recover genomes from multiple metagenomic datasets. *Bioinformatics* **32**: 605–607.

Zhang, R., Debeljak, P., Blain, S., and Obernosterer, I. (2023) Seasonal shifts in Fe-acquisition strategies in Southern Ocean microbial communities revealed by metagenomics and autonomous sampling. *Environmental Microbiology* **25**: 1816–1829.

Zhou, Z., Tran, P.Q., Breister, A.M., Liu, Y., Kieft, K., Cowley, E.S., et al. (2022) METABOLIC: high-throughput profiling of microbial genomes for functional traits, metabolism, biogeochemistry, and community-scale functional networks. *Microbiome* **10**: 33.

Supplementary material

Supplementary Results

Prokaryotic community composition across samples

Differences in prokaryotic community composition between different size fractions were observed through the visualization of Bray-Curtis dissimilarity in the NMDS plot (Fig. S1A). In addition, the prokaryotic community composition varied across surface waters or water masses, both in the free-living or particle-attached prokaryotes communities (Fig. S1B and S1C). In the surface waters of the free-living prokaryotes samples, they were all dominated by SAR11, SAR86 and SAR116. However, significant differences in prokaryotic community composition were observed when comparing different surface waters. Specifically, STSW exhibited a high abundance of *Cyanobiaceae*, while SASW, PFSW, and ASW exhibited a high abundance of *Flavobacteriaceae* and *Rhodobacteraceae*. Additionally, ASW featured abundant *Thioglobaceae*. And there are some differences in the composition of prokaryotic communities between particle-attached and free-living samples in surface water. First, *Flavobacteriaceae* exhibits a consistently high abundance across all surface water of the particle-attached samples, and also *Cyanobiaceae* is not only dominated in STSW but also dominated in SASW.

In the free-living prokaryotes samples obtained from various water masses, *Nitrosopumilaceae*, SAR324, SAR406, and Marine Group II exhibited consistently high abundance. Although SAR11 was detected, its presence was notably lower, especially in comparison to surface waters. Moreover, distinct variations were observed in the prokaryotic community composition among different water masses. For instance, in WW, AAIW, UCDW and LCDW, there was a high abundance of *Thioglobaceae*. The LCDW and NADW had a high abundance of *Pseudoalteromonadaceae*. In the samples of particle-attached prokaryotes collected from various water masses, a consistently high abundance of *Moraxellaceae* was observed. Distinct prokaryotic community compositions were also identified among the various water masses within the particle-attached prokaryote samples. For instance, there was a high abundance of *Comamonadaceae* in STMW, and a high abundance of *Pseudoalteromonadaceae* in NADW.

Abundance of trace metal transporters in different water masses of PA samples

In all FL samples, the abundance of genes associated with ferric transport was higher than that of genes linked to ferrous transport (Fig. 3A). However, this contrast was not evident in

the particle-attached samples, where gene abundance was lower compared to the FL samples (Fig. S3A). Among PA samples, genes associated with ferrous transport were predominantly present in deeper water masses such as LCDW, NADW, and AABW, except for *yfeAB*. Conversely, most genes associated with ferric transport exhibited higher abundance in PFSW and ASW, with the exception of *futA1/A2* and *futC*, which also displayed high abundance in NADW (Fig. S3A). The difference in Mn transporters between surface and deeper water masses in PA samples, when compared to FL samples, was not significant except for ASW (Fig. S3C). A distinct pattern of gene abundance emerged in PA samples compared to FL samples, with lower gene abundance observed in surface water and the highest abundance recorded in NADW (Fig. S3D). This may be attributed to a decrease in the abundance of *cbiOMQ* observed in surface seawater of PA samples, as indicated by the PAN index (Fig. S5). The abundance of *cbik* was very high in surface water in FL samples, but in the PA samples, the abundance of *cbiK* was higher in ASW, LCDW and NADW, with lower abundance in SASW and PFSW compared to FL samples (Fig. S3D).

Supplementary Figures

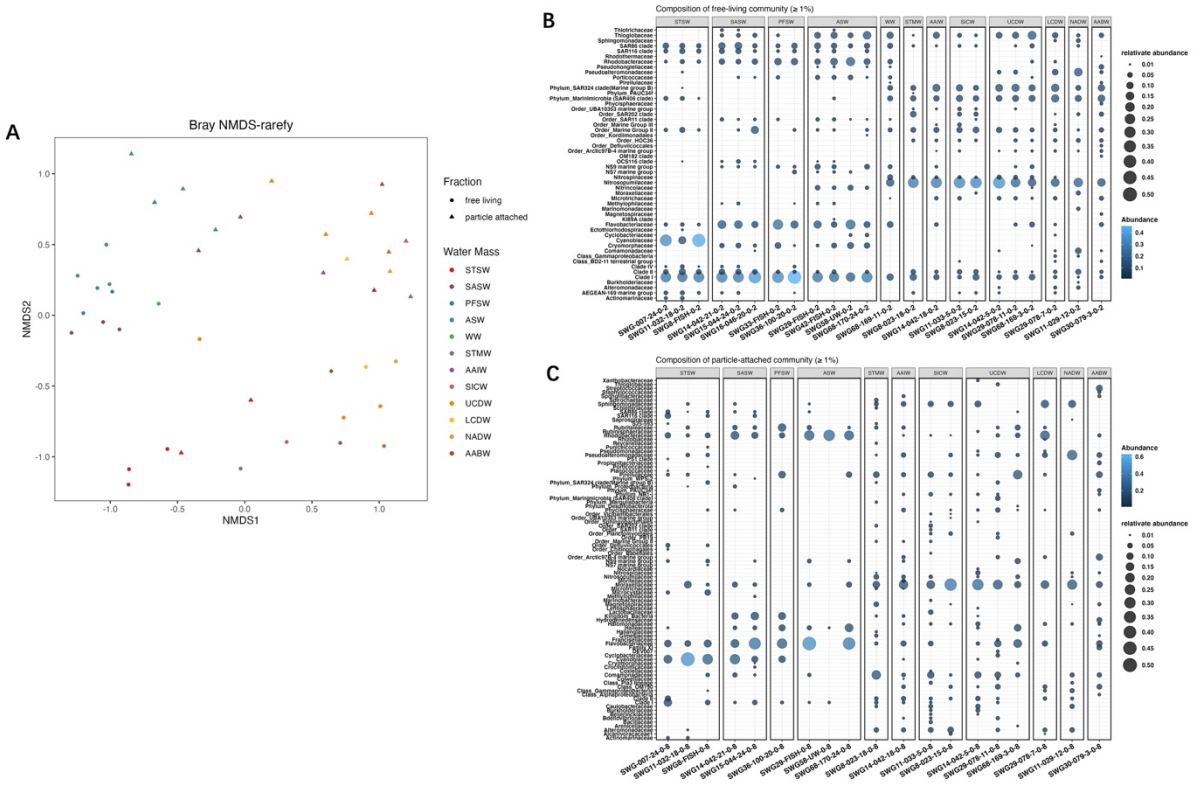

Fig. S1 A. Non-Metric Multidimensional Scale (NMDS) plots of free-living (circles) and particle-attached (triangles) prokaryotic communities based on Bray-Curtis dissimilarity. Composition of the free-living prokaryotic communities (B) and particle-attached prokaryotic communities (C) in samples of the present study. Taxonomic assignments are based on the Family level and only ASVs with a relative abundance of more than 1% in at least one sample are shown.

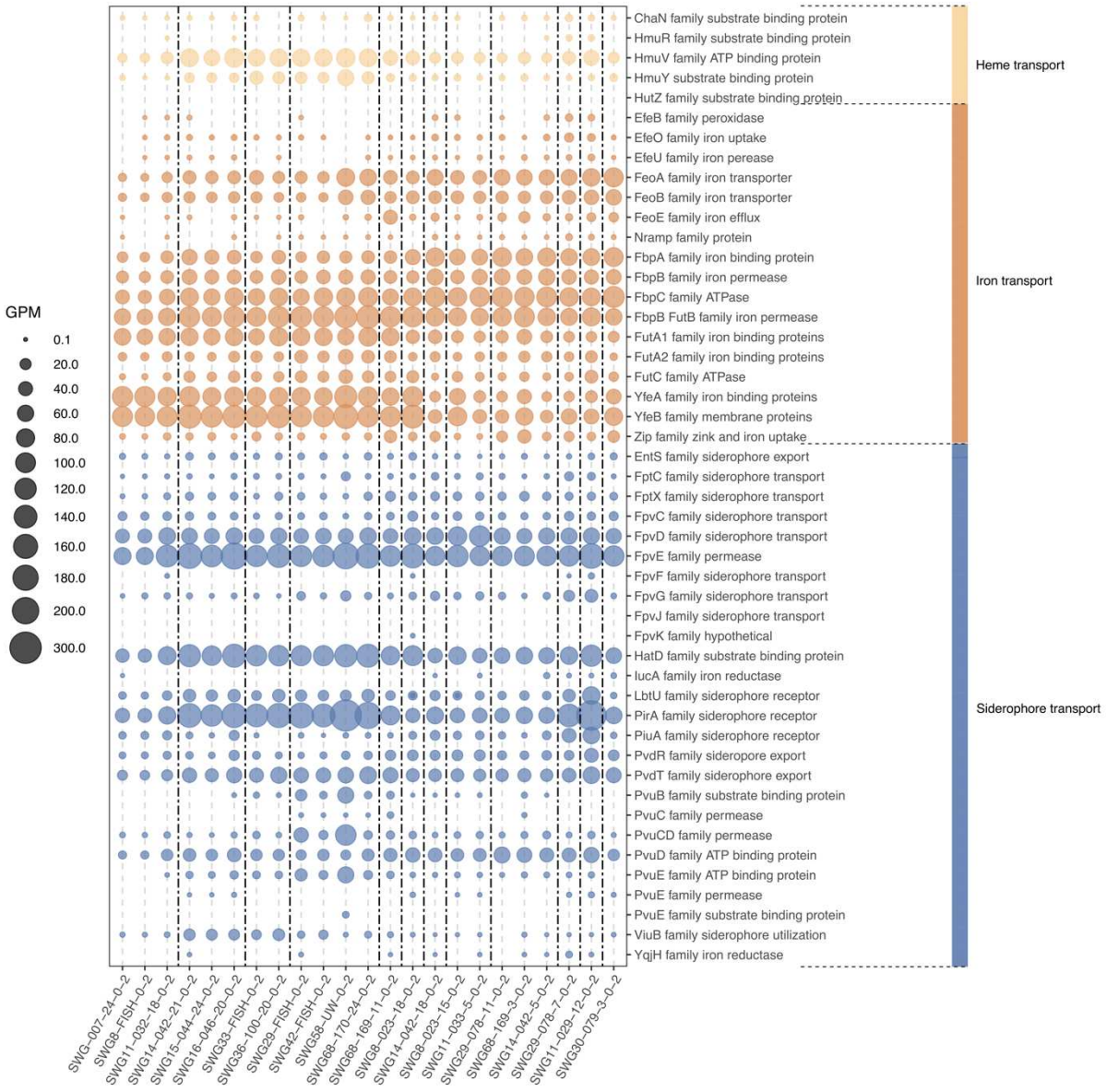

Fig. S2 The abundance of genes in free-living samples for heme, Fe^{2+} and Fe^{3+} and siderophore transporters. Normalized gene abundances are given in genes per kilobase million (GPM).

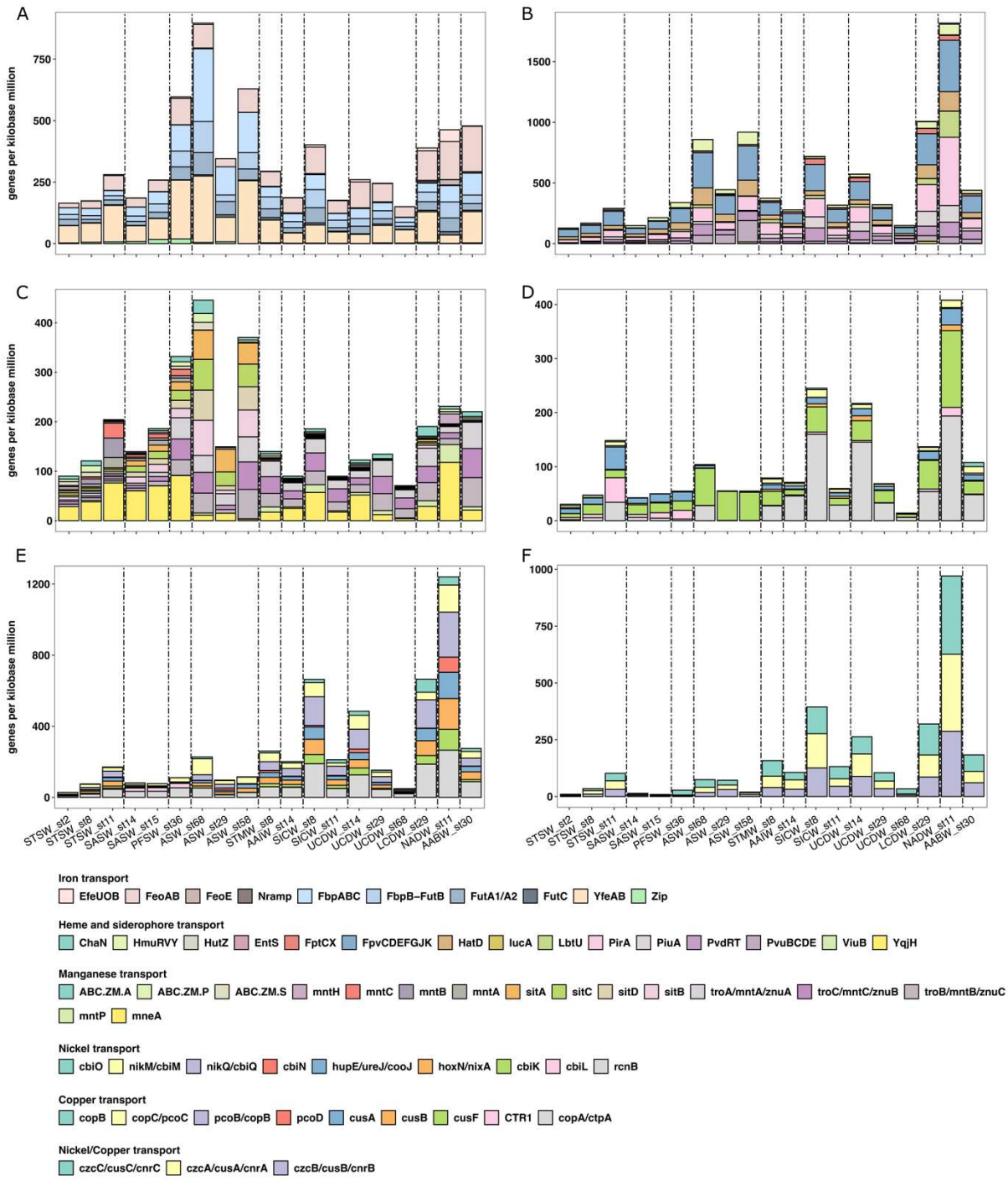

Fig. S3 The abundance of genes in particle-attached samples for heme and siderophore transporters (A), Fe^{3+} and Fe^{2+} transporters (B), copper transporters (C), nickel transporters (D), manganese transporters (E), and nickel/copper transporters (F). Normalized gene abundances are given in genes per kilobase million (GPM).

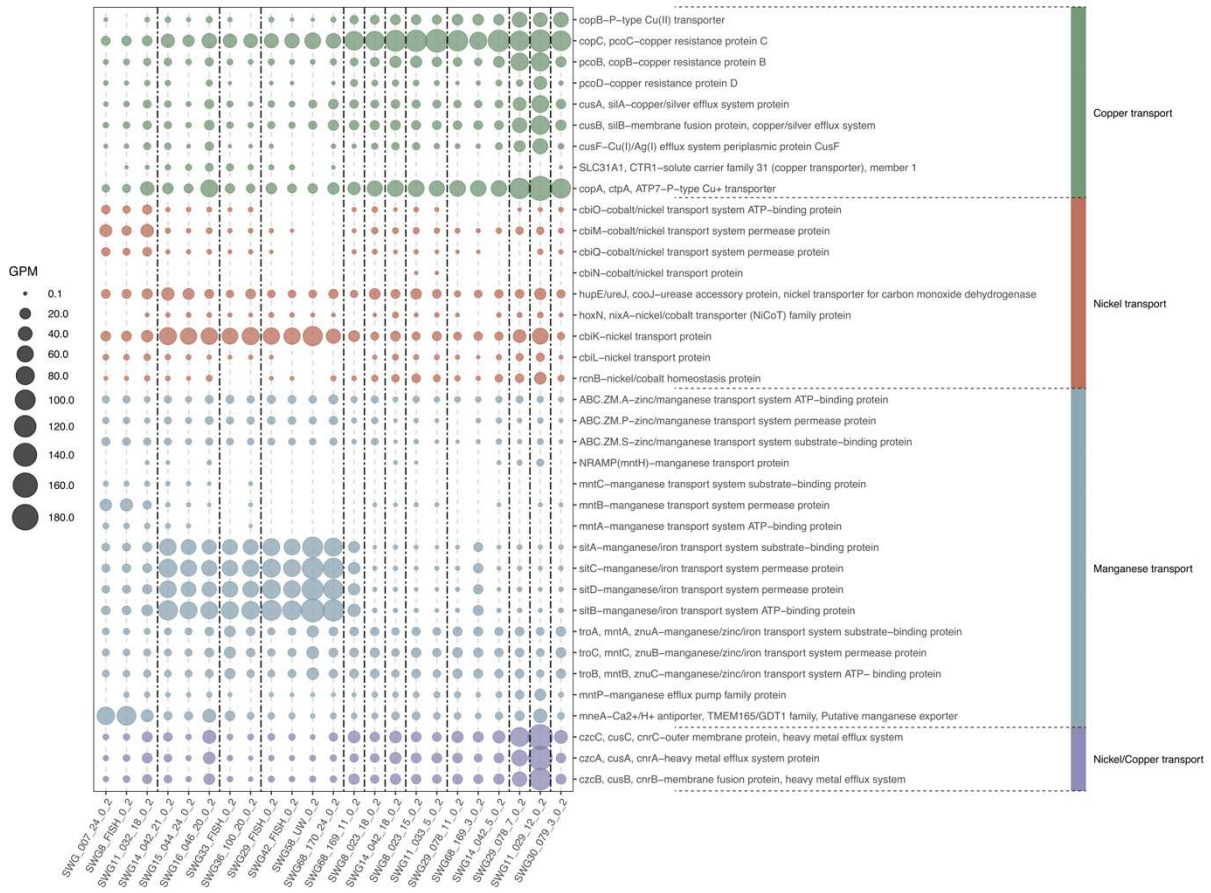

Fig. S4 The abundance of genes in free-living samples for copper, nickel, manganese and nickel/copper transporters. Normalized gene abundances are given in genes per kilobase million (GPM).

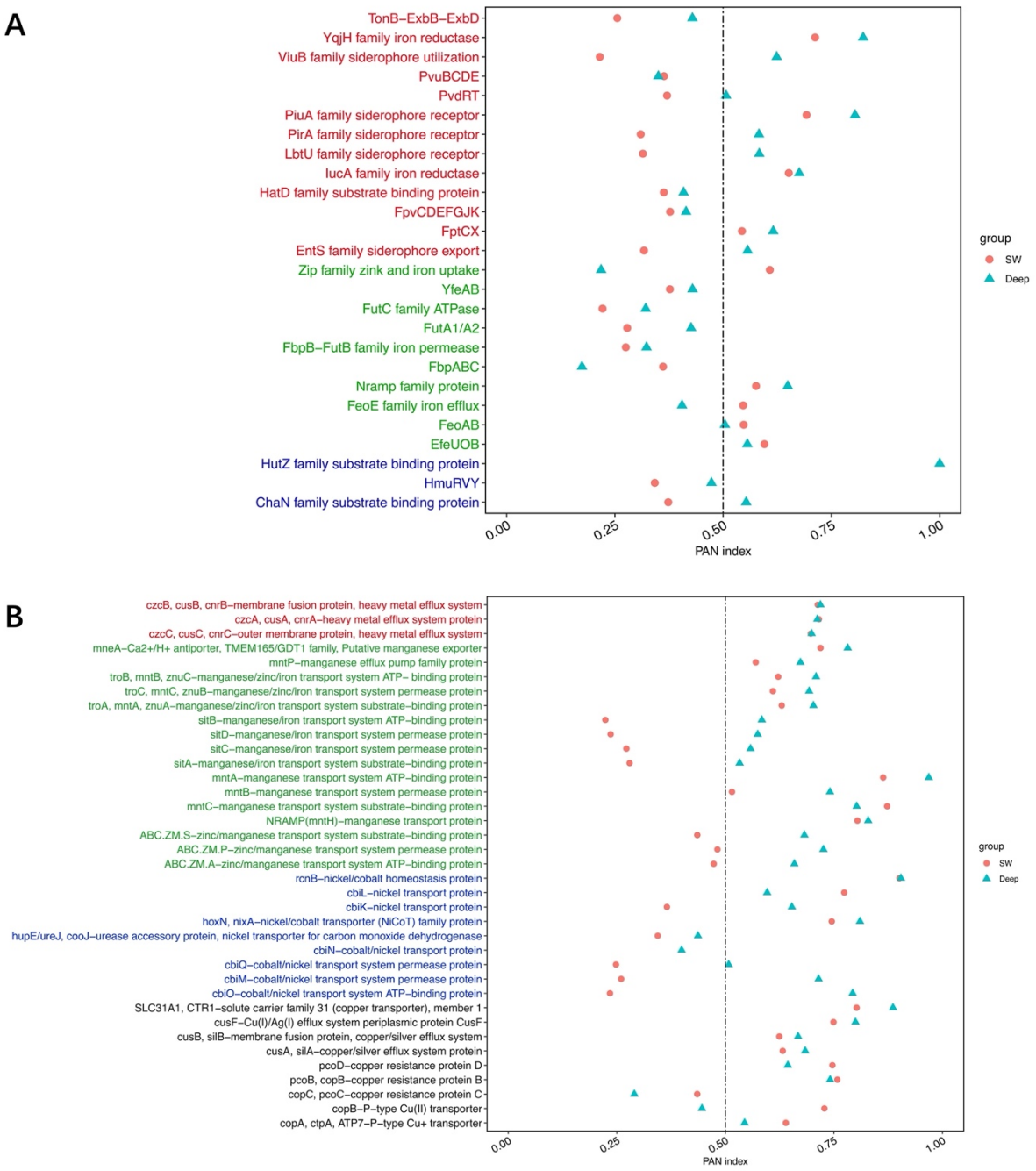

Fig. S5 Particle-association niche (PAN) index of the genes realted to iron (A) and Mn, Ni, Cu (B) transport. Different colors represent different transport pathway; A. siderphore transport genes in red, Fe^{3+} and Fe^{2+} transport genes in green, heme transport genes in blue; B. copper transport genes in black, nickel transport genes in blue, manganese transport genes in green, nickel/copper transport genes in red.

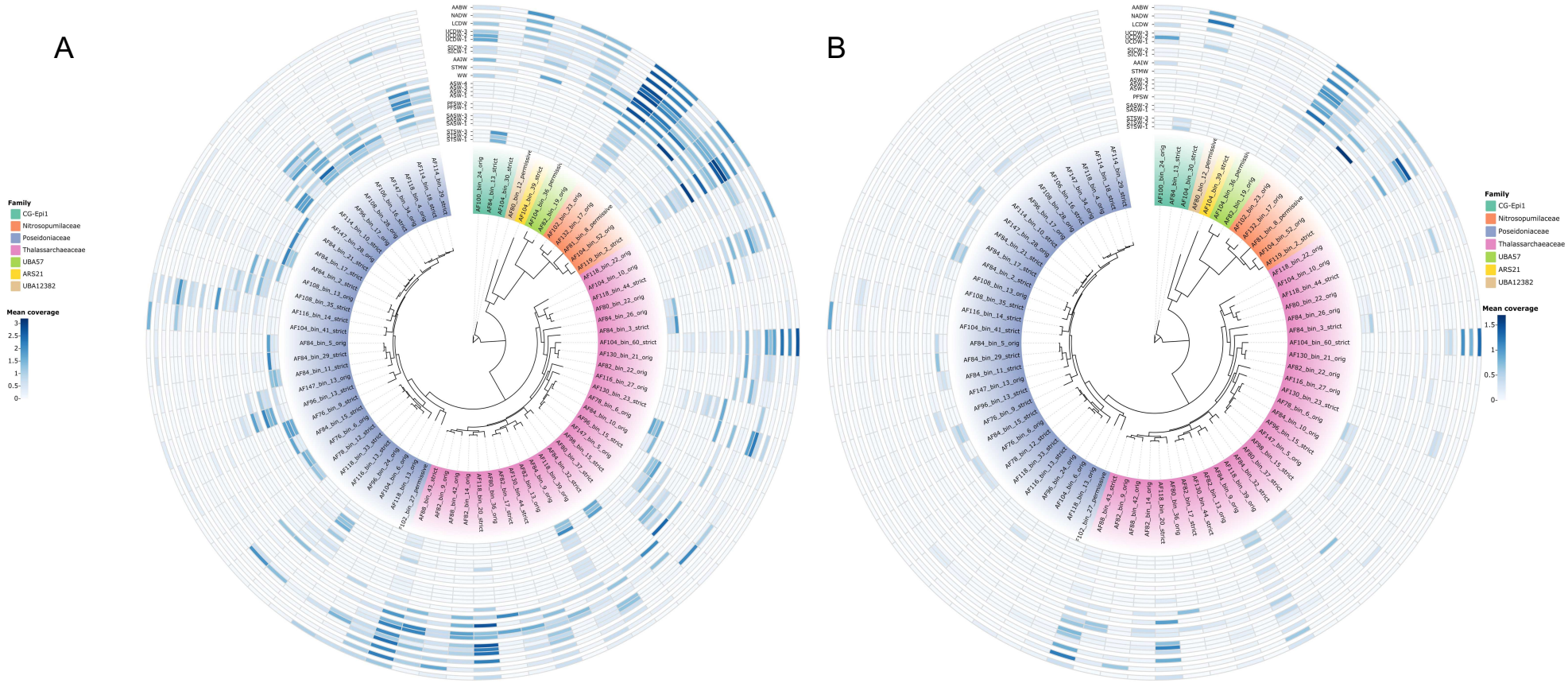

Fig. S6 Phylogenetic tree of all archaea species-level MAGs. The heatmap shows the mean coverage of each MAG in each free-living (A) and particle-attached (B) sample. Colour intensity is determined by log transformed mean coverage of each MAG.

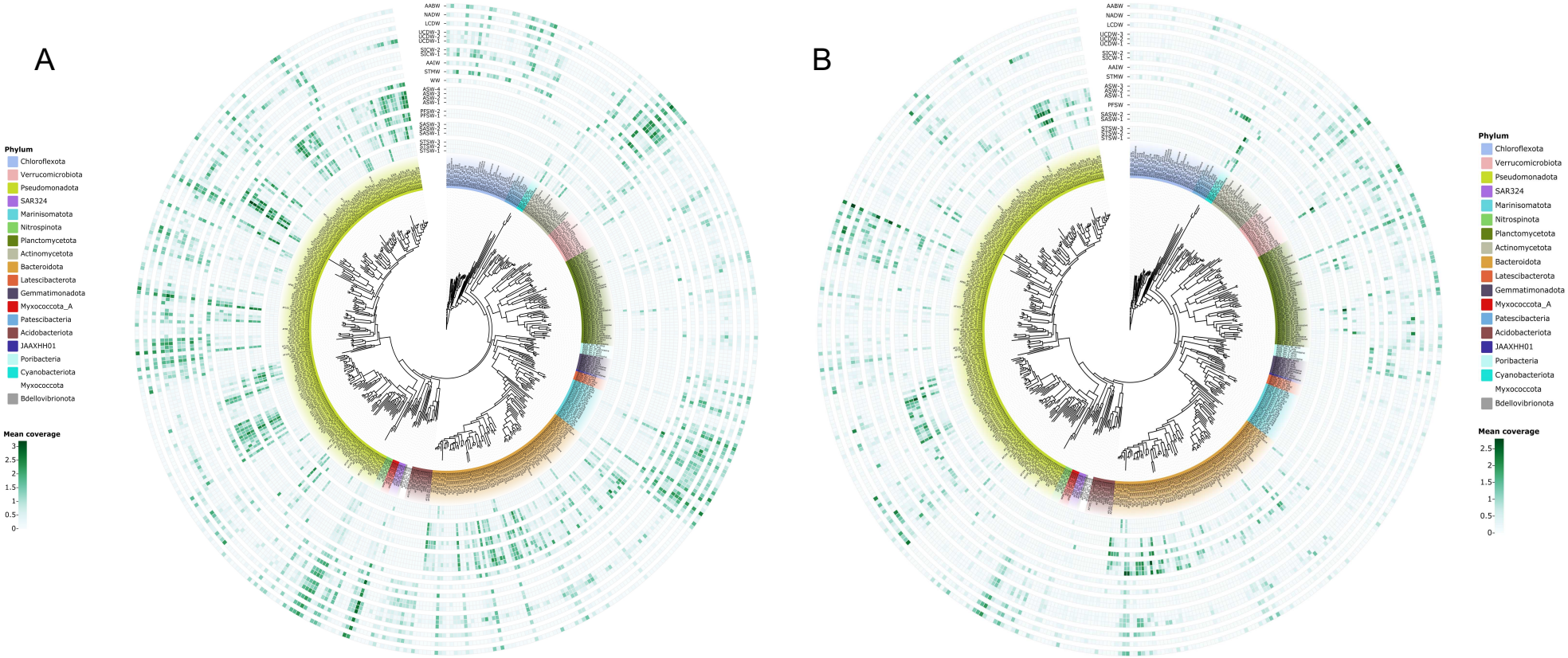

Fig. S7 Phylogenetic tree of all bacterial species-level MAGs. The heatmap shows the mean coverage of each MAG in each free-living (A) and particle-attached (B) sample. Colour intensity is determined by log transformed mean coverage of each MAG.

Supplementary Tables

Table S1. Geographic location and total number of sequences obtained per sample

Code	Sample Name	Station	Size	Lon	Lat	Total sequences
AFQF-76	SWG-007-24-0-2	2	free-living	39.988	-28.638	114457156
AFQF-77	SWG-007-24-0-8	2	particle-attached	39.988	-28.638	124434938
AFQF-78	SWG8-FISH-0-2	8	free-living	34.471	-35.218	115938727
AFQF-79	SWG8-FISH-0-8	8	particle-attached	34.471	-35.218	103538227
AFQF-80	SWG8-023-18-0-2	8	free-living	34.471	-35.218	115749381
AFQF-81	SWG8-023-18-0-8	8	particle-attached	34.471	-35.218	110015341
AFQF-82	SWG8-023-15-0-2	8	free-living	34.471	-35.218	118449789
AFQF-83	SWG8-023-15-0-8	8	particle-attached	34.471	-35.218	120342949
AFQF-84	SWG11-032-18-0-2	11	free-living	36.390	-39.812	107884402
AFQF-85	SWG11-032-18-0-8	11	particle-attached	36.390	-39.812	103423496
AFQF-88	SWG11-029-12-0-2	11	free-living	36.379	-39.801	102961698
AFQF-89	SWG11-029-12-0-8	11	particle-attached	36.379	-39.801	111859692
AFQF-90	SWG14-042-21-0-2	14	free-living	36.174	-44.862	111859692
AFQF-91	SWG14-042-21-0-8	14	particle-attached	36.174	-44.862	100652635
AFQF-93	SWG14-042-18-0-8	14	particle-attached	36.174	-44.862	101704024
AFQF-95	SWG14-042-5-0-8	14	particle-attached	36.174	-44.862	104214398
AFQF-96	SWG15-044-24-0-2	15	free-living	36.231	-44.854	109595520
AFQF-97	SWG15-044-24-0-8	15	particle-attached	36.231	-44.854	107639186
AFQF-98	SWG29-FISH-0-2	29	free-living	49.380	-52.397	117442856
AFQF-100	SWG29-078-11-0-2	29	free-living	49.380	-52.397	121366046
AFQF-101	SWG29-078-11-0-8	29	particle-attached	49.380	-52.397	106485424
AFQF-102	SWG29-078-7-0-2	29	free-living	49.380	-52.397	112539556
AFQF-103	SWG29-078-7-0-8	29	particle-attached	49.380	-52.397	112458066
AFQF-104	SWG30-079-3-0-2	30	free-living	49.383	-52,902	103337371
AFQF-105	SWG30-079-3-0-8	30	particle-attached	49.383	-52,902	108404070
AFQF-106	SWG33-FISH-0-2	33	free-living	51.889	-46.120	112216585
AFQF-108	SWG36-100-20-0-2	36	free-living	56.411	-47.086	116667266
AFQF-109	SWG36-100-20-0-8	36	particle-attached	56.411	-47.086	129008243
AFQF-110	SWG42-FISH-0-2	42	free-living	68.501	-50.701	112906568
AFQF-112	SWG58-UW-0-2	58	free-living	81.924	-57.690	112906568
AFQF-114	SWG68-170-24-0-2	68	free-living	72.300	-50.800	111610535
AFQF-115	SWG68-170-24-0-8	68	particle-attached	72.300	-50.800	112906568
AFQF-116	SWG68-169-11-0-2	68	free-living	72.300	-50.800	112906568
AFQF-118	SWG68-169-3-0-2	68	free-living	72.300	-50.800	123727617
AFQF-119	SWG68-169-3-0-8	68	particle-attached	72.300	-50.800	114136983
AFQF-126	SWG11-033-5-0-2	11	free-living	36.404	-39.817	110567727
AFQF-127	SWG11-033-5-0-8	11	particle-attached	36.404	-39.817	108854881
AFQF-130	SWG14-042-18-0-2	14	free-living	36.174	-44.862	119639443

AFQF-132	SWG14-042-5-0-2	14	free-living	36.174	-44.862	108468196
AFQF-135	SWG29-FISH-0-8	29	particle-attached	49.379	-52.397	106876734
AFQF-143	SWG58-UW-0-8	58	particle-attached	81.924	-57.690	106177217
AFQF-147	SWG16-046-20-0-2	16	free-living	36.602	-46.501	109686895

Table S2. The list of genes associated with trace metal transport detected in this study

Module	Gene		Description	KO
Heme transport		ChaN	ChaN-family-substrate-binding-protein	
	HmuRVY	HmuR	HmuR-outer-membrane heme utilization receptor	K16089
		HmuV	HmuV-family-heme transport system ATP-binding protein	K10834
		HmuY	HmuY-substrate-binding-protein	
		HutZ	HutZ family substrate binding protein	
Iron transport Fe^{2+} (ferrous)	EfeUOB	EfeB	EfeB-family peroxidase; deferrochelatase/peroxidase EfeB [EC:1.11.1.-]	K16301
		EfeO	EfeO-family-iron-uptake	K07224
		EfeU	EfeU-family-iron-perease; high-affinity iron transporter	K07243
	FeoAB	FeoA	FeoA-family- ferrous iron transport protein A	K04758
		FeoB	FeoB-family-ferrous iron transport protein B	K04759
		FeoE	FeoE-family-iron-efflux; export excess Fe^{2+} from the MR-1 cytoplasm	
		Nramp	Nramp-family-protein; natural resistance-associated macrophage protein	K12347, K21398
	YfeAB	YfeA	YfeA-family-iron-binding-proteins; manganese/iron transport system substrate-binding protein	K11604
		YfeB	YfeB-family-membrane-proteins; manganese/iron transport system ATP-binding protein	K11607
Iron transport Fe^{3+} (ferric)	FbpABC	FbpA	FbpA-family-iron-binding-protein; afuA, fbpA; iron(III) transport system substrate-binding protein	K02012
		FbpB	FbpB-family-iron-permease; afuB, fbpB; iron(III) transport system permease protein	K02011
		FbpC	FbpC-family-ATPase; afuC, fbpC; iron(III) transport system ATP-binding protein [EC:7.2.2.7]	K02010
		FbpB-FutB	FbpB-FutB-family-iron-permease	
	FutA1/A2	FutA1	FutA1-family-iron_ABC_transporter-iron-binding-proteins	
		FutA2	FutA2-family-iron_ABC_transporter-iron-binding-proteins	
		FutC	FutC-family-iron_ABC_transporter-ATPase	
Iron transport		Zip	Zip-family-zink-and-iron-uptake	
Siderophore transport		EntS	EntS-enterobactin exporter; MFS transporter, ENTS family, enterobactin (siderophore) exporter	K08225
		FptC	FptC-ferripyochelin transport	

	FptCX Ferripyochelin uptake	FptX	FptX-ferripyochelin transport; MFS transporter, PAT family, beta-lactamase induction signal transducer AmpG	K08218
	FpvCDEFGJK Pyoverdin siderophore uptake	FpvC	FpvC-family-siderophore-transport; Sid_FpvC_metal_ion_transport_PA2407_Paeruginosa_PAO1_180602	
		FpvD	FpvD-family-siderophore-transport; Sid_FpvD_ATPase_PA2408_Paeruginosa_PAO1_180602	
		FpvE	FpvE-family-permease; PF01032-FecCD-YfhA-FpvE-YfeCD_transport_family	
		FpvF	FpvF-family-siderophore-transport; Sid_FpvF_metal_ion_transport_PA2410_Paeruginosa_PAO1_180602	
		FpvG	FpvG-family-siderophore-transport; Sid_FpvG_iron_reductase_PA2403_Paeruginosa_PAO1_180602	
		FpvJ	FpvJ-family-siderophore-transport; Sid_FpvJ_PA2405_Paeruginosa_PAO1_180602	
		FpvK	FpvK-family-hypothetical	
		HatD	HatD-aerobactin binding protein	
		LbtU	LbtU-legiobactin receptor	
		PirA	PirA-ferric enterobactin receptor (TonB_dependent_receptor)	K19611
		PiuA	PiuA-catecholate siderophore receptor	K16090
	PvdRT Pyoverdine export	PvdR	PvdR-pyoverdine export; membrane fusion protein, macrolide-specific efflux system	K13888
		PvdT	PvdT-pyoverdine export; macrolide transport system ATP-binding/permease protein [EC:7.6.2.-]	K05685
	PvuBCDE Vibrioferrin uptake; the ABC transport system for ferric vibrioferrin	PvuB	PvuB-family-substrate-binding-protein	K25282
		PvuC	PvuC-family-permease; Ferrichrome ABC transporter (permease)	K23183
		PvuCD	PvuCD-family-permease; ferric citrate transport system permease protein	K23183, K23182
		PvuD	PvuD-family-ATP-binding-protein; ferric citrate transport system permease protein	K23182
		PvuE	PvuE-family-ATP-binding-protein; ferric citrate transport system ATP-binding protein [EC:7.2.2.18]	K23184
			PvuE-family-permease	
			PvuE-family-substrate-binding-protein	
		ViuB	ViuB-vibriobactin utilization protein	
		YqjH	YqjH-ferric chelate reductase (NADPH) [EC:1.16.1.9]	K07229
	ExbB-ExbD-TonB	ExbB	ExbB-family	K03561
		ExbD	ExbD-family	K03559
		TonB	TonB-family	K03832

Copper transport	copB	copB-P-type Cu(II) transporter [EC:7.2.2.9], copper Efflux System	K01533
	copC/pcoC	copC, pcoC-copper resistance protein C	K07156
	pcoB/copB	pcoB, copB-copper resistance protein B	K07233
	pcoD	pcoD-copper resistance protein D	K07245
	cusA	cusA, silA-copper/silver efflux system protein	K07787, K15726
	cusB	cusB, silB-membrane fusion protein, copper/silver efflux system	K07798, K15727
	cusF	cusF-Cu(I)/Ag(I) efflux system periplasmic protein CusF	K07810
	CTR1	SLC31A1, CTR1-solute carrier family 31 (copper transporter), member 1	K14686
	copA/ctpA	copA, ctpA, ATP7-P-type Cu+ transporter, copper Efflux System	K17686
Nickel transport	cbiO	cbiO-cobalt/nickel transport system ATP-binding protein	K02006
	nikM/cbiM	cbiM-cobalt/nickel transport system permease protein | Substrate-specific component NikM of nickel ECF transporter	K02007
	nikQ/cbiQ	cbiQ-cobalt/nickel transport system permease protein | nikQ; Transmembrane component of energizing module of nickel ECF transporter	K02008
	cbiN	cbiN-cobalt/nickel transport protein	K02009
	ddpD	ddpD-peptide/nickel transport system ATP-binding protein_ABC.PE.A	K02031
	ddpF	ddpF-peptide/nickel transport system ATP-binding protein_ABC.PE.A1	K02032
	ABC.PE.P	ABC.PE.P-peptide/nickel transport system permease protein	K02033
	ABC.PE.P1	ABC.PE.P1-peptide/nickel transport system permease protein	K02034
	ABC.PE.S	ABC.PE.S-peptide/nickel transport system substrate-binding protein	K02035
	hupE/ureJ, cooJ	hupE/ureJ, cooJ-urease accessory protein | hupE/ureJ protein; urease accessory protein | cooJ; nickel transporter for carbon monoxide dehydrogenase	K03192
	HoxN/nixA	hoxN, nixA-nickel/cobalt transporter (NiCoT) family protein	K07241
	cbiK	cbiK-nickel transport protein	K10094
	cbiL	cbiL-nickel transport protein	K16915
	rcnB	rcnB-nickel/cobalt homeostasis protein	K23243
Manganese transport	ABC.ZM.A	ABC.ZM.A-zinc/manganese transport system ATP-binding protein	K02074
	ABC.ZM.P	ABC.ZM.P-zinc/manganese transport system permease protein	K02075
	ABC.ZM.S	ABC.ZM.S-zinc/manganese transport system substrate-binding protein	K02077
	mntH	NRAMP(mntH)-manganese transport protein	K03322

	mntC	mntC-manganese transport system substrate-binding protein	K11601, K19975
	mntB	mntB-manganese transport system permease protein	K11602, K19976
	mntA	mntA-manganese transport system ATP-binding protein [EC:7.2.2.5]	K11603, K19973
	sitA	sitA-manganese/iron transport system substrate-binding protein; ABC transporters	K11604
	sitC	sitC-manganese/iron transport system permease protein	K11605
	sitD	sitD-manganese/iron transport system permease protein	K11606
	sitB	sitB-manganese/iron transport system ATP-binding protein	K11607
	troA/mntA/znuA	troA, mntA, znuA-manganese/zinc/iron transport system substrate-binding protein	K11707
	troC/mntC/znuB	troC, mntC, znuB-manganese/zinc/iron transport system permease protein	K11708
	troB/mntB/znuC	troB, mntB, znuC-manganese/zinc/iron transport system ATP- binding protein [EC:7.2.2.5]	K11710
	mntP	mntP-manganese efflux pump family protein	K23242
	mneA	mneA-Ca2+/H+ antiporter, TMEM165/GDT1 family, Putative manganese exporter	K23541
Ni/Cu transport	czcC/cusC/cnrC	czcC, cusC, cnrC-outer membrane protein, heavy metal efflux system	K15725
	czcA/cusA/cnrA	czcA, cusA, cnrA-heavy metal efflux system protein	K15726
	czcB/cusB/cnrB	czcB, cusB, cnrB-membrane fusion protein, heavy metal efflux system	K15727

Table S3. The taxa classification of the top 10 MAGs in STSW, SASW, PFSW and ASW of the free-living samples

MAGs	Kingdom	Phylum	Class	Order	Family	Genus	Species
AF106_bin_11	Bacteria	Bacteroidota	Bacteroidia	Flavobacteriales	Schleiferiaceae	UBA10364	UBA10364 sp003487785
AF106_bin_16	Archaea	Thermoplasmatota	Poseidoniia	Poseidoniales	Poseidoniaceae	MGIIa-L1	NA
AF106_bin_17	Bacteria	Bacteroidota	Bacteroidia	Flavobacteriales	Flavobacteriaceae	Arcticimaribacter	Arcticimaribacter sp018608425
AF106_bin_2	Bacteria	Pseudomonadota	Gammaproteobacteria	Pseudomonadales	Pseudohongiellaceae	UBA9145	NA
AF108_bin_15	Bacteria	Pseudomonadota	Alphaproteobacteria	Rhodobacterales	Rhodobacteraceae	CPC320	CPC320 sp002336405
AF108_bin_22	Bacteria	Pseudomonadota	Gammaproteobacteria	Pseudomonadales	HTCC2089	UBA4421	UBA4421 sp002336645
AF110_bin_22	Bacteria	Pseudomonadota	Gammaproteobacteria	Pseudomonadales	Porticoccaceae	Porticoccus	NA
AF110_bin_26	Bacteria	Pseudomonadota	Gammaproteobacteria	Pseudomonadales	Porticoccaceae	HTCC2207	NA
AF110_bin_30	Bacteria	Bacteroidota	Bacteroidia	Flavobacteriales	Flavobacteriaceae	MS024-2A	NA
AF110_bin_9	Bacteria	Bacteroidota	Bacteroidia	Flavobacteriales	Schleiferiaceae	UBA10364	UBA10364 sp003487785
AF112_bin_15	Bacteria	Bacteroidota	Bacteroidia	Flavobacteriales	Flavobacteriaceae	Arcticimaribacter	NA
AF112_bin_6	Bacteria	Bacteroidota	Bacteroidia	Flavobacteriales	Flavobacteriaceae	Patiriisocius	Patiriisocius sp003450155
AF114_bin_10	Archaea	Thermoplasmatota	Poseidoniia	Poseidoniales	Poseidoniaceae	MGIIa-L1	NA
AF114_bin_12	Bacteria	Pseudomonadota	Gammaproteobacteria	Pseudomonadales	Porticoccaceae	HTCC2207	HTCC2207 sp905181925
AF114_bin_17	Bacteria	Pseudomonadota	Alphaproteobacteria	Rhodobacterales	Rhodobacteraceae	Amylibacter	Amylibacter sp905182285
AF114_bin_18	Archaea	Thermoplasmatota	Poseidoniia	Poseidoniales	Poseidoniaceae	MGIIa-L1	NA
AF114_bin_20	Bacteria	Bacteroidota	Bacteroidia	Flavobacteriales	UA16	UBA974	UBA974 sp002339135
AF114_bin_3	Bacteria	Bacteroidota	Bacteroidia	Flavobacteriales	Schleiferiaceae	TMED14	TMED14 sp913049755
AF114_bin_32	Bacteria	Pseudomonadota	Gammaproteobacteria	Pseudomonadales	Pseudohongiellaceae	UBA9145	NA
AF114_bin_38	Bacteria	Pseudomonadota	Gammaproteobacteria	Pseudomonadales	Porticoccaceae	HTCC2207	NA
AF114_bin_4	Bacteria	Pseudomonadota	Alphaproteobacteria	Sphingomonadales	Emcibacteraceae	Pseudemcibacter	Pseudemcibacter sp018675425
AF114_bin_42	Bacteria	Bacteroidota	Bacteroidia	Flavobacteriales	UBA7312	JABAYQ01	JABAYQ01 sp018608925
AF115_bin_9	Bacteria	Pseudomonadota	Gammaproteobacteria	Pseudomonadales	Porticoccaceae	TMED48	NA
AF118_bin_26	Bacteria	Pseudomonadota	Gammaproteobacteria	Pseudomonadales	Nitrincolaceae	ASP10-02a	ASP10-02a sp002312935
AF147_bin_14	Bacteria	Pseudomonadota	Gammaproteobacteria	Burkholderiales	Burkholderiaceae_B	Aquabacterium	Aquabacterium sp001770725

AF147_bin_28	Archaea	Thermoplasmatota	Poseidoniia	Poseidoniales	Poseidoniaceae	MGIIa-L1	NA
AF147_bin_30	Bacteria	Bacteroidota	Bacteroidia	Flavobacteriales	UBA7430	GCA-2707145	GCA-2707145 sp002707145
AF147_bin_6	Bacteria	Pseudomonadota	Gammaproteobacteria	Woeseiales	Woeseiaceae	SP4260	NA
AF78_bin_2	Bacteria	Actinomycetota	Acidimicrobiia	Acidimicrobiales	UBA11606	UBA11606	UBA11606 sp002699625
AF78_bin_6	Archaea	Thermoplasmatota	Poseidoniia	Poseidoniales	Thalassarchaeaceae	MGIIb-O2	MGIIb-O2 sp002504905
AF78_bin_8	Bacteria	Bacteroidota	Bacteroidia	Flavobacteriales	UA16	UBA11663	UBA11663 sp002863145
AF79_bin_1	Bacteria	Bacteroidota	Bacteroidia	Flavobacteriales	Flavobacteriaceae	UBA3537	UBA3537 sp002725015
AF79_bin_2	Bacteria	Cyanobacteriota	Cyanobacteriia	Cyanobacteriales	Microcystaceae_A	Atelocyanobacterium	Atelocyanobacterium thalassa
AF79_bin_3	Bacteria	Cyanobacteriota	Cyanobacteriia	PCC-6307	Cyanobiaceae	Parasynechococcus	Parasynechococcus sp000012625
AF83_bin_6	Bacteria	Pseudomonadota	Gammaproteobacteria	Enterobacterales_A	Alteromonadaceae	Pseudoalteromonas	Pseudoalteromonas gelatinilytica
AF84_bin_1	Bacteria	Pseudomonadota	Gammaproteobacteria	Pseudomonadales	Halieaceae	Luminiphilus	NA
AF84_bin_11	Archaea	Thermoplasmatota	Poseidoniia	Poseidoniales	Poseidoniaceae	Poseidonia	NA
AF84_bin_15	Archaea	Thermoplasmatota	Poseidoniia	Poseidoniales	Poseidoniaceae	MGIIa-K1	MGIIa-K1 sp002689565
AF84_bin_16	Bacteria	Bacteroidota	Bacteroidia	Flavobacteriales	Flavobacteriaceae	UBA724	NA
AF84_bin_17	Archaea	Thermoplasmatota	Poseidoniia	Poseidoniales	Poseidoniaceae	MGIIa-L1	NA
AF84_bin_21	Archaea	Thermoplasmatota	Poseidoniia	Poseidoniales	Poseidoniaceae	MGIIa-L1	MGIIa-L1 sp8160u
AF84_bin_23	Bacteria	Pseudomonadota	Alphaproteobacteria	NA	NA	NA	NA
AF84_bin_4	Bacteria	Pseudomonadota	Gammaproteobacteria	Pseudomonadales	Litoricolaceae	HIMB30	NA
AF84_bin_5	Archaea	Thermoplasmatota	Poseidoniia	Poseidoniales	Poseidoniaceae	Poseidonia	Poseidonia sp002714305
AF84_bin_8	Bacteria	Pseudomonadota	Alphaproteobacteria	Parvibaculales	RS24	UBA7378	NA
AF90_bin_31	Bacteria	Pseudomonadota	Gammaproteobacteria	Pseudomonadales	HTCC2089	UBA4421	UBA4421 sp002390555
AF90_bin_9	Bacteria	Pseudomonadota	Gammaproteobacteria	Pseudomonadales	Porticoccaceae	HTCC2207	HTCC2207 sp913031645
AF91_bin_4	Bacteria	Bacteroidota	Bacteroidia	Flavobacteriales	Flavobacteriaceae	Hel1-33-131	Hel1-33-131 sp913052445
AF96_bin_1	Bacteria	Pseudomonadota	Gammaproteobacteria	Pseudomonadales	Porticoccaceae	TMED48	NA
AF96_bin_17	Archaea	Thermoplasmatota	Poseidoniia	Poseidoniales	Poseidoniaceae	MGIIa-L1	MGIIa-L1 sp9513u
AF96_bin_18	Bacteria	Bacteroidota	Bacteroidia	Flavobacteriales	Schleiferiaceae	TMED14	TMED14 sp913043005
AF96_bin_26	Bacteria	Pseudomonadota	Alphaproteobacteria	Rhodobacterales	Rhodobacteraceae	MED-G52	NA
AF96_bin_9	Bacteria	Pseudomonadota	Gammaproteobacteria	Pseudomonadales	Pseudohongiellaceae	UBA9145	NA

AF97_bin_3	Bacteria	Pseudomonadota	Alphaproteobacteria	Rhodobacterales	Rhodobacteraceae	LFER01	NA
AF98_bin_22	Bacteria	Bacteroidota	Bacteroidia	Cytophagales	Cyclobacteriaceae	UBA4465	UBA4465 sp002470835

Table S4. The functional annotation results of the top 10 MAGs in STSW, SASW, PFSW and ASW of the free-living samples based on the Metabolic_v4.0 database

Pathway	Amino acid utilization	Ethanol fermentation	Fatty acid degradation	Aromatics degradation	Complex carbon degradation	Fermentation	C1 metabolism	Nitrogen cycling	Oxidative phosphorylation	Oxidative phosphorylation Complex IV	Urea utilization	Halogenated compound utilization	Nitrile hydration	Sulfur cycling enzymes
AF78_bin_2	7	0	2	0	4	2	4	0	7	2	0	0	0	22
AF78_bin_6	2	0	1	1	0	1	0	0	2	1	0	0	0	7
AF79_bin_3	3	0	0	1	2	1	0	0	7	2	3	0	0	16
AF84_bin_1	8	0	6	1	4	1	3	1	6	3	0	0	0	13
AF84_bin_8	2	0	2	0	2	1	0	0	10	1	0	0	0	13
AF79_bin_1	4	0	0	0	4	1	0	0	3	0	0	0	0	4
AF84_bin_11	1	0	2	1	0	1	0	0	2	1	0	0	0	3
AF79_bin_2	1	0	0	1	1	1	0	3	6	2	0	0	0	9
AF84_bin_4	5	1	0	0	1	1	5	0	6	4	3	0	0	18
AF96_bin_26	5	0	1	0	0	1	5	0	5	1	0	1	0	21
AF83_bin_6	6	1	6	1	11	3	2	3	5	11	0	1	0	23
AF78_bin_8	0	0	1	0	3	0	0	0	3	0	0	0	0	1
AF84_bin_17	1	0	2	1	0	1	0	0	2	1	0	0	0	4
AF84_bin_21	1	0	2	1	0	1	0	0	2	0	0	0	0	4
AF84_bin_5	1	0	2	2	0	1	0	0	2	1	0	0	0	4
AF84_bin_15	0	0	2	1	0	1	0	0	2	0	0	0	0	5
AF84_bin_23	3	0	1	1	1	0	0	0	2	3	0	0	0	6
AF147_bin_14	7	1	3	1	1	3	2	6	9	7	3	0	0	23
AF84_bin_16	5	0	1	0	2	1	0	0	4	0	0	0	0	10
AF90_bin_9	6	1	4	1	5	1	5	0	6	3	0	0	0	16
AF96_bin_18	3	0	1	0	6	2	0	0	2	0	0	0	0	13
AF91_bin_4	5	0	2	0	7	1	0	0	5	0	0	0	0	7
AF96_bin_1	7	1	7	1	2	0	4	0	8	2	0	0	0	12

AF96_bin_9	5	1	4	1	1	1	3	0	7	2	0	1	0	10
AF97_bin_3	6	1	2	0	3	4	7	0	6	2	0	1	2	22
AF90_bin_31	5	0	8	0	3	1	5	0	5	2	0	0	2	23
AF147_bin_28	1	0	2	1	0	1	0	0	1	0	0	0	0	4
AF147_bin_6	4	0	1	0	1	0	0	0	4	0	0	0	0	6
AF96_bin_17	1	0	2	1	0	1	0	0	0	1	0	0	0	8
AF108_bin_22	6	0	6	0	3	1	5	0	5	2	0	0	2	19
AF108_bin_15	6	0	4	0	2	3	13	0	8	4	0	1	2	20
AF106_bin_16	1	0	1	1	0	1	0	0	0	1	0	0	0	4
AF147_bin_30	5	0	2	1	3	1	0	0	3	0	0	0	0	6
AF114_bin_12	5	0	4	0	3	1	4	0	8	3	0	0	0	12
AF112_bin_6	4	0	1	0	4	2	0	0	3	0	0	0	0	6
AF114_bin_3	4	0	2	0	4	2	0	0	2	0	0	0	0	13
AF110_bin_30	5	0	0	0	3	2	0	0	2	0	0	0	0	11
AF106_bin_11	4	0	2	0	4	2	0	0	2	0	0	0	0	5
AF115_bin_9	7	1	5	1	4	1	4	0	8	2	0	0	0	13
AF110_bin_26	4	0	3	0	6	1	1	0	6	1	0	0	0	12
AF114_bin_17	5	0	1	0	2	1	4	0	10	4	0	1	0	21
AF106_bin_2	2	4	2	0	1	1	8	0	5	3	0	1	2	12
AF114_bin_18	0	0	2	0	0	1	0	0	2	1	0	0	0	6
AF114_bin_10	1	0	2	1	0	2	0	0	2	1	0	0	0	4
AF114_bin_20	4	0	1	0	4	2	0	0	3	0	0	0	0	12
AF110_bin_22	6	0	0	1	1	1	0	0	7	2	0	0	0	10
AF112_bin_15	3	0	3	0	2	1	0	0	5	0	0	0	0	13
AF98_bin_22	8	0	2	0	6	1	2	0	5	0	0	0	0	14
AF118_bin_26	6	0	2	1	1	1	4	0	5	2	0	1	0	35
AF106_bin_17	5	0	3	0	2	2	0	0	3	0	0	0	0	11
AF110_bin_9	4	0	2	0	4	2	0	0	3	0	0	0	0	6

AF114_bin_42	3	0	1	1	4	1	0	0	3	0	0	0	0	10
AF114_bin_38	6	0	5	1	3	1	5	0	8	2	0	0	0	16
AF114_bin_32	6	1	5	1	1	1	3	0	8	2	0	0	2	19
AF114_bin_4	8	0	0	1	1	1	3	1	9	2	0	0	0	23

Table S5. The taxa classification of the top 10 MAGs in WW, AAIW, SICW, UCDW, LCDW and NADW of the free-living samples

MAGs	Kingdom	Phylum	Class	Order	Family	Genus	Species
AF100_bin_17	Bacteria	Verrucomicrobiota	Verrucomicrobiae	Pedosphaerales	UBA1096	UBA1096	UBA1096 sp015658765
AF100_bin_28	Bacteria	Marinisomatota	Marinisomatia	Marinisomatales	UBA1611	GCA-002717915	GCA-002717915 sp002717915
AF100_bin_8	Bacteria	Actinomycetota	Acidimicrobiia	Acidimicrobiales	MedAcidi-G1	S20-B6	S20-B6 sp002699725
AF101_bin_5	Bacteria	Pseudomonadota	Gammaproteobacteria	Arenicellales	UBA868	REDSEA-S09-B13	REDSEA-S09-B13 sp002456995
AF102_bin_39	Bacteria	Pseudomonadota	Gammaproteobacteria	Enterobacterales_A	Alteromonadaceae	Pseudoalteromonas	Pseudoalteromonas lipolytica_A
AF102_bin_48	Bacteria	Pseudomonadota	Alphaproteobacteria	Sphingomonadales	Sphingomonadaceae	Qipengyuania	Qipengyuania citrea
AF104_bin_29	Bacteria	Marinisomatota	Marinisomatia	Marinisomatales	TCS55	GCA-002701945	GCA-002701945 sp913062595
AF104_bin_3	Bacteria	Marinisomatota	Marinisomatia	Marinisomatales	TCS55	TCS55	TCS55 sp002715035
AF104_bin_60	Archaea	Thermoplasmatota	Poseidoniia	Poseidoniales	Thalassarchaeaceae	MGIIb-O1	MGIIb-O1 sp002498525
AF105_bin_2	Bacteria	Actinomycetota	Acidimicrobiia	Acidimicrobiales	MedAcidi-G1	UBA9410	UBA9410 sp012961035
AF110_bin_26	Bacteria	Pseudomonadota	Gammaproteobacteria	Pseudomonadales	Porticoccaceae	HTCC2207	
AF114_bin_12	Bacteria	Pseudomonadota	Gammaproteobacteria	Pseudomonadales	Porticoccaceae	HTCC2207	HTCC2207 sp905181925
AF114_bin_13	Bacteria	Pseudomonadota	Gammaproteobacteria	Pseudomonadales	Porticoccaceae	HTCC2207	HTCC2207 sp014381985
AF116_bin_12	Bacteria	Marinisomatota	Marinisomatia	Marinisomatales	TCS55	TCS55	
AF116_bin_14	Archaea	Thermoplasmatota	Poseidoniia	Poseidoniales	Poseidoniaceae	MGIIa-L1	
AF116_bin_28	Bacteria	Actinomycetota	Acidimicrobiia	Acidimicrobiales	MedAcidi-G1	UBA9410	UBA9410 sp014240365
AF116_bin_3	Bacteria	Bacteroidota	Bacteroidia	Flavobacteriales	Flavobacteriaceae	SCGC-AAA160-P02	SCGC-AAA160-P02 sp000383355
AF118_bin_20	Archaea	Thermoplasmatota	Poseidoniia	Poseidoniales	Thalassarchaeaceae	Thalassarchaeum	Thalassarchaeum sp002495735
AF126_bin_14	Bacteria	Gemmatimonadota	Gemmatimonadetes	Longimicrobiales	UBA6960	UBA1138	
AF130_bin_24	Bacteria	Pseudomonadota	Gammaproteobacteria	UBA11654	UBA11654	CACPJA01	
AF132_bin_6	Bacteria	Pseudomonadota	Alphaproteobacteria	HIMB59	GCA-002718135	MarineAlpha5-Bin3	MarineAlpha5-Bin3 sp002938255
AF147_bin_14	Bacteria	Pseudomonadota	Gammaproteobacteria	Burkholderiales	Burkholderiaceae_B	Aquabacterium	Aquabacterium sp001770725
AF147_bin_32	Bacteria	Pseudomonadota	Alphaproteobacteria	Sphingomonadales	Sphingomonadaceae	Sphingopyxis	Sphingopyxis sp001468395
AF81_bin_8	Archaea	Thermoproteota	Nitrososphaeria	Nitrososphaerales	Nitrosopumilaceae	Nitrosopelagicus	Nitrosopelagicus brevis
AF82_bin_18	Bacteria	Pseudomonadota	Gammaproteobacteria	Pseudomonadales	Pseudohongiellaceae	UBA9145	UBA9145 sp002712055

AF82_bin_2	Bacteria	Chloroflexota	Dehalococcoidia	UBA3495	UBA3495	UBA9611	UBA9611 sp002697005
AF82_bin_23	Bacteria	Pseudomonadota	Gammaproteobacteria	Pseudomonadales	Pseudomonadaceae	Halopseudomonas	Halopseudomonas pachastrellae
AF82_bin_4	Bacteria	Chloroflexota	Dehalococcoidia	SAR202	UBA826	GCA-002712965	GCA-002712965 sp009391195
AF82_bin_5	Bacteria	Actinomycetota	Acidimicrobiia	Acidimicrobiales	MedAcidi-G1	UBA9410	UBA9410 sp022452035
AF82_bin_8	Bacteria	Actinomycetota	Acidimicrobiia	Acidimicrobiales	TK06	UBA2110	UBA2110 sp002705305
AF83_bin_13	Bacteria	Pseudomonadota	Gammaproteobacteria	Pseudomonadales	Moraxellaceae	Acinetobacter	Acinetobacter junii
AF83_bin_6	Bacteria	Pseudomonadota	Gammaproteobacteria	Enterobacterales_A	Alteromonadaceae	Pseudoalteromonas	Pseudoalteromonas gelatinilytica
AF88_bin_40	Bacteria	SAR324	SAR324	SAR324	NAC60-12	Arctic96AD-7	Arctic96AD-7 sp002082305
AF88_bin_43	Archaea	Thermoplasmatota	Poseidoniia	Poseidoniales	Thalassarchaeaceae	Thalassarchaeum	Thalassarchaeum sp002507125
AF98_bin_1	Bacteria	Pseudomonadota	Gammaproteobacteria	Pseudomonadales	Porticoccaceae	HTCC2207	
AF98_bin_15	Archaea	Thermoplasmatota	Poseidoniia	Poseidoniales	Thalassarchaeaceae	MGIIb-O2	MGIIb-O2 sp023700255

Table S6. The functional annoation results of the top 10 MAGs in WW, AAIW, SICW, UCDW, LCDW and NADW of the free-living samples based on the Metabolic_v4.0 database

Pathway	Amino acid utilization	Ethanol fermentation	Fatty acid degradation	Aromatics degradation	Complex carbon degradation	Fermentation	C1 metabolism	Methane metabolism	Nitrogen cycling	Oxidative phosphorylation	Urea utilization	Halogenated compound utilization	As cycling	Sulfur cycling enzymes
AF100_bin_17	8	0	0	1	0	2	0	0	1	6	3	0	0	11
AF100_bin_28	5	0	2	0	9	1	6	0	0	6	0	0	0	10
AF100_bin_8	7	0	4	0	2	2	7	0	0	7	0	0	0	16
AF101_bin_5	10	0	7	1	1	1	4	0	0	6	0	1	1	37
AF102_bin_39	4	1	4	1	6	1	2	0	1	5	0	1	1	18
AF102_bin_48	5	0	5	0	3	1	3	0	0	9	0	0	1	16
AF104_bin_29	4	0	3	0	10	1	3	0	1	10	0	0	0	10
AF104_bin_3	4	0	2	0	6	1	0	0	2	6	0	0	1	11
AF104_bin_60	2	0	2	1	0	2	0	0	0	2	0	0	0	5
AF105_bin_2	8	0	4	0	3	2	8	0	0	7	0	0	0	21
AF110_bin_26	4	0	3	0	6	1	1	0	0	6	0	0	1	12
AF114_bin_12	5	0	4	0	3	1	4	0	0	8	0	0	1	12
AF114_bin_13	6	0	8	1	3	1	4	0	0	6	0	0	0	16
AF116_bin_12	6	0	1	0	10	1	0	0	0	4	0	0	0	10
AF116_bin_14	1	0	1	1	0	1	0	0	0	1	0	0	0	6
AF116_bin_28	8	0	4	0	2	2	9	0	0	7	0	0	0	19
AF116_bin_3	5	0	2	0	3	2	0	0	0	3	0	0	1	9
AF118_bin_20	2	0	1	1	0	1	0	0	0	2	0	0	0	3
AF126_bin_14	3	3	0	0	2	2	4	0	0	4	0	1	0	12
AF130_bin_24	5	0	2	1	2	1	4	0	0	5	0	0	0	13
AF132_bin_6	4	0	0	0	1	1	5	0	0	7	0	1	0	12
AF147_bin_14	7	1	3	1	1	3	2	1	6	9	3	0	1	23
AF147_bin_32	6	0	10	2	3	2	3	1	2	10	0	1	2	26

AF81_bin_8	4	0	0	0	0	0	0	0	3	2	3	0	0	5
AF82_bin_18	7	1	5	1	1	2	7	0	0	6	4	1	2	15
AF82_bin_2	8	0	3	1	0	3	5	0	0	6	0	2	1	11
AF82_bin_23	8	2	6	1	1	3	6	0	4	6	3	0	1	26
AF82_bin_4	4	0	2	1	0	0	6	0	0	6	0	3	0	4
AF82_bin_5	4	0	4	0	1	2	5	0	0	7	0	0	0	14
AF82_bin_8	7	0	7	0	1	1	6	0	0	7	0	0	0	27
AF83_bin_13	9	2	4	0	1	3	3	0	3	6	0	0	1	28
AF83_bin_6	6	1	6	1	11	3	2	0	3	5	0	1	1	23
AF88_bin_40	3	0	0	0	1	1	6	1	0	5	0	0	0	15
AF88_bin_43	2	0	3	1	0	1	0	0	0	2	0	0	0	3
AF98_bin_1	6	0	8	1	6	3	10	0	0	4	0	0	1	13
AF98_bin_15	2	0	2	1	0	1	0	0	0	2	0	0	0	8

Conclusions and perspectives

1. Summary and general discussion

This thesis investigates microbial carbon and trace metal transport strategies in the ocean, providing a comprehensive analysis from both temporal and spatial perspectives. Based on a rich dataset comprising 187 seawater samples, encompassing the surface and the deep ocean, microbial taxonomic and functional diversity was determined through 16S rRNA gene sequencing and metagenomic approaches. The study covers regions from the Subtropical to the Southern Ocean, among which the Southern Ocean is one of the most unstudied marine environments on Earth. The work in this thesis contributes to our understanding of trace metal transport strategies in marine microbes and provides insights on how trace metals could shape microbial communities.

1.1 Temporal and Spatial dynamics of carbon and trace metals transporters

Although the distribution of genes encoding trace element-dependent proteins as well as iron transporters have been investigated on a global ocean scale (Toulza *et al.*, 2012; Xu *et al.*, 2021), there is still limited research on these aspects in the Southern Ocean. In this thesis, studies of prokaryotes revealed the temporal and spatial variations in genes associated with carbon and trace metal transport. Twelve surface seawater samples, were collected from the Kerguelen Plateau (Station A3) in the Indian sector of the Southern Ocean using a Remote Access Sampler (RAS-500®, Mac Lane) between 25 October 2016 and 24 February 2017. Through the sequencing of metagenomes and subsequent annotation of assemblies, a distinct seasonal pattern of genes related to carbon and iron transport was observed, and this seasonal variation is related to the organic carbon substrate provided by phytoplankton and the seasonal succession of prokaryotes (Chapter 1). Seasonal variations in microbial communities and processes during phytoplankton blooms have been investigated in previous studies (Teeling *et al.*, 2016; Liu *et al.*, 2020; Zhou *et al.*, 2020). Despite these studies, comprehensive seasonal observations in the Southern Ocean are still lacking. Here, this thesis provides the first seasonal metagenomics dataset collected from the Kerguelen region, covering both the spring and the summer phytoplankton blooms.

The analysis of Chapter 1 was limited to the FL prokaryotic communities, lacking consideration of the PA prokaryotic communities. However, in Chapter 3, the sampling scope was expanded by collecting 42 seawater samples from surface water in various geographic regions and in water masses across STZ, SAZ, PFZ and AAZ during the SWINGS cruise (10th January to 8th March 2021). These samples encompassed both the FL and PA size

fractions. Through metagenome sequencing and analysis, differences in the presence of trace metals (Fe, Mn, Cu and Ni) transport related genes between the FL and PA prokaryotic communities were observed, as well as variances across different water masses. This pattern might be less associated with the concentration of trace metals but rather with prokaryotic community composition (Chapter 3). Leu *et al*. have shown differences in the metabolism between FL and PA prokaryotic communities across the water column, and observed metabolic variations between different depths (Leu *et al.*, 2022). There are, however, fewer studies in the Southern Ocean, in particular those focusing on trace metal metabolism. Hence, this thesis makes a significant contribution to the understanding of microbial-mediated trace metal cycling in oceanic environments.

1.2 Different taxa harbor different carbon and trace metals transporters

Different prokaryotic taxa carry different genes related to carbon and trace metal transport. In Chapter 1, the focus is on four key genes categories associated with iron transport: *fbp* (Fe^{3+}), *feo* (Fe^{2+}), *hmu* (heme), and *pir* (siderophore ferric enterobactin receptor). Each of these genes exhibited unique seasonal trends. Taxonomic assignments revealed that different prokaryotic taxa contributed to these genes during different seasons. For instance, the *fbp* gene was dominated by different taxa in different seasons, *Pseudomonadaceae*, *Pelagibacteraceae*, *Rhodobacteraceae* and *Nitrincolaceae* were major contributors. Conversely, the major contributors of the *feo* gene were *Sphingomonadaceae* and *Flavobacteriaceae*. Additionally, our functional annotation analysis of MAGs (SAR11, *Nitrincolaceae*, *Rhodobacteracea* and *Polaribacter*) revealed variations in metabolic gene pools among different taxa. This finding was also observed by Debeljak *et al*. (2019), highlighting the taxon-specific gene repertoire related to iron transport. The findings of this chapter, combined with the seasonal dynamics in microbial community composition (Liu *et al.*, 2020), offer novel insights into the adaptive strategies of prokaryotes in the Southern Ocean, particularly in response to iron limitation and dynamic organic carbon inputs from phytoplankton.

In Chapter 3, a total of 556 high quality MAGs from 42 metagenomes were assessed, from which the most abundant MAGs in each water mass were selected to analyze their metabolic profiles from a genomic perspective. This analysis revealed the variations in metabolic genes across different MAGs. For example, the abundant MAGs identified in SICW (*Acinetobacter Junii*) contained genes associated with the transport of trace metals such as Fe, Ni, and Cu. The abundant MAGs observed in LCDW and NADW, such as *Pseudoalteromonas* and *Aquabacterium*, show a diverse possibility of metabolic capabilities including heme and

siderophore transport, aromatic degradation, nitrogen metabolism, and sulfur metabolism. Moreover, the investigation revealed that a MAG affiliated to *Cyanobiaceae* with high abundance in STSW harbored genes related to Mn transport. Previous studies have also described the metabolic strategies of MAGs observed from surface to deep, but mostly focused on major metabolic pathways such as carbon fixation, recalcitrant organic substrate utilization, while giving less attention to the strategies of trace metal transport (Cao *et al.*, 2020; Coutinho *et al.*, 2021; Royo-Llonch *et al.*, 2021; Tran *et al.*, 2021; Leu *et al.*, 2022; Dutta *et al.*, 2023). the findings of this thesis underscore the diverse metabolic strategies of prokaryotes to adapt to the dynamic open ocean, and provide new insights for the adaptation of prokaryotes in response to varying trace metals conditions of the ocean.

1.3 The links between prokaryotes and trace metals in water masses

In Chapter 2, the potential links between prokaryotes and environmental factors within marine water masses were analyzed, employing partial least squares regression (PLSR). Through this method, the combinations of spatial distributions of prokaryotic taxa, micronutrients, and AOU contribute to distinguishing various water masses were found. Furthermore, by analyzing regression coefficients extracted from the PLSR model, the regression between prokaryotic taxa and trace metals were identified. For example, found that some ASVs have positive regressions with Cu, indicating their adaptation to high Cu concentrations. Specifically, taxa affiliated with *Nitrosopumilaceae* (ASV 29 and 119), SAR324 (ASV 188), *Alteromonadaceae* (ASV 180), and *Pseudoalteromonadaceae* (ASV 36) displayed this positive regression with Cu. This positive regression was further supported by the functional annotation of MAGs that were constructed in Chapter 3. For instance, one MAG (AF81_bin_8) affiliated with *Nitrosopumilaceae*, exhibited a high abundance in SICW and was found to harbor genes associated with Cu transport. Additionally, three MAGs belonging to SAR324 (AF100_bin_21, AF104_bin_13 and AF88_bin_40) were constructed, all of which contained genes related to Cu transport. Notably, MAG (AF88_bin_40) is prevalent and highly abundant in all water masses. Furthermore, seven MAGs associated with *Alteromonadaceae* were identified, all of which contained genes linked to Cu transport. Among these, two MAGs (AF102_bin_39 and AF83_bin_6) exhibited significant abundance in LCDW and NADW, aligning with our observations in Chapter 2 regarding their relative abundance in these water masses. Importantly, the detected Cu transport genes within these MAGs all are efflux or resistance genes, which suggests that these MAGs regulate intracellular copper homeostasis, and thus can adapt to the high Cu concentrations

environment. Moreover, while the analysis of Chapter 2 highlighted three ASVs with high relative abundance in WW and positive regression coefficients with Mn, and although MAGs belonging to these three ASVs were not detected in high abundance in WW, the other MAGs with high abundance in WW were found to harbor genes associated with Mn transport (*sitABCD*), suggesting their role in Mn cycling within this environment.

2. Perspectives

These observations can provide some new guidelines for future research.

Firstly, regarding the first chapter of the study, it would have been of interest to measure the concentrations of DOM and dFe, which would have allowed to confirm some conclusions of this thesis. Measurements of particulate trace metal concentrations could have provided further insights, it has been shown that particulate matter has a strong influence on PA prokaryotes (Teeling *et al.*, 2012; Manna *et al.*, 2020; Zhang *et al.*, 2020; Dithugoe *et al.*, 2023).

In this thesis metagenomics analysis and 16S rRNA gene sequencing were used, and both of these analyses yielded results of relative abundance and therefore lacked a quantitative analysis of the gene abundance. To determine the abundance of prokaryote-related trace metal transporter genes in the ocean quantitatively qPCR could be used to explore the spatial and temporal dynamics. Currently, the methods of omic analysis are becoming more and more diversified, allowing us to perform metatranscriptomic and metaproteomic analyses. In Chapter 1, through the results of metagenome annotation analysis, different prokaryotic taxa carry different iron transporter genes were found. However, a possible bias in this analysis is related to the short length of the sequences the taxonomic annotation. Another perspective is the verification of proposed hypotheses in the laboratory, such as by obtaining pure cultures by isolation, and obtaining a more comprehensive information by genome annotation of cultured isolates. By addressing these areas for further research, can refine the understanding of prokaryotic involvement in trace metal element cycling in the ocean and contribute to advancements in this field.

Reference

Cao, S., Zhang, W., Ding, W., Wang, Meng, Fan, S., Yang, B., et al. (2020) Structure and function of the Arctic and Antarctic marine microbiota as revealed by metagenomics. *Microbiome* **8**: 47.

Coutinho, F.H., Von Meijenfeldt, F.A.B., Walter, J.M., Haro-Moreno, J.M., Lopéz-Pérez, M., Van Verk, M.C., et al. (2021) Ecogenomics and metabolic potential of the South Atlantic Ocean microbiome. *Science of The Total Environment* **765**: 142758.

Debeljak, P., Toulza, E., Beier, S., Blain, S., and Obernosterer, I. (2019) Microbial iron metabolism as revealed by gene expression profiles in contrasted Southern Ocean regimes. *Environ Microbiol* **21**: 2360–2374.

Dithugoe, C.D., Bezuidt, O.K.I., Cavan, E.L., Froneman, W.P., Thomalla, S.J., and Makhalanyane, T.P. (2023) Bacteria and Archaea Regulate Particulate Organic Matter Export in Suspended and Sinking Marine Particle Fractions. *mSphere* **8**: e00420-22.

Dutta, A., Connors, E., Trinh, R., Erazo, N., Dasarathy, S., Ducklow, H.W., et al. (2023) Depth drives the distribution of microbial ecological functions in the coastal western Antarctic Peninsula. *Front Microbiol* **14**: 1168507.

Leu, A.O., Eppley, J.M., Burger, A., and DeLong, E.F. (2022) Diverse Genomic Traits Differentiate Sinking-Particle-Associated versus Free-Living Microbes throughout the Oligotrophic Open Ocean Water Column. *mBio* **13**: e01569-22.

Liu, Y., Blain, S., Crispi, O., Rembauville, M., and Obernosterer, I. (2020) Seasonal dynamics of prokaryotes and their associations with diatoms in the Southern Ocean as revealed by an autonomous sampler. *Environ Microbiol* **22**: 3968–3984.

Manna, V., Malfatti, F., Banchi, E., Cerino, F., De Pascale, F., Franzo, A., et al. (2020) Prokaryotic Response to Phytodetritus-Derived Organic Material in Epi- and Mesopelagic Antarctic Waters. *Front Microbiol* **11**: 1242.

Royo-Llonch, M., Sánchez, P., Ruiz-González, C., Salazar, G., Pedrós-Alió, C., Sebastián, M., et al. (2021) Compendium of 530 metagenome-assembled bacterial and archaeal genomes from the polar Arctic Ocean. *Nat Microbiol* **6**: 1561–1574.

Teeling, H., Fuchs, B.M., Becher, D., Klockow, C., Gardebrecht, A., Bennke, C.M., et al. (2012) Substrate-Controlled Succession of Marine Bacterioplankton Populations Induced by a Phytoplankton Bloom. *Science* **336**: 608–611.

Teeling, H., Fuchs, B.M., Bennke, C.M., Krüger, K., Chafee, M., Kappelmann, L., et al. (2016) Recurring patterns in bacterioplankton dynamics during coastal spring algae blooms. *eLife* **5**: e11888.

Toulza, E., Tagliabue, A., Blain, S., and Piganeau, G. (2012) Analysis of the Global Ocean Sampling (GOS) Project for Trends in Iron Uptake by Surface Ocean Microbes. *PLoS ONE* **7**: e30931.

Tran, P.Q., Bachand, S.C., McIntyre, P.B., Kraemer, B.M., Vadeboncoeur, Y., Kimirei, I.A., et al. (2021) Depth-discrete metagenomics reveals the roles of microbes in biogeochemical cycling in the tropical freshwater Lake Tanganyika. *The ISME Journal* **15**: 1971–1986.

Xu, Y., Cao, J., Jiang, L., and Zhang, Y. (2021) Biogeographic and Evolutionary Patterns of Trace Element Utilization in Marine Microbial World. *Genomics, Proteomics & Bioinformatics* **19**: 958–972.

Zhang, Y., Jing, H., and Peng, X. (2020) Vertical shifts of particle-attached and free-living prokaryotes in the water column above the cold seeps of the South China Sea. *Marine Pollution Bulletin* **156**: 111230.

Zhou, J., Lao, Y., Song, J., Jin, H., Zhu, J., and Cai, Z. (2020) Temporal heterogeneity of microbial communities and metabolic activities during a natural algal bloom. *Water Research* **183**: 116020.

Appendices

Appendix. 1 – Poster for SAME17

Seasonal shifts in Fe-acquisition strategies in Southern Ocean microbial communities revealed by metagenomics and autonomous sampling

Rui Zhang[1], Pavla Debeljak[2], Stephane Blain[1], Ingrid Obernosterer[1]

[1]Sorbonne Université, CNRS, Laboratoire d'Océanographie Microbienne (LOMIC), Banyuls/mer, France

[2]SupBiotech, Villejuif, France

For correspondence E-mail: rui.zhang@obs-banyuls.fr

Context

Iron (Fe) governs the cycling of organic carbon in large parts of the Southern Ocean. The strategies of diverse microbes to acquire the different chemical forms of Fe under seasonally changing organic carbon regimes remain, however, poorly understood. Here, we report high-resolution seasonal metagenomic observations from the region off Kerguelen Island (Indian Sector of the Southern Ocean) where natural Fe-fertilization induces consecutive spring and summer phytoplankton blooms. Our study provides novel insights to Fe-related ecological strategies of diverse marine prokaryotes and how the acquisition of this element is linked to organic carbon.

Observations from a remote autonomous sampler

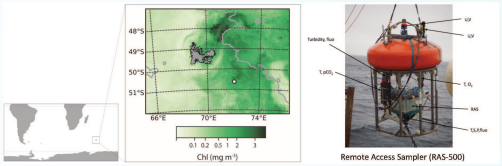

- Collection of seawater samples with a Remote Access Sampler (RAS-500®, Mac Lane) from Oct. 2016 to Feb. 2017 in surface waters (40 m) above the Kerguelen plateau.
- Seasonal picture of environmental parameters and microbial community composition and functioning (Blain et al. 2021, Liu et al. 2020, Zhang et al. 2023)

Results

Pronounced seasonal changes of genes related to prokaryotic Fe- and C- acquisition

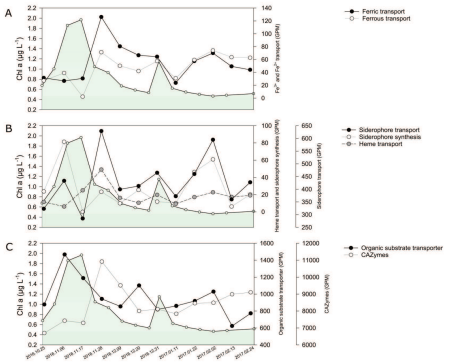

Fig. 1 Temporal changes of Chlorophyll a (green shaded area) and abundance of genes for Fe^{3+} and Fe^{2+} transporters (A), siderophore-bound Fe and heme transporters, and siderophore biosynthesis (B) and carbon substrate transporters and carbohydrate-active enzymes (CAZymes) (C). Normalized gene abundances are given in genes per kilobase million (GPM).

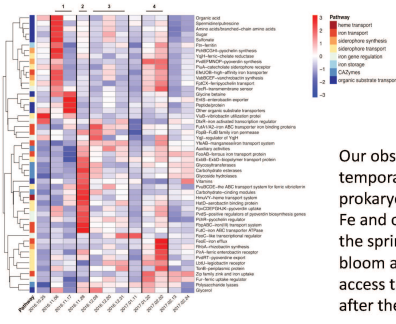

Fig. 2 Seasonal patterns of genes involved in Fe and organic substrate transporters and related processes.

Our observations suggest a temporal decoupling in the prokaryotic requirements of Fe and organic carbon during the spring phytoplankton bloom and a concerted access to these resources after the summer bloom.

Different prokaryotic groups harbor genes of Fe and organic carbon uptake

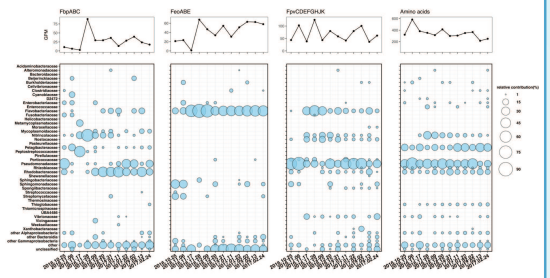

Fig. 3 Temporal changes of gene abundance and relative contribution of prokaryotic groups to specific genes.

Taxonomically diverse MAGs reveal distinct repertoires of genes involved in Fe and organic substrate utilization

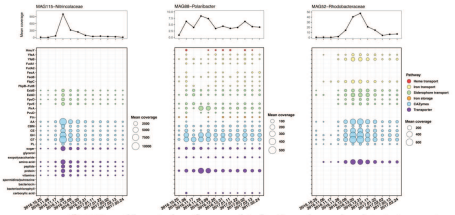

Fig. 4 Mean coverage of MAGs and inventories of genes related to Fe and organic substrate transport and CAZymes.

Conclusion

The pronounced, but distinct seasonal patterns in the abundance of genes implicated in the transport of different forms of Fe and organic substrates, of siderophore biosynthesis and carbohydrate active enzymes (CAZymes), likely result from temporal changes in the requirements of Fe and organic carbon. Our results suggest that the functional capabilities to acquire the different chemical forms in which Fe and organic carbon are present are drivers of microbial community succession in the Southern Ocean (Liu et al. 2021). Together, these observations provide new insights on the potential ecological niches of prokaryotes in the Fe- and organic carbon- constrained Southern Ocean.

Acknowledgements

This research was funded by the Southern Ocean and Climate (SOCLIM, PI Stéphane Blain) project of the Climate Initiative of the BNP Paribas Foundation, and it was supported by the CNRS, the IPEV and the Sorbonne University. R.Z. received PhD grant from the China Scholarship Council (CSC). We thank the Association Francophone d'Ecologie Microbienne (AFEM) and SAME17 for the travel grant.

References:

Blain, S., Rembauville, M., Crispi, O. & Obernosterer, I. (2021) Synchronized autonomous sampling reveals coupled pulses of biomass and export of morphologically different diatoms in the Southern Ocean. *Limnology & Oceanography*, 66, 753– 764.

Liu, Y., Blain, S., Crispi, O., Rembauville, M., and Obernosterer, I. (2020) Seasonal dynamics of prokaryotes and their associations with diatoms in the Southern Ocean as revealed by an autonomous sampler. *Environ Microbiol* 22: 3968–3984.

Zhang, R., Debeljak, P., Blain, S., and Obernosterer, I. (2023) Seasonal shifts in Fe-acquisition strategies in Southern Ocean microbial communities revealed by metagenomics and autonomous sampling. *Environ Microbiol* DOI: 10.1111/1462-2920.16397

Appendix. 2 – Communications – Academic Trainings – Publications

Communications

2023 **Rui Zhang**, Pavla Debeljak, Stephane Blain, Ingrid Obernosterer. Seasonal shifts in Fe-acquisition strategies in Southern Ocean microbial communities revealed by metagenomics and autonomous sampling. **SAME17 Symposium of Aquatic Microbial Ecology**, Aug. 20-25, 2023 *Tartu, Estonia*; poster

2022 **Rui Zhang**, Pavla Debeljak, Stephane Blain, Ingrid Obernosterer. Metagenomics reveal seasonal shifts in Fe-acquisition by diverse microbial communities in the Southern Ocean. **InterLab Meeting Banyuls-Barcelona**, Oct. 13-14, 2022 *Banyuls-sur-mer, France*; oral presentation

Academic Trainings

2022 Défis majeurs océans polaires: biogéochimie et écosystèmes (MU5MRM08), Paris, France

2022 Fundamentals in Statistics, Paris, France

2021 the EBAME Workshop on computational Microbial Ecogenomics, Brest, France

Publications

Rui Zhang, Pavla Debeljak, Stephane Blain, Ingrid Obernosterer. Seasonal shifts in Fe-acquisition strategies in Southern Ocean microbial communities revealed by metagenomics and autonomous sampling. *Environmental Microbiology* 2023;25;1816-1825.

Rui Zhang, Stéphane Blain, Corentin Baudet, Hélène Planquette, Frédéric Vivier, Philippe Catala, Olivier Crispi, Audrey Guéneuguès, Barbara Marie, Pavla Debeljak, Ingrid Obernosterer. Tagging of water masses with covariance of trace metals and prokaryotic taxa in the Southern Ocean. *Limnology and Oceanography Letters. accepted*.

Rui Zhang, Pavla Debeljak, Sharvari Gadegaonkar, Corentin Baudet, Hélène Planquette, Stéphane Blain, Ingrid Obernosterer. Spatial variations in microbial trace metal transporters across surface and deep water masses of the Southern Ocean. *in preparation*

Appendix. 3 – Co-author papers

1. Yanhui Kong, **Rui Zhang**, Stéphane Blain, Ingrid Obernosterer. Dynamics in microbial trace metals transporters during phytoplankton blooms in the Southern Ocean. *accepted*

2. Rhea Thoppil, **Rui Zhang**, Stéphane Blain, Philippe Catala, Olivier Crispi, Audrey Guéneuguès, Barbara Marie, Ingrid Obernosterer. Response of marine microbes to iron contained in nanoparticles of glacial origin in the Southern Ocean. *in preparation*

3. Corentin Baudet, Eva Bucciarelli, Géraldine Sarthou, Cédric Boulart, Ewan Pelleter, Millie Goddard-Dwyer, Hannah Whitby, **Rui Zhang**, Ingrid Obernosterer, David Gonzalez-Santana, Morgane Léon, Pieter van Beek, Virginie Sanial, Catherine Jeandel, Frédéric Vivier, Maria-Elena Vorrath, Wen-Hsuan Liao, Yoan Germain, Hélène Planquette. A hydrothermal plume on the SouthWest Indian Ridge revealed by a multi-proxy approach: impact on iron and manganese distributions (GEOTRACES GS02). *Marine Chemistry.* 2024,265-266:104401

Appendix. 3. 1

Dynamics in microbial trace metals transporters during phytoplankton blooms in the Southern Ocean

Yanhui Kong[1,2], Rui Zhang[2], Stéphane Blain[2], Ingrid Obernosterer[2]

Affiliations

1 - School of Oceanography, Shanghai Jiao Tong University, 1954 Huashan Rd., Shanghai 200030, China

2- Sorbonne Université, CNRS, Laboratoire d'Océanographie Microbienne, LOMIC, Banyuls-sur-Mer, France

Preface

I guided Yanhui Kong in the bioinformatic analyses and carried out some of the anlayses

Abstract

Trace metals are required as co-factors in metalloproteins that are essential in microbial metabolism and growth. The microbial requirements of diverse metals and the capabilities of prokaryotic taxa to acquire these remains poorly understood. We present here results from metagenomic observations over an entire season in the region off Kerguelen Island (Indian Sector of the Southern Ocean). We observed seasonal patterns in the abundance of prokaryotic transporters of 7 trace elements (Zn, Mn, Mo, W, Cu, Co, Ni). The consecutive spring and summer phytoplankton blooms were strong drivers of the temporal trends. Taxonomic affiliation of the functional genes revealed that each of the trace metal transporter was associated to different microbial assemblages. Our observations suggest that *Rhodobacteraceae* had the broadest repertoire of trace metal transporters (Mn, Zn, Ni, W, Mo) and a more restricted set was observed for *Flavobacteriaceae* (Zn) and *Nitrincolaceae* (Ni, W). The prevalence of one or more trace metal transporter within a prokaryotic group, as determined on the family level, was overall confirmed in representative metagenome assembled genomes. Our results point to varying capabilities of trace metal acquisition among prokaryotic groups, suggesting these groups could contribute to the cycling of metals in surface waters of the Southern Ocean.

Appendix. 3. 2

Response of marine microbes to iron contained in nanoparticles of glacial origin in the Southern Ocean

Rhea Thoppil[1], Rui Zhang[1], Stéphane Blain[1], Philippe Catala[1], Olivier Crispi[1], Audrey Guéneuguès [1], Barbara Marie[1], Ingrid Obernosterer[1]

1 CNRS, Sorbonne Université, Laboratoire d'Océanographie Microbienne, LOMIC, F-66650 Banyuls/mer, France.

∗ Corresponding author

Preface

I carried out the DNA extractions and performed the 16S rRNA amplicon analyses.

Abstract

Biogeochemical processes in the Southern Ocean (SO) are crucial for global ocean balance. Being the largest high-nutrient-low-chlorophyll region, surface waters in the SO hold a large potential for biological activity, in particular carbon dioxide drawdown and the "greening" of the SO. But these biological processes are limited by the essential nutrient iron (Fe). The accelerated melting of glaciers in the SO could be a significant source of Fe but whether this glacial Fe is bioavailable to microorganisms is poorly understood. Moreover, not all chemical forms of Fe are equally bioavailable. Answering such questions is vital for a better understanding of the influence of glacial Fe on marine microbes and their contribution to the carbon cycle. One pathway of interest is siderophores, low molecular weight compounds that can strongly bind to Fe in seawater and thereby render Fe bioavailable. In this study, we provided colloids obtained from lakes influenced or not by glacial melt to SO coastal marine microbial communities. Taxonomic profiling displayed significant differences in microbial community compositions between treatments, with known siderophore synthesizers contributing for about half of the relative abundance in incubations amended with glacial-lake colloids. Furthermore, Fe-related gene annotation analyses showed a higher relative abundance of siderophore synthesis and transport genes in these incubations. This indicates that natural bacterial communities can utilize siderophores to access Fe from glacial nanoparticles hence exhibiting different metabolic responses to a novel resource of Fe in the SO.

Appendix. 3. 3

A hydrothermal plume on the SouthWest Indian Ridge revealed by a multi-proxy approach: impact on iron and manganese distributions (GEOTRACES GS02)

Corentin Baudet[1*], Eva Bucciarelli1[†], Géraldine Sarthou1[†], Cédric Boulart[2], Ewan Pelleter[3], Millie Goddard-Dwyer[4], Hannah Whitby[4], Rui Zhang[5], Ingrid Obernosterer[5], David Gonzalez-Santana[1,6], Morgane Léon[7], Pieter van Beek[7], Virginie Sanial[8], Catherine Jeandel[7], Frédéric Vivier[9], Maria-Elena Vorrath[10], Wen-Hsuan Liao[1,11], Yoan Germain[3], Hélène Planquette[1†*]

1 Univ Brest, CNRS, IRD, Ifremer, UMR 6539, LEMAR, F-29280 Plouzane, France

2 UMR 7144 AD2M, CNRS, Sorbonne Université, Station Biologique de Roscoff, 29680 Roscoff, France

3 IFREMER, CNRS, Univ Brest, UBS, UMR6538, Laboratoire Geo-Ocean, F-29280 Plouzane, France

4 Department of Earth, Ocean and Ecological Sciences, University of Liverpool, L69 3GP, UK

5 CNRS, Sorbonne Université, Laboratoire d'Océanographie Microbienne, LOMIC, F-66650 Banyuls/mer, France

6 Instituto de Oceanografía y Cambio Global (IOCAG), Universidad de Las Palmas de Gran Canaria, Spain

7 LEGOS (CNRS, CNES, IRD, UPS, Université de Toulouse) 14 avenue Edouard Belin, 31400 Toulouse

8Université de Toulon, Aix Marseille Univ., CNRS, IRD, MIO, Toulon, France

9 LOCEAN-IPSL, CNRS, Sorbonne Université, Paris, France

10 Institute for Geology, University Hamburg, Germany

11 Department of Earth Sciences, National Cheng Kung University, Tainan, Taiwan

† These authors contributed equally

Preface

I carried out the metagenomic analysis.

Abstract

Iron (Fe) and Mn (manganese) are crucial micronutrients that limit oceanic primary productivity in the Southern Ocean. It has been recently suggested that hydrothermal activity may be an important source of oceanic dissolved iron yet, this contribution is still not fully understood and only one active hydrothermal site has been reported on the SouthWest Indian Ridge (SWIR), south of 40°S.

Using a multi-proxy approach, this study demonstrates the occurrence of hydrothermal venting on the SWIR in the near vicinity of the location 44°51.690 S, 36°10.460 E, which is likely to be a clear fluid. Indeed we report high values of dissolved methane to manganese ratios (up to 11.1 ± 1.2 mol mol-1), low particulate iron (pFe) and manganese (pMn) concentrations (with maximum values of 0.7 nmol L-1 and 0.06 nmol L-1, respectively) associated with the presence of few oxyhydroxides, as well as high 223Radium (Ra) and 224Ra activities near the seafloor. The Fe and Mn data revealed a significant enrichment at depths influenced by hydrothermal circulation on the seafloor, within the Upper Circumpolar Deep Water. Dissolved iron (dFe) and dissolved Mn (dMn) concentrations were enriched by 3- and 7-fold, respectively, and pFe and pMn by 2- and 1.5-fold, respectively, compared to a reference station located outside the SWIR. They were however lower than concentrations reported so far near high temperature vents, suggesting a weaker influence of a clear fluid system on deep Fe and Mn reservoirs. We show that a large fraction of the dFe could be stabilized by the combined presence of colloidal Fe (up to 43 ± 8 % of dFe) and organic complexation with humic substances (eHS, estimated 27 - 60 % of dFe). High prokaryotic abundance related to the proximity of the hydrothermal vent suggests that other Fe-complexing ligands of biological origin might also stabilize Fe in its dissolved form. Although the system is a source of both dFe and dMn to the deep ocean, the low current velocities and the bathymetry likely limit the fertilization of surface water by dFe and dMn along this section of the SWIR.

Appendix. 4 – Response of Marine Microbes to Colloids of Glacial vs Non-Glacial Origin (master student)

Response of Marine Microbes to Colloids of Glacial vs Non-Glacial Origin

Alyssa Vanderkuylen, Rui Zhang and Ingrid Obernosterer
Microbial Oceanography Laboratory (LOMIC), Banyuls sur mer, France

Introduction:

- Southern Ocean is the largest HNLC region where Fe limits biological activity
- The Kerguelen Islands are an archipelago located within the Southern Indian Ocean.
- Glaciers on Ker I are rapidly melting
- Input of Fe to marine environment

Question?

Is Fe glacial origin available to marine microbes?

Objectives:

- To determine the composition of prokaryotic communities that grow in the presence of colloids of glacial and non-glacial origin.
- To investigate whether communities responding to glacial colloids are different to those responding to glacial particles
- To identify taxa that are specific to colloids from glacial origin.

Experimental Design:

Sampling sites on Kerguelen Island

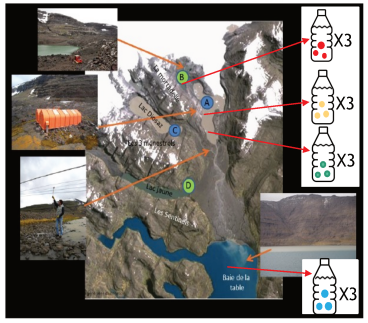

Figure 1. Water samples taken from Lake AMP (A) with the addition of colloids (green) and particles (orange) and Lake ADN (B) with the addition of colloids (red) compared to three control replicates (blue) of coastal seawater. Project BINGO (IPEV)

- Microbial incubation experiments
- Prokaryotic communities from a coastal site (Bay de la Table) were incubated with colloids and particles from glacial (Lake AMP) and non-glacial (Lake ADN) influenced environments (Fig 1)
- Incubations were carried out in the dark and community composition was determined at the end of the incubation time (10 days)

What are Colloids?

- Non-living, sub-micrometer particles made of organic matter and inorganic elements
  - Used ultrafiltration to concentrate colloids in the size fraction 0.02 µm – 0.2 µm.

Data Analysis:

- Non-metric Multi-dimensional Scaling (NMDS) Plot (R studio) to condense the data into a two-dimensional ordination
- Histograms (R studio) to plot the relative abundances of the microbial groups in the different incubations.
- A simper statistical analysis test was performed (R studio) to determine the significantly different ASVs between incubations of non-glacial and glacial origins.

Results:

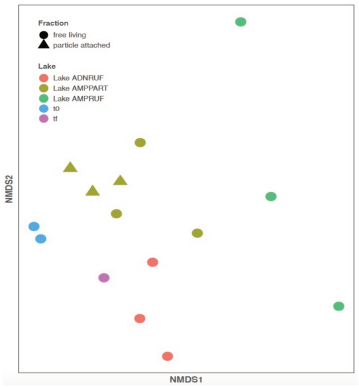

Figure 2. NMDS Plot demonstrating the similarities between 15 samples including the control, lake ADN colloids, Lake AMP colloids and Lake AMP particles.

Colloids
Non-glacial **Glacial**

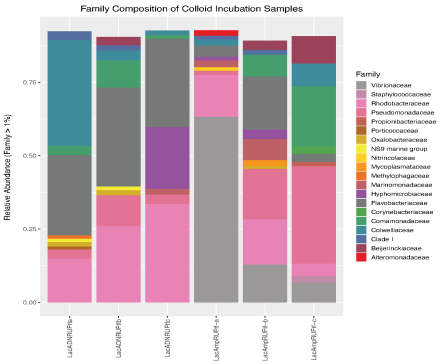

Figure 3. Family composition histogram plotting the marine microbial communities for six colloid samples, three treatments from non-glacial influenced colloids (Lake AND) and three treatments from glacial influenced colloids (Lake AMP).

Prokaryotes and Glacial Influenced Particles
Free-living **Particle-Attached**

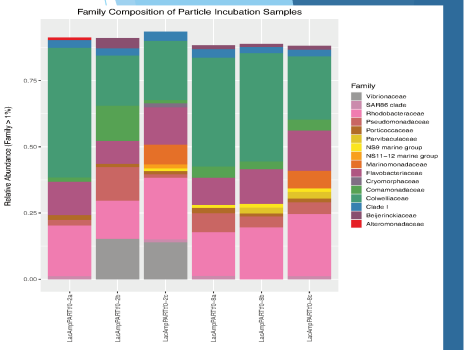

Figure 4. Family composition histogram plotting the marine microbial communities for six particle samples from Lake AMP, three treatments from the size fraction < 0.8 µm (free-living prokaryotes) and three treatments from the size fraction > 0.8 µm (particle-attached prokaryotes).

Table 1. The significant difference between eight ASV samples and their corresponding marine microbial communities extracted from colloids of glacial and non-glacial origin. Collected in Kerguelen Islands, Jan 2020.

ASV #	Glacial Colloid Abundance	Non-Glacial Colloid Abundance	Family Taxonomy	Genus Taxonomy
ASV_6	10-55%	0%	Vibrionaceae	Vibrio
ASV_122	0.35-0.7%	0%	Vibrionaceae	Vibrio
ASV_24	0-1%	8-15%	Flavobacteriaceae	Flavobacterium
ASV_59	0-1%	3-4%	Flavobacteriaceae	Flavobacterium
ASV_92	0%	1-2%	Flavobacteriaceae	Flavobacterium
ASV_113	0%	1-2%	Flavobacteriaceae	Flavobacterium
ASV_126	0%	0-1.6%	Flavobacteriaceae	Flavobacterium
ASV_125	0.5-2%	0-0.3%	Pseudomonadaceae	Pseudomonas

Discussion:

- Vibrionaceae and Pseudomonadaceae are highly abundant in the incubations amended with glacial influenced colloids. Because these colloids are rich in iron, the prevalence of these groups could be due to their ability to produce one or more siderophores with high affinities to iron. (1)
- While only few prokaryotes possess genes for siderophore synthesis, many prokaryotes have the capabilities for siderophore uptake, also known as "cheaters", as they can up-take the iron from the siderophores without expending the energy for synthesis. (1)
- Flavobacteriaceae are more abundant in the incubations with non-glacial influenced colloids. These colloids were rich in organic carbon. Members of Flavobacteriaceae contain a diverse repertoire of enzymatic capabilities for the degradation of complex organic compounds. (2)
- Since Vibrionaceae can secrete siderophores for iron uptake, it could be potentially used determine if the Kerguelen Island is a source of iron nanoparticles for the ocean.
- However, we cannot confirm this just based on the taxonomic level. We could prove this result by using a functional approach like metagenomics.

References:
1. Payne et al. 2016. *Vibrio* Iron Transport: Evolutionary Adaptation to Life in Multiple Environments. *NCBI*. 80(1): 69-90
2. Hernandez-Magana et al. 2021. Prokaryotic diversity and activity in contrasting productivity regimes in late summer in the Kerguelen region (Southern Ocean). ELSEVIER. 1-12

Acknowledgments. This work is part of the project BINGO (Bioavailability of Iron contained in Nanoparticles of Glacial Origin), supported by the IPEV.